UNIVERSIDAD AUTÓNOMA DE MADRID

FACULTAD DE CIENCIAS

PROGRAMA DE DOCTORADO EN BIOCIENCIAS MOLECULARES

The metabolic basis of renal fibrosis: role of microRNAs and insight from genetic models targeting lipid metabolism

TESIS DOCTORAL

VERÓNICA MIGUEL HERRANZ

Madrid, 2019

UNIVERSIDAD AUTÓNOMA DE MADRID

FACULTAD DE CIENCIAS

PROGRAMA DE DOCTORADO EN BIOCIENCIAS MOLECULARES6

Memoria presentada por

VERÓNICA MIGUEL HERRANZ

LICENCIADA EN BIOTECNOLOGÍA

The metabolic basis of renal fibrosis: role of microRNAs and insight from genetic models targeting lipid metabolism

Para optar al grado de

DOCTORA EN BIOCIENCIAS MOLECULARES

Dirigida por

Dr. SANTIAGO LAMAS PELÁEZ

Tutor: **Dr. Miguel Ángel Íñiguez Peña**

Realizada en el Centro de Biología Molecular "Severo Ochoa", CSIC-UAM

CSIC
CONSEJO SUPERIOR DE INVESTIGACIONES CIENTÍFICAS
UAM
Universidad Autónoma de Madrid
CENTRO DE BIOLOGÍA MOLECULAR SEVERO OCHOA

22 de mayo de 2019

A la atención de la Comisión de Doctorado de la Universidad Autónoma de Madrid:

D. **Santiago Lamas Peláez**, Profesor de Investigación de OPIs destinado en el Centro de Biología Molecular "Severo Ochoa", (CSIC-UAM).

CERTIFICA

Que Dña. **Verónica Miguel Herranz**, Licenciada en Biotecnología por la Universidad de León, ha realizado bajo mi dirección la presente Tesis Doctoral titulada **"The metabolic basis of renal fibrosis: role of microRNAs and insight from genetic models targeting lipid metabolism"**, y que dicho trabajo reúne los requisitos necesarios para su presentación y defensa en el departamento de Biología Molecular de la Universidad Autónoma de Madrid.

Fdo.: Dr. Santiago Lamas Peláez

Este trabajo ha sido realizado en el Centro de Biología Molecular Severo Ochoa (CSIC-UAM) bajo la dirección de Dr. Santiago Lamas Peláez, Profesor de investigación del CSIC en el Centro de Biología Molecular "Severo Ochoa". Además, parte de los resultados fueron obtenidos en la Universidad de Yale (New Haven, USA) bajo la supervisión de Dr. Carlos Fernández Hernando.
La realización de esta Tesis ha sido posible gracias a un contrato predoctoral para la formación de doctores 2013 (BES-2013-065986) del Ministerio de Economía y Competitividad. La autora también ha recibido tres ayudas de movilidad para estancias breves de la misma entidad.

A mis padres

A Alba

“La alegria de ver y entender es el más perfecto don de la naturaleza”

Albert Einstein

“May your choices reflect your hopes, not your fears”

Nelson Mandela

Agradecimientos/ Acknowledgments

Una historia no tiene ni comienzo ni fin: uno elige el momento de la experiencia desde el cual mirar hacia atras o hacia delante. Sin duda, estos años han constituido una etapa intensa de crecimiento profesional y personal, marcados por la gente que me ha acompañado, y de la que tanto he aprendido. Quiero mostrar mi agradecimiento a todas estas personas que, de una u otra forma, han hecho posible este trabajo.

Santiago, sin duda esta tesis ha sido posible gracias a ti. Gracias por darme la oportunidad de trabajar en el laboratorio, por confiar en mí desde el principio, por tus consejos y tu apoyo. Gracias por tu dedicación, por estar siempre dispuesto a escucharme y por tener en cuenta mis ideas. Gracias por ofrecerme la mejor formación y darme la libertad necesaria para aprender equivocándome. Gracias por saber motivarme y enseñarme a disfrutar de este trabajo.

También quiero dar las gracias a todos los compañeros con los que he compatido más o menos tiempo durante esta etapa. Oscar y Cris, todavía me acuerdo cuando me decíais que sin darme cuenta estaría imprimiendo la tesis; hoy sé que teníais razón. Gracias por todo lo que me enseñasteis y por preocuparos tanto por mi cuando llegué al laboratorio. Cris, gracias en especial por tu amistad, por estar siempre dispuesta a ayudarme, por tener respuesta para todas mis dudas y estar preparada para hacer un viaje! A Maria Ángeles, Jose, Fernando, Estrella, Marta y Eva, por echarme una mano cuando la necesitaba. A Nacho y Hassan, qué habría hecho yo con los ratones sin vosotros! A Carlos y Jessy, por compartir experiencias y experimentos, y por hacer el día a día más divertido. A los estudiantes que han pasado por el laboratorio, especialmente a Miriam, Alba y Elena, gracias por vuestra gran ayuda con el proyecto de CPT1A. A Patricia y Tamara, por compartir esta experiencia conmigo desde el principio, por vuestra gran amistad y por hacer que los días sean siempre más fáciles. A Diana, por poner ese punto diferente en las conversaciones de las comidas. A Macarena, gracias por cargar los viajes de anécdotas! A Jose Luis, Tania y Cris, gracias por las conversaciones en el CBM y por vuestra ayuda con las dudas sobre doctorado.

A los grupos de investigación donde he realizado estancias en el extranjero. Dr. Victor Thannickal (UAB), Dr. Carlos Fernandez-Hernando (Yale) and Dr. Katalin Susztak (UPenn) and their research groups. Thank you so much for the opportunity to work in your lab, for your help and support. It was a big pleasure to be there, to learn and enjoy a different way of working and thinking. Also I am very thankful to all people in your lab. Special thanks to Karen and Naomi (UAB), Nathan (Yale) and Shizheng (UPenn). It was fantastic working with you!

Al resto de grupos de investigación que han colaborado en este proyecto: Diego Rodríguez-Puyol, Loreto y Carolina (Hospital de Alcalá), Marta Ruiz Ortega y su grupo (Fundación Jimenez Diaz), Coral Barbas y Paula (Universidad CEU San Pablo), Ricardo Ramos (Parque Científico), Laura Garcia Bermejo (Hospital Ramón y Cajal), Laura Herrero (Universidad de Barcelona) y Miguel López (Universidad de Santiago de Compostela). A los laboratorios de Jorgina Satrustegui y JM Cuezva en el CBM por su generosidad con el uso del equipo Seahorse. A Valeria Valez y Susana Cadenas por la ayuda con el equipo Oroboros. A Marisa Toribio por la ayuda con el análisis de los experimentos de citometría de flujo. A los servicios cientificos que han participado: Microscopía Óptica y Confocal (CBMSO), Citometría de Flujo (CBMSO), Transgénesis (CNB) y Unidad de Ratones Transgénicos (CNIO). A Miguel Ángel Íñiguez, mi tutor académico, gracias por tu ayuda con las correciones de la tesis y con los trámites del doctorado.

A la fundación IMFAHE, por incorporarme a su programa de mentoring internacional. Gracias por permitirme disfrutar de una nueva experiencia en USA en el laboratorio del Dr. Samir Parikh los próximos meses. Gracias a mi mentor, Ángel, por compartir tu experiencia conmigo y por tus valiosos consejos.

Sin embargo, mi trabajo en el laboratorio comenzó en la dpto. de Fisiología Animal de la Universidad de León. Mil gracias Ana, por permitirme descubrir el trabajo de investigación, por todo lo que aprendí de ti, por el tiempo que me dedicaste, y sobre todo, por toda la energia y entusiasmo por la ciencia que me transmitiste. Gracias, Borja y Andoni, y al resto del grupo por el esfuerzo en enseñarme a trabajar en el laboratorio cuando apenas sabía pipetear. Trabajar en vuestro laboratorio hizó realmente enriquecedora mi etapa formativa allí. Son infinitos los recuerdos de dentro y fuera de la Universidad. Cris, Raquel, Unai, Nacho, Raul, Marta (s), Esther, Isa…gracias por todos esos momentos, y por estar siempre ahí aunque nos veamos poco. Raquel, gracias por esa amistad tan especial y por los planes improvisados siempre que vienes a Madrid. Mil gracias Carlos, por tu ayuda, paciencia, comprensión y por hacer que la distancia sólo sea un número.

También quiero agradecer a mi familia. A mis abuelos, por ser esa fuente tan grande de cariño y por transmitirme tantos valores. A mis tíos y a mis primos: Sergio, Pablo, Marina, Fer, Raúl y Marta, porque desde un mundo tan ajeno a este, me habéis sabido comprender y apoyar. Gracias a mis padres por la educación y el valor del esfuerzo. Por permitirme aprender tanto de vosotros, y por todo lo que me seguís enseñando. Por facilitarme el camino que he querido seguir en cada momento. Gracias por vuestro apoyo incondicional. Y sobre todo a mi hermana, Alba. Eres el mejor ejemplo de fortaleza, constancia y superación. Gracias por tu cariño y complicidad.

¡Gracias a todos!

Table of contents

TABLE OF CONTENTS **15**
ABBREVIATIONS **21**
SUMMARY – RESUMEN **29**
1.INTRODUCTION **35**
1.1 Chronic kidney disease **37**
1.1.1. –Chronic kidney disease: a major public health concern *37*
1.1.2. –Kidney physiology *37*
1.1.2.1. –Kidney structure and function *37*
1.1.2.2. –Nephron structure and function *37*
1.1.3. –Fibrosis: the final outcome of CKD *38*
1.1.3.1. –Organ fibrosis *38*
1.1.3.2. –Renal tubulointerstitial fibrosis *39*
1.1.3.3. –Animal models for the study of kidney fibrosis *39*
1.1.3.4. –Phenotypic characterization of kidney-associated myofibroblasts *40*
1.1.3.5. –Cellular origin of myofibroblasts in kidney fibrosis *40*
1.1.3.6. –Inflammatory cells in kidney fibrosis *41*
1.1.3.7. –Molecular signaling pathways in kidney fibrosis *43*
1.1.3.7.1. –TGF-β signaling pathways *43*
1.2 MicroRNAs **44**
1.2.1. –microRNAs as crucial regulators of gene expression *44*
1.2.2. –microRNA biogenesis and function *45*
1.2.2.1. –MicroRNA processing in the nucleus: Drosha and DGCR8 ..... *45*
1.2.2.2. –MicroRNA processing in the cytoplasm: DICER *45*
1.2.2.3. –mRNA degradation and translational repression *45*
1.2.2.4. –Mechanisms of action of microRNAs and its regulation *46*
1.2.2.5. –microRNA turnover *47*
1.2.3. –microRNA nomenclature *47*
1.2.4. –microRNA gain- and loss- of- function strategies *47*
1.2.5. –Regulation of kidney fibrosis by microRNAs *47*
1.2.5.1. –Regulation of TGF-β-induced signaling pathways by microRNAs *48*
1.2.5.2. –Regulation of epithelial to mesenchymal transition (EMT) *48*
1.2.5.3. –Regulation of metabolic pathways and redox responses *49*
1.2.5.4. –Regulation of extracellular matrix (ECM) and other cellular mechanisms *49*
1.3 Metabolism in the kidney **50**
1.3.1. –The kidney as a metabolic organ *50*
1.3.2. –Fatty acid oxidation *50*
1.3.2.1. –Carnitine palmitoyl-transferase 1 ..... *51*
1.3.2.1.1. –Structure and function of CPT1 ..... *52*
1.3.2.1.2. –CPT1 gene regulation *53*
1.3.3. –Energy metabolism in renal proximal tubular cells during CKD *53*

1.3.4. –microRNAs regulation of lipid metabolism *55*
1.3.4.1. –miR-33 ..... *55*
2.AIMS **57**
3.METHODS **61**
3.1 Generation of a transgenic mouse model for inducible *Cpt1a* gene **63**
3.1.1. –Molecular cloning and gene targeting in ES cells *63*
3.1.2. –Generation of mice *65*
3.1.3. –Doxycycline induction *65*
3.1.4. –Genotyping *65*
3.2 miR-33 KO animals **66**
3.3 Cell lines and culture conditions **66**
3.4 Isolation of primary kidney epithelial cells **67**
3.5 Transfection procedure **67**
3.6 Immunoblot **67**
3.7 RNA extraction **68**
3.8 Analysis of mRNA expression **68**
3.9 Quantification of miRNA expression **69**
3.10 Mouse models of kidney fibrosis **70**
3.10.1. –Unilateral ureteral obstruction (UUO) *71*
3.10.2. –Folic acid-induced nephropathy (FAN) *71*
3.10.3. –Adenine-induced renal failure (ADN) *71*
3.11 microRNA profiling **72**
3.12 Triglyceride measurement **74**
3.13 [1-^{14}C] Palmitate oxidation **74**
3.14 TaqMan gene expression assay **75**
3.15 Mitochondrial copy number determination **75**
3.16 Assessment of kidney function **76**
3.17 miRNA analysis in blood plasma from CKD patients **77**
3.18 Quantification of kidney cell populations by flow cytometry **77**
3.19 Immunofluorescence **78**
3.20 Histological analysis **78**
3.21 Electron microscopy examination **79**
3.22 Measurements of oxygen consumption rate **79**
3.23 Mitochondrial membrane potential (MMP) **81**
3.24 Mitochondrial superoxide radical anion production **81**
3.25 Adenovirus-mediated CPT1A overexpression **82**
3.26 Statistical analysis **83**
4.RESULTS **85**
4.1 Generation of a transgenic mouse model with inducible renal overexpression of CPT1A (*Cpt1a* knock-in) **87**

4.1.1. –Generation process of the transgenic mouse model for inducible Cpt1a gene in renal epithelial cells 87
4.1.2. –Evaluation of Dox-induced GFP expression in CPT1A clones 87
4.1.3. –Genotypic characterization of the Pax8-rtTA$^{tg/0}$:tetO-Cpt1a$^{tg/0}$ mice 88
4.1.4. –Characterization of Dox-inducible Cpt1a gene overexpression in renal epithelial cells 89
4.1.5. –Dox-inducible Cpt1a gene overexpression in renal tubular epithelial cells improved kidney FAO rate 90
4.2 Effects of FAO gain-of-function in kidney fibrosis 92
4.2.1. –CPT1A as a protective enzyme for kidney fibrosis development 92
4.2.2. –CPT1A overexpression prevents histological changes associated to experimental renal fibrosis 92
4.2.3. –CPT1A prevents the increased expression of fibrotic, apoptotic and inflammatory markers associated to kidney fibrosis 94
4.2.4. –CPT1A prevents impaired mitochondrial morphology and fatty acid oxidation defect induced by fibrosis in the kidney 98
4.2.5. –Increased levels of CPT1A reduces the monocyte/macrophage infiltration pro-inflammatory profile in fibrotic kidneys 100
4.2.6. –Genetic CPT1A overexpression prevents AMP-activated protein kinase (AMPK) activation associated to kidney fibrosis 102
4.3 Evaluation of TGF-β-induced profibrotic responses in renal cellular models of CPT1A overexpression 104
4.3.1. –Renal tubule epithelial cells overexpressing CPT1A exhibit higher levels of FAO-associated oxygen consumption rate (OCR) and decreased glucose utilization 104
4.3.2. –CPT1A overexpression in renal epithelial cells prevents TGF-β-induced dedifferentiation 107
4.4 Identification of specific miRNAs that regulate the fibrotic outcome in the kidney through metabolic pathways 109
4.4.1. –miRNA expression data in UUO-induced fibrotic kidneys 109
4.4.2. –Determination of the contribution of miR-33 in regulating kidney FAO and renal fibrosis using the miR-33 knockout mouse model 111
4.4.2.1. –Loss of miR-33 protects against kidney fibrosis 111
4.4.2.2. –Loss of miR-33 enhances FAO-dependent mitochondrial respiration and reduces renal lipid accumulation 113
4.4.2.3. –miR-33 impairs fatty acid oxidation and promotes kidney dysfunction in human patients. 116
4.4.3. –Role of miR-150, miR-495 as regulators of the profibrotic response by regulating mitochondrial function. 117
4.4.3.1. –MiR-150 and miR-495 increase the TGF-β profibrotic response in the Human Tubular Renal Epithelial Cell line HKC-8 117
4.4.3.2. –MiR-150 and miR-495 suppress CPT1A expression and reduce FAO-associated oxygen consumption rate (OCR) in HKC-8 cells 119

4.4.3.3. –MiR-150 and miR-495 do not alter mitochondrial transmembrane potential (ΔΨm) and mitochondrial superoxide radical anion production 120

4.4.3.4. –MiR-150 and miR-495 levels are not affected in plasma and kidney samples from CKD patients 121

5.DISCUSSION 123

5.1 Cpt1a enzyme has a protective impact on the outcome of kidney fibrosis 125

5.1.1. –Protective role of CPT1A in kidney fibrosis development 125

5.1.2. –Differences among animal models used for the study of kidney fibrosis 125

5.1.3. –Characterization of in vivo CPT1A overexpression among transgenic mouse models 126

5.1.5. –Molecular mechanisms underlying mitochondrial defects in kidney fibrosis mouse models ... 129

5.1.6. –Effect of restoring lipid metabolism on renal epithelial damage 130

5.1.7. –Macrophage population profile in renal epithelial damage 131

5.2 MiR-33, a quintessential regulator of lipid metabolism with a new role in kidney fibrosis 132

5.2.1. –miR-33 as a new regulator of lipid metabolism during kidney fibrosis 132

5.2.2. –Global control of lipid metabolism by miR-33 132

5.2.3. –The profibrotic role of miR-33 133

5.2.4. –Lipid and miR-33 alterations in plasma samples from CKD patients 134

5.3 miR-150 and miR-495 as new regulators of the metabolic derangements of renal fibrosis 135

5.3.1. –Regulation of mitochondrial function by miR-150 and miR-495 enhance profibrotic responses in renal tubular epithelial cells 135

5.3.2. –MicroRNA regulation of mitochondrial function in renal fibrosis 135

5.3.3. –Serum levels of microRNAs as potential biomarkers for CKD progression 137

6.CONCLUSIONS – CONCLUSIONES 139

7.SUPPLEMENTARY MATERIAL 145

8.REFERENCES 151

Abbreviations

ABCA1: ATP-binding cassette sub-family A member 1

ACC: Acetyl-CoA carboxylase

ACCORD: Action to control cardiovascular risk in diabetes

ACoA: Acyl-Coenzyme A

***Acox1*:** Peroxisomal acyl-CoA oxidase 1

***Acox2*:** Peroxisomal acyl-CoA oxidase 2

***Acta2*:** Alpha smooth muscle actin

ADAM19: ADAM metallopeptidase domain 19

***Adgre1*:** Adhesion G protein-coupled receptor E1 (F4/80)

ADN: Adenine-induced nephrotoxicity

AGO: Argonaute (AGO)

AKI: Acute kidney injury

AKT: AKT serine/threonine kinase 1

Alb: albumin

AMPK: AMP activated kinase

Ang II: Angiotensin II

***Apaf1*:** Apoptotic peptidase activating factor 1

ApoA1: Apolipoprotein A-I

***Bax*:** Bcl-2-associated X protein

***Bcl2*:** B-cell lymphoma 2

Bcl2l1: BCL2-like 1

BUN: Blood urea nitrogen

c-ABL: Abelson non receptor tyrosine kinase

CAT: Carnitine-acyl-carnitine translocase

CD: Collecting duct

CD86: CD86 antigen

***Cdc42*:** Cell division cycle 42

***Cdh16*:** Cadherin 16

CDS: Coding sequence

CKD: Chronic kidney disease

CKD-EPI: Chronic kidney disease epidemiology collaboration

CMC: Carboxymethyl cellulose

CMV: Cytomegalovirus

***Col1a1*:** Collagen type I alpha 1 chain

Col3a1: Collagen type III alpha 1 chain

***Col4a1*:** Collagen type IV alpha 1 chain

***Cpt1a*:** Carnitine palmitoyltransferase 1A

***Cpt2*:** Carnitine palmitoyltransferase 2

CREB: cAMP-response element-binding protein

CROT: Carnitine O-octanoyltransferase

CTGF: Connective tissue growth factor

DAMP: Danger-associated molecular pattern

DAPI: 4,6-diamidino-2-phenylindole

DC: Dendritic cells

DGCR8: DiGeorge syndrome critical region 8

Dicer 1: Double-stranded RNA-specific endoribonuclease

Dox: Doxycycline

***E-cadh*:** E-cadherin

ECAR: Extracellular acidification rate

ECM: Extracellular matrix proteins

EMC: Extracellular matrix

EMT: Epithelial–mesenchymal transition

EndoMT: Endothelial-mesenchymal transition

EpCAM: Epithelial cell adhesion molecule

EQ: relative quantification

ERK: Extracellular signal-regulated kinase

ES: Embryonic stem

FA: Fatty acid

FABP7: Fatty acid-binding protein 7

FAN: Folic acid-induced nephropathy

FAO: Fatty acid oxidation

FASN: Fatty acid synthase

FBS: Fetal bovine serum

FCCP: Carbonyl cyanide-p-trifluoromethox- yphenyl-hydrazon

FDR: False discovery rate

FGF2: Fibroblast growth factor 2

FIELD: Fenofibrate intervention and event lowering in diabetes

FN: Fibronectin

FOXD1: Forkhead Box D1

FRT: Flippase recombination targets

FXR: Farnesoid X receptor

***G6pc*:** Glucose-6-phosphatase catalytic subunit

***Gapdh*:** Glyceraldehyde-3-phosphate dehydrogenase

GFR: Glomerular filtration rate

GLI1: GLI family zinc finger 1

GSH: Glutathione reduced

HADH: Hydroxyacyl-CoA dehydrogenase

Havrc1: Hepatitis A virus cellular receptor 1

HBSS: Hank's balanced salt solution

HDL: High-density lipoprotein

***Hk1*:** Hexokinase 1

HMGA2: High mobility group A2

Hspa9: Heat shock protein family A (Hsp70) member 9

IGFBP3: Insulin-like growth factor binding protein 3

IGFBP5: Insulin like growth factor binding protein 5

IL1b: Interleukin 1 beta

iNOS: Nitric oxide synthase

ITS: Insulin-transferrin-selenium

JNK: c-Jun N-terminal kinase

KDIGO: Kidney disease improving global outcomes

KI: Knock-in

KIM1: Kidney injury molecule 1

KO: Knock-out

LCFA: Long-chain fatty acids

***Ldh1*:** L-lactate dehydrogenase 1

***Ldh2*:** L-lactate dehydrogenase 2

LNA: Locked nucleic acid

lncRNA: Long non-coding RNA

LPS: Lipopolysaccharide

Lrpprc: Leucine-rich PPR motif-containing protein

MAPK: Mitogen-activated protein kinase

MC: Mast cells

MCD: Malonyl-CoA decarboxylase

MCFA: Medium-chain fatty acid

MDRD: Modification of diet in renal disease

MicroRNA: miRNA

MINCLE: Macrophage-inducible C-type lectin

MMP: Matrix metalloproteinase

MMP12: Matrix metalloproteinase 12

MP: Mitochondrial membrane potential

MPL: membrane phospholipid

Mrc1: Macrophage mannose receptor 1 (CD206)

MSC: Mesenchymal stem cell

MVB: Multivesicular bodies

ncRNA: Non-coding RNA

***Ndufv2*:** NADH:ubiquinone oxidoreductase core subunit V2

***Nos2*:** Nitric oxide synthase 2

NR: Nuclear receptors

***Nrf2*:** Nuclear factor erythroid 2-related factor 2

ns: no significant

OCR: Oxidation-associated oxygen consumption rate

OCT: Optimal cutting temperature

ORF: Open reading frame

P2A: 2A self-cleaving peptide

PAI-1: Plasminogen activator inhibitor-1

PAMP: Pathogen-associated molecular patterns

PAX8: Paxillin-8

P-Bodies: Processing bodies

PBS: Phosphate buffered saline

PDCD4: Programmed cell death 4

PDGFRβ: Platelet-derived growth factor receptor-beta

PGC-1α: Peroxisome proliferator-activated receptor γ coactivator 1α

PGK: Phosphoglycerate kinase

***Pgk1*:** Phosphoglycerate Kinase 1

PI3K: Phosphatidylinositol 3 kinase

PKD: Polycystic kidney disease

***Pkfm*:** Phosphofructokinase 1

***Pkm*:** Pyruvate kinase

PLA2: phospholipase A2

PLA2: Phospholipase A2

***Ppargc1a*:** PPARG Coactivator 1 Alpha

PPAR-α: Peroxisome proliferator-activated receptor alpha

pre-miRNA: Precursor microRNAs

pri-miRNA: Primary miRNA

PTCs: proximal tubule cells

RCT: Reverse cholesterol transport

RISC: RNA-induced silencing complex (RISC)

ROS: Reactive oxigen species

RT: Reverse transcription

RTEC: Renal tubular epithelial cells

RXRα: Retinoid X receptor alpha

SBE: Smad-binding elements

SCFA: Short-chain fatty acid

***Sdha*:** Succinate Dehydrogenase Complex Flavoprotein Subunit A

SHP: Small heterodimer partner

***Slc2a1*:** Glucose transporter protein type 1

***Snai1*:** Snail Family Transcriptional Repressor 1

SREBP: Sterol regulatory element-binding protein

TAG: Triglycerides

TCA: Tricarboxylic acid

TEC: Tubular epitelial cell

***Tfam*:** Mitochondrial transcription factor 1

***Tgfb1*:** Transforming growth factor beta 1

TGF-βRII: TGF-β receptor type II

TIMP: Tissue inhibitor of metalloproteinases

TIMP-1: Metalloproteinase inhibitor 1

TLR: Toll- like receptor

TLR4: Toll-like receptor 4

TMRM: Tetramethylrhodamine methyl ester

***Tnf*:** Tumor necrosis factor

TR: Thyroid hormone receptor

TRBP: Transactivation response element RNA-binding protein

TRE: Tetracycline-responsive promoter element

TRE: Thyroid hormone response element

TWEAK: Tumor necrosis factor-like weak inducer of apoptosis

***Twist1*:** Twist family BHLH transcription factor 1

UCP: Uncoupling proteins

UTR: Untranslated region

UUO: Unilateral ureteral obstruction

VEGF: Vascular endothelial growth factor

***Vim*:** Vimentin

VLCFA: Very long-chain fatty acids

***Zeb1*:** Zinc finger E-box binding homeobox 1

α-SMA: Alpha-smooth muscle actin

Summary – Resumen

Chronic kidney disease (CKD) involves the progressive deterioration of kidney function and affects around 10% of the worldwide population. Chronic injury of renal epithelial cells conveys a persistent inflammatory and profibrogenic response, which ultimately results in tubulointerstitial fibrosis and a progressive loss of renal function. Mitochondrial dysfunction and defective fatty acid oxidation (FAO), which compromise the main source of energy for the renal tubular epithelial cell (RTEC), have been proposed to be fundamental contributors to the development and progression of kidney fibrosis.

To determine if a functional gain in FAO could protect the kidney from fibrosis, we generated a conditional transgenic mouse model with specific overexpression of the fatty acid shuttling enzyme carnitine palmitoyl-transferase 1 A (CPT1A) in RTECs. This was achieved by crossing mice expressing the rtTA transactivator under the paxillin-8 promoter with the newly generated TRE/CPT1A mice. CPT1A expression was upregulated by 10-fold after doxycycline induction and showed the expected mitochondrial localization. This was reflected in an increased rate of palmitate oxidation and ATP production. Studies in *Cpt1a* knock-in mice subjected to the experimental models of renal fibrosis, unilateral ureteral obstruction (UUO), folic acid nephropathy (FAN) or adenine-induced renal failure (ADN) exhibited decreased expression of fibrotic markers compared with wild type animals (WT). In the FAN model, CPT1A overexpression reduced the abundance of the pro-inflammatory M1 subpopulation. This FAO gain-of-function partially prevented the decrease in FAO rate 3 days after UUO, FAN and ADN models but not in kidneys after 7 days of UUO. Furthermore, both primary renal tubule epithelial cells isolated from transgenic mice and HKC-8 cells transduced with adenoviral particles for CPT1A were protected from TGF-β-induced dedifferentiation. These cells exhibited higher levels of FAO-associated oxygen consumption rate (OCR) and decreased glucose utilization. Tissue from kidneys corresponding to mice overexpressing CPT1A also presented a reduced proportion of damaged epithelial cells in the UUO and FAN models. These results support that overexpression of CPT1A has a protective impact on the outcome of kidney fibrosis, most likely due to the enhancement of FAO in RTECs.

MicroRNAs (miRNAs), which regulate gene expression post-transcriptionally, have been reported to control renal fibrogenesis. To identify miRNAs involved in the metabolic derangement of renal fibrosis, we performed a miRNA array screen in the renal fibrosis mouse model of unilateral ureteral obstruction (UUO). MiR-150-5p, miR-495-3p and miR-33-5p were selected for their link to human pathology, their role in mitochondrial metabolism and their targeting of CPT1A. Studies in miR-33a-deficient mice (KO) subjected to UUO and FAN showed decreased kidney fibrosis and lipid accumulation compared with wild type animals. MiR-33 analogs reduced FAO-related OCR while miR-33 antagonists increased it in HKC-8 cells. MiR-495-3p and miR-150-5p were upregulated both in the UUO and folic FAN models. These miRNAs synergized with TGF-β regarding their profibrotic effects and reduced FAO-associated OCR in the human epithelial renal cell line HKC-8. These data support that miR-150, miR-495 and miR-33 can be exploited as targets to prevent the metabolic impairment leading to renal fibrosis.

Overall, this work proposes that strategies directed towards restoring FAO may prove useful for the prevention or treatment of kidney fibrosis.

La enfermedad renal crónica (ERC) implica el deterioro progresivo de la función renal y afecta a alrededor del 10% de la población. La lesión crónica de las células epiteliales renales se manifiesta con una respuesta inflamatoria y profibrogénica persistente, que en última instancia produce fibrosis tubulointersticial y una pérdida progresiva de la función renal. Se ha propuesto que la disfunción mitocondrial y una oxidación de ácidos grasos (FAO) deficiente, que comprometen la principal fuente de energía de las células epiteliales tubulares renales, contribuyen de manera fundamental al desarrollo y a la progresión de la fibrosis renal.

Para determinar si una ganancia funcional en la FAO podría proteger el riñón de la fibrosis, generamos un modelo de ratón transgénico condicional de sobreexpresión específica de la enzima transportadora de ácidos grasos carnitina palmitoiltransferasa 1 A (CPT1A) en células epiteliales tubulares renales. Esto se logró cruzando ratones que expresaban el transactivador rtTA bajo el promotor de paxilina 8 con los ratones TRE/CPT1A generados *de novo*. La expresión de CPT1A se incrementó 10 veces tras la inducción con doxiciclina y presentó la esperada localización mitocondrial. Esto se reflejó en una mayor tasa de oxidación de palmitato y producción de ATP. Los estudios en ratones con sobreexpresión de CPT1A sometidos a los modelos experimentales de fibrosis renal, obstrucción unilateral del uréter (UUO), nefropatía inducida por ácido fólico (FAN) o fallo renal inducido por adenina (ADN) mostraron una expresión reducida de marcadores fibróticos en comparación con animales de fenotipo silvestre (WT). En el modelo de FAN, la sobreexpresión de CPT1A redujo la abundancia de la subpoblación de macrófagos proinflamatorios M1. Esta ganancia de función de FAO impidió parcialmente la disminución de la tasa de FAO en los modelos de 3 días tras UUO, FAN y ADN pero no en los riñones sometidos a 7 días de UUO. Además, tanto las células primarias epiteliales del túbulo renal aisladas de ratones transgénicos como la línea celular humana de túbulo renal HKC-8 transducidas con partículas adenovirales para CPT1A mostraron una reducción de la desdiferenciación inducida por TGF-β. Estas células también presentaron niveles más altos de la tasa de consumo de oxígeno (OCR) asociada a la FAO y una menor utilización de glucosa. En los riñones sometidos a UUO o FAN que sobreexpresaban CPT1A se observó una reducción del número de células epiteliales dañadas. Estos resultados respaldan que la sobreexpresión de CPT1A tiene un efecto protector sobre la fibrosis renal, muy probablemente debido al aumento de la FAO en las células epiteliales del túbulo renal.

Los microRNA (miRNAs), que regulan la expresión génica de manera post-transcripcional, controlan la fibrogénesis renal. Para identificar los miRNAs implicados en la regulación metabólica de la fibrosis renal, se realizó un *array* de miRNAs en el modelo de ratón de fibrosis renal de UUO. Los microRNAs miR-150-5p, miR-495-3p y miR-33-5p fueron seleccionados por su vínculo con la patología humana, su papel en el metabolismo mitocondrial y porque tenían como diana a CPT1A. Estudios en ratones deficientes en miR-33a (KO) sometidos a UUO y FAN mostraron una disminución de la fibrosis renal y de la acumulación de lípidos en comparación con los animales WT. Los análogos de miR-33 redujeron el OCR asociado con la FAO en las células HKC-8, mientras que los antagonistas de miR-33 lo aumentaron. MiR-495-3p y miR-150-5p presentaron una expresión incrementada tanto en los modelos de UUO como de FAN. Estos miRNAs demostraron sinergia con TGF-β con respecto a sus efectos profibróticos y redujeron la OCR asociada a la FAO en las células HKC-8. Estos datos apoyan que miR-150, miR-495 y miR-33 pueden ser explorados como dianas terapéuticas con el objetivo de prevenir el deterioro metabólico que conduce a la fibrosis renal.

En conjunto, este estudio propone que las estrategias encaminadas a restaurar la FAO pueden ser útiles para la prevención o el tratamiento de la fibrosis renal.

1.Introduction

1.1 Chronic kidney disease

1.1.1. –Chronic kidney disease: a major public health concern

Chronic kidney disease (CKD) is a clinical condition where the reduction of renal function is maintained. It is generally considered to be irreversible and progressive. It represents an important public health problem that can affect 12–14% of the general population [1]. It may be present in about 30-40% of patients with highly prevalent pathologies such as diabetes mellitus and hypertension, where it contributes to dictate evolution and prognosis. Other less common causes of CKD include genetic diseases such as polycystic kidney disease (PKD), glomerulopathies of immune origin and exposure to environmental toxins. Acute kidney injury (AKI) is a predisposing cause and an occasional precedent of CKD, whereas CKD is a major risk factor for AKI [2]. Costs for the treatment of CKD in the US now exceed $42 billion/year [3]. This translates into 1.4 million patients reaching end-stage renal disease (ESRD) each year globally, which requires lifelong dialysis or kidney transplantation and it is the cause of more than 950,000 deaths. Currently, about 20,000 patients require some type of dialysis in Spain [4]. Although over the last few years multipronged interventions have been applied to defer the progression of CKD, including intensive glycemic control, strict control of blood pressure, correction of dyslipidemia, discontinuation of potentially nephrotoxic drugs or smoking and blockade of the renin-angiotensin system to lower glomerular capillary pressure, none of the current strategies have revealed themselves effective to revert the progression to ESRD [5]. Regardless of the disease etiology, progression of CKD leads to tubulointerstitial and glomerular fibrosis as a result of excessive deposition of extracellular matrix (ECM) [6].

1.1.2. –Kidney physiology

1.1.2.1. –Kidney structure and function

Kidneys are retroperitoneal organs located at both sides of the vertebral column. On the medial surface is a hilus, through which the renal artery and vein, the lymphatics and a nerve plexus enter the kidney. The parenchyma consists of the tubular system, the interstitium and the vasculature and can be divided into cortex (outer region) and medulla (inner region). In humans, the medulla is divided into 8 to 18 renal pyramids [7]. The base of each pyramid extends towards the renal pelvis, forming a papilla where urine is collected and flows through the ureter and the bladder [8].

The global mission of the kidney is to maintain the homeostasis of the internal milieu, which is essentially equivalent to the extracellular fluid. Thus, it regulates the concentration of water and preservation of solutes by filtering the blood, reabsorbing essential metabolites and excreting the rest as urine. Beyond the elimination of waste products, the kidney also controls blood pressure, levels of electrolytes and metabolites and regulates blood pH [9]. These functions are partly related to the endocrine system to which the kidney also contributes by generating hormones such as erythropoietin [10]; calcitriol, [11]; synthesis of arachidonic acid derivatives [12] and renin [13].

1.1.2.2. –Nephron structure and function

The functional unit of the kidney is the nephron. The human kidney contains about 0.4-1.2 x 10^6 nephrons. The nephron consists of the renal corpuscle (glomerulus and Bowman's capsule) connected to the renal tubular system and ending in the collecting duct [14].

Ultrafiltration of blood takes place in the glomerulus. Blood enters the glomerulus through the afferent arteriole and leaves it via the efferent arteriole. The filtration barrier between the blood and urinary space is composed of a fenestrated endothelium, glomerular basement membrane and the slit pores between the foot processes of the podocytes. Physical forces affecting these arterioles and the glomerular capillaries together with the juxtaglomerular apparatus form the basis of the autoregulation of glomerular filtrate [15].

The tubular system is involved in reabsorption and secretion functions. Its components include the proximal convoluted tubule, the loop of Henle, the distal convoluted tubule, and the collecting duct [16]. In the tubules, water and solutes are absorbed or secreted depending on the segment and conditions generating a primordial urine (**Figure 1**).

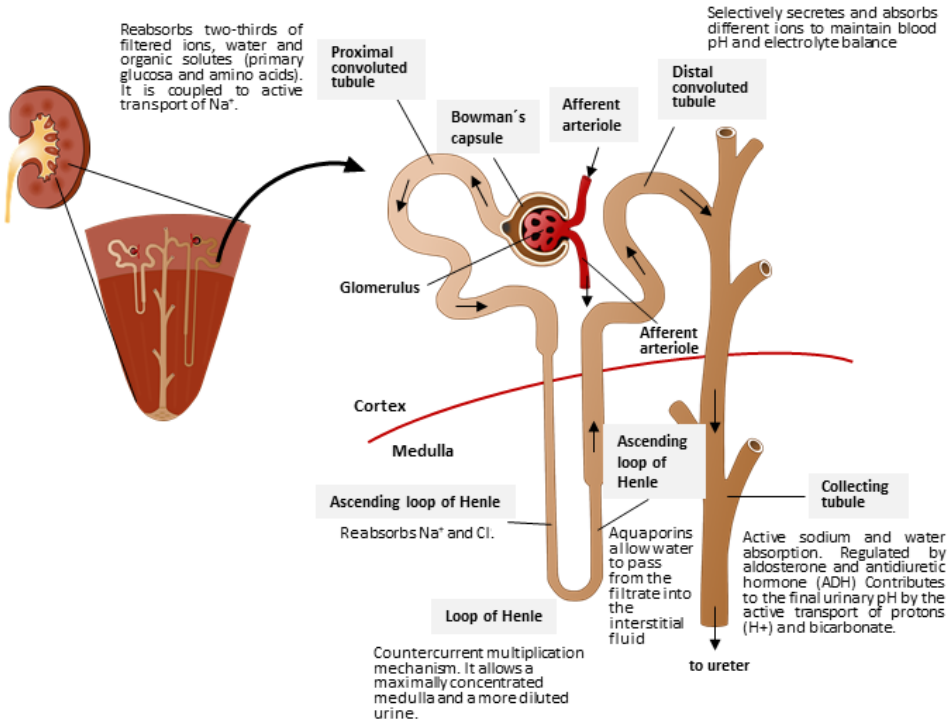

Figure 1. Kidney structure and physiology. Nephrons are the functional units of the kidney. They are composed of glomeruli and tubules. The glomerulus filters the blood while retaining cells and large proteins. The filtrate enters the tubule to produce the final urine by removing substances from the tubular fluid (reabsorption) or adding substances to the tubular fluid (secretion). The kidneys maintain the homeostasis of the internal milieu by preserving the balance of water, minerals, electrolytes and hydrogen ions and eliminating the toxic substances produced by the body.

1.1.3. –Fibrosis: the final outcome of CKD

1.1.3.1. –Organ fibrosis

Tissue fibrosis is the formation of non-functional scar tissue in response to a non-resolving inflammation after a sustained injury or insult [17]. It is a worldwide leading cause of morbidity and mortality associated with organ failure in various chronic diseases including idiopathic pulmonary fibrosis, liver cirrhosis, systemic sclerosis and nephrosclerosis as well as several cardiac diseases [18]. Tissue damage promoted by infectious agents, metabolic derangements, autoimmune processes or genetic causes, triggers pro-inflammatory signals and cellular responses elicited by cells participating in both innate and adaptive immune responses. Both profibrotic cytokines and mechanical forces produced by infiltrating macrophages or resident cells, promote the migration, proliferation and activation of the population of mesenchymal cells that eventually become myofibroblasts. These cells share many features with smooth muscle cells, including

their morphology and contractile capacity [19]. Their phenotypic transformation correlates with the expression of alpha-smooth muscle actin (α-SMA) and the production of extracellular matrix (ECM) proteins. Although this transient activation of the mesenchyme in response to tissue injury represents an evolutionarily conserved adaptive response, this maladaptive repair reaction can culminate in organ fibrosis [20]. In this pathophysiological wound healing response, activation of myofibroblasts becomes persistent and leads to an excessive deposition of extracellular matrix (ECM) components, such as hyaluronic acid, fibronectin (FN), proteoglycans and interstitial collagens, replacing functional cells and resulting in a loss of function of the affected tissues [21]. Transforming growth factor-β (TGF-β) is considered a crucial ubiquitous pro-fibrogenic cytokine. TGF-β1 can induce fibrosis via both canonical (Smad-dependent) and noncanonical (Smad-independent) signaling pathways [20]. Myofibroblasts can derive from several cell types according to the nature of the insult and the organ [22]. The cell type giving origin to the transformation into myofibroblasts is a tissue-dependent process. In specific tissues these cells may derive not only from resident fibroblasts, but also from epithelial and endothelial cells (via epithelial–mesenchymal transition (EMT)/endothelial-mesenchymal transition (EndoMT), stellate cells, pericytes, and bone marrow precursors [23].

The capacity for fibrosis resolution may differ depending on the organ involved and the nature and chronicity of the injury [24]. It encompasses different mechanisms including degradation of ECM and the elimination of fibrogenic myofibroblasts thought apoptosis, dedifferentiation, senescence or reprogramming [25]. ECM degradation is mediated by matrix metalloproteinases (MMPs); the fine balance between MMPs and tissue inhibitor of metalloproteinases (TIMPs) also appears to be altered in patients with tubulointerstitial fibrosis [26]. Although several important pathogenetic mechanisms driving fibrosis have been identified, a deeper and more precise knowledge of organ-specific molecular mechanisms is still required [27, 28]. This is even more imperative as no effective therapy for the prevention, deferment or resolution of organ fibrosis is yet available.

1.1.3.2. –Renal tubulointerstitial fibrosis

Tubulointerstitial fibrosis is the expansion of the space between tubular basement membrane and peritubular capillaries through the deposition of matrix proteins (predominantly collagens type I and III and fibronectin) in association with inflammatory cells, tubular cell loss, myofibroblast accumulation and rarefaction of the peritubular microvasculature. Fibrogenesis initiates in small areas at random sites of inflammation and then expands to become diffuse if profibrotic drivers persist [29].

1.1.3.3. –Animal models for the study of kidney fibrosis

Experimental mouse models are widely used to study the mechanisms involved in the progression of renal fibrosis. The latter can be induced by organic chemicals such as folic acid, adriamycin or adenine; by surgical procedures: 5/6 renal mass reduction, unilateral ureteral obstruction, ischemia-reperfusion or by genetic modifications in transgenic mouse models: mice lacking collagen alpha 3(IV) (same genetic defect that the autosomal form of human Alport syndrome) or the epithelial-specific inducible, active, cleaved Notch1 overexpressing mouse model (ICNotch1) [30].

1.1.3.4. –Phenotypic characterization of kidney-associated myofibroblasts

Myofibroblasts are contractile cells with characteristic cytoplasmic features including dense rough ER, moderate stress fibers of the actin cytoskeleton and a paucity of lysosomes [31]. Intermediate filament α-SMA has been widely used as a marker of myofibroblasts and the specific ablation of proliferating α-SMA+ myofibroblasts caused a 50–60% reduction in collagen accumulation and interstitial fibrosis in several different renal fibrosis models [32]. Of note, α-SMA cannot be considered a specific myofibroblast marker as several other cell types such as vascular smooth muscle, neonatal pericytes and stromal cells are positive for it. Other myofibroblast markers include the ECM proteins fibronectin (FN), vimentin (VIM) and collagen-1α1 (Col1a1) **(Figure 2**). Studies with the reporter mouse model of cells expressing Collagen Iα1 (Col1a1) (*Coll-GFP*^{Tg}) were performed with the aim of characterizing this population. This lineage analysis *in vivo* showed that Col1a1 protein producing cells express αSMA, whereas a minority of αSMA+ cells produce Col1a1 protein [33]. These Col1a1-producing cells express several typical pericyte or mesenchymal stem cell markers including platelet-derived growth factor receptor-beta (PDGFRβ), PDGFRα, CD73, CD44 and variable levels of CD105 and CD90 as well as a number of other mesenchymal markers including CD248. However, they do not express leucocyte, endothelial or epithelial markers [34]. Therefore, evidence suggests ECM-producing cells overlap with the pericyte and mesenchymal cell population. However, the lack of specific well-established markers for myofibroblasts points to the strong need for better markers to distinguish stromal cell subtypes.

1.1.3.5. –Cellular origin of myofibroblasts in kidney fibrosis

The origin of myofibroblasts in kidney fibrosis is not completely defined and the precise contributions of different cell types to overall matrix mass varies among studies. Previous reports suggested that myofibroblasts originate from resident stromal cells (pericytes, perivascular fibroblasts and mesenchymal stem cell–like cells) or vascular and tubule cells undergoing endoMT or EMT or from migration and differentiation of cells from bone marrow origin [35, 36] (**Figure 2**). By exploiting the ablation of Snail and Twist in tubular epithelial cells they concluded that partial EMT is a contributor to the interstitial myofibroblast pool [37, 38]. Partial EMT refers to an epithelial dedifferentiation and transformation into myofibroblasts, also accompanied by the epithelial secretion of factors that favor interstitial myofibroblast proliferation and inflammation. However, recent data using fate-mapping strategies suggest that local resident fibroblasts or differentiated bone marrow-derived mesenchymal stem cells (MSCs) are the major source of myofibroblasts in the kidney, whereas endothelial and proximal tubular cells only account for 5% and 10% of the total of interstitial myofibroblasts, respectively [39] (**Figure 2**). Single cell RNA-sequencing data have provided additional strong evidence suggesting that resident mesenchymal cells such as pericytes are the major source of myofibroblasts in the kidney, while hematopoietic cells act through indirect mechanisms activating resident mesenchymal cells [40]. This concept supports the model of perivascular cell detachment from capillaries and transdifferentiation into myofibroblasts, contributing to the deposition of pathological extracellular matrix. Notwithstanding, epithelial and endothelial cells as well as leukocytes play also important roles during fibrogenesis by the action of paracrine signaling pathways [17].

Genetic lineage analysis has also been employed to identify myofibroblast precursors. It has been reported that perivascular Gli1+ mesenchymal MSC-like cells were identified as progenitors of

myofibroblasts. Genetic fate tracing experiments indicate that Gli1+ cells only contribute to a subfraction of myofibroblasts (<50%), while genetic ablation of the myofibroblast progenitors reduced fibrosis by the same percentage [41] (**Figure 2**). Others map the source of kidney myofibroblasts to a single pool of nephrogenic intermediate mesoderm progenitors, which express the transcription factor OSR1 which, in turn, subsequently differentiates into FoxD1+ cortical stroma progenitors [42, 43]. PDGFR-α is exclusively expressed by kidney pericytes and PDGFR-β is expressed by kidney pericytes as well as by glomerular mesangial cells and vascular smooth muscle cells. PDGFR-β+ kidney cells derive from FoxD1+ progenitors, and Gli1+ cells are also PDGFR-β+ in the adult kidney, suggesting that Gli1+ cells also derive from the FoxD1 population [44]. This lack of unanimity evidences the complex heterogeneity of stromal cell population in their contribution to kidney fibrosis [45]. New technologies such as single-cell RNA sequencing will likely aid in defining cellular hierarchies in the renal interstitium and to the potential discovery of novel cell types.

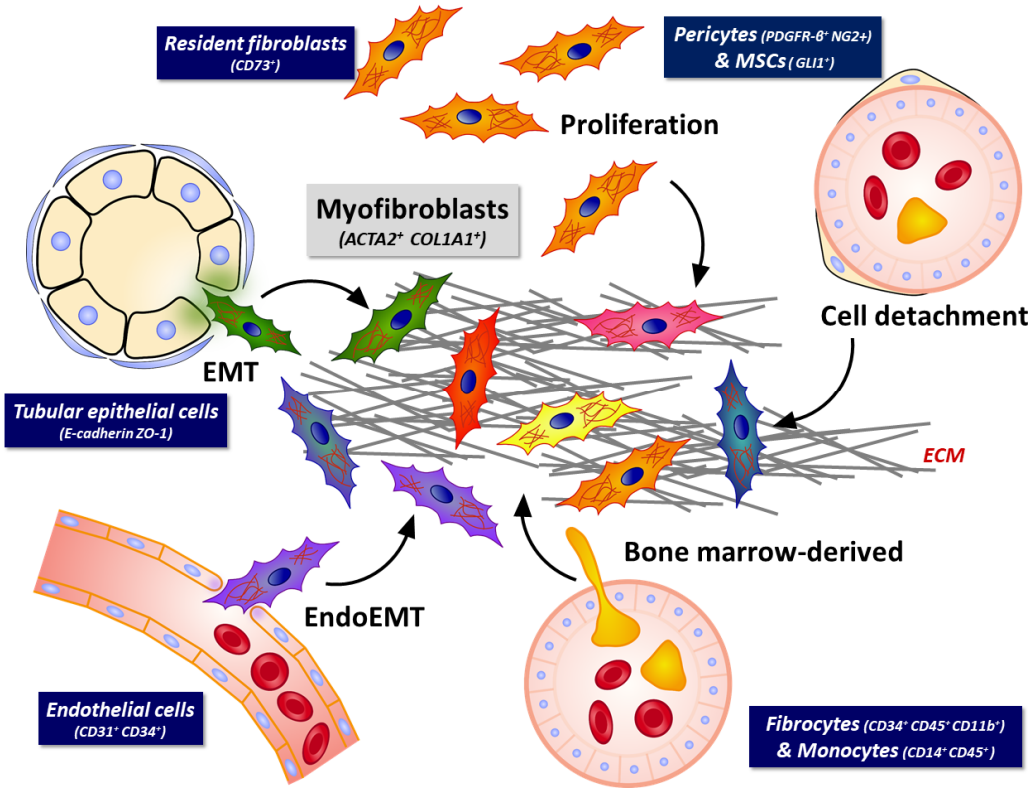

Figure 2. Origin of scar-producing myofibroblasts in the kidney. It is controversial whether myofibroblasts are derived from resident fibroblasts, circulating bone marrow–derived fibrocytes and monocytes, or transition from either epithelial (EMT) or endothelial cells (EndoMT). Recent studies suggest that stromal cells (pericytes, Gli1+ perivascular fibroblasts and mesenchymal stem cell–like cells) are the main contributors to the myofibroblast population. ECM: extracellular matrix proteins.

1.1.3.6. –Inflammatory cells in kidney fibrosis

Early stages of tubulointerstitial fibrosis are typically characterized by the infiltration of inflammatory cells including lymphocytes, macrophages, dendritic cells and mast cells [46] (**Figure 3**). Most studies indicate that fibrillar matrix-producing cells arising from bone marrow are exceptionally rare [47]. Inflammation contributes significantly to fibrogenesis [48], while recent evidence also highlights the antifibrotic effects of various subsets of lymphocytes and macrophages [49].

Lymphocyte infiltration precedes the influx of macrophages. Rag-2 null mice, which lack both mature B and T lymphocytes, are protected from fibrosis [50]. Long-term renal fibrosis after ischemia-reperfusion injury also depends on persistent infiltration of effector-memory T lymphocytes.[51].

When monocytes are recruited to the interstitium they transdifferentiate into macrophages. Macrophages are plastic cells and their gene expression patterns and functions adapt rapidly to the dynamics of the renal microenvironment. There is a strong correlation between macrophage infiltration and the extent of fibrosis [52]. Although somewhat debated, the division of macrophages in two archetypal populations, M1 and M2, is still functional [53, 54]. Monocyte differentiation into discrete populations of kidney macrophages is quantified by the levels of cell surface markers such as F4/80, Ly6C or TREM1. This allowed to establish that circulating classical monocytes ($CD11b^{+}$ $Ly6C^{high}$ in the mouse or $CD14^{high}CD16^{low}$ in humans) are recruited to the kidney [55]. M1 polarization occurs during the early phase of renal injury and can be triggered by several stimuli including pathogen- associated molecular patterns (PAMPs), lipopolysaccharide (LPS), danger- associated molecular patterns (DAMPs) like S100A9 and IL-1α and pro- inflammatory cytokines such as interferon gamma (IFNγ) and tumor necrosis factor (TNF) [56]. It is characterized by the upregulation of cell surface activation markers and molecules involved in antigen presentation, such as major histocompatibility complex (MHC) class II, CD16, CD32, CD80, CD86 and IL-1 receptor (IL-1R), as well as by the production of a range of pro- inflammatory molecules, such as IL-1, IL-6, IL-12, IL-23, inducible nitric oxide synthase (iNOS), matrix metalloproteinase 12 (MMP12) and macrophage- inducible C- type lectin (MINCLE) [56, 57]. Macrophages adopt a M2 phenotype throughout the later stages of tissue repair. M2 macrophages can be divided in 3 subpopulations: M2a–M2c on the basis of their phenotype and function [58, 59]. Macrophage polarization into M2 phenotypes is driven by a diverse range of stimuli: IL-4 and IL-13 induce the differentiation of M2a macrophages [60]; immune complexes and Toll- like receptor (TLR) and/or IL-1R ligands induce the differentiation of M2b macrophages [61] and IL-10, transforming growth factor- β (TGF-β) and glucocorticoids induce the differentiation of M2c macrophages [62]. The subtypes of M2 macrophages have distinct but overlapping functions: M2a macrophages induce an anti- inflammatory TH2-like immune response and promote wound healing and tissue fibrosis; M2b macrophages participate in immunoregulation and contribute to TH2-like activation and M2c macrophages contribute to immunosuppression, matrix remodeling and tissue repair [59] (**Figure 3**).

The switch into a specific macrophage phenotype is also associated with a metabolic fuel preference signature. Thus, M1 macrophages exhibit glycolytic cellular metabolism and tricarboxylic acid cycle impairment, while M2 macrophages present increased mitochondrial abundance and function and enhanced fatty acid oxidation [63]. The transition of macrophages from an M1 to an M2 phenotype is well documented in animal models of acute kidney injury (AKI), in which M1 cells are replaced by M2 cells during the repair response. Whether the early M1 macrophages switch their phenotype to become M2 macrophages or whether these are separate cell populations remains unclear [64].

Dendritic cells (DCs), defined as $CD11c^{hi}$MHC class II^{+} cells, interface with the adaptive immune system initiating autoimmune responses and stimulating T cells, which results in macrophage activation and kidney tissue damage [65]. Mast cells (MCs) can initiate and amplify innate and adaptive immune responses. Their number correlates with the extent of interstitial fibrosis [66]. Initially, they were considered to contribute to the pathogenesis of renal diseases through the release of TGF-β, MMP-9, and a variety of proteases (tryptase and chymase); however, recent data have demonstrated that these protective actions are mediated by neutralizing fibrotic factors [67] (**Figure 3**).

Several new biological modifiers of the immune system reduce interstitial fibrosis. Peroxisome

proliferator-activated receptor gamma (PPAR-γ) agonists reduce the number of macrophages by attenuating TGF-β expression [68], and three independent studies report that the administration of a C-C Motif Chemokine Receptor 1 (CCR1) antagonist, anti-TNF-α blocking antibodies or an IL-1 receptor antagonist are sufficient to ameliorate renal fibrosis, even after starting the treatment in advanced stages of the disease [69-71]. These studies corroborate the role of inflammation not only in the instauration, but also in the perpetuation of fibrosis though the profibrotic effects of different immune cell such as lymphocytes, M1 macrophages and DCs, or the antifibrotic response of M2 macrophages or MCs.

1.1.3.7. –Molecular signaling pathways in kidney fibrosis

The global set of pathological events above described is mainly instigated by the cytokine TGF-β1 [72]. Aside from it, other key fibrogenic factors include PDGF, fibroblast growth factor 2 (FGF2), connective tissue growth factor (CTGF), Insulin Like Growth Factor Binding Protein 5 (IGFBP5), Tumor necrosis factor-like weak inducer of apoptosis (TWEAK), and angiotensin II (Ang II) [44], which involve the activation of TGF-β, Notch, Wnt/β-Catenin, PDGF and Ang II/reactive (ROS)-signaling pathways, which are critical for kidney fibrosis development. Increased Notch activity in renal epithelial cells is associated with epithelial dedifferentiation, myofibroblast activation, matrix deposition, and the inflammatory response [73]. Increased tubule-specific β-catenin expression has been also described in CKD. Wnt/β-catenin signalling in pericytes and interstitial fibroblasts exhibits spontaneous myofibroblast differentiation. Wnt signaling pathway regulates cytoskeleton rearrangement, cell adhesion and cell movement via the kinases Rho, Rac and Cell Division Cycle 42 (Cdc42) [74], while Ang II-induced ROS are important for renal growth processes, inflammation, and fibrosis [75] (**Figure 3**).

1.1.3.7.1. –TGF-β signaling pathways

Many cell types in the kidney generate TGF-β, including endothelial, epithelial and mesangial cells as well as macrophages, in response to various stimuli, including high glucose, angiotensin II and reactive oxygen species [76]. The profibrotic effects of TGF-β1 are primarily accomplished by the canonical Smad-dependent pathways. However, Smad-independent pathways, including the mitogen-activated protein kinase (MAPK) pathway via extracellular signal-regulated kinase (ERK), p38MAPK, c-Jun N-terminal kinase (JNK), TGF-β1 activated kinase 1, phosphatidylinositol 3 kinase (PI3K)/AKT, Abelson non receptor tyrosine kinase (c-ABL) and Rho GTPase pathways, have also been reported [77]. The binding of TGF-β1 to the TGF-β receptor type-2 results in recruitment and activation of TGF-β receptor type-1 (TGFBR1) [78]. This activates Smad2 and Smad3 by phosphorylation, allowing their binding to Smad4 and translocation of the complex into the nucleus. The transactivation of cis-regulatory Smad binding sites (SBS) in the promoter regions of specific target genes sustains the mechanism of transcriptional regulation. The Smad7 cytoplasmic protein is a negative modulator of the pathway [77, 79, 80]. TGF-β transcriptionally increases the expression of ECM-related proteins including collagens, fibronectin, plasminogen activator inhibitor-1 (PAI-1), metalloproteinase inhibitor 1 (TIMP-1), a disintegrin and metalloproteinase domain 19 (ADAM19), CTGF, Vascular Endothelial Growth Factor (VEGF) and α-SMA [81].

Therapeutically, blockade of TGF-β1 signaling using TGF-β1 neutralizing antibodies or specific inhibitors of TGF-β1 receptors might be a promising therapeutic approach for CKD [82]. However, their

pleiotropic effects limit this potential clinical application [83]. Major efforts and encouraging results have been based on angiotensin II antagonism. However, no substantial advances have been made in halting progression to end-stage renal disease, a condition that requires renal replacement therapy by dialysis or kidney transplantation [84]. Biologically, besides important progress in the understanding of cellular and molecular mechanisms, several conundrums pervade the field. The discovery of miRNAs has fostered important research on their potential use as therapeutic agents or targets in almost every clinical setting, including kidney disease [85].

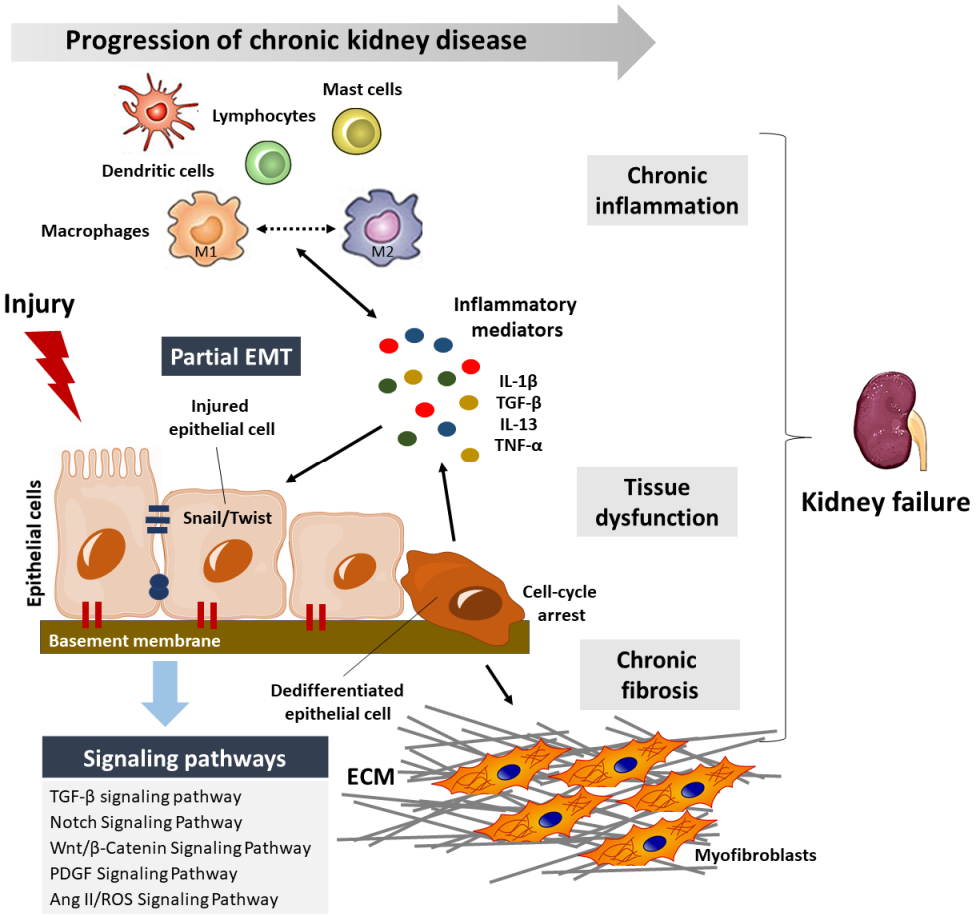

Figure 3. Maladaptive repair leads to kidney fibrosis. Persistent injury overcomes normal repair mechanisms. Macrophages and monocytes are recruited, releasing pro-inflammatory and profibrotic factors. Epithelial cells can undergo an incomplete EMT to avoid apoptosis, with the loss of some epithelial markers and acquisition of mesenchymal markers. Pro-inflammatory factors are also secreted by TECs further activating different inflammatory cells and driving proliferation of myofibroblasts, responsible for collagen synthesis and ECM deposition. ECM: extracellular matrix proteins.

1.2 MicroRNAs

1.2.1. –microRNAs as crucial regulators of gene expression

MicroRNAs (miRNAs) are a large family of conserved, small, non-coding RNAs (ncRNAs) of 20–25 nucleotides (nt) long that repress translation and/or induce degradation of their mRNA targets [86]. Their mechanism of action is based on the Watson-Crick base-pair complementarity between miRNAs and target sequences mainly located in the 3′ untranslated region (UTR) of mRNAs. However, functional miRNA binding sites can be also found in the 5´ UTR and open reading frame regions (ORFs) [87]. This feature makes possible that a single miRNA can potentially target hundreds or thousands of mRNAs and that one mRNA can be regulated by several miRNAs, with cooperative repression achieved by binding closely spaced target sites. Furthermore, entire cellular pathways can be regulated by individual miRNAs or miRNA clusters [88].

Since the discovery of the first miRNA, Lin-4, in *Caenorhabditis elegans* in 1993, thousands of miRNAs have been uncovered in many multicellular organisms, often with high levels of conservation across phylogeny [89, 90]. More than a third of human genes appear to have been under selective pressure to maintain their pairing to miRNA seeds [91]. The human miRNAome is composed of 1,917 precursor microRNAs (pre-miRNAs) and 2,654 mature miRNAs, which regulate at least 60% of protein-coding genes (miRbase, v22.1, May 2019). They show very specific expression patterns that differ among tissues and cell types and are involved in virtually every cellular process. Thus, miRNAs have been proven crucial for animal development, cell differentiation and tissue homeostasis while their dysregulation is frequently associated with numerous diseases [92].

1.2.2. –microRNA biogenesis and function

The biogenesis of microRNAs (miRNAs) is a tightly regulated multistep process (**Figure 4**). MiRNAs are transcribed by RNA polymerase II / III as precursor molecules termed primary miRNAs (pri-miRNAs) [93, 94]. Approximately 80% of them derive from introns of protein-coding genes (miRtrons), while the remaining 20% arise from independent genes or long non- coding RNAs (lncRNAs) [95]. MiRNAs tissue-specific expression patterns are primarily regulated transcriptionally. The expression of miRtrons is usually governed by the promoter of the host gene. Intergenic miRNAs generally bear their own promoters, while clustered miRNAs usually share one promoter [96].

1.2.2.1. –MicroRNA processing in the nucleus: Drosha and DGCR8

These pri-miRNAs, which can be over 1000 nt in length, present 5´Cap and 3´Poly-A Tail and form imperfect stem-loop structures [97]. Pri-miRNAs act as substrates for a processing complex formed by the RNAse III enzyme Drosha and the RNA binding protein DiGeorge syndrome critical region 8 (DGCR8) in the nucleus, resulting in a precursor miRNA (pre-miRNA) of 100 - 70 nt in length [98] (**Figure 4**).

1.2.2.2. –MicroRNA processing in the cytoplasm: DICER

Pre-miRNAs are exported to the cytoplasm mainly by the nuclear export receptor Exportin 5 in a Ran-GTP dependent manner, through the recognition of 2-nt 3′ overhang. Once in the cytoplasm, pre-miRNAs are shortened by the RNase III enzyme DICER, yielding a double stranded RNA molecule of approximately ~22 nucleotides (mature miRNA) [99]. Alternative cleavage by DROSHA or DICER leads to the production of isomirsA [88]. They associate with specific mRNAs within the multiprotein complex of Argonaute (AGO) proteins, constituting the core of the RNA-induced silencing complex (RISC) [93] (**Figure 4**).

1.2.2.3. –mRNA degradation and translational repression

One strand of the mature miRNA (‘guide strand’), mostly generated from the 5´ arm of the pre-miRNA hairpin, is loaded into AGO, whereas the other strand (‘passenger strand’) is mainly degraded [100, 101] (**Figure 4**). When the match is perfect, miRNAs promote mRNA cleaving, while partial matching favors mRNA translation repression, the most frequent mechanism in mammals. The process of mRNA degradation involves the recruitment of the deadenylation multicomplex, which removes or shortens the poly-A tail, inducing decapping of the 5´ end of the transcript and its rapid degradation by 5´-3´ exoribonucleases [102].

Translational repression can occur by different mechanisms: inhibition of translation initiation, inhibition of translation elongation, co-translational protein degradation or premature termination of translation. [103] (**Figure 4**).

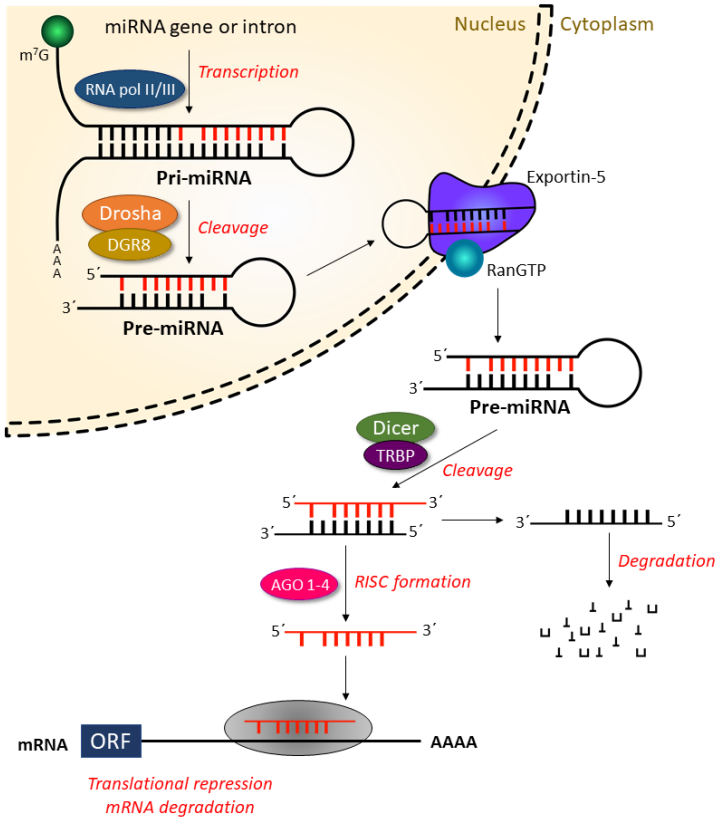

Figure 4. microRNA biogenesis and function. Pri-miRNA are transcribed and cleaved by the microprocessor complex Drosha–DGCR8 in the nucleus. Resulting pre-miRNA is exported to cytoplasm by Exportin-5–Ran-GTP. There, the RNase Dicer in complex with the HIV-1 TAR RNA binding protein (TRBP) cleaves the pre-miRNA yielding its mature form. The functional mature miRNA strand is loaded together with Ago proteins into RISC, which promotes the silencing of target mRNAs through mRNA cleavage, translational repression or deadenylation, whereas the passenger strand is degraded.

1.2.2.4. –Mechanisms of action of microRNAs and its regulation

MiRNAs are grouped into families on the basis of their nucleotide similarity in positions 2-8 in the miRNA, the so called `seed sequence´, which is essential for pairing with the target mRNA (**Figure 5**)**.** General features of site context in the mRNA that boost site efficacy include AU-rich nucleotide composition near the site, proximity to sites for co-expressed miRNAs (which may lead to cooperative action) and proximity to residues pairing to miRNA nucleotides 13-16. The position within the 3'UTR of at least 15 nt from the stop codon and away from the center of long UTRs is also important [104].

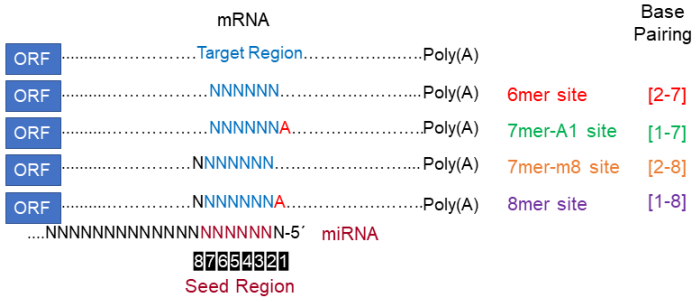

Figure 5. miRNA seed types. Based on the conservation of sites in orthologous UTRs, seed regions have been classified in four types: 6mer, 7mer-A1, 7mer-m8 and 8mer, with increasing repressive effectiveness.

1.2.2.5. –microRNA turnover

Selective cytoplasmic compartmentalization in processing bodies (P-Bodies) and multivesicular bodies (MVB) participate in mRNA storage, degradation and miRNA secretion. This not only constitutes an essential mechanism for dynamic intercellular communication, but also gives rise to miRNA application as biomarkers in body fluids such as blood or urine [105]. Additional sources of such extracellular miRNAs include passive leakage from broken cells or active secretion using microvesicle-free systems, such as RNA-binding proteins or lipoproteins, which protect them from degradation by ribonucleases [106]. However, further optimization of these procedures is required before they can be used in routine clinical practice [107]. As a consequence of this alternative multistep regulation process of miRNA biogenesis and function, they present distinct half-lives varying from hours to days [108, 109].

1.2.3. –microRNA nomenclature

New knowledge of miRNA origins, biogenesis, and function has required a revision of their nomenclature to avoid redundancies and to facilitate the identification and localization of microRNA precursor molecules [110] (**Figure 6**).

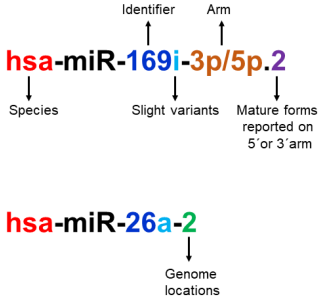

Figure 6. Schematic of miRNAs nomenclature. Mature miRNAs are named as 'miR' followed by a numerical identifier (in dark blue). A three-letter prefix defines the species name (in red). Lettered suffixes denote closely related mature miRNA sequences expressed from different precursors or genomic loci (in light blue), while identical mature miRNA sequences are named with numbered suffixes (in green). Two different mature miRNAs generated from the 3′ and 5′ arms of the pre-miRNA hairpin are indicated with the suffixes -3p and -5p (in orange). IsomiRs are distinguished with a number suffix after a dot (in purple).

1.2.4. –microRNA gain- and loss- of- function strategies

Different approaches have been developed to manipulate miRNA expression and investigate their functions [111]. Liposomes, polymeric nanoparticles, and adenoviral/lentiviral viral systems are some of the delivery systems for these miRNA tools [112]. Promising results in halting renal fibrosis have been obtained by knocking down miR-21, miR-29c, miR-214 and miR-433 or overexpressing miR-29b through successful kidney transfection by intraperitoneal, intravenous or subcutaneous administration [113]. Recently, pHLIP peptides have been used as an antimiR delivery platform for cancer. They penetrate cell membranes in acidic environments, delivering cargoes (such as anti-miR–peptide conjugates based on peptide nucleic acids (PNAs)) into the cytoplasm, and releasing them by disulfide cleavage [114]. However, many obstacles must be overcome before miRNA-based therapies for CKD can be translated into clinical practice [115].

1.2.5. –Regulation of kidney fibrosis by microRNAs

In the kidney, miRs have been shown to play critical roles in nephrogenesis, homeostasis and disease [116]. Recently, a group of miRNAs has emerged as capable of regulating fibrotic processes and have been termed "fibromiRs" [117]. Thus, Gomez et al. identified 24 miRNAs that were commonly upregulated both in

human CKD and animal models of kidney injury with fibrosis due to unilateral ureteral obstruction (UUO) or ischemic injury, suggesting a “fibrotic” miR signature in the kidney [118]. Aberrant expression of microRNAs can drive the initiation and progression of CKD.

MiRNA-mediated control of kidney fibrosis mainly occurs thought the regulation of TGF-β1 signaling in a cell-dependent and context-dependent manner, through Smad signaling [119]. In keeping, Dicer1 deficiency promotes fibrosis in different organs by upregulating Smad2/3 [120, 121]. Consistently, Smad7 suppresses renal fibrosis via altering expression of TGF-β/Smad3-regulated microRNAs [122]. TGF-β signaling, in turn, can regulate the transcription of miRNAs through Smad proteins by binding to Smad-binding elements (SBEs) in the DNA. These proteins can also associate with conserved consensus sequences within the stem region of pri-miRNAs, which provides a landing site for the Drosha/DGCR8 complex. In addition, Smad-activated auxiliary factors such as the RNA helicase p68, a component of the Drosha microprocessor complex, can facilitate recruitment of Drosha/DGCR8 to specific pri-miRNAs for efficient processing [123]. Therefore, manipulation of miRNA expression by *in vivo* delivery of miRNA mimics or inhibitors has emerged as a promising novel therapeutic strategy for CKD [124]. In addition, circulating miRNAs have been proposed as possible diagnostic and even prognostic biomarkers in an effort to avoid invasive kidney biopsies, even though no definitive data have yet been translated to the clinic through the demonstration of their usefulness in large cohort studies [125].

1.2.5.1. –Regulation of TGF-β-induced signaling pathways by microRNAs

MiR-21 is one of the most characterized fibromiRNAs associated with fibrosis in multiple organs and one of the first to be described in the kidney [126, 127]. In the kidney, the expression of miR-21 is increased by TGF-β in tubular epithelial cells and in human fibrotic kidney samples [128]. Its expression is regulated by TGF-β/SMAD3, but not SMAD2 [126]. TGF-β signaling is in turn regulated by miR-21 [128]. It induces Smad3 and Akt signaling due to the downregulation of Smad7 and PTEN, respectively [129, 130]. Further, kidneys from miR-21 KO mice showed marked protection against the development of renal fibrosis [131]. Serum circulating miR-21 levels also correlates with kidney fibrosis [132]. MiR-433 promotes renal fibrosis by amplifying the TGF-β/Smad3-Azin1 pathway [133]. High levels of miR-433 correlate with increased levels of antizyme, which induces the degradation of ornithine decarboxylase involved in polyamine biosynthesis. Low levels of polyamines in turn activate and sustain the TGF-β1-induced profibrotic effect in an amplification loop. *In vivo* knockdown of miR-433 attenuates the induction and progression of fibrosis [133]. miR-23b levels were increased in the kidneys of TGFβ transgenic mice and in TGF-β-treated renal epithelial cells. MiR-23b targets include TGF-β receptor type II (TGF-βRII), SMAD3, and TGF-β, suggesting a negative feedback loop-regulating TGF-β signaling [134]. MicroRNA-196a/b mitigates renal fibrosis silencing TGF-β-Smad signaling by targeting TGF- βRII [135].

1.2.5.2. –Regulation of epithelial to mesenchymal transition (EMT)

Although its contribution to fibrosis is still an object of debate, some authors claim that partial EMT may account for the renal fibrotic phenotype [37, 38]. MiR-200 family members have been closely related to EMT. Targets of miR-200a include EMT-related factors such as TGF-β2, β-catenin and the Zinc finger E-box binding homeobox 1 (Zeb1) which negatively modulates E-cadherin [136-138]. MiR-192 prevents TGF-β-

mediated downregulation of E-cadherin by targeting ZEB1/2 in animal models of diabetic and obstructive nephropathy [139]. The highly conserved Let-7 family has been associated with the progression of fibrosis in several organs including the kidney [140-142]. Let-7d target genes include high mobility group A2 (HMGA2) [143], a key factor in the TGF-β-induced EMT, which contributes to Snail and Twist suppression, preventing the downregulation of epithelial proteins such as E-cadherin and the upregulation of mesenchymal proteins. Of interest, miR-214, which is highly expressed in the kidney appears to promote fibrosis in both a TGF-β-dependent and independent way, is inducible by TWIST and hypoxia and represses the expression of E-cadherin [144, 145]. MiRNAs can also regulate EMT by modulating the Notch signaling pathway. This is the case of miR-34c, which attenuates epithelial-mesenchymal transition and kidney fibrosis by targeting the TGF-β-mediated upregulation of the Notch ligand Jagged 1 (JAG1) [146].

1.2.5.3. –Regulation of metabolic pathways and redox responses

MiR-21 (see above) was arguably the first miRNA shown to promote fibrosis by silencing metabolic pathways by targeting PPAR-α [131]. Generation of ROS also contributes to renal fibrosis. Mpv17-like protein is located in the mitochondrial inner membrane and regulates the production of ROS and protects against mitochondrial oxidative stress and apoptosis [147]. This protein is also downregulated by miR-21 during kidney injury [131]. Anti-miRNA-21 oligonucleotides based therapy has also confirmed these findings in the model of renal disease of Alport nephropathy [148]. MicroRNA-27a also promotes renal tubulointerstitial fibrosis via suppressing PPAR-γ pathway in diabetic nephropathy. MiR-433 (see above) can target glutathione (GSH) biosynthetic enzymes in an Nrf2-independent manner, impairing endothelial function and favoring kidney and liver fibrosis [149]. TGF-β1 suppresses miR-30e expression, resulting in increased expression of uncoupling 2 (UCP2), an anion carrier protein that regulates mitochondrial ATP production. Dysregulation of the miR-30e/UCP2 axis has been linked to decreased ATP generation that ultimately causes kidney fibrosis [150].

1.2.5.4. –Regulation of extracellular matrix (ECM) and other cellular mechanisms

The miR-29 family includes the best characterized microRNAs that regulates ECM production in several organs including the kidney [151]. TGF-β/Smad3 signaling promotes renal fibrosis by inhibiting miR-29 in tubular epithelial cells. *In vivo* studies have proven that administration of miR-29 analogues decreased expression of collagens I and III in these organs during fibrosis [152, 153]. Several genes that have been identified as targets for the miR-29 family code for ECM proteins such as collagens, fibrillins, laminins, and elastin suggesting an anti-fibrogenic function for the miR-29 family [154]. MiR-21 also has a role in ECM homeostasis through the regulation of MMPs and TIMPs. CTGF is known as a potent inducer of tissue fibrosis in multiple tissues and with a clear role in kidney fibrosis [155, 156]. The downregulation of miR-30c, which targets CTGF, has been related to renal fibrosis in the context of diabetic nephropathy [157]. Myofibroblast proliferation and apoptosis imbalance determines the accumulation of ECM-producing cells during fibrosis. Silencing of microRNA-132 reduces renal fibrosis by selectively inhibiting myofibroblast proliferation by regulating Foxo3a/p300 [158]. Of note, the targeting by miR-324-3p of prolyl endopeptidase, an enzyme involved in the metabolism of angiotensins, was shown to represent a novel mechanism for progressive nephropathy and ACE inhibition-dependent protection [159].

1.3 Metabolism in the kidney

1.3.1. –The kidney as a metabolic organ

The kidney requires a high energy input and is the second organ in mitochondrial content and oxygen consumption after the heart [160]. This energy is consumed in the removal of waste from the blood, nutrient reabsorption and general homeostatic functions concerning fluid and electrolyte balance, acid–base equilibrium and blood pressure regulation [161].

Glucose enters cells through specialized glucose transporter proteins and further it is converted to pyruvate. From here, the presence or absence of oxygen dictates the fate of pyruvate. During aerobic respiration, pyruvate is substrate for the tricarboxylic acid (TCA) cycle, while anaerobic respiration leads to lactate production [162]. During kidney development, self-renewing or proliferating cells rely mainly on glycolysis to supply energy, replenish reducing equivalents and generate nucleotides. However, terminally differentiated cell types rely more heavily on fatty acid oxidation and mitochondrial oxidative phosphorylation, likely as an adaptation to higher energy demands [163]. Peroxisome proliferator-activated receptor γ coactivator 1α (PGC-1α) is a main transcriptional regulator of mitochondrial biogenesis and function, while mitochondrial transcription factor A (TFAM) is key in the genome replication of this organelle. Both are essential to maintain an appropriate mitochondrial mass [164].

The mature nephron is comprised of distinct segments and each segment utilizes metabolic pathways to varying degrees depending on their specific function [163]. Proximal tubules require a higher degree of active transport than other renal cell types because they reabsorb 80% of the filtrate that traverses the glomerulus. They present high levels of baseline energy consumption and use fatty acid oxidation (FAO) as a preferential energy source due to its capacity to generate large amounts of ATP as reviewed in [165]. Historical studies by Weidemann and Krebs were the first to report that in dog kidneys these droplets can be used in case of energy scarcity [166]. Proximal tubules also rely on gluconeogenesis and the kidney is unique in that it is the only organ aside from the liver able to perform this metabolic program. In fact, the kidney has recently been shown to contribute to up to 20% of all glucose production [167]. It is utilized to maintain glucose homeostasis by generating glucose from noncarbohydrate molecules such as glutamine. The resulting glucose can then be metabolized to help maintain blood glucose levels and utilized for other pathways [168]. By contrast, glomerular cells, including podocytes, endothelial cells and mesangial cells exhibit a lower degree of oxidative capacity also likely adapted to their function: i.e. to filter blood, remove small molecules (glucose, urea, water and salts) and retain large proteins such as hemoglobin [169].

Metabolic alterations of cells are emerging as an integral indicator of developmental abnormalities and disease susceptibility. Particularly, impaired energy metabolism and mitochondrial dysfunction have gained importance as potential pathogenetic factors in the progression of kidney diseases [170, 171].

1.3.2. –Fatty acid oxidation

A fatty acid (FA) is a carboxylic acid with a long aliphatic tail. It can be produced by FA synthesis or by hydrolysis of triglycerides (TAG) or phospholipids; conversely, TAG are the storage form of FA [166]. Fatty acid oxidation occurs in the mitochondrial and peroxisomal compartments. PPAR-α is the main regulator of the uptake, utilization, and catabolism of fatty acids by upregulation of genes involved in fatty acid transport, fatty acid binding and activation and peroxisomal and mitochondrial fatty acid β-oxidation [172].

FAs must first be supplied, either by extracellular uptake through the FA transport protein CD36, by in situ cytosolic synthesis, or by the deacylation of cellular phospholipids under the action of phospholipase A2 (PLA2) [173]. Second, FAs need to be transported from the cytosol to the respective organelles in order to be oxidized and provide the cell with ATP. Fatty acids of total carbon atom numbers from 1 to 6 are usually classified as short-chain fatty acids (SCFAs), those of 7 to 12 carbon atoms are defined as medium-chain fatty acids (MCFAs), whereas fatty acids longer than 12 carbon atoms are considered long-chain fatty acids (LCFAs), of which C16 and C18 LCFAs are the most abundant in mammalian cells. Very long-chain fatty acids (VLCFA), which have more than 22 carbons, are metabolized in peroxisomes [174]. Since peroxisomes do not contain respiratory chain enzymes, peroxisomal FAO is not directly coupled to generation of ATP and most of the energy is released as heat [175]. SCFAs and MCFAs can simply diffuse through the membranes of the mitochondrion, while LCFAs are not permeable and need to use a specific transporter named as the carnitine shuttle. They need to be activated by coenzyme A in the cytosol, under the action of an acyl-CoA synthetase, which is located at the outer membrane of the organelle. The resulting long-chain acyl-CoA products will then interact with a carnitine molecule to regenerate coenzyme A and produce a long-chain acyl carnitine (LCAC) [176]. This step requires the rate-limiting enzyme of the carnitine shuttle, the carnitine palmitoyl-transferase 1 (CPT 1), located at the outer membrane [177]. Then, LCACs are able to cross the inner membrane through the carnitine-acyl-carnitine translocase (CACT). The carnitine palmitoyl-transferase 2 ensures the reverse reaction regenerating the carnitine molecule using coenzyme A, resulting again in an acyl-CoA product, which will undergo β-oxidation [178]. During β-oxidation, bond cleavage of every two carbons to form acetyl-CoA occurs every cycle. Each cycle involves 4 steps: dehydrogenation, hydratation, oxidation and thiolysis. The process continues until all of the carbons in the fatty acid are turned into acetyl-CoA. Electron carriers flavine adenine dinucleotide (FAD^+) and nicotine adenosine dinucleotide (NAD^+) will accept electrons which will be transferred to the electron transfer chain, while acetyl-CoA molecules are incorporated to the Krebs cycle. The energy yield of FA β-oxidation has an average of 106 ATP equivalents per FA (palmitate), as opposed to 36 during the oxidation of carbohydrates (glucose) [179] (**Figure 7**).

1.3.2.1. –Carnitine palmitoyl-transferase 1

The CPT family (EC.2.3.1.21) comprises 3 CPT1 isoforms: CPT1A, CPT1B, CPT1C and another independent enzyme, CPT2. They differ in their intracellular location, tissue distribution and structure. CPT1A is mostly expressed in liver and kidney, CPT1B in cardiac and skeletal muscle and CPT1C in the brain. The CPT2 enzyme is ubiquitously expressed in all tissues [180].

The *CPT1A* gene is composed of 20 exons, spanning 60 kb of DNA. The open reading frame of rat and human *CPT1A* is 2319 bp and encodes a protein of 773 amino acids. Within the 5'upstream region of the gene, two alternate promoters and numerous transcription factor-binding sites have been identified, while its 3' untranslated region is 2 kb long. Human CPT1A and CPT1B share a 63% sequence homology at protein level, although in the active site it is notably higher (82%) and the sequence similarity is close to 80%. The homology among human, rat, and mouse enzymes is rather high. All isoforms coded by *CPT1* from different species have the same first 18 N-terminal amino acids [181]. CPT1A and CPT1B have different kinetic characteristics, particularly, with respect to their affinity for one of the substrates (L-carnitine) and the allosteric inhibition by malonyl-CoA. CPT1A has a much higher affinity for carnitine (Km=30μM for the rat

enzyme) than CPT1B (Km = 500 μM for the rat enzyme) [182]. There is evidence that CPT1 activity is controlled by phosphorylation and nitration, although it has also been proposed that CPT is constitutively phosphorylated [183, 184].

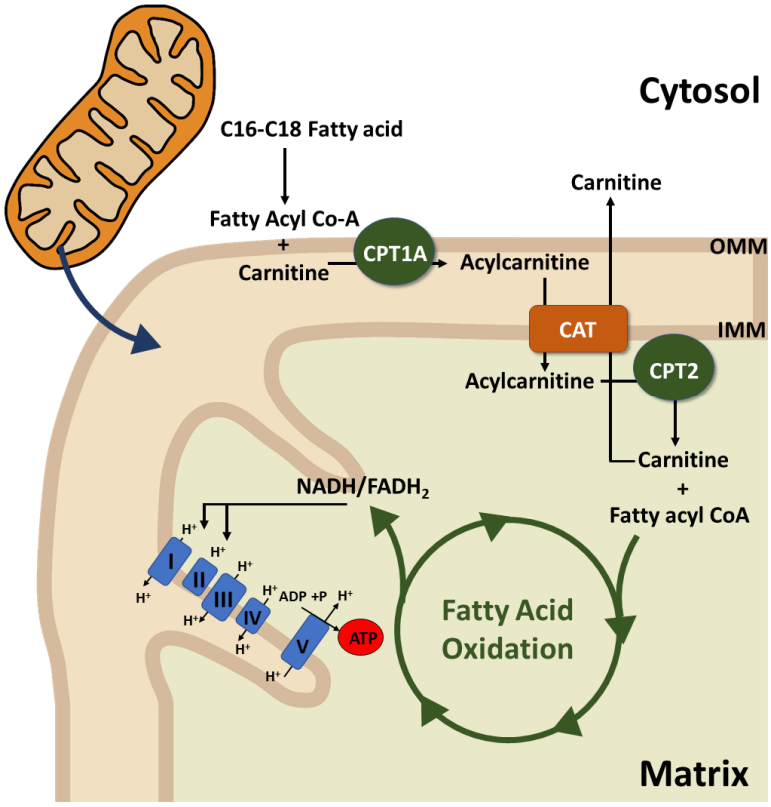

Figure 7. Mitochondrial carnitine palmitoyltransferase system. It transfers long chain fatty acids from the cytoplasm into mitochondrial matrix for oxidation. CPT1 converts acyl-CoAs into acylcarnitines. CACT exchanges acylcarnitine and carnitine between the outer and inner membranes of the mitochondria and finally acylcarnitine is converted back into acyl-CoAs by CPT2. Acyl-CoAs of β-oxidation generates acetyl-CoA that fuels the tricarboxylic acid cycle that ultimately leads to ATP production.

1.3.2.1.1. –Structure and function of CPT1

The yet unsolved challenge to solubilize CPT1 without losing enzyme activity has hampered the obtention of a complete structure through crystallization. This certainly attests to appropriate membrane anchoring for its activity. Nevertheless, a 3-D structural model with the functional domains for CPT1A has been proposed based on the crystal structure of the homologous enzyme, mouse carnitine acetyltransferase (CAT) and CPT2 [185]. The CPT1 isoforms are located on the cytosolic side of the external mitochondrial membrane and are anchored to the membrane via a transmembrane portion comprising two hydrophobic stretches of amino acids at the N-terminal side of the protein. The N-terminus itself (~47 residues) is also located on the cytosolic side, providing a hairpin polytopic conformation. The only part of the protein exposed to the intermembrane space is composed by a 27-residue loop [186] (**Figure 8**).

The N-terminal region is critical for the physiological inhibition by malonyl-CoA, due its binding capacity to the amino acid residues E3 and H5 [187]. Docking analysis has proposed two separate binding sites for malonyl-CoA inhibition: a high-affinity binding site “O side” (the amino acid residue Arg^{243} was found critical for this interaction) and a second low-affinity site “A side” (His^{473} is involved in this interaction) that corresponds to the catalytic site and where acyl-CoA binds. Both are located in the C-terminal region [188]. It is postulated that the A binding site promotes a contact interaction between the N- and C-terminal segments of the protein, which explains the sensitivity to membrane fluidity as well as the loss of sensitivity to malonyl-

CoA if the N-terminal portion of the protein is deleted or mutated [189]. These two sites share the carnitine-binding locus. Met^{593}, which is located in the C-terminal domain, is essential for malonyl-CoA sensitivity affecting both O and A sites (**Figure 8**). A conserved STS (685-687) motif is indispensable for enzyme activity, while the signature motif, (--RTETXR--) is described to be involved in carnitine binding [185]. Faye et al. described the existence of CPT1 trimers and their potential to assemble into hexamers [190].

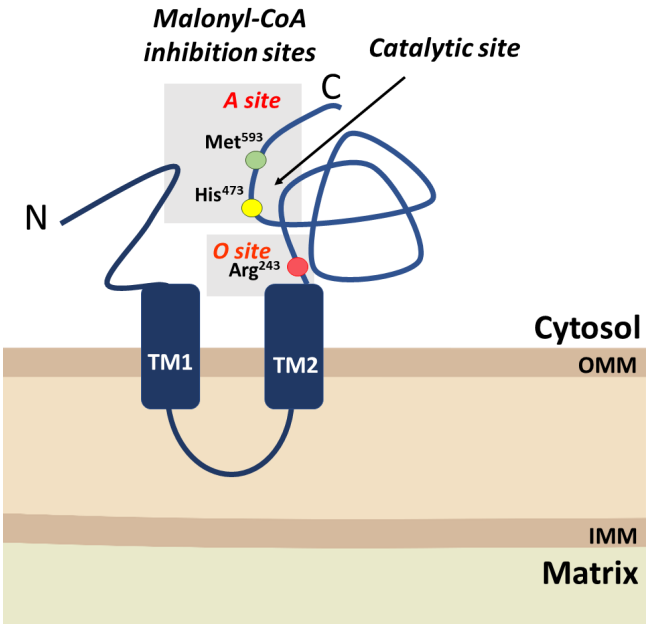

Figure 8. Carnitine palmitoyl-transferase 1 A structure. CPT1A consists of a short, well defined N-terminal regulatory domain and a large C-terminal catalytic domain, which are linked by two transmembrane (TM) segments that span the OMM. Critical residues have been identified in two malonyl-CoA inhibitions sites (see text for details).

1.3.2.1.2. –CPT1 gene regulation

Peroxisomal proliferator-activated receptor gamma coactivator (PGC-1α), a coactivator for many factors of the nuclear hormone receptor family including PPAR-α, the glucocorticoid receptor, the thyroid hormone receptor, and several orphan receptors, up-regulates the expression of the *CPT1* gene [191]. The coactivator PGC-1 in combination with HNF4-α has been described to regulate the *CPTIA* gene in the liver by interacting with a cAMP-response element-binding protein (CREB) [192].

1.3.3. –Energy metabolism in renal proximal tubular cells during CKD

Recent data in genome wide-associated and transcriptomic profiles have allowed to identify common metabolic derangements in the process of renal fibrogenesis. In this line, it has been shown that mitochondrial dysfunction and defective FAO in renal tubular epithelial cells play an important role in the development of kidney fibrosis. TGF-β was able to suppress FAO in a SMAD3- and PGC1A-dependent manner, which regulate the levels of proteins involved in fatty acid uptake and oxidation, including CPT1A. SMAD3 binding overlaps with the active enhancer histone tail modification H3K4me1 of the PPARGC1A promoter sequence, resulting in the blocking of the progression transcription machinery [171, 193] (**Figure 9**). Alterations in FAO finally result in intracellular lipid accumulation and ATP depletion. Genes related to glucose utilization in fibrotic samples from ICNotch1 mice and FAN presented a downregulated expression. Glucose in TEC is used mainly for anaerobic glycolysis. Inhibition of CPT1A shifted metabolism to more glycolysis and the glycolytic phenotype did not improve the development of fibrosis [171]. Facing those metabolic constraints,

surviving TECs exhibit a phenotypic switch that includes cytoskeletal rearrangement and production of extracellular matrix proteins [194]. Although cell-specific overexpression of CD36 in tubular epithelial cells from mice leads to lipid accumulation, it is not sufficient to drive spontaneous renal fibrogenesis [195]. Therefore, it appears that defects in energy production have detrimental consequences beyond mere lipid accumulation. A decrease in PPAR-α and PGC-1α expression and fatty acid oxidation is commonly observed in patient samples and mouse models with acute and chronic kidney disease [196]. Evidence suggests that restoring mitochondrial function protects against CKD. Han et al found that enhanced expression of PGC-1α protected mice against Notch-induced kidney fibrosis and could even reverse the mitochondrial defects associated with this model [197]. Thus, it has been reported that proximal tubule PPAR-α attenuates renal fibrosis and inflammation caused by UUO [198]. Consistently, in a murine model of AKI based on renal ischemia-reperfusion, the protective role of PGC1α and NAD^+ has been documented [199]. However, podocytes and endothelial cells are less metabolically active and have a narrow PGC-1α tolerance. [200].

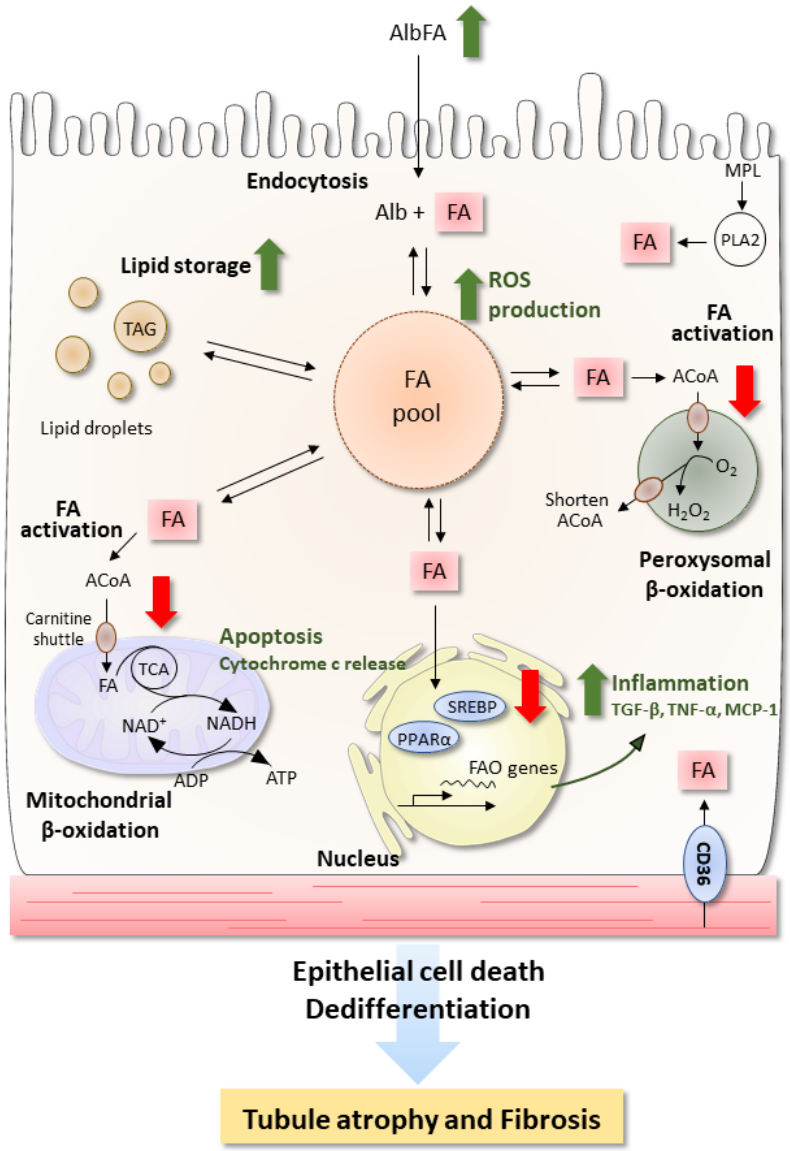

Figure 9. Defects in fatty acid oxidation contribute to tubulointerstitial fibrosis. FAs enter the cell either free or albumin-bound. They can also be produced after hydrolysis of membrane phospholipids by phospholipase A2. Intracellular FAs are then routed to anabolic or catabolic pathways; FAs are stored in the global triglyceride pool or oxidized in mitochondria or peroxisome to produce ATP. A carnitine shuttle gives access to the matrix of these two organelles. FAO enzymes are positively retro-controlled by FAs accumulation at the transcriptional level by the activation of SREBP1c and PPAR-α. Red and green arrows indicate what is being down-regulated or up-regulated during fibrosis, respectively. Depressed FAO is associated with intracellular lipid accumulation and kidney fibrosis development. ACoA, acyl-Coenzyme A; Alb, albumin; MPL, membrane phospholipid; PLA2, phospholipase A2.

Of interest, a recent genomic screening in kidney samples from CKD patients exhibited increased electron transport chain (ETC) protein expression but these proteins had overall decreased activity, leading to high levels of ROS, suggesting the potential therapeutic benefits of molecules with antioxidant properties in treating CKD [201]. Thus, a prevailing concept in the field with increasing momentum is that restoring an appropriate energy balance may represent a powerful therapeutic approach to defer or prevent TEC injury and inflammation, contributing to a halt and eventually to a reversion in the fibrotic process.

1.3.4. –microRNAs regulation of lipid metabolism

MiRNAs are critical regulators of lipid synthesis, fatty acid oxidation and lipoprotein formation and secretion [202]. Nuclear receptors (NRs) are ligand-activated transcription factors, which regulate lipid metabolism and also the expression of miRNAs [203]. For example, the promoter activity of miR-29a was significantly increased by the NR FXR through a FXR-responsive element [204]. MiR-199a-3p was also reported to be repressed by FXR19 [205]. By the same token, several representative miRNAs have been shown to have a significant impact on lipid homeostasis. Both global or conditional liver miR-122-deletion showed a marked decrease in total serum cholesterol and triglyceride (TG) levels. Anti-miR-122 therapy resulted in a significant reduction (~30%) of circulating cholesterol levels. The expression of miR-21 was decreased in liver from high-fat fed mice [206]. Overexpression of miR-21 markedly blocked stearic acid (SA)-induced intracellular lipid accumulation by targeting fatty acid-binding protein 7 (FABP7) [207]. PPAR-*α* and insulin-like growth factor binding protein 3 (IGFBP3) were also targeted directly by miR-21. Several other miRNAs (miR-758, miR-26, and miR-106b) also regulate lipid metabolism by targeting ABCA1 whereas miR-370 targets CPT1A and miR-24 targets insulin induced gene 1 (INSIG1) [208]. Both miR-27a and miR-27b target retinoid X receptor alpha (RXR*α*), which through the formation of a heterodimer with PPAR-*γ* regulates adipogenesis. Furthermore, PPAR-*γ* is a target of miR-27b and ATP-binding cassette sub-family A member 1 (ABCA1) a target of miR-27a. Overexpression of miR-27a accelerates adipolysis by releasing more glycerol and free fatty acids in the adipocytes and repressing lipid storage in cells. In addition, miR-27a inhibits the expression of many lipid metabolism genes, including fatty acid synthase (FASN), SREBP-1, SREBP-2, PPAR-*α* and PPAR-*γ*, as well as ApoA1, ApoB100 and ApoE3 [209].

1.3.4.1. –miR-33

The family miR-33 is highly conserved in organisms ranging from Drosophila to humans and includes two members: miR-33a and miR-33b. These two miR-33 genes are present in humans: miR-33b, which is located in intron 17 of the Srebp-1 gene on chromosome 17, and miR-33a, which is part of intron 16 within the Srebp-2 gene on chromosome 22. In mice there is only one miR-33 gene, which is conserved with human miR-33a and located within intron 15 of the mouse Srebp-2 gene (**Figure 10**). Although miR-33a and b differ by only 2 nucleotides in the mature form of the 3′ region, they are identical in their seed sequence, and thus they are predicted to repress the same subset of genes. The SREBP transcription factors are crucial modulators of cellular cholesterol and fatty acid metabolism, while miR-33 members co-express with their host genes regulating these mechanisms [210].

During conditions of low intracellular cholesterol, miR-33a is co-transcribed with *Srebp-2* and orchestrates an increase cellular cholesterol levels by reducing cholesterol export through the reverse cholesterol transport (RCT) [211, 212]. The RCT pathway is the only mechanism by which peripheral tissues,

including the macrophages that make up atherosclerotic plaques, can remove excess cholesterol for transportation to and degradation by the liver [213]. Through its ability to target genes involved in cholesterol efflux (ABCA1, ABCG1), high-density lipoprotein (HDL) biogenesis (ABCA1), and bile acid metabolism, miR-33 has been established as an important regulator of this process [214, 215] (**Figure 10**). Consistent with this, antagonism or loss of miR-33 has been shown to increase circulating levels of HDL-C in both rodents and non-human primates [211, 216]. Moreover, a number of studies have demonstrated that treatment with anti-miR-33 therapeutic agents can significantly reduce plaque burden in mouse models of atherosclerosis [215, 217]. Nevertheless, while antagonizing miR-33 may appear as an attractive strategy for raising plasma HDL levels and protect against atherosclerosis, this approach should be carefully considered because long-term silencing of miR-33 may promote adverse outcomes including hypertriglyceridemia and hepatic steatosis [218]. Similarly, when *Srebp-1c* is induced during hyperinsulinemia or insulin resistance, miR-33b is co-transcribed resulting in reduced fatty acid metabolism by targeting CPT1, carnitine O-octanoyltransferase (CROT) and hydroxyacyl-CoA dehydrogenase β (HADHβ); insulin signaling by modulating insulin Receptor Substrate 2 (IRS2) and Sirtuin 6 (SIRT6), and mitochondrial function by regulating AMP Activated Kinase (AMPK) and PGC1α [219, 220]. The ability of miR-33 to regulate such a wide array of metabolic functions suggests that miR-33 may be involved in the differential regulation of lipid metabolism across organs and tissues.

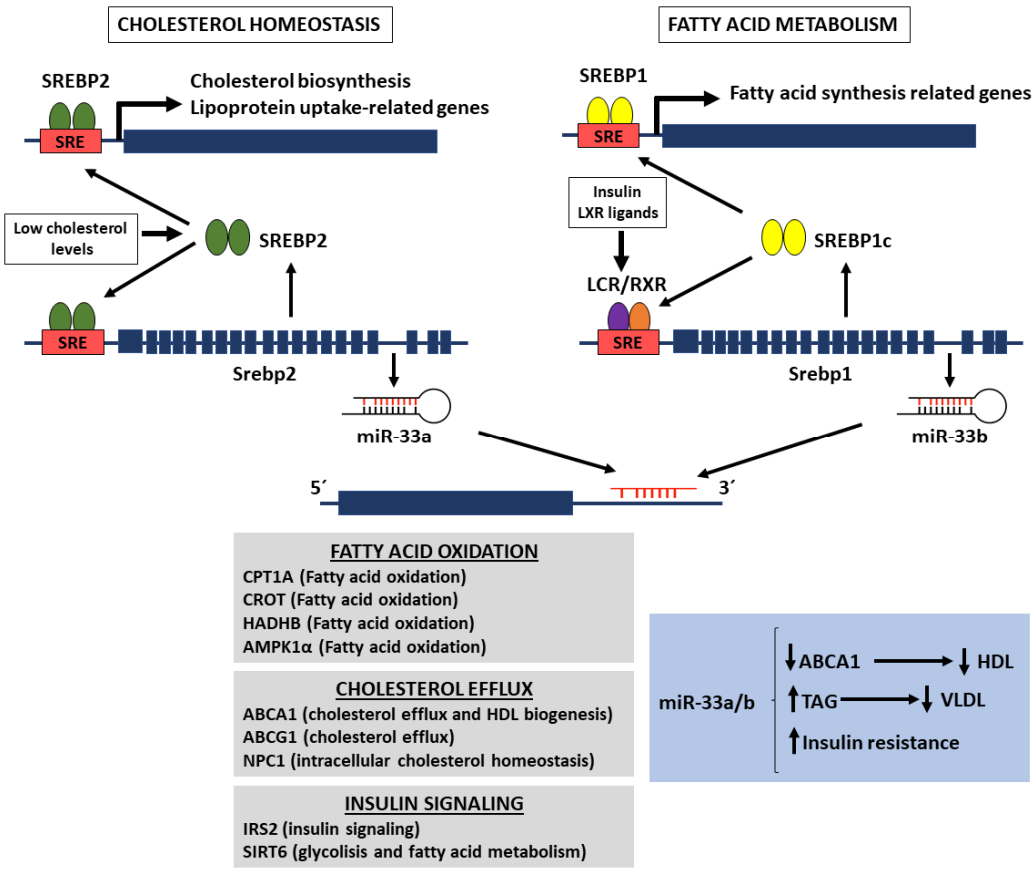

Figure 10. miR-33a and miR-33b regulation of lipid metabolism. Conditions of low intracellular cholesterol enhance the expression of SREBP2, leading to increased lipoprotein uptake and endogenous cholesterol biosynthesis. Hyperinsulinemia induces SREBP1 expression, promoting an increase in hepatic fatty acid and triglyceride synthesis. The activation of SREBPs transcription induces miR-33a and miR-33b expression, decreasing HDL levels by targeting hepatic ABCA1 expression. They also target IRS2 impairing insulin signaling. Importantly, they also inhibit cellular β-oxidation by targeting different fatty acid oxidation enzymes.

2.Aims

The general aim of this thesis is to explore the question as to whether a major change in metabolism can dictate a different fate in the progression of kidney fibrosis.

The specific aims are:

1. Study the possible prevention or reversion of the fibrotic phenotype in the kidney by gain-of-function strategies in fatty acid oxidation involving the generation of a knock-in mouse overexpressing CPT1A in tubular epithelial cells.

2. Explore the role of miRNAs that may regulate the renal fibrotic phenotype through the modification of metabolic pathways and specifically in a mouse model null for miR-33.

3.Methods

3.1 Generation of a transgenic mouse model for inducible *Cpt1a* gene

Generation of an inducible conditional transgenic mouse model for *Cpt1a* overexpression in the renal epithelium was based on a 2nd generation Tet-On system with site-specific recombination in embryonic stem (ES) cells [221, 222]. Mice harboring the transgene of *Cpt1a* gene under the control of the tetracycline-responsive promoter element (TRE) (*tetO-Cpt1a* mice) were generated in the transgenic mice core unit from the National Cancer Research Center (CNIO, Spain). Next, these mice were crossed with mice providing renal epithelial tissue specificity, *Pax8-rtTA* (Jackson labs, Bar Harbor, Ma). The resulting mice express an optimized reverse tetracyclin-controlled transactivator (rtTA2s-M2) under the control of the Paxillin-8 (Pax8) gene promoter, which allows for specific expression of *Cpt1a* gene bearing TRE in proximal and distal tubules and collecting ducts after doxycycline (Dox) administration (**Figure 11**). Extra-renal expression only occurs at the level of the thyroid and this fact does not interfere with any kidney phenotype [223].

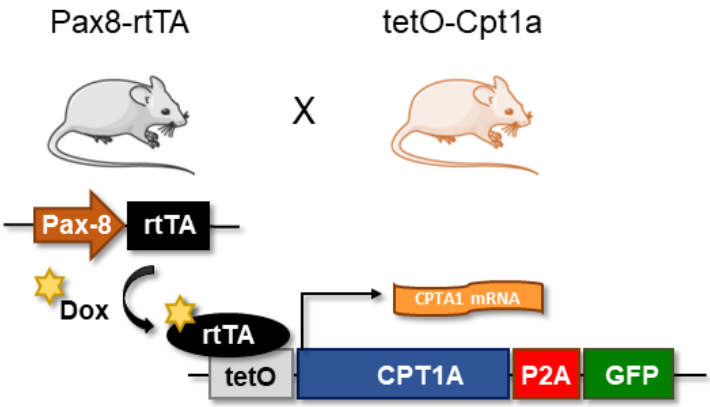

Figure 11. Schematic depicting the strategy to generate mice with inducible renal tubular epithelial-specific overexpression of CPT1A. Pax8-rtTA mice, which express the rtTA transactivator specifically in renal tubular epithelial cells driven by the Pax-8 promoter, were crossed with mice harboring the tetO-Cpt1a gene construction where the *Cpt1a* gene is under the control of a doxycycline-responsive promoter element. The yellow star indicates doxycycline-dependent activation of the transactivator. The construct bears an autoproteolytic P2A site, facilitating independent expressions of CPT1A and GFP (see text for details).

3.1.1. –Molecular cloning and gene targeting in ES cells

The CPT1A transgene containing the 5'UTR of the *Cpt1a* gene, the *Cpt1a* open reading frame (ORF) (Genbank accession number NM_013495.2), the 2A self-cleaving peptide (P2A), the gene encoding for green fluorescent protein (GFP) and the 3´UTR of the *Cpt1a* gene (**Figure 12A**) were cloned into a unique EcoRI site of pBS31 vector (OriGene Technologies, Rockville, Maryland). This vector contains the phosphoglycerate kinase (PGK) promoter followed by an ATG start codon and a FRT recombination site, a splice acceptor-double polyA cassette, the tetracycline operator with a cytomegalovirus (CMV) minimal promoter and an SV40 polyA signal, assembled in Bluescript (**Figure 12B**).

By using FRT/flippase-mediated recombination system, which permits the generation of single copy transgenes in predetermined integration sites [221, 222], the CPT1A transgene was targeted into the downstream region of the collagen 1a1 (Col1a1) locus of KH2 embryonic stem (ES) cells containing a frt-flanked PGK-neomycin-resistance gene followed by a promoterless, ATG-less hygromycin-resistance gene (**Figure 13**). These cells also contained the M2-rtTA under control of the endogenous ROSA26 promoter [224].

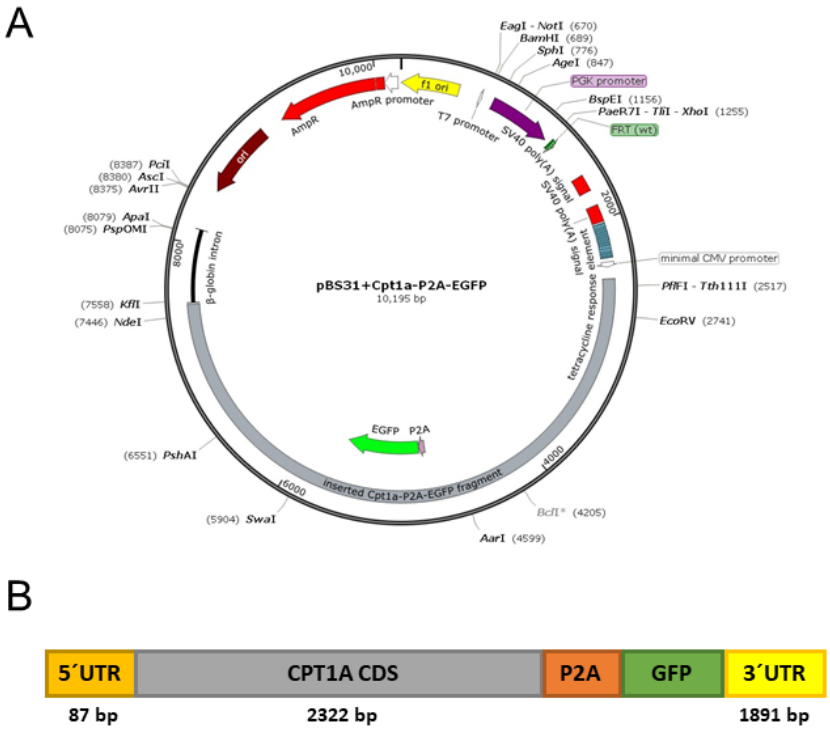

Figure 12. Map of the pBS31 vector (A) containing the CPT1A transgene (B). Aside from the coding sequence (CDS) the 5' and 3' UTRs of the CPT1A mRNA were included.

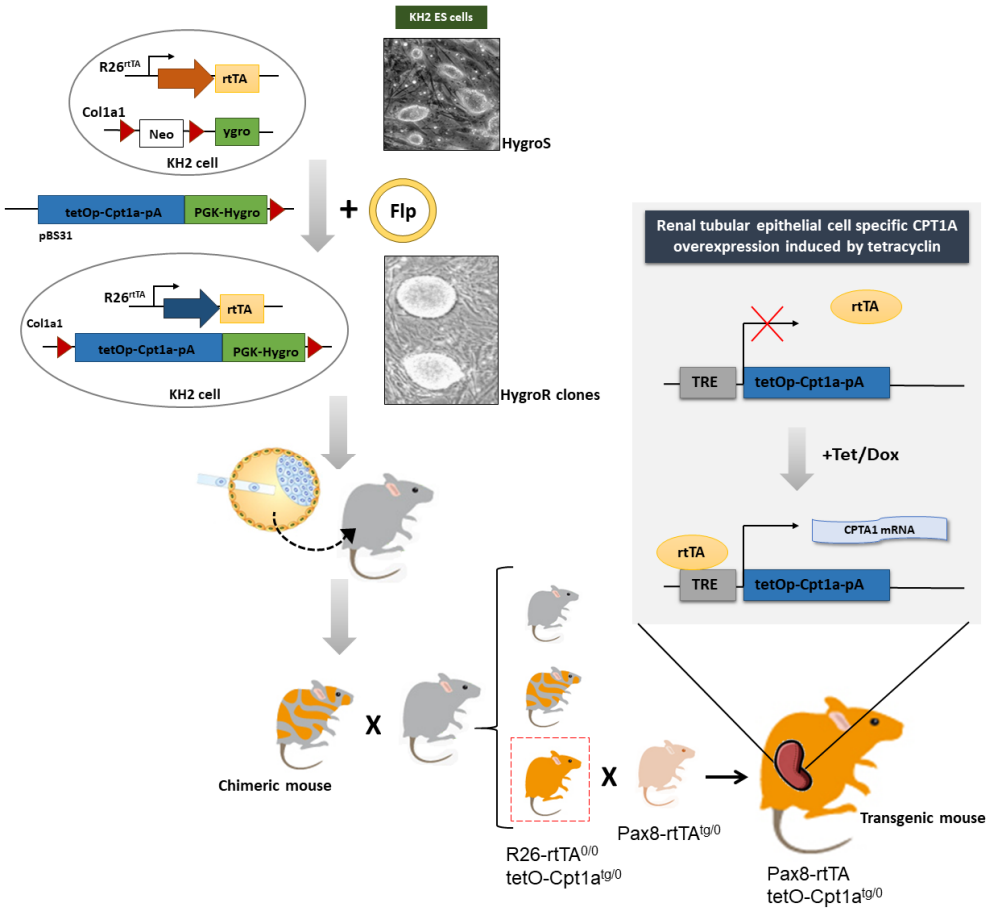

Figure 13. Schematic of the generation of mice with renal overexpression of CPT1A. The CPT1A transgene was inserted downstream of a tetracycline response element (TRE) by flippase (Flp)-mediated recombination in the Col1a1 locus of KH2 embryonic stem cells. Cells that undergo FRT site-specific recombination acquire hygromycin resistance. Positive clones were injected into blastocysts of C57/Bl6-J female mice and transferred into CD1 foster mothers to generate chimeric mice able to transmit the mutant gene to their progeny. *Cpt1a* knock-in (tetO-Cpt1a$^{tg/0}$) mice were bred with Pax8-rtTA (R26-rtTA $^{tg/0}$) mice to generate mice overexpressing CPT1A in renal epithelial tubular cell after doxycycline induction.R26: Rosa 26 locus, PGK: phosphoglycerate kinase, ygro: hygromycin resistance gene. See figure 11 and text for details.

For gene targeting, 50 µg pBS31 vector and 25 µg vector encoding the flippase (pCAGGS-FLP) [225] were co-electroporated with 1.5 x 10^7 KH2 ES cells at 400 V and 125 µf using two pulses in a Gene PulserII (Bio-Rad, Hercules, CA). Recombination between FRT sites such that the entire plasmid is inserted within the PGK promoter and the ATG initiation codon upstream and in frame with the hygromycin resistance gene was used to select correctly targeted cells. ES cells were treated with 140 µg/ml hygromycin B (Carl Roth, Karlsruhe, Germany) after 48 h post electroporation to select clones that had undergone site-specific recombination and individual clones were picked after 8-14 days. Individual ES clones were tested *in vitro* by treating them with 1µg/ml doxycycline (Sigma, St. Louis, MO) in the culture media for 4 days. Then, GFP was measured in a BD FacsCanto™ II cytometer (BD Bioscience, San José, CA) to assess the electroporation efficiency and cells expressing GFP were sorted. Dox-induced CPT1A was also analyzed by immunoblot as described above.

3.1.2. –Generation of mice

Mice were generated by diploid blastocyst injection. Blastocysts were harvested at 3.5 days post coitum (dpc) from C57/BL6-J strain females. Between 10 and 15 KH2 ES cells were injected per blastocyst. Approximately 30 injected blastocysts were transferred into pseudo-pregnant CD1 strain recipient females (transgenic mice core unit, CNIO, Spain). Chimeras from the litter with a high percentage agouti coat colour (>80%) were then crossed with C57/BL6-J mice to evaluate germline transmission (**Figure 13**). Male *tetO-Cpt1a*$^{tg/0}$ mice were bred with *Pax8-rtTA*$^{tg/0}$ female mice to generate double heterozygous *Pax8-rtTA*$^{tg/0}$*:tetO-Cpt1a*$^{tg/0}$ mice and their control littermates in a B6N;129Sv mixed genetic background.

3.1.3. –Doxycycline induction

To induce CPT1A expression, 8-wk-old *Pax8-rtTA*$^{tg/0}$*:tetO-Cpt1a*$^{tg/0}$ mice and corresponding *Pax8-rtTA*$^{0/0}$*:tetO-Cpt1a*$^{tg/0}$ (WT) mice were fed with doxycycline (Sigma, St. Louis, MO) at concentrations of 1 mg/ml *via* drinking water for 3 weeks. Mice were housed in colony cages with a 12:12-h light-dark cycle in a temperature- and humidity-controlled environment with free access to water.

3.1.4. –Genotyping

Mice were genotyped by PCR using DNA extracted from tail biopsies and the primers listed in **Table 1**. DNA extraction was performed by using the AccuStart™ II Mouse Genotyping Kit according to the manufacturer's instructions.

PCR name	PCR product	5´- 3´ primer sequence	PCR Amplicons	PCR protocol
Rosa26-rtTA	Rosa26	RV1: GCGAAGAGTTTGTCCTCAACC RV2: GGAGCGGGAGAAATGGATATG FW: AAAGTCGCTCTGAGTTGTTAT	Mutant allele: 300 bp Wild type allele: 650 bp	Denature: 94º 30' Annealing: 59º 45" Extension: 65º 2'30" 40x
Pax8-rtTA	Pax8-rtTA construct	FW: CTGGAGAACGCACTGTACGC RV: CCA ATACGCAGCCCAGTGT	Mutant allele: 450 bp Wild type allele: no band	Denature: 95º 3' Annealing: 95º 5" Extension: 60º 30" 40x
FRT	Col1a1	FW1 (A):GCAGAAGCGCGGCCGTCTGG RV (B):CCCTCCATGTGTGACCAAGG FW2 (C): GCACAGCATTGCGGACATGC	Mutant allele: 450 bp Wild type allele: 300 pb	Denature: 94º 30' Annealing: 59º 45" Extension: 65º 2'30" 40x
GFP	Col1a1	FW (A): AGCAGCAGGTGGAACTGTTT RV (B):CTGAACTTGTGGCCGTTTAC	Mutant allele: 400 bp Wild type allele: no band	Denature: 94º 30' Annealing: 59º 45" Extension: 65º 2'30" 40x
Exon	Col1a1	FW (A): CCAGGCTACAGTGGGACATT RV (B):GAACTTGCCCATGTCCTTGT	Mutant allele: 209 bp Wild type allele: no band	Denature: 94º 30' Annealing: 59º 45" Extension: 65º 2'30" 40x

Table 1. Primer sequences for CPT1A KI mice genotyping.

3.2 miR-33 KO animals

miR-33 knockout (KO) mice was generated and characterized as previously described [226]. Male C57BL/6JRccHsd (WT) mice were purchased from The Jackson Laboratory (Bar Harbor, ME, USA). They were used as controls for the miR-33 KO mice. All mice were maintained under constant temperature and humidity in a 12 h controlled dark/light cycle.

3.3 Cell lines and culture conditions

Human proximal tubular epithelial cells (HKC-8) were cultured in DMEM/F12 (Dulbecco's modified Eagle's medium 1:1 (v/v)) (Corning, New York, NY) supplemented with 15 mM Hepes, 5% (vol/vol) fetal bovine serum (FBS) (HyClone Laboratories, Logan, UT), 1x Insulin-Transferrin-Selenium (ITS) (Gibco, Rockville, MD), 0.5 µg/ml hydrocortisone (Sigma, St. Louis, MO), 50 units/mL penicillin and 50 µg/mL streptomycin (Gibco, Rockville, MD) at 37ºC and 5% CO_2. Human renal epithelial cells (HRECs) were cultured in Epithelial Cell Medium (EpiCM) supplemented with 2% fetal bovine serum (FBS), 1% Epithelial Cell Growth Supplement (EpiCGS) and 1% penicillin/streptomycin solution (P/S solution) (all the components from Innoprot, Derio, Spain) at 37ºC and 5% CO_2. HKC-8 cells were kindly provided by Dr. Susztak´s lab (Philadelphia, Pennsylvania, USA) and HRECs were purchased from Innoprot. HEK293A cells are cultured in DMEM supplemented with 10% (v/v) FBS (HyClone Laboratories, Logan, UT) and 1% penicillin /streptomycin (Gibco, Rockville, MD) at 37ºC and 5% CO_2. All cells were treated with trypsin every five days for sub-culturing. Cell from the embryonic stem cell line KH2 derived from 129/Bl6-J mice were cultured on irradiated murine embryonic fibroblast (MEF) cells according to standard procedures [227]. Briefly, cells were seeded at a density of 3×10^4 cells/cm^2 in DMEM supplemented with leukemia inhibitory factor (LIF) at 1000 units/ml (Corning, New York, NY), 15% ES qualified fetal bovine serum (FBS), non-essential amino acids and sodium pyruvate (Gibco, Rockville, MD), and passaged every other day. Treatments with human recombinant 10 ng/ml TGF-β1 (R&D Systems, Minneapolis, MN) were performed after serum-free starvation of HKC-8 for 12 hours (h).

3.4 Isolation of primary kidney epithelial cells

Kidneys from CPT1A KI and wild-type (WT) mice (3- to 5-week-old males) were collected after sacrifice by cervical dislocation and perfusion with PBS. The capsule was removed and the cortex from 2 kidneys was dissected, placed in 1 mL ice-cold phosphate buffered saline (PBS) (Corning, New York, NY), and minced into pieces of approximately 1 mm^3. These pieces were digested with 10 ml HBSS containing 2 mg/mL collagenase I (Thermo Scientific, Rockford, IL) for 30 minutes at 37°C with gentle stirring and supernatants were sieved through a 100-µm nylon mesh. After centrifugation for 10 minutes at 3000 rpm, the pellet was resuspended in sterile red blood cell lysis buffer (8.26 g NH4Cl, 1 g KHCO3, and 0.037 g EDTA per 1 L ddH2O) and seeded in 10-cm culture dishes. Cells were cultured in RPMI 1640 (Corning, New York, NY) supplemented with 10% FBS (HyClone Laboratories, Logan, UT), 20 ng/mL EGF (Sigma, St. Louis, MO), 20 ng/ml bFGF (Sigma, St. Louis, MO), 50 units/mL penicillin and 50 µg/mL streptomycin (Gibco, Rockville, MD) at 37ºC and 5% CO2. Media were changed 24 hours after plating and every 48–72 hours thereafter. Cells were used between days 7 and 10 of culture. Treatments (10 ng/ml) with human recombinant TGF-β1 (R&D Systems, Minneapolis, MN) were performed after serum-free starvation of cells for 12 h.

3.5 Transfection procedure

Cells were seeded into 60 mm culture dishes to reach a confluence of 70%. They were transfected with 40 nM of either mirVana™ miRNA mimic of miR-150, miR-495 or miR-33, miR-33 inhibitor or mirVana™ miRNA mimic/inhibitor negative control (Ambion company, USA) using lipofectamine 2000 (Invitrogen, Carlsbad, CA). Cells were incubated with the lipofectamine-pre-miRNA 37 °C for 6 h. Subsequently, 5 ml fresh medium containing 10% FBS were added to the culture dishes and the cells were maintained in culture until used for subsequent experiments.

3.6 Immunoblot

Cells were washed in PBS, homogenized and lysed in 100 µL RIPA lysis buffer containing 150 mM NaCl, 0.1% SDS, 1% sodium deoxycholate, 1% NP-40 and 25 mM Tris–HCl pH 7.6, in the presence of protease (Complete, Roche Diagnostics, Mannheim, Germany) and phosphatase inhibitors (Sigma-Aldrich, St. Louis, MO) and harvested by scraping. A quarter piece of each kidney sample (obtained after dissection in half both lengthwise and crosswise) was homogenized in 300 µl RIPA buffer above described with 5 mm stainless steel beads (Qiagen, Valencia, CA) using TissueLyser LT (Qiagen, Valencia, CA) vibrating at 50 Hz for 15 min at 4°C. Samples were clarified by centrifugation at 10,000 *g* for 15 min at 4°C. The pellet was then discarded, and the supernatant was kept as protein lysate. Protein concentrations were determined by the BCA Protein Assay Kit (Thermo Scientific, Rockford, IL) and was measured in Glomax®-Multi Detection system (Promega, Madison, WI). Equal amounts of protein (10–50 µg) from the total extract were separated on 8–10% SDS–polyacrylamide gels and transferred onto nitrocellulose blotting membranes (GE Healthcare, Chicago, IL) at 12 V for 20 min in a semi-dry Trans-Blot Turbo system (Bio-Rad, Hercules, California). Membranes were blocked by incubation for 1 h with 5% non-fat milk in PBS containing 0.5% Tween-20 and blotted overnight with the specific antibodies listed in (**Table 2**). After incubation with IRDye 800 goat anti-rabbit and IRDye 600 goat anti-mouse (1:15,000, LI-COR Biosciences, Lincoln, NE) secondary antibodies,

membranes were imaged in triplicates with the Odyssey Infrared Imaging System (LI-COR Biosciences, Lincoln, NE). Band densitometry was performed using the ImageJ 1.48 software (http://rsb.info.nih.gov/ij) and relative protein expression was determined by normalizing to GAPDH. Fold changes were normalized to values of control condition.

Protein	Species	Reference	Dilution	Experimental conditions
CPT1A	Mouse	Ab128568, Abcam	1:1000	4°C O/N
α-tubulin	Mouse	T9026, Sigma-Aldrich	1:5000	1h RT
β-actin	Mouse	A1978, Sigma-Aldrich	1:15000	1h RT
GFP	Mouse	AB10145, Sigma-Aldrich	1:5000	4°C O/N
FN1	Rabbit	F7387, Sigma,	1:1000	4°C O/N
α-SMA	Mouse	sc-32251, Santa Cruz Biotechnology	1:1000	4°C O/N
GAPDH	Mouse	MAB374, Millipore	1:15000	1h RT
p-ACC-Ser^{79}	Rabbit	07-303, Sigma-Aldrich	1:1000	4°C O/N
p-AMPKα-Thr^{172}	Rabbit	2535, Cell signaling	1:1000	4°C O/N
COL III	Mouse	Ab6310, Abcam	1:1000	4°C O/N
ABCA1	Mouse	Ab18180, Abcam	1:1000	4°C O/N

Table 2. Primary antibodies for western blot analysis. O/N: overnight, RT: room temperature.

3.7 RNA extraction

Total RNA was extracted from HKC-8 or mouse kidneys using the miRNeasy Mini Kit (Qiagen, Valencia, CA) according to the manufacturer's instructions. RNA quantity and quality were determined at 260 nm by a Nanodrop-1000 spectrophotometer (Thermo Scientific, Rockford, IL).

3.8 Analysis of mRNA expression

Reverse transcription (RT) was carried out with 500 ng of total RNA using the iScript™ cDNA Synthesis kit (Bio-Rad, Hercules, CA) using the the program described in **Table 3A**. qRT–PCR was carried out with the iQ™SYBR Green Supermix (Bio-Rad, Hercules, CA), using a 96-well Bio-Rad CFX96 RT–PCR System with a C1000 Thermal Cycler (Bio-Rad, Hercules, CA) according to the manufacturers' instructions (**Table 3B**). A C_t value was obtained from each amplification curve using CFX96 analysis software provided by the manufacturer. Relative mRNA expression was determined using the $2^{-\Delta\Delta Ct}$ method [228] (**Figure 14**). The 18S gene was used for normalization purposes. The primer sequences used for mRNA quantification are listed in **Table 4**. Fold changes were normalized to values of control condition.

A

Time (min)	Temperature (°C)
5	25
30	42
5	85
Hold	4

B

Cycle	Step	Time	Temperature (°C)
Initial denaturation (x1)	Denaturation/ polymerase activation	3 min	95
Thermal cycling (x40)	Denaturation	10 sec	95
	Annealing/ Extension	30 sec	60

Table 3. PCR protocols for RT (A) and qRT-PCR (B) of mRNA expression analyses.

$$\text{Relative expression level} = 2^{-\Delta\Delta Ct}$$

$$\Delta Ct = Ct_{\text{target gene}} - Ct_{\text{control gen}}$$

$$\Delta\Delta Ct = \Delta Ct_{\text{Exp. condition}} - \Delta Ct_{\text{control condition}}$$

Figure 14. $2^{-\Delta\Delta Ct}$ method for relative quantification of RT-PCR expression data.

Gene	5´- 3´ primer sequence
Mouse	
Cpt1a	FW: GGTCTTCTCGGGTCGAAAGC
	RV: TCCTCCCACCAGTCACTCAC
Acta2	FW: CTGACAGAGGCACCACTGAA
	RV: CATCTCCAGAGTCCAGCACA
Col1a1	FW: CTGCTGGCAAAGATGGAGA
	RV: ACCAGGAAGACCCTGGAATC
Fn1	FW: ACCGACAGTGGTGTGGTCTA
	RV: CACCATAAGTCTGGGTCACG
Cdh1	FW: ACCTCCGTGATGAAGGTCTC
	RV: CCGGTGTCCCTATTGACAGT
Ppargc1a	FW: CCCTGCCATTGTTAAGACC
	RV: TGCTGCTGTTCCTGTTTTC
Tgfb1	FW: AGCGGACTACTATGCTAAAGAGGTCAACCC
	RV: CCAAGGTAACGCCAGGAATTGTTGCTATA
Col3a1	FW: ACAGCTGGTGAACCTGGAAG
	RV: ACCAGGAGATCCATCTCGAC
18s	FW: TCAAGAACGAAAGTCGGAGG
	RV: GGACATCTAAGGGCATCAC
Human	
CPT1A	FW: TGCTTTACAGGCGCAAACTG
	RV: TGGAATCGTGGATCCCAAA
ACTA2	FW: TTCAATGTCCCAGCCATGTA
	RV: GAAGGAATAGCCACGCTCAG
COL1A1	FW: CGGACGACCTGGTGAGAGA
	RV: CATTGTGTCCCCTAATGCCTT
FN1	FW: GTGTTGGGAATGGTCGTGGGGAATG
	RV: CCAATGCCACGGCCATAGCAGTAGC
PPARGC1A	FW: TGCCCTGGATTGTTGACATGA
	RV: TTTGTCAGGCTGGGGGTAGG
CROT	FW: TGTTCACCACAGGGATACAAGCCT
	RV: TACCTTGGCCTCCCACCGTGCTAA
HADHB	FW: TCACCATGGCTTGTATCTCTGCCA
	RV: AGACAGTCGCTGGCCCATAGATTT
TFAM	FW: CATCTGTCTTGGCAAGTTGTCC
	RV: CCACTCCGCCCTATAAGCATC
18S	FW: AGCTATCAATCTGTCAATCCTGTC
	RV: GCTTAATTTGACTCAACACGGGA

Table 4. Primer sequence for qPCR analysis.

3.9 Quantification of miRNA expression

Quantification of miRNAs expression was performed using the miRCURY Locked Nucleic Acid (LNA) miRCURY LNA RT Kit (Exiqon, Vedback, Denmark) using the program described in **Table 5A**. Following RT, the cDNA template was amplified using microRNA-specific LNA primers for mature miR-150-5p, miR-495-3p or miR-33-5p (Exiqon, Vedback, Denmark). qRT–PCR was performed in a 96-well Bio-Rad CFX96 RealTime PCR System with a C1000 Thermal Cycler using iQ™ SYBR Green Supermix (Bio-Rad, Hercules, CA) according to the manufacturers' instructions (**Table 5B**) (**Figure 15**). A C_t value for triplicate wells was

obtained from each amplification curve using the CFX Manager Bio-Rad software (Bio-Rad, Hercules, CA). C_t values were normalized to the endogenous control 5S rRNA. Plasma lipid levels were to miR-103a-5p. Relative miRNA expression was determined using the $2^{-\Delta\Delta Ct}$ method [228]. Fold changes were normalized to values of control condition.

A

Time (min)	Temperature (ºC)
60	25
5	95
Hold	4

B

Cycle	Step	Time	Temperature (ºC)
Initial denaturation (x1)	Denaturation/ polymerase activation	15 min	95
Thermal cycling (x40)	Denaturation	15 sec	95
	Annealing	30 sec	55
	Extension	30 sec	70

Table 5. PCR protocols for RT (A) and qRT-PCR (B) of miRNA expression analyses.

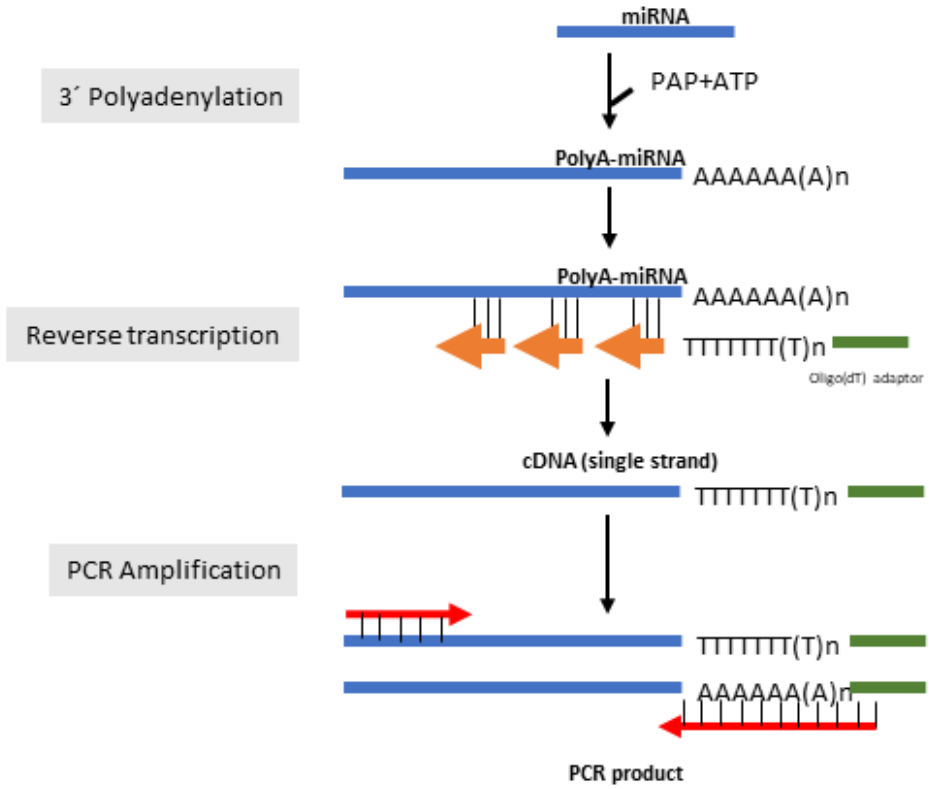

Figure 15. Schematic depicting the principle of the microRNA real-time PCR. A poly(A) tail is added to the mature miRNA template (in blue) and cDNA is synthesized using a poly(dT) primer with a 3' degenerate anchor (orange arrows) and a 5' universal tag (in green). The cDNA template is then amplified using miRNA-specific and LNA-enhanced forward and reverse primers (in red). Sybr Green is used for detection. PAP: poly(A) polymerase.

3.10 Mouse models of kidney fibrosis

Mice were housed in the Specific-pathogen-free (SPF) animal facility at the CBMSO in accordance with EU regulations for all the procedures. Animals were handled in agreement with the Guide for the Care and Use of Laboratory Animals contained in Directive 2010/63/EU of the European Parliament. Approval was granted by the local ethics review board of the Centro de Biología Molecular "Severo Ochoa" in Madrid, the Ethics committee at CSIC and the Regulatory Unit for Animal Experimental Procedures from the Comunidad de Madrid.

3.10.1. –Unilateral ureteral obstruction (UUO)

UUO surgery procedure was performed as previously described [229] (**Figure 16.**) Briefly, mice were anesthetized with isofluorane (3-5% for induction and 1-3% for maintenance) and divided into two experimental groups: the UUO group and the sham operation group. In the UUO group, mice were shaved on the left side of the abdomen, a vertical incision was made through the skin with a scalpel and the skin was retracted. A second incision was made through the peritoneum to expose the kidney. The left ureter was ligated twice 15 mm below the renal pelvis with surgical silk and the ureter was then severed between the two ligatures. Then, the ligated kidney was placed gently back into its correct anatomical position and sterile saline was added to replenish loss of fluid. The incisions were sutured and mice were individually caged. The sham operation was performed in a similar manner, but without ureteral ligation. Buprenorphine was used as an analgesic. A first dose was administered 30 minutes before surgery and then every 12 hours for 72 hours, at a dose of 0.05 mg / kg subcutaneously. In this model, renal blood flow and glomerular filtration rate become significantly reduced within 24 h and interstitial inflammation (peak at 2–3 days), tubular dilation, tubular atrophy and fibrosis are evident after 7 days. The obstructed kidney reaches maximal dysfunction around 2 weeks after the procedure. Mice were sacrificed by CO_2 overdose and control and obstructed kidney and blood samples were harvested after perfusion with PBS at 3 and 7 days after UUO.

3.10.2. –Folic acid-induced nephropathy (FAN)

In this model kidney fibrosis was induced by intraperitoneal (i.p) injection with 250 mg folic acid (Sigma-Aldrich, St. Louis, MO) per kg body weight dissolved in 0.3 M sodium bicarbonate (vehicle) as previously described [230]. Control animals received 0.3 ml of vehicle (i.p). Mice were sacrificed by CO_2 overdose and kidneys and blood samples were harvested after perfusion with PBS after 15 days of FA administration (**Figure 16.**

3.10.3. –Adenine-induced renal failure (ADN)

Adenine (Sigma-Aldrich, St. Louis, MO) was administered daily to mice at 50 mg/kg body weight in 0.5% carboxymethyl cellulose (CMC) (Wako Pure Chemical Industries Ltd., Osaka, Japan) by oral gavage for 28 days as previously described [231]. Control animals received daily 0.5% CMC administered by oral gavage for the same period of time. Mice were sacrificed by CO_2 overdose and kidneys and blood samples were harvested after perfusion with PBS after 28 days of the first adenine dose administration (**Figure 16.**

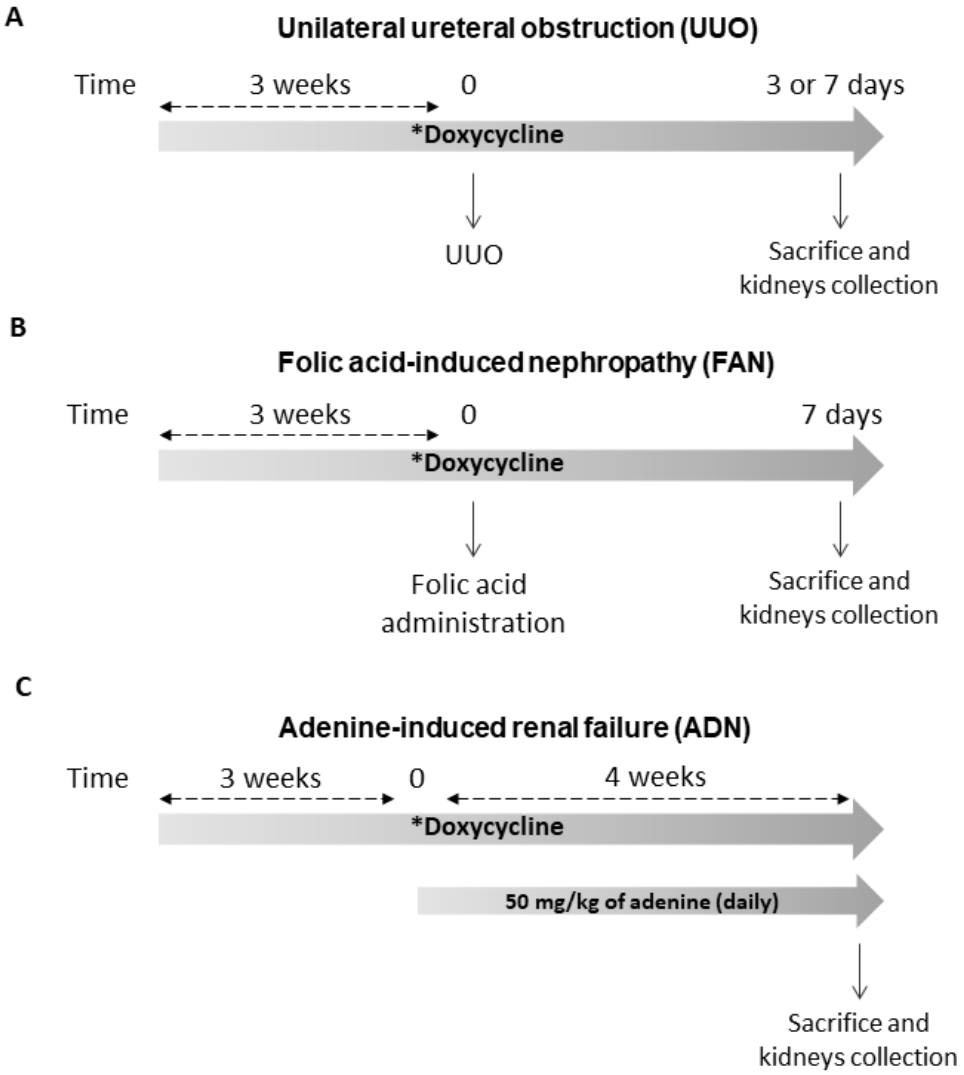

Figure 16. Schematic of the protocols for mouse models of kidney fibrosis. Temporal diagrams of the experimental procedures for the UUO (A), FAN (B) and ADN (C) models (see text for details). *When these models were performed in CPT1A KI mice, doxycycline was administered for 3 weeks prior to the induction of kidney fibrosis (time 0) and was maintained until tissue collection.

3.11 microRNA profiling

To identify specific miRNAs that regulate the fibrotic outcome, a Custom miRCURY LNA microRNA array (Exiqon, Vedback, Denmark) was selected as the platform for microRNA profiling. This platform consisted of a total of 175 unique assays specific for mouse miRNAs present in the Sanger miRBase v22.1 (http://microrna.sanger.ac.uk, listed in **Table 6**). For each microRNA, the prevailing strand was selected for analysis. miR selection was based on predicted target genes related to renal fibrosis, mitochondrial metabolism, redox processes and circadian rhythm. This analysis was done with the bioinformatics tools for sequence-based miRNA target prediction, microcosm [232] (www.ebi.ac.uk/enright-srv/microcosm), Targetscan 4.1 [233] (www.targetscan.org/vert_40/) and Pictar I [234] (www.pictar.mdc-berlin.de), miRWalk [235] (www.mirwalk.umm.uni-heidelberg.de/) and miRanda [236] (www.microrna.org/microrna/).

Biological process	microRNA	Biological function	microRNA	Biological process	microRNA	Biological process	microRNA
Organ fibrosis	let-7d	Kidney fibrosis	miR-491	*In silico* Cpt1	miR-546	Previous miRNA arrays with UUO samples	miR-130b
	miR- 355		miR-125b		miR-380		miR-877
	miR-1		let-7c		miR-544		miR-223
	miR-101		let-7g		miR-715		miR-3072
	miR-107		miR-195		miR-760		miR-199a
	miR-132		miR-214		miR-211		miR-1224
	miR-133a		miR-328		miR-674		miR-17
	miR-140	Fatty acid oxidation	miR-33		miR-322		miR-96
	miR-141		miR-122		miR-692-1		miR-199b
	miR-142		miR-370		miR-466b-3		miR-18a
	miR-146a		miR-335		miR-188		miR-199a
	miR-15		miR-125a		miR-692-2		miR-342
	miR-150		miR-375		miR-324		miR-148a
	miR-155		miR-758		miR-541		miR-34b
	miR-15b		let-7		miR-679		miR-181d
	miR-16		miR-143		miR-297b		let-7e
	miR-17		miR-103		miR-328		miR-350
	miR-192		miR-148		miR-680-1		miR-181b
	miR-194		miR-221		miR-330		miR-19a
	miR-196		miR-126		miR-202		miR-301
	miR-199		miR-149		miR-680-2		miR-301a
	miR-19b	Mitochondrial metabolism	miR-183		miR-703		miR-181a
	miR-20		miR-743a		miR-680-3		miR-181c
	miR-200 a/b/c		miR-761		miR-204		miR-652
	miR-204		miR-499		miR-338		miR-130a
	miR-206		miR-761		miR-511		miR-709
	miR-208		let7b		miR-468		miR-100
	miR-21		mir-146a		miR-466l		miR-467b
	miR-211		miR-19b		miR-1192		miR-99b
	miR-215		miR-20a		miR-340		miR-31
	miR-216		miR-494		miR-495		miR-500
	miR-217		miR-696	*In silico* Nrf2	miR-137		miR-676
	miR-23a	Redox	miR-153		miR-142		miR-135a
	miR-24		miR-142		miR-146b		miR-10a
	miR-26 a/b		miR-144		miR-707		miR-872
	miR-27 a/b		miR-28		miR-20a		miR-127
	miR-29 a/b/c		miR-34 a/b/c		miR-876		miR-705
	miR-30		miR-23b		miR-410		miR-532
	miR-32		miR-451		miR-25		
	miR-338		miR-210		miR-93		
	miR-377		miR-128a		miR-302		
	miR-382		miR-145	*In silico* Circadian rhythm-related genes	miR-346		
	miR-433	Circadian rhythm	miR-142		miR-98		
	miR-449		miR-185		miR-106 a/b		
	miR-503		miR-122		miR-152		
	miR-590		miR-182		miR-182		
	miR-9		miR-191		miR-90		
	miR-92a		miR-383		miR-203		
	miR-94		miR-219		miR-367		

Table 6. Selected microRNAs for array-based profiling.

After RNA extraction from 7 day-UUO kidney samples, the miRNA fraction present in 20 ng of total RNA was subjected to reverse transcription using miRCURY LNA RT Kit (Exiqon, Vedback, Denmark) according to the manufacturer's instructions. The resultant cDNAs were analyzed with the miRCURY miRNA PCR Panels in a Roche LightCycler 480 Real-Time PCR system using miRCURY LNA SYBR Green PCR Master Mix (Exiqon, Vedback, Denmark). Each sample was analyzed by duplicate. This procedure was performed in the Genomic Facility of the Fundación Parque Científico de Madrid (Madrid, ES).

The LC480 software was utilized to obtain Cq values (C_q) for each miRNA. The delta C_t (ΔC_t) value was calculated by normalizing C_t values to the endogenous housekeeping snRNAU6. The heat map was generated with the real-time PCR data presented as ΔC_t. A hierarchical clustering was made according to ΔC_t values. The delta delta Ct ($\Delta\Delta C_t$) value was calculated by subtracting the ΔC_t of the reference sample group (control kidney) from the ΔC_t of each obstructed kidney sample. Relative quantification (RQ) or fold-change of each miRNA was generated using the $2^{-\Delta\Delta C_t}$ method [228]. Differentially expressed miRNAs were identified by the parametric Limma test. To take the multiple hypotheses testing into account, *P*-values

were adjusted (adj.) using the Benjamini–Hochberg false discovery rate (FDR) correction [237]. Results were graphed in a volcano plot.

3.12 Triglyceride measurement

Total lipids from tissue were sequentially extracted by the method of Bligh and Dyer [238] in the presence of internal standards including dieicosanoyl-PC, ditetradecanoyl-PE and cholesteryl heptadecanoate. Extracted renal lipids were resuspended in methanol/chloroform (4:1, by vol.) to a dilution of ~20 pmol of lipid per µL and analyzed by ESI-MS in the direct infusion mode at a flow rate of 3 µL/min using a Thermo Electron TSQ Quantrum Ultra® instrument. Results were normalized to the protein content.

3.13 [1-^{14}C] Palmitate oxidation

Measurement of fatty acid oxidation (FAO) rates was performed in mouse kidney tissue and cells as previously described [239]. Kidneys from renal fibrosis mouse models were decapsulated, diced, and then homogenized in 5 volumes of chilled STE buffer by a Dounce homogenizer. Crude homogenates were centrifuged at 420 g for 10 min at 4 °C. Thirty µL of tissue homogenate supernatant was mixed with 370 µL of the oxidation reaction mixture containing 7% BSA/5 mM palmitate/0.01 µCi/µL ^{14}C-palmitate (PerkinElmer, Waltham, MA) and incubated at 37 °C for 30 min. In the case of cells, they were seeded in 12-well dishes to reach a confluence of 70% and were infected with CPT1A adenoviruses as described in the adenovirus-mediated CPT1A overexpression procedure section. Then, cells were incubated in 500 µL of media containing 0.3% BSA/100 µM palmitate/0.4 µCi/mL ^{14}C-palmitate at 37 °C for 3 h. Each sample was assayed in triplicate. The reaction was stopped by the addition of 200 µl of 1 M perchloric acid. The rate of palmitate oxidation was measured as released $^{14}CO_2$ trapped in a filter paper disk with 20 µL of 1 M NaOH in the top of sealed vials. $^{14}CO_2$ traps were transferred to scintillation vials to determine ^{14}C-palmitate-derived $^{14}CO_2$. The remaining acid solution for each sample was centrifuged at 14,000 × g for 10 min at 4 °C and 400 µL of supernatant was also added to scintillation vials for the quantification of ^{14}C-palmitate-derived acid-soluble metabolites (**Figure 18**). Control incubations without cells or tissue samples were also run in parallel. ^{14}C products were counted in an LS6500 liquid scintillation counter (Beckman Instruments Inc., Brea, CA). Scintillation values were converted to mmol $^{14}CO_2$ or acid-soluble metabolites by multiplying with the specific activity (**Figure 17**) and normalized to the protein content.

$$\text{Specific activity} = \frac{\text{DPM of input}}{\text{Total nmol of palmitate}}$$

Figure 17. Calculation of the radioactive specific activity. DPM (disintegrations per minute).

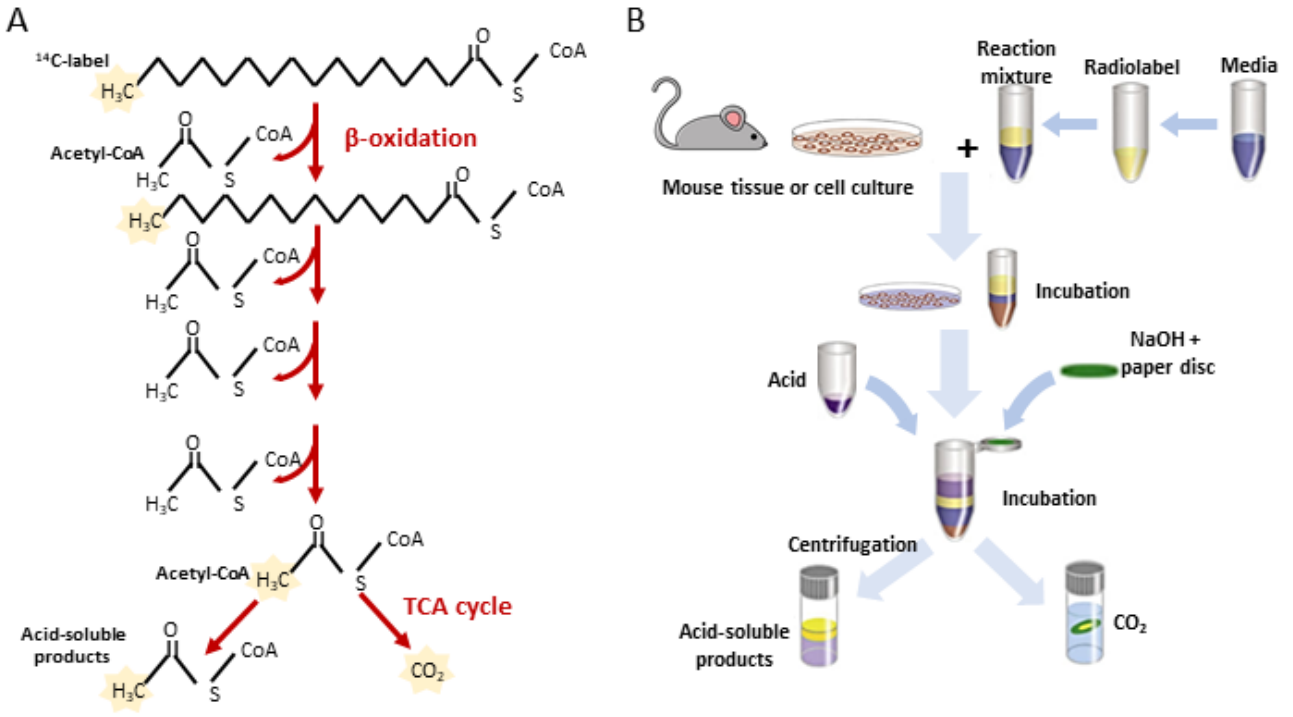

Figure 18. Schematic of the protocol for measurement of fatty acid oxidation rates in animal tissues and cell lines. (A)^{14}C-palmitate is oxidized via β-oxidation to generate acetyl-CoA, which can then enter the tricarboxylic acid (TCA) cycle or incorporate into acid-soluble products. (B) Tissue or cells are incubated in a reaction mixture containing ^{14}C-palmitate. Addition of a strong acid is used to stop the reaction and precipitate palmitate. The amounts of ^{14}C in the acid-soluble metabolite fraction and the CO_2 fraction retained in the paper disc were measured by scintillation counting.

3.14 TaqMan gene expression assay

TaqMan Array Plates (Thermo Scientific, Rockford, IL) were selected as the platform for gene expression profiling. This panel consisted of a total of 43 unique TaqMan probes specific for mouse gene related with fibrosis, apoptosis, mitochondrial metabolism, glucose utilization and inflammation listed in **(Table 7) (Supplementary table 1)**. RNA from kidney samples was performed as described in the RNA extraction procedure section. Two µg of total RNA were subjected to reverse transcription using High-Capacity cDNA Reverse Transcription Kit (Thermo Scientific, Rockford, IL) according to the manufacturer's instructions. PCR amplification was performed using TaqMan® master (Thermo Scientific, Rockford, IL) with the Roche LightCycler 480 Real-Time PCR system (AB7900HT). This procedure was performed in the Genomic Facility of the Fundación Parque Científico de Madrid (Madrid, Spain).

The ABI TaqMan SDS v2.4 software was utilized to obtain Cq values (C_q) for each gene. The C_q data were analyzed with the StatMiner 4.2.8 software (Integromics; Madrid, Spain). The delta C_t (ΔC_t) value was calculated by normalizing C_t values to the endogenous housekeeping 18S. Relative mRNA expression was determined using the $2^{-\Delta\Delta Ct}$ method [228]. Fold changes were normalized to values of control condition.

3.15 Mitochondrial copy number determination

Genomic DNA was extracted from mouse kidneys using the DNeasy Blood & Tissue Kit (Qiagen, Valencia, CA) according to the manufacturer's instructions. DNA quantity and quality were determined at 260 nm by a Nanodrop-1000 spectrophotometer (Thermo Scientific, Rockford, IL). Mitochondrial abundance was determined with the Mouse Mitochondrial DNA Copy Number Assay Kit (Detroit R&D, Detroit, MI). Relative mtDNA copy number was presented as the mtDNA-to-nuclear DNA ratio.

Biological function	Abbreviation	Gene name
Apoptosis	*Apaf1*	Apoptotic Peptidase Activating Factor 1
	Bax	Bcl-2-associated X protein
	Bcl2	B-cell lymphoma 2
	Bcl2l1	(BCL2-like 1)
Fatty acid oxidation	*Cpt1a*	Carnitine palmitoyltransferase I
	Cpt2	Carnitine palmitoyltransferase II
	Ppara	Peroxisome proliferator-activated receptor alpha
	Ppargc1a	PPARG Coactivator 1 Alpha
	Acox1	Peroxisomal Acyl-CoA Oxidase 1
	Acox2	Peroxisomal Acyl-CoA Oxidase 2
Fibrosis	*Acta2*	alpha smooth muscle actin
	Cdh16	Cadherin 16
	Col1a1	Collagen type I alpha 1 chain
	Col3a1	Collagen type III alpha 1 chain
	Col4a1	Collagen type IV alpha 1 chain
	Fn1	Fibronectin
	Havrc1	Kidney Injury Molecule-1
	Snai1	Snail Family Transcriptional Repressor 1
	Tgfb1	Transforming Growth Factor Beta 1
	Twist1	Twist Family BHLH Transcription Factor 1
	Vim	Vimentin
Glycolysis	*G6pc*	Glucose-6-Phosphatase Catalytic Subunit
	Gapdh	Glyceraldehyde-3-Phosphate Dehydrogenase
	Hk1	Hexokinase 1
	Ldh1	L-lactate dehydrogenase 1
	Ldh2	L-lactate dehydrogenase 2
	Pgk1	Phosphoglycerate Kinase 1
	Pkfm	fosfofructoquinasa-1
	Pkm	pyruvate kinase
	Slc2a1	Glucose transporter protein type 1
Inflammation	*Adgre1*	F4/80
	Agr1	Arginase-1
	Cd86	CD86 Antigen
	IL1b	Interleukin 1 Beta
	IL6	Interleukin 6
	Mrc1	Macrophage mannose receptor 1 (CD206)
	Nos2	Nitric Oxide Synthase 2
	Tnf	Tumor Necrosis Factor
Mitochondria	*Hspa9*	Heat Shock Protein Family A (Hsp70) Member 9
	Lrpprc	Leucine-rich PPR motif-containing protein
	Ndufv2	NADH:Ubiquinone Oxidoreductase Core Subunit V2
	Sdha	Succinate Dehydrogenase Complex Flavoprotein Subunit A
	Tfam	Mitochondrial Transcription Factor 1

Table 7. Genes analyzed with TaqMan probes.

3.16 Assessment of kidney function

Animal kidney function was determined by analyzing the indicators, serum creatinine and Blood Urea Nitrogen (BUN). They were analyzing by using the QuantiChrom TM Creatinine Assay Kit (Bioassay systems, Hayward, CA) and the Blood Urea Nitrogen (BUN) Colorimetric Detection Kit (Ann Arbor, MI), respectively, according to the manufacturers' instructions. Serum was obtained from blood samples by centrifugation at 3000 rpm for 15 min.

Evaluation of kidney function in humans is based in the universal clinical guidelines for the evaluation of CKD, Kidney Disease Improving Global Outcomes (KDIGO). It defined CKD as kidney structural damage and/or glomerular filtration rate (GFR) <60 mL/min/1.73 m^2 for 3 months or more, irrespective of cause. Kidney damage in many kidney diseases can be ascertained by the presence of albuminuria, defined as albumin-to-creatinine ratio >30 mg/g in two of three spot urine specimens. GFR can be estimated from calibrated serum creatinine and estimating equations, such as the Modification of Diet in Renal Disease (MDRD) Study equation, Chronic Kidney Disease Epidemiology Collaboration (CKD-EPI) or the Cockcroft-Gault formula. The average glomerular filtration rate reference values for the MDRD and CKD-EPI cohorts

assessed for equation development were 39,8 and 68,0 mL/min per 1,73 m^2, respectively. Kidney disease severity is classified into five stages according to the level of GFR [240].

GFR was estimated in stage 3-4 CKD patients (Hospital Principe de Asturias) by assessing creatinine, MDRD and CKD-EPI indicators. A cohort of 100 CKD patients was selected for the analysis of microRNAs plasma levels. It included two clearly differentiated subgroups differentiated by the evolution of their renal function base on the MDRD indicator over a period of 24 months: 50 patients presented less than 10% of kidney function deterioration while the rest of them had experienced at least a 40% reduction in kidney function or had initiated renal replacement therapy (dialysis). Triglyceride plasma level was also reported for these patients. Relevant clinical information for these patients can be found in **Supplementary table 2** and **Supplementary table 3**.

Fibrosis degree was stimated in kidney biopsies from 26 patients with graft dysfunction following kidney transplantation (Hospital Ramón y Cajal). All biopsies were evaluated according to the Banff 2007 criteria [241].

3.17 miRNA analysis in blood plasma from CKD patients

The levels of selected microRNAs were analyzed in plasma samples from the cohort of 100 CKD patients described above (Hospital Universitario Principe de Asturias, Madrid, ES). Peripheral venous blood was collected in EDTA spray-coated vacutainers (BD, Franklin Lakes, NJ). To obtain plasma blood was centrifuged at 400 g for 20 min, supernatant was transferred into a new tube and centrifuged at 800 g for 20 min. Plasma was collected and stored frozen in aliquots at −80 °C. Plasma miRNA was extracted from blood using miRCURY™ RNA Isolation Kit—Biofluids and UniSp2 Spike-in RNA (Exiqon, Vedbaeck, Denmark). Analysis of miR-33 and miR-150 levels in these samples were performed as described in the quantification of miRNA expression procedure section.

3.18 Quantification of kidney cell populations by flow cytometry

Multiparametric flow cytometry was used for the identification of macrophage and epithelial cell population. Kidneys were decapsulated, diced, then incubated at 37ºC for 30 min with 0.5 mg/ml liberase DL (Roche Basel, Switzerland) and 100 U/ml DNase (Roche Basel, Switzerland) in serum free DMEM. After centrifugation (10 min, 2500 rpm at 4ºC), cells were resuspended in 5ml of buffer (1% BSA and 1% FBS in PBS) and filtered (40µm). For staining, 10^6 cells were dissolved in 50 µl of buffer and pre-incubated with 0.25 µl CD16/CD32 (BioLegend, San Diego, CA) to block interactions with the Fc domain of immunoglobulins. Three µl of 4,6-diamidino-2-phenylindole (DAPI) (1:15000) (Sigma, St. Louis, MO) was added to stain dead cells. Cell suspensions were incubated with specific fluorochrome-conjugated antibodies (BioLegend, San Diego, CA) listed in (**Table 8**). For each experiment, flow minus one (FMO) controls was performed for each fluorophore to establish gates by using corresponding antibodies listed in **Table 8**. Fluorescence intensity was measured in a BD FacsCantoTM II cytometer (BD Bioscience, San José, CA) and analyzed with the FlowJo 10.2 software (FlowJo, LLC, Ashland, OR). For each kidney sample, at least 20.000 singlets were analyzed in triplicates. Negative gates were set to exclude other cell types from the positive selection by using appropriate isotype control antibodies. Cells gating was initially based in the Forward versus Side scatter (FSC vs SSC) plot. Next, dead cells were excluded. Identification of the macrophage cell population

was based on the presence of CD45, expressed in inflammatory and hematopoietic cells and F4/80, a specific macrophage surface marker. CD86 and CD206 were used to determine M1 and M2 macrophage subpopulations, respectively. Identification of the epithelial cell population was based on the presence of the epithelial cell adhesion molecule (EpCAM) and the absence of CD45. The subsequent display of positive CD24 determined injured proximal tubule epithelia. Numbers in quadrants indicate cell proportions in percent of cells that co-express both markers.

Antibody	Antibody Reference	Isotype control antibody	Isotype control antibody Reference
APC anti-human CD45	368511 (Clone 2D1)	APC Rat IgG2b	400611 (clone RTK4530)
FITC anti-mouse F4/80	123107 (Clone BM8)	FITC Rat IgG2a	400505 (Clone RTK2758)
APC anti-mouse CD86 Antibody	105113 (Clone PO3)	APC Rat IgG2b	400611 (Clone RTK4530)
PE anti-mouse CD206	141705 (Clone C068C2)	PE Rat IgG2a	400507 (Clone RTK2758)
APC/Cy7 anti-mouse CD326 (Ep-CAM)	118217 (Clone G8.8)	APC/Cy7 Rat IgG2a	400523 (Clone RTK2758)
PE anti-mouse CD24	101807 (Clone M1/69)	PE Rat IgG2b	400607 (Clone RTK4530)

Table 8. Antibodies for flow cytometry analysis. All were from Biolegend (San Diego, CA)

3.19 Immunofluorescence

A quarter piece of each kidney sample (obtained after dissection in half both lengthwise and crosswise) was immersed sequentially in 4% neutral buffered formalin for 24 hous, in 30% sucrose in PBS until tissue sank (6-12 h) and embedded in Tissue-Tek® OCT for cryoprotection at -80ºC. OCT blocks were cut in serial frozen sections (10µm thickness). These sections were fixed with 4% PFA for 10 min and permeabilized with 0.25% Triton X-100 in PBS for 5 min at room temperature (RT). Next, they were washed with PBS, blocked with 1% BSA in PBS for 30 min at RT and incubated for 1 h for staining with specific primary antibodies: anti-CPT1A antibody (1:1000, ab128568, Abcam, Cambridge, UK), biotinylated lotus tetragonolobus lectin (LTL) (1:1000, B-1325, Vector Laboratory, (Burlingame, CA) anti-β-F1-ATPase (clone 11/21-7 A8, 1: 1.000), kindly provided by Dr. Jose Manuel Cuezva (UAM, ES [242]. Subsequently, sections were washed with PBS incubated with the corresponding fluorochrome-conjugated secondary antibodies: Alexa Fluor 555 anti-Mouse antibody (1:1000, A-21137, Thermo Scientific, Rockford, IL), (1:1000, A-21206, Thermo Scientific, Rockford, IL), Streptavidin Alexa Fluor™ 555 Conjugate (1:400, S32355, Thermo Scientific, Rockford, IL), respectively for 1h at RT. Nuclei were stained with DAPI (Sigma, St. Louis, MO) for 5 min at RT. The cover slips were mounted on slides using mowiol (Calbiochem). Tissue fluorescence was visualized by a LSM 510 Meta Confocal microscope with a 40X/1.3 oil Plan-Neofluar M27 objective (Zeiss, Oberkochen, Germany).

3.20 Histological analysis

A quarter piece of each kidney sample (obtained after dissection in half both lengthwise and crosswise) was immersed in 4% neutral buffered formalin for 24 hous, embedded in paraffin, cut in serial sections (5µm thickness) and stained with hematoxylin and eosin, Masson´s trichome and Sirius red stainings as described previously [243]. All stainings were performed in the histology facility of the National Center of

Biotechnology (Madrid, Spain). Fibrosis was quantified in Sirius red-stained sections in order to detect collagen fibers. The area of interstitial fibrosis was identified, after excluding the vessel area from the region of interest, as the ratio of interstitial fibrosis or collagen deposition to total tissue area and expressed as %FA (fibrotic area). For each kidney, 10–15 fields were analyzed with a 40X objective lens under transmitted light microscopy by using a digital camera (Nikon D3) connected to a Nikon's Eclipse TE2000-U light microscope (Nikon Instruments Europe B.V., Badhoevedorp, The Netherlands). All measurements were performed blind in an automated mode using the ImageJ 1.48 software (http://rsb.info.nih.gov/ij). Furthermore, qualitative evaluation of the tissue was performed by a renal pathologist in a blinded fashion.

3.21 Electron microscopy examination

The number of mitochondrial and their structure was analyzed by standard transmission electron microscopy. Renal cortex pieces were cut into small blocks (1 mm^3) and fixed by immersion in fixative (4% paraformaldehyde/2% glutaraldehyde in 0.1 M phosphate buffer) for overnight at 4ºC. After washing with cold PBS and incubated in 1% osmium tetroxide and 1% potassium ferricyanide in water for 1 hour at 4ºC. Pieces were sequentially stained with 0.15% tannic acid (in 0.1 M phosphate buffer) for 1 min at room temperature (RT), and 2% uranyl acetate in water for 1 hore at RT. Next, they were dehydrated in graded ethanol, and embedded in EmBed812 resin (Electron Microscopy Sciences, Fort Washington, PA). Serial ultrathin sections (70 nm) of the tissue were collected on copper mesh grids. Three grids from each sample were examined using a JEOL 1230 transmission electron microscope, and digital photographs were captured by real-time digital imaging.

3.22 Measurements of oxygen consumption rate

Fatty acid oxidation-associated oxygen consumtion rate (OCR) (ligated to oxidative phosphorylation) and extracellular acidification rate (ECAR) (associated with lactate production and glycolysis) were studied using SeaHorse Bioscience metabolic analyzer according to the manufacturer's instructions [244]. HKC-8 cells were seeded in a p60 plate and microRNA transfection or adenovirus-mediated CPT1A overexpression was performed (as shown in the transfection procedure and adenovirus-mediated overexpression sections, respectively) when they reached a confluence of 70% and 48 hours later, HKC-8 cells were treated with 10 ng/ml TGF-β1 for 48 h. In the case of primary kidney epithelial cells, they were seeded in a p60 plate and when they reached a confluence of 70%, they were treated with 10 ng/ml TGF-β1 for 48 h. In all cases, cells were then seeded at 2×10^4 cells per well in a Seahorse Bioscience XFe24 cell culture microplate (Seahorse Bioscence, North Billerica, MA). After cell adherence, growth medium was replaced with substrate-limited medium, Dulbecco's Modified Eagle Medium (DMEM) supplemented with 0.5 mM Glucose and 1 mM Glutamate. One hour before the assay measurement, cells were incubated with Krebs-Henseleit Buffer (KHB) assay medium supplemented with 0.2% carnitine at 37ºC without CO_2. Fifteen minutes before the assay, the CPT1 inhibitor Etomoxir (Eto) (Sigma-Aldrich, St. Louis, MO) 400 µM was added to the corresponding wells and cells were incubated at 37ºC without CO_2. Finally, just before starting the assay, BSA or 200 mM Palmitate-BSA FAO Substrate (Agilent Technology, Santa Clara, CA, USA) was added.

Immediately, XF Cell Mito Stress Test was performed in a Seahorse XFe24 energy analyzer by adding sequentially during the assay several modulators of mitochondrial function. First the ATP synthase inhibitor

oligomycin (Sigma-Aldrich, St. Louis, MO) (1 μM) was used following basal measurement. This decreases electron flow through the ETC, resulting in a reduction in mitochondrial respiration. Next, the uncoupling agent cyanide 4-(trifluoromethoxy) phenylhydrazone (FCCP) (Sigma-Aldrich, St. Louis, MO) (3 μM), that collapses the proton gradient and disrupts the mitochondrial membrane potential was added. As a result, electron flow through the ETC is uninhibited, and oxygen consumption by complex IV reaches its maximum. The third and last injection is a mixture of the complex III and I inhibitors antimycin/rotenone (Sigma-Aldrich, St. Louis, MO) (1 μM). This combination shuts down mitochondrial respiration and enables the calculation of non-mitochondrial respiration driven by processes outside the mitochondria. Substrates/inhibitors were prepared in the same medium in which the experiment was conducted and were injected from the reagent ports automatically at the times indicated.

Measurements were registered for 3-minute periods of time (over a total period of 2 hours) and values were normalized for total protein content. Protein was extracted from wells with 0.1% NP-40-PBS solution, and quantified with BCA protein assay (Thermo Scientific, Rockford, IL). Four wells were used for each experimental group. The seahorse XFp Cell Mito Stress Test profile showing the key parameters of mitochondrial function is represented in **Figure 19**. Basal mitochondrial respiration, ATP-linked respiration, proton leak (non-ATP–linked oxygen consumption), maximal respiration, non-mitochondrial respiration and reserve respiratory capacity were determined as described [245].

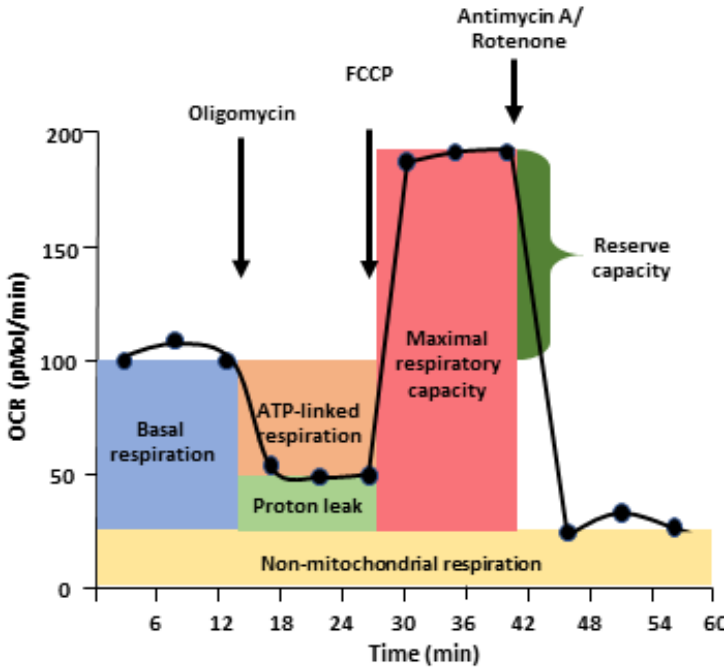

Figure 19. Representative curve of OCR dynamics with commonly used reagents used for the study of mitochondrial respiration. Oxygen consumption rate (OCR) is measured before and after the addition of inhibitors to calculate the magnitude of several phases and parameters of mitochondrial respiration. Oligomycin: ATP synthesis inhibitor; FCCP: membrane potential uncoupler; Antimycin A: complex III inhibitor; Rotenone: Complex I inhibitor.

The absence or limitation of exogenous substrates other than palmitate in combination with Etomoxir allows to determine the intrinsic rate and capacity of a cell to oxidize fatty acids (FAs) including exogenous FAs, endogenous FAs or uncoupling by FAs (**Figure 20**).

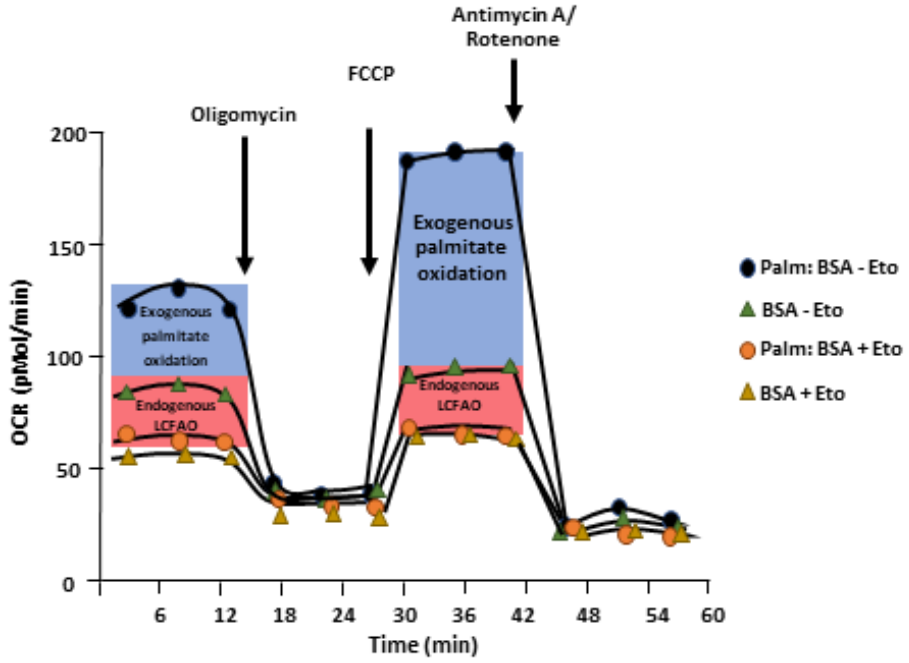

Figure 20. Representative curve of OCR dynamics with commonly used reagents used for the study of mitochondrial respiration. Oxygen consumption rate (OCR) is measured in the presence or absence of Palmitate-BSA and the CPT1 inhibitor, Etomoxir (Eto), before and after the addition of mitochondrial complexes inhibitors to calculate the magnitude of the contribution of endogenous and exogenous fatty acid to overall mitochondrial respiration. Oligomycin: ATP synthesis inhibitor; FCCP: membrane potential uncoupler; Antimycin A: complex III inhibitor; Rotenone: Complex I inhibitor; Eto: Etomoxir; LCFAO: long chain fatty acid oxidation.

3.23 Mitochondrial membrane potential (MMP)

Changes in MMP were determined as differences in tetramethylrhodamine methyl ester (TMRM) fluorescence (Invitrogen, Carlsbad, CA, USA). It accumulates in negatively charged polarized mitochondria and fluoresces in orange. When mitochondrial membrane potential collapses in apoptotic or metabolically stressed cells, the TMRM reagent is dispersed throughout the cell cytosol and fluorescence levels drop dramatically.

HKC-8 or HREC cells were cultured and transfected as described in the cell culture and transfection procedure sections, respectively and 48 hours later cells were treated with 10 ng/ml TGF-β1 for 48h. Next, growth medium was replaced by phenol-red free Hank's Balanced Salt Solution (HBSS) with 10 mM Hepes. Treatments with oligomycin (5 µM) and FCCP (4 µM) for 5 min were used as positive and negative control conditions. Next, cells were stained with 250 nM TMRM for 30 min at 37 °C. Mitotracker® GREEN FM (100 µM) (Invitrogen, Carlsbad, CA, USA) was used as counterstaining. Cells were harvested with trypsin, centrifuged (3000 rpm, 5 min) and the pellet was resuspended in 200 µL HBSS with 1% Bovine Serum Albumin (BSA) and 5mM ethylenediaminetetraacetic acid (EDTA). Fluorescence intensity was measured by flow cytometry using an emission wavelength of 516 nm and 570 nm for Mitotracker® GREEN FM (FL1) and TMRM (FL2), respectively [246] in a BD FacsCanto™ II system (BD Bioscience, San José, CA) and analyzed with the FlowJo 10.2 software (FlowJo, LLC, Ashland, OR). For each experimental condition, at least 20,000 singlets were analyzed in triplicates.

3.24 Mitochondrial superoxide radical anion production

Evaluation of superoxide radical anion production was performed by using MitoSOX™ Red mitochondrial superoxide radical anion indicator (Invitrogen, Carlsbad, CA, USA), a highly selective

fluorogenic dye for mitochondrial superoxide radical anion in live cells, according to the manufacturer's instructions.

HKC-8 or HREC cells were cultured and transfected as described in the cell culture and transfection procedure sections, respectively and 48 hours later, cells were treated with 10 ng/ml TGF-β1 for 48h. Next, growth medium was replaced by phenol-red free Hank's Balanced Salt Solution (HBSS) with 10 mM Hepes. Treatment with antimycin A (150 µM) and FCCP (50 µM) for 5 min were used as positive and negative control conditions. Next, cells were stained with 5 µM MitoSOX™ Red for 30 min at 37 °C. Mitotracker® GREEN FM (100 µM) (Invitrogen, Carlsbad, CA, USA) was used as counterstaining. Cells were harvested as described in the mitochondrial membrane potential section. Fluorescence intensity was measured by flow cytometry using an emission wavelength of 516 nm and 580 nm for Mitotracker® GREEN FM (FL1) and MitoSOX™ Red (FL2), respectively [247] in a BD FacsCanto™ II system (BD Bioscience, San José, CA) and analyzed with the FlowJo 10.2 software (FlowJo, LLC, Ashland, OR). For each experimental condition, at least 20,000 singlets were analyzed in triplicates.

3.25 Adenovirus-mediated CPT1A overexpression

CPT1A overexpression in cells was driven and transduced by adenoviral particles. Adenoviruses carrying GFP (AdGFP) and CPT1A (AdCPT1A) were kindly provided by Dr. Laura Herrero (Universidad de Barcelona, ES). Adenoviruses were amplified, purified and titrated according to [248]. Briefly, adenovirus production consisted of two rounds of amplification. In the first amplification round, HEK293A cells in a 100 cm^2 dish at 70% confluence growing in complete medium supplemented with 5% of FBS (infection media) were infected with 50 µl of the adenovirus stock, while in the second amplification round, 10 X 100 cm^2 dishes of 70% confluent HEK 293A cells /virus type were infected with 400 µl of the first amplification of the adenovirus. After 20 h, cells from all dishes were harvested together by scraping and centrifuged (1,000 rpm for 5 min at 4ºC). The cell pellet was disrupted by 3 cycles of freeze and thaw using liquid N_2 and resuspended in 5 mL of infection media. Cell debris was discarded by centrifugation at 3,000 rpm for 10 min at 4ºC and supernatant containing adenoviruses was stored in 500 µl aliquots to be used throughout the experiments (**Figure 21**). Titration was performed by using the Adeno-X™ Rapid Titer Kit (Clontech Laboratories, Palo Alto, CA) according to the manufacturer's instructions, which is based on the antibody specific detection of the adenoviral hexon protein by peroxidase (HRP).

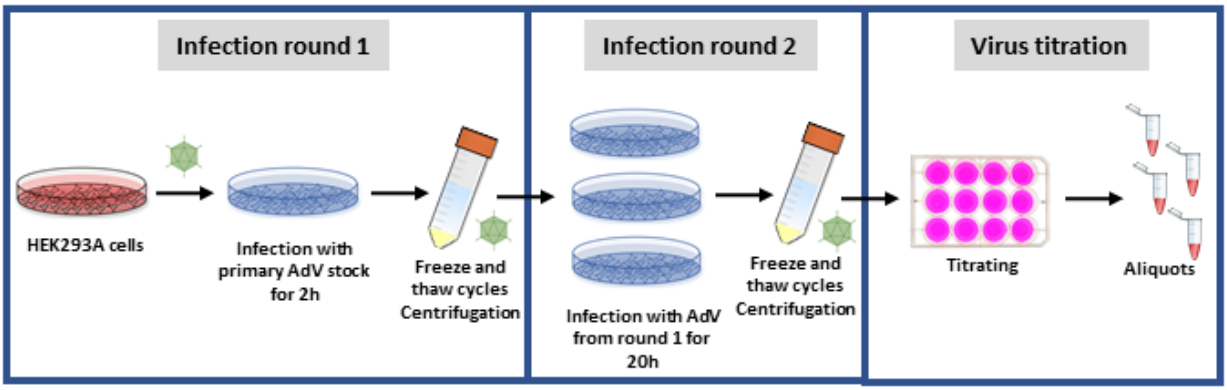

Figure 21. Workflow scheme for adenovirus amplification and titration. HEK293A cells are infected with adenoviruses (AdV) carrying GFP (AdGFP) and CPT1A (AdCPT1A) in two sequential amplification rounds. Adenovirus production was titrated and stored at -80ºC. See text for details.

HCK8 cells were seeded into 60 mm culture dishes to reach a confluence of 70%. They were infected with adenoviruses AdGFP and AdCPT1A [100 moi (multiplicity of infection)] for 24 h in serum-free DMEM/F12 (supplemented with 15 mM Hepes, 5% FBS, 1x ITS, 0.5 µg/ml hydrocortisone, 50 units/mL penicillin and 50 µg/mL streptomycin) and then the medium was replaced with complete medium for additional 24 h. Adenovirus infection efficiency was assessed in AdGFP-infected cells by immunofluorescence.

3.26 Statistical analysis

Data were analyzed using nonparametric tests except where indicated. The difference between two independent groups was examined with Mann-Whitney test, while more than two groups were compared with Kruskall-Wallis test. A *P*-value of 0.05 or less was considered statistically significant ($^{*/\#}$: $P < 0.05$, $^{**/\#\#}$: $P < 0.01$, $^{***/\#\#\#}$: $P < 0.001$). Data were analyzed using GraphPad Prism 6.0 (GraphPad Software, La Jolla, CA). Data are reported as mean ± standard error of mean (SEM).

4.Results

4.1 Generation of a transgenic mouse model with inducible renal overexpression of CPT1A (*Cpt1a* knock-in)

4.1.1. –Generation process of the transgenic mouse model for inducible *Cpt1a* gene in renal epithelial cells

In order to test the *in vivo* relevance of CPT1A and FAO for renal fibrosis, a mouse model with conditional, inducible expression of *Cpt1a* in the renal tubular epithelium was engineered as described in Methods. Next, these mice were crossed with mice providing renal epithelial tissue specificity, *Pax8-rtTA*. The resulting mice expressed an optimized reverse tetracyclin-controlled transactivator (rtTA2s-M2) under the control of the Paxillin-8 gene promoter, which permits tissue specific expression of *Cpt1a* gene bearing TRE in proximal and distal tubules and collecting duct after doxycyclin administration (**Figure 11**). Extrarenal expression only occurs at the level of the thyroid [223].

4.1.2. –Evaluation of Dox-induced GFP expression in CPT1A clones

To assess the electroporation efficiency and the inducibility of the Tet-on system in individual ES clones, Dox-induced GFP expression was measured by flow cytometry. Dox-induced CPT1A was also analyzed by western blot. The percentage of GFP positive cells was determined in 13 different clones before and after doxycycline is listed in **Figure 22**. This percentage ranged from 2 to 10 among different clones. ES clones numbered 6, 11, 20 and 25 (in bold in **Figure 22**) presented the higher induction in GFP levels. In all cases, we did not observe any leakiness of the system due to GFP expression in the absence of dox. Dox-induced CPT1A protein abundance was also analyzed in these clones to assess the inducibility of this system. Clones numbered 10, 12 and 25 showed significant increase in CPT1A protein expression after doxycycline treatment (**Figure 23**). ES cells from clone number 12 displayed the higher Tet-on system inducibility. To improve the amount of positive cells of these clones, cells expressing GFP were sorted, expanded and the proportion of GFP cells re-evaluated. After a second sorting round, the percentage of GFP cells was around 30%. Correct transgene integration was confirmed by sequencing and cells were used to generate chimeric mice.

A

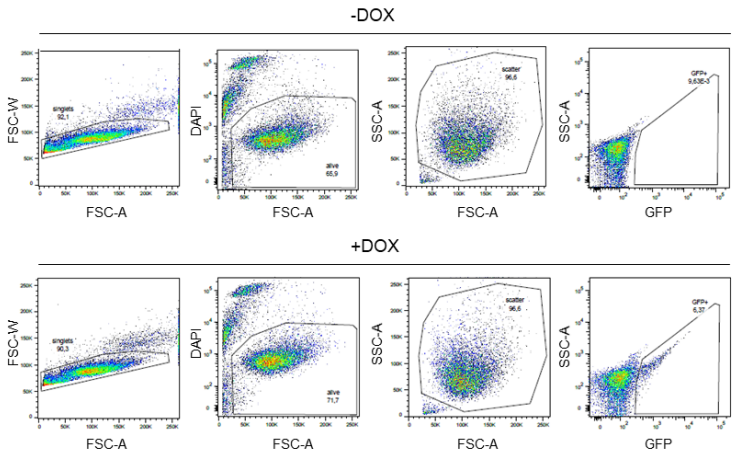

B

Clone number	% GFP (-DOX)	% GFP (+DOX)
6	**9,63 x 10^{-3}**	**6.37**
8	0	2.81
9	0	5.76
10	0	1.47
11	**0,019**	**9.61**
12	0	4.16
13	0	2.78
16	0	5.12
19	0	2.78
20	**0**	**6.29**
22	0	5.41
23	0	5.75
25	**0**	**6.36**

Figure 22. Evaluation of Dox-induced GFP expression in ES clones. (A) Dot plots representing the sequence from left to right of the flow cytometry-based strategy for the analysis of the proportion of cells that express GFP in each generated ES clone. FSC-W: forward light scatter width, FSC-A: forward-scattered light area, SSC-A: side-scattered light area. (B) Percentage of GFP positive cells determined for each one of the 13 different clones before and after doxycycline treatment. ES clones numbered 6, 11, 20 and 25 (in bold) presented the higher induction in GFP levels.

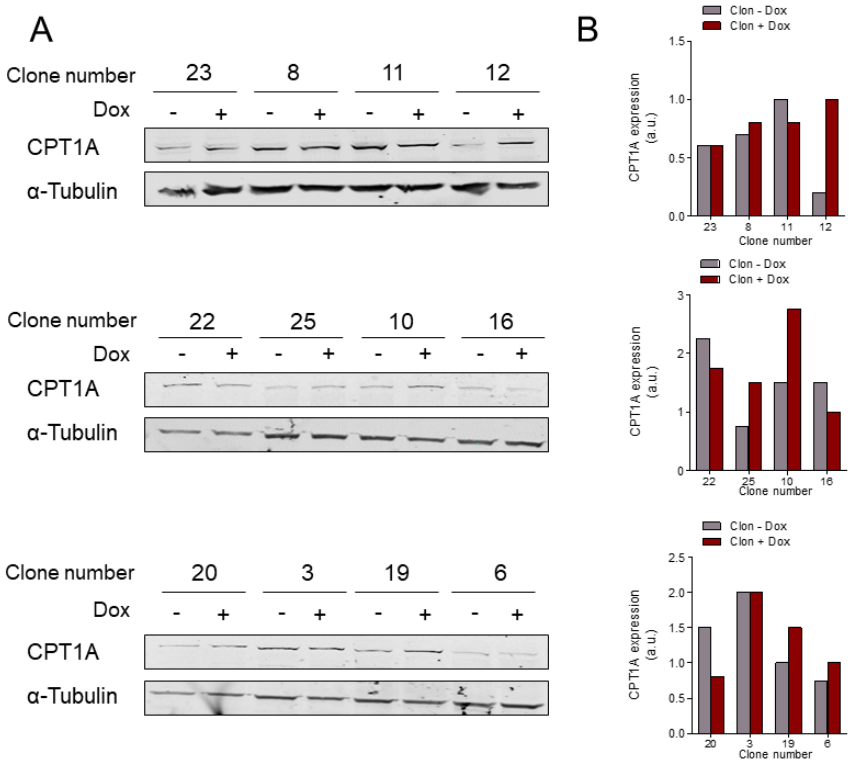

Figure 23. Evaluation of Dox-induced CPT1A expression in ES clones. (A) Western blots of CPT1A protein levels in each individual ES clone before (-) and after (+) doxycycline treatment. (B) Bar graphs represent densitometric values (arbitrary units, a.u.) of CPT1A expression in the ES clones described in (A). α-tubulin was used for normalization purposes.

4.1.3. –Genotypic characterization of the Pax8-rtTA$^{tg/0}$:tetO-Cpt1a$^{tg/0}$ mice

Generated mice were genetically characterized by PCR analysis of genomic DNA. Different alternative PCR strategies were designed for CPT1A^{tetO}, ROSA26-M2-rtTA and Pax8-rtTA alleles identification (**Figure 24**).

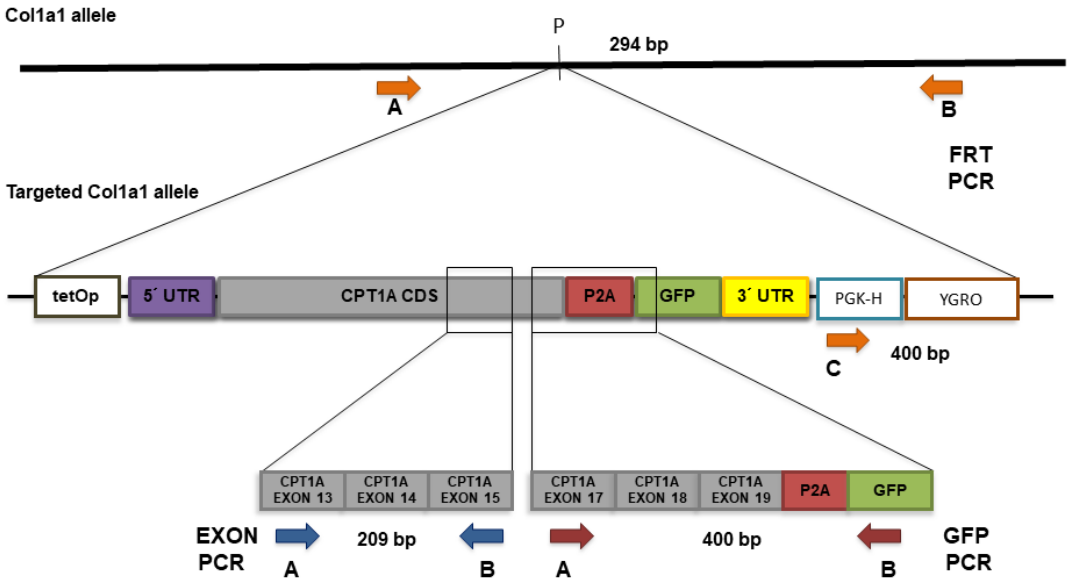

Figure 24. Genetic validation of tetO-Cpt1a$^{tg/0}$ mice. Schematic of the wild-type Col1a1 allele (top) and targeted with the *Cpt1a* gene construction (expanded). The lower diagram is a further blow-up of the indicated regions in the targeting construct. Genomic DNA analysis for the CPT1A^{tetO} allele was performed with 3 different PCR strategies, named as referred in Table 1: FRT, Exon and GFP. The positions of primers for these PCR strategies are indicated by colored arrows: FRT, orange; Exon, blue; GFP, red. For FRT PCR, amplicons are 294 bp (AB primers) and 400 bp (CB primers) corresponding to the WT and CPT1A^{tetO} alleles, respectively. For GFP PCR the amplicon is 400 bp. For Exon the amplicon is 209 bp. In both cases they correspond to the CPT1A^{tetO} allele. P: PstI restriction site. See figure 11 and table 1 for further details.

To avoid ubiquitous CPT1A overexpression, animals harboring *Cpt1a* gene bearing TRE and lacking positive ROSA26-M2-rtTA allele (**Figure 25A, lane 3**) were selected for breeding with *Pax8-rtTA$^{tg/0}$ mice.* Possible genotypes to be obtained after breeding *Pax8-rtTA$^{tg/0}$ and tetO-Cpt1a$^{tg/0}$* mice are depicted in **Figure 25B**. As expected, we detected the PCR product for the GFP gene in the case of mice with positive CPT1A^{tetO} allele (**Figure 25B, lane 1 and lane 2**). In this case, we detected the presence of the positive CPT1A^{tetO} allele as well as of the corresponding negative allele, supporting that these mice are heterozygous for that gene. Expected band sizes for the *Pax8-rtTA allele* PCR product were present in **lane 1 and lane 3 from Figure 25B**. However, only PCR products in **lane 1** represent a double heterozygous *Pax8-rtTA$^{tg/0}$:tetO-Cpt1a$^{tg/0}$* mouse. These mice can be considered as *Cpt1a* knock-in (CPT1A KI) mice and will be named hereafter as Pax8-CPT1A.

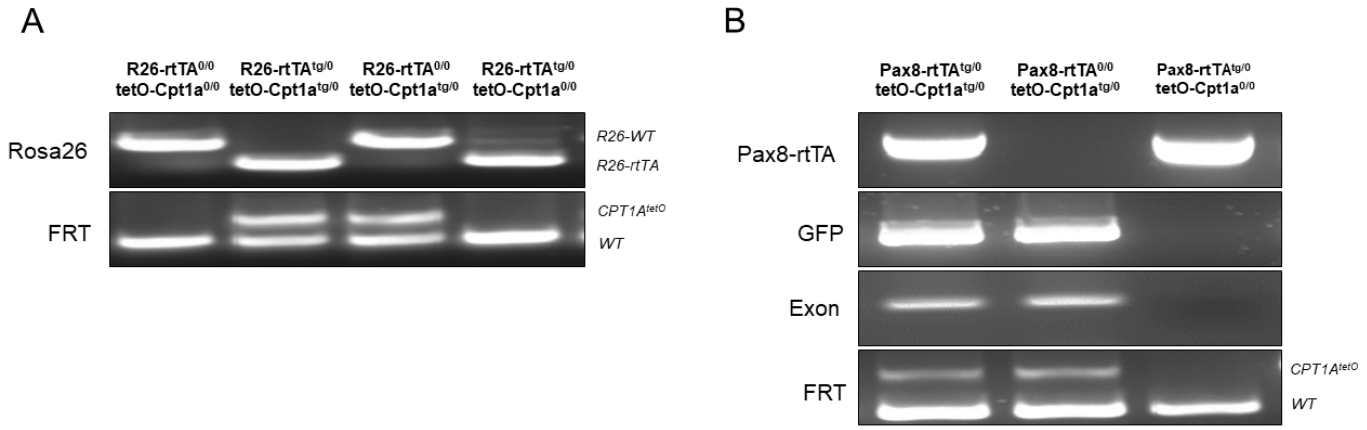

Figure 25. PCR analysis of genomic DNA for the Rosa26 and CPT1A alleles. (A) Genomic DNA analysis by PCR for the Rosa26 allele variants generates 650-bp and 300-bp amplicons for WT (R26-WT) and ROSA26-M2-rtTA (R26-rtTA) alleles, respectively as indicated in table 1. The FRT PCR is detailed in Figure 24, the presence of two bands (lanes 2 and 3) denotes heterozygosity. Animals harboring CPT1A^{tetO} allele and lacking ROSA26-M2-rtTA allele (**lane 3**) were selected for crossing with Pax8-rtTA$^{tg/0}$ mice (see Methods for details). (B) PCR analysis of offspring genotypes from these crosses. Genomic DNA analysis by PCR for the Pax8-rtTA allele generates a 595-pb band (table 1). The GFP, Exon and FRT PCRs are described in Figure 24. Double heterozygous *Pax8-rtTA$^{tg/0}$:tetO-Cpt1a$^{tg/0}$* mice (**lane 1**) were selected for experiments.

4.1.4. –Characterization of Dox-inducible *Cpt1a* gene overexpression in renal epithelial cells

We next characterized the renal specific overexpression of CPT1A in this newly generated genetic mouse model based on the doxycycline inducible transgenic system Tet-On. *Pax8-rtTA$^{0/0}$:tetO-Cpt1a$^{tg/0}$* mice (WT) were used as controls for the *Pax8-rtTA$^{tg/0}$:tetO-Cpt1a$^{tg/0}$* (CPT1A KI) mice experiments. CPT1A KI mice after doxycycline administration presented a 10-fold increase in CPT1A mRNA level in the whole kidney tissue compared with WT mice (**Figure 26A**). By contrast, the level of CPT1A protein expression in the whole kidney was 2.7-fold higher in CPT1A KI mice than in control ones (*WT*) (**Figure 26B**). Of note, no differences were observed when the liver tissue was analyzed. In the kidney, double transgenic mice after doxycycline treatment consistently displayed GFP fluorescence. Tubules were labeled by lotus tetragonolobus lectin (LTL), a marker for proximal tubules (**Figure 27A**). Similarly, induced expression of CPT1A and GFP proteins colocalized in tubule segments as evaluated by immunohistochemistry (**Figure 27B**). Importantly, overexpressed CPT1A presented a mitochondrial localization pattern, which was observed by double immunostaining by using the ATP synthase beta-subunit as a marker (**Figure 27C**). This whole set of results is consistent with a Dox-inducible expression of CPT1A in renal epithelial mitochondria in Pax8-rtTA$^{tg/0}$:tetO-Cpt1a$^{tg/0}$ mice.

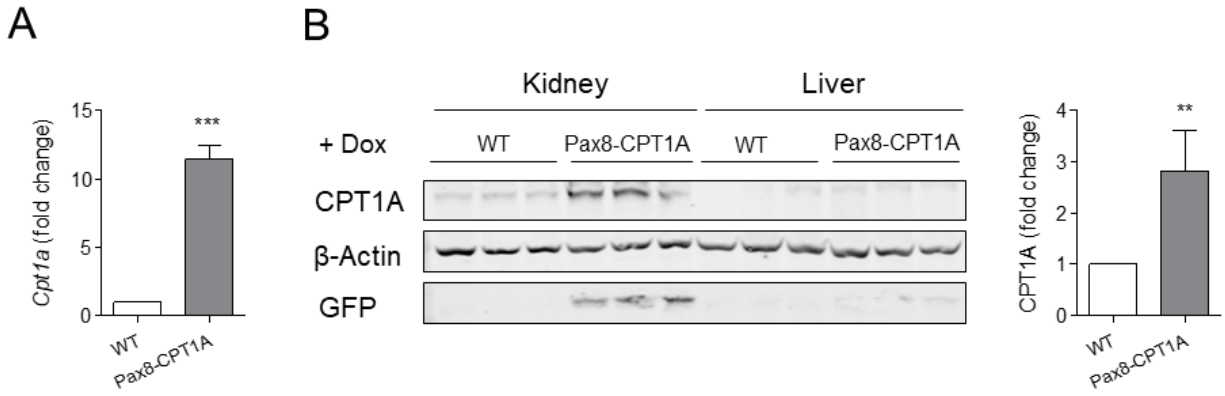

Figure 26. Dox-inducible *Cpt1a* gene overexpression in the kidney. (A) mRNA levels of *Cpt1a* gene was determined by qRT-PCR in total kidney tissue of mice treated with doxycycline for 3 weeks. (B) Immunoblots depicting protein levels of CPT1A and GFP in kidneys and livers of 3 individual mice per group. β-actin was used for normalization purposes. Bar graphs represent the mean ± s.e.m of fold changes corresponding to densitometric analyses (n = 6 mice per group). **P < 0.01, ***P < 0.001 compared to kidneys from WT mice.

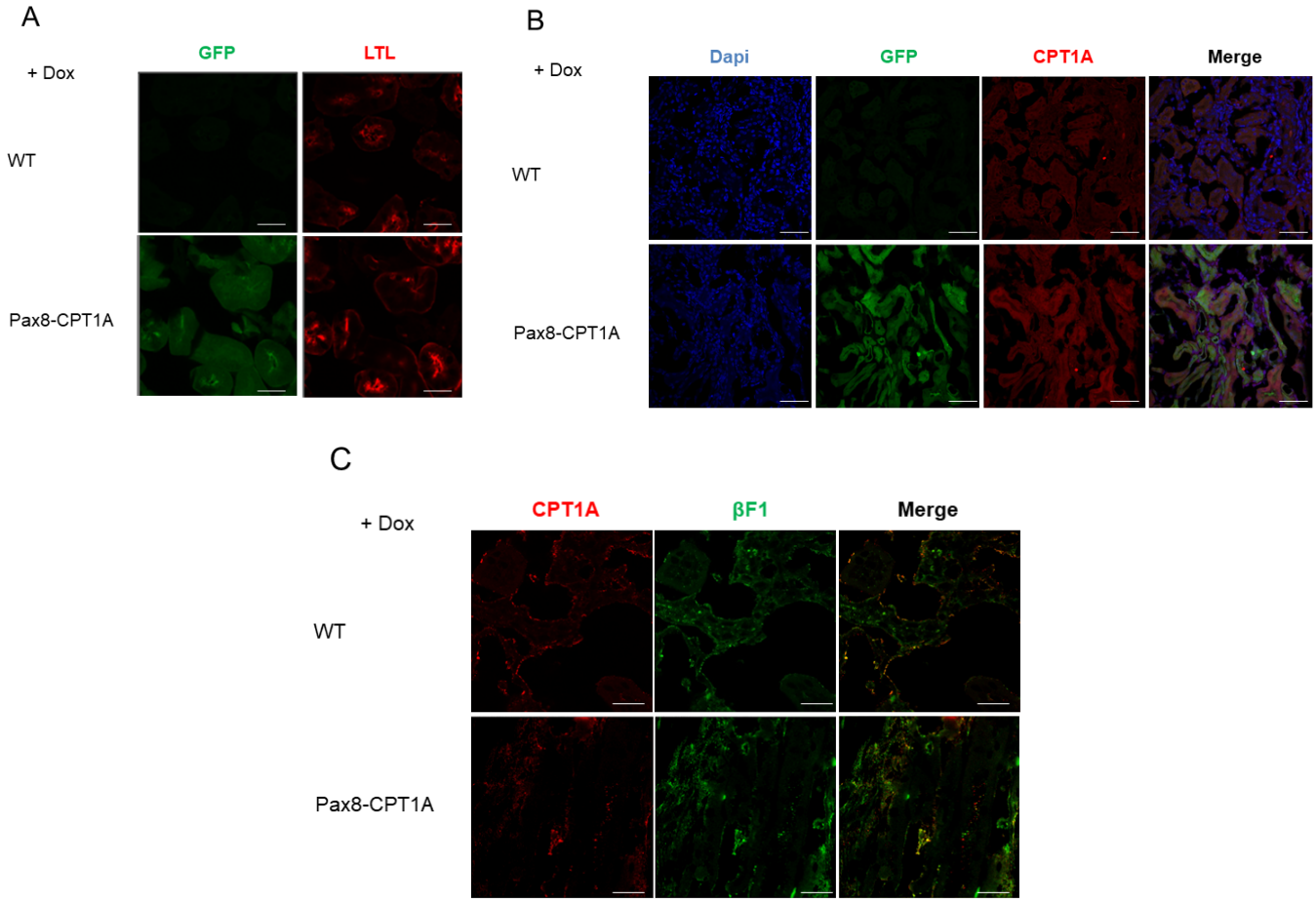

Figure 27. CPT1A and GFP proteins in kidneys from CPT1A KI mice are expressed in renal tubules. (A) Representative images of double immunofluorescence staining with the proximal tubular marker lotus tetragonolobus lectin (LTL) and GFP. (B) Staining with DAPI (nuclei), CPT1A, GFP and merge of all three. (C) Staining with CPT1A and the mitochondrial marker ATP synthase beta-subunit (βF1). All panels show immunofluorescence images of kidneys from WT and Pax8-CPT1A mice after doxycycline administration. Scale bar, 20 µm (A) and 100 µm (B and C)

4.1.5. –Dox-inducible *Cpt1a* gene overexpression in renal tubular epithelial cells improved kidney FAO rate

To assess the magnitude of CPT1A overexpression on FAO, we analyzed the capacity to oxidize radiolabeled palmitate by the renal tissue. As expected, the 2-fold increase in CPT1A protein levels in the renal epithelium increased the capacity of kidney tissue to oxidize ^{14}C-palmitate by 1.5-fold as reflected in

the levels of both ^{14}C-palmitate-derived $^{14}CO_2$ as well as in ^{14}C-palmitate-derived acid-soluble metabolites (**Figure 28**).

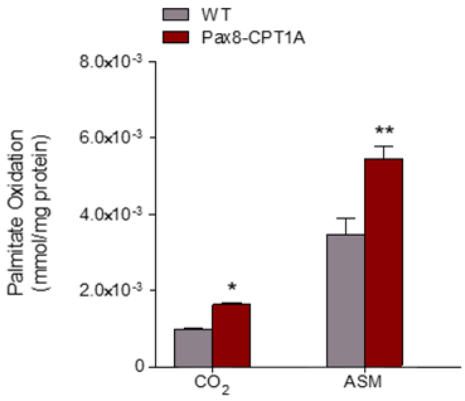

Figure 28. CPT1A overexpression in renal tubular epithelial cells enhances kidney palmitate oxidation. Radiolabeled palmitate-derived CO_2 and acid-soluble products (ASP) were determined after incubation of ^{14}C-palmitate with kidney tissue from WT or Pax8-CPT1A mice after doxycycline treatment. Bar graphs represent the mean ± s.e.m (n = 4 mice per group). *P < 0.01, **P < 0.01 compared to kidneys from WT mice.

4.2 Effects of FAO gain-of-function in kidney fibrosis

4.2.1. –CPT1A as a protective enzyme for kidney fibrosis development

As previously commented in the Introduction section, defective fatty acid oxidation in renal tubular epithelial cells has been proposed to play a key role in the development of kidney fibrosis. CPT1A is considered the rate-limiting enzyme in FAO and is critically involved in the shuttling of long chain fatty acids inside the mitochondria [174]. We hypothesized that correcting the metabolic defect in FAO may prevent CKD. To address this question, we employed different models of renal fibrosis in mice with inducible genetic overexpression of CPT1A in the renal epithelium, namely unilateral ureteral obstruction, folic acid induced nephropathy and adenine-induced renal failure.

4.2.2. –CPT1A overexpression prevents histological changes associated to experimental renal fibrosis

The UUO model generates progressive renal fibrosis. In this model, renal blood flow and glomerular filtration rate in the affected kidney are significantly reduced within 24 h, interstitial inflammation is maximal at 2–3 days while tubular dilation, tubular atrophy and fibrosis are evident after 7 days [229]. To determine whether FAO-gain-of-function could mitigate kidney fibrosis, the latter was assessed by performing UUO for 3 and 7 days in mice overexpressing CPT1A in TECs. Animals were treated with doxycycline starting three weeks prior to UUO surgery. Obstructed kidneys from WT animals showed significant tubulointerstitial architectural and histological changes 7 days after UUO, characterized by tubular atrophy, tubular dilatation and interstitial fibrosis. The extent of tubular atrophy and dilatation was markedly reduced in kidneys with increased levels of CPT1A (**Figure 29A**). To determine the effect of CPT1A on fibrosis, sirius red staining was performed to quantify the collagen content in the kidneys. Evaluation of renal lesions by light microscopy showed increased collagen deposition in the interstitial area after 7 days of the procedure in the obstructed kidneys compared to the contralateral ones in WT mice. A significant protective effect of CPT1A was observed by a reduction of 20-40% in the collagen deposition (**Figure 29A**).

To confirm the protective effect provided by the *Cpt1a* knock-in strategy we evaluated the folic acid-induced injury model. Animals were treated with doxycycline starting three weeks prior to folic acid injection. Histological parameters were evaluated in tissue samples from mice seven days after intraperitoneal (IP) injection of FA. Tubule dilation was significantly attenuated and fibrosis was markedly ameliorated in *Pax8-rtTA*$^{tg/0}$*:tetO-Cpt1a*$^{tg/0}$ compared with WT mice (**Figure 29B**).

Disruption of organ tissue architecture associated to kidney fibrosis leads to the detriment of renal function. Common parameters indicative of kidney function, blood urea nitrogen (BUN) and creatinine, were increased in animals injected with folic acid, but this variation was blunted in mice overexpressing CPT1A (**Figure 30B**). However, as expected, circulating levels of BUN and creatinine were not different between WT and *Cpt1a* knock-in mice after 7 days of UUO due to the remaining functional kidney (**Figure 30A**).

Hence, data from both models support that CPT1A overexpression exerts a protective action on the development of kidney fibrosis.

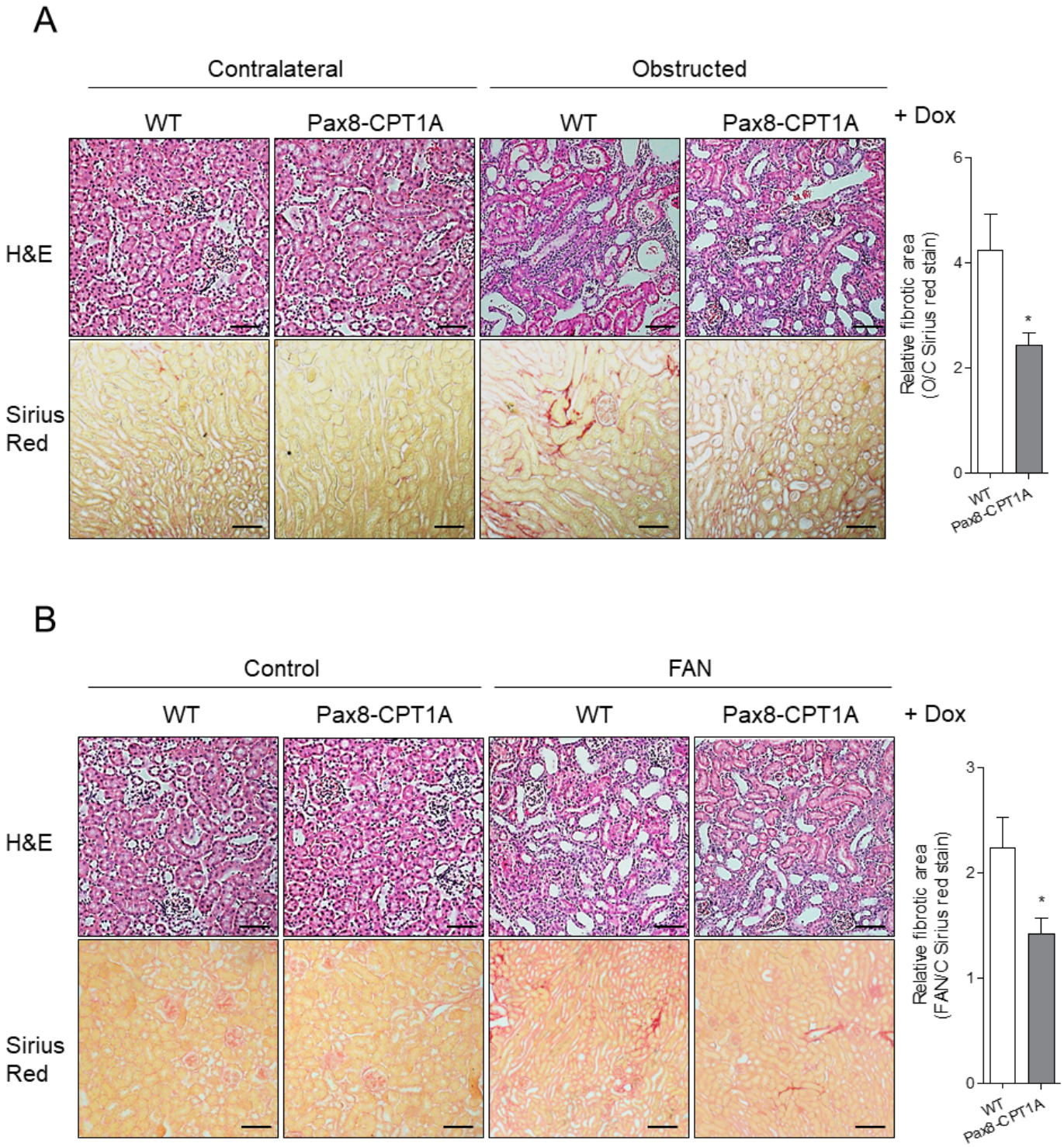

Figure 29. CPT1A overexpression prevents histological alterations associated with kidney fibrosis. Representative microphotographs from one mouse per group of hematoxylin and eosin (H&E) (upper panels) and Sirius Red (lower panels) staining of kidneys from WT and Pax8-CPT1A mice subjected to UUO for 7 days (A) and FAN (B) after doxycycline treatment (Dox). The fibrotic area is represented as Sirius Red staining of obstructed kidneys (O) related to their corresponding contralateral (C) kidneys from mice in (A) and FA-treated mouse kidneys (FAN) related to control kidneys (C) of mice from (B). Scale bars: 50 µm. For each model, quantification of Sirius Red staining was calculated as a ratio of the stained area over the total area and bar graphs represent the mean ± s.e.m, n = 6 mice per group. *P < 0.05, compared to O/C kidneys and FAN/C kidneys in WT mice, respectively.

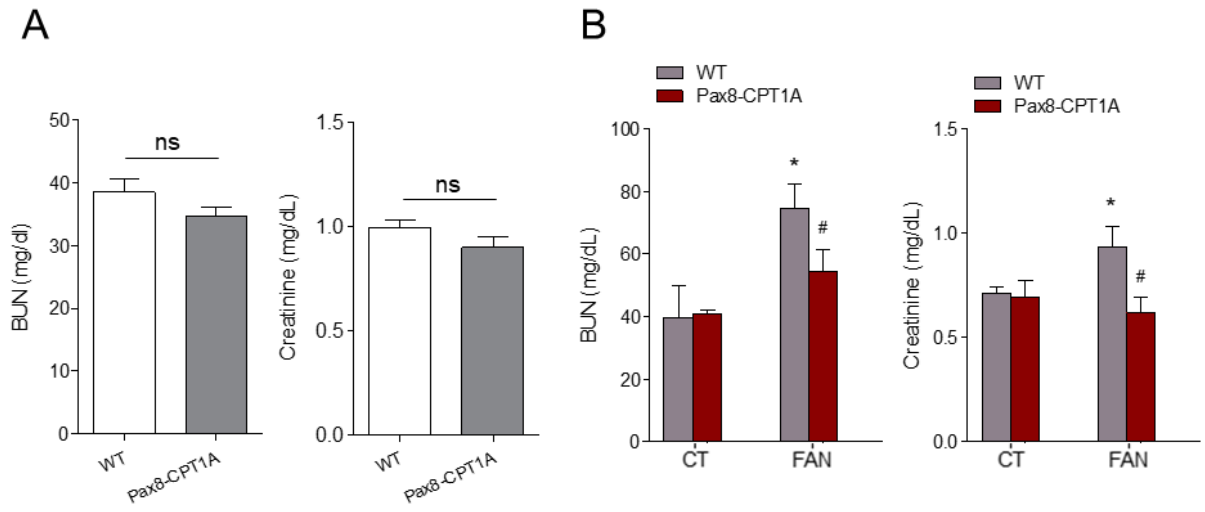

Figure 30. FAN-associated kidney function deterioration is blunted in mice overexpressing CPT1A. Serum blood urea nitrogen (BUN) and creatinine levels of WT and Pax8-CPT1A mice subjected to UUO for 7 days (A) or FAN (B) after doxycycline treatment. Data represent the mean ± s.e.m (n = 6 mice per group). *P < 0.05 compared to its respective experimental control (CT) condition; #P < 0.05, compared to WT mice with the same experimental condition; ns: no significant.

4.2.3. –CPT1A prevents the increased expression of fibrotic, apoptotic and inflammatory markers associated to kidney fibrosis

To understand the mechanisms underlying the protective action of CPT1A on renal fibrosis, we performed expression analysis of whole kidney from WT or CPT1A KI mice subjected to the UUO procedure for 7 days. Expression of genes related to critical cellular mechanisms for the initiation and perpetuation of tubular dysfunction and chronic tissue damage was analyzed by using specific TaqMan probes. They included subsets of genes related to metabolism (oxidative phosphorylation (OXPHOS), tricarboxylic acid cycle (TCA) and glycolysis), apoptosis, extracellular matrix proteins (ECM), epithelial to mesenchymal transition (EMT) and inflammation. Specific tubule induction of CPT1A protein prevented the increased expression of fibrosis-associated genes such as *Acta2* and *Col1α1* in the UUO model (**Figure 31A**). These results were supported by a parallel decrease in the fibrotic markers α-SMA and FN protein levels induced by UUO (**Figure 31B**), further supporting a role for CPT1A function in renal fibrogenesis. Noteworthy, there was an effect of CPT1A overexpression on the levels of *Havcr1*, whose gene encodes the renal proximal tubule injury marker KIM-1 (Kidney Injury Molecule-1), supporting an inhibitory effect of CPT1A in preventing epithelial dedifferentiation (**Figure 31A**). According to some authors, partial EMT is sufficient to induce tubular function impairment, triggering cell cycle arrest and promoting the release of cytokines that activate interstitial myofibroblasts [249].

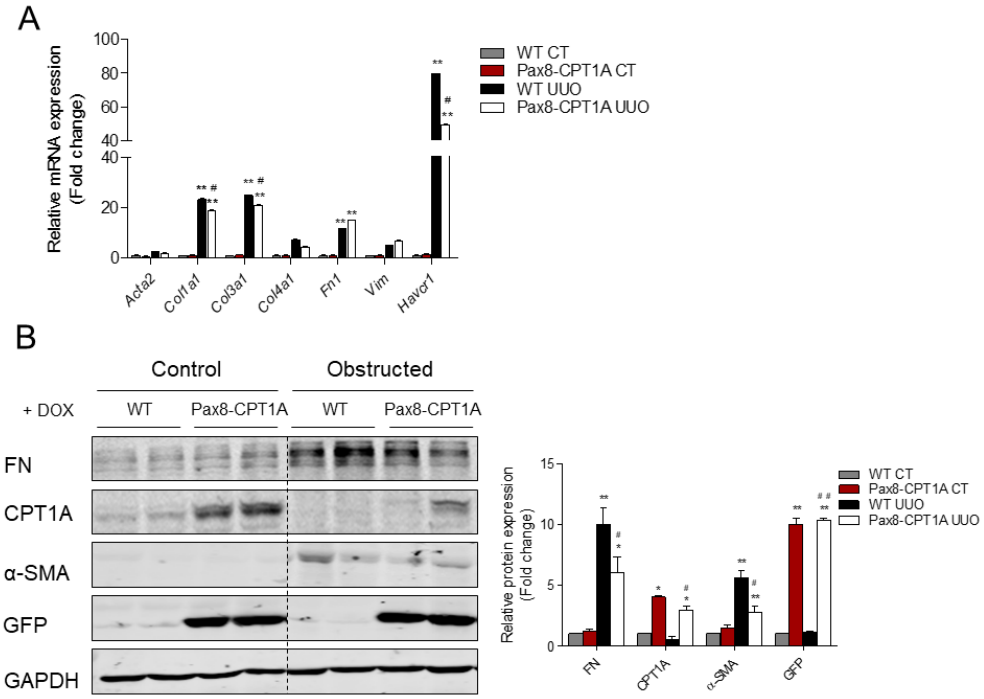

Figure 31. Renal tubule overexpression of CPT1A prevents UUO-dependent increased expression of fibrosis-associated markers. (A) mRNA levels of fibrosis-associated genes were determined by qRT-PCR using TaqMan qPCR probes in contralateral (CT) and obstructed (UUO) kidneys from WT and Pax8-CPT1A mice subjected to UUO for 7 days after doxycycline induction (see methods for details). Bar graphs represent the mean ± s.e.m. of fold changes (n = 6 mice per group). (B) Immunoblots depicting fibronectin (FN), carnitine palmitoyltransferase 1A (CPT1A), green fluorescence protein (GFP) and alpha-smooth muscle actin (α-SMA) protein levels in contralateral (CT) and obstructed (UUO) kidneys from 3 WT and 3 Pax8-CPT1A mice. Bar graphs represent the mean ± s.e.m. of fold changes corresponding to densitometric analyses (n = 6 mice per group). Glyceraldehyde-3-phosphate dehydrogenase (GAPDH) was used for normalization purposes. *P < 0.05, **P < 0.01 compared to their corresponding contralateral (CT) kidneys; #P < 0.05, ##P < 0.01 compared to kidneys from WT mice with the same experimental condition. For detailed gene nomenclature see **Supplementary table 1**.

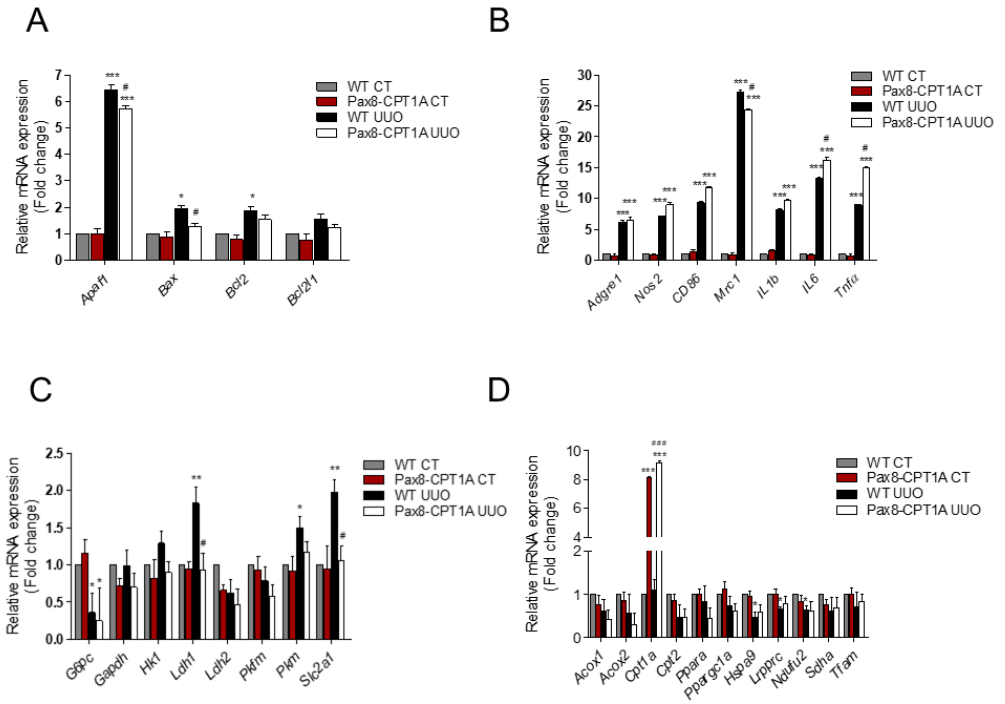

Figure 32. Renal tubule overexpression of CPT1A modifies the UUO response to apoptosis and inflammation. The mRNA levels of apoptosis- (A), inflammation- (B), glucose utilization- (C) and peroxisomal/mitochondrial function- (D) associated genes were determined by qRT-PCR using TaqMan qPCR probes in contralateral (CT) and obstructed (UUO) from kidneys of WT and Pax8-CPT1A mice subjected to UUO for 7 days after doxycycline induction. Bar graphs represent the mean ± s.e.m. of fold changes (n = 6 mice per group). *P < 0.05, **P < 0.01, ***P < 0.01 compared to their corresponding contralateral (CT) kidneys; #P < 0.05, ###P < 0.001 compared to kidneys from WT mice with the same experimental condition. For detailed gene nomenclature see **Supplementary table 1**.

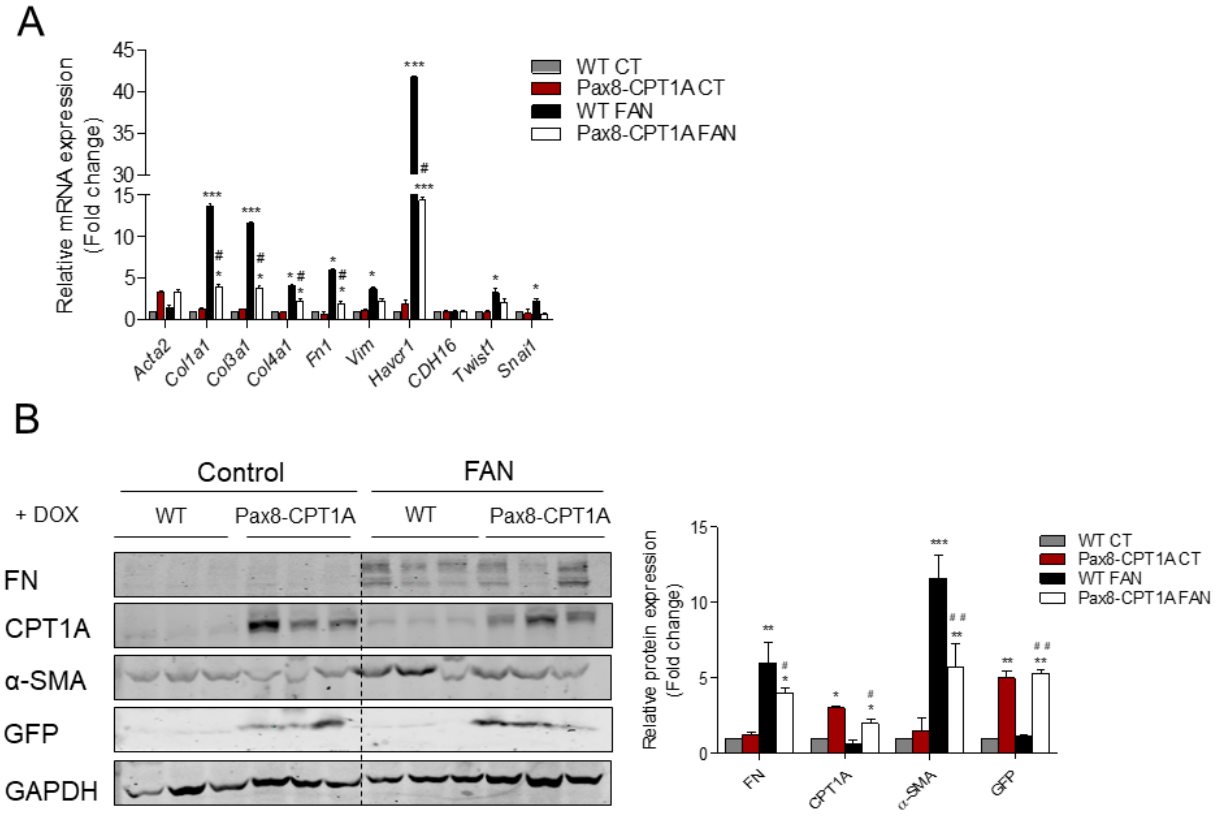

Figure 33. Renal tubule overexpression of CPT1A prevents FAN-dependent increased expression of fibrosis-associated markers. (A) mRNA levels of fibrosis-associated genes were determined by qRT-PCR using TaqMan qPCR probes in kidneys from control (CT) and FA-treated (FAN) WT and Pax8-CPT1A mice after doxycycline induction (see methods for details). Bar graphs represent the mean ± s.e.m. of fold changes (n = 6 mice per group). (B) Immunoblots depicting fibronectin (FN), carnitine palmitoyltransferase 1A (CPT1A), green fluorescence protein (GFP) and alpha-smooth muscle actin (α-SMA) protein levels in kidneys from control (CT) and FA-treated (FAN) WT and Pax8-CPT1A mice after doxycycline induction. Bar graphs represent the mean ± s.e.m. of fold changes corresponding to densitometric analyses (n = 6 mice per group). Glyceraldehyde-3-phosphate dehydrogenase (GAPDH) was used for normalization purposes. *P < 0.05, **P < 0.01, ***P < 0.001 compared to their corresponding control (CT) kidneys; #P < 0.05, ##P < 0.01 compared to kidneys from WT mice with the same experimental condition. For gene nomenclature see **Supplementary table 1**.

Some of these data were confirmed by mRNA quantitative analysis using Sybr green. Thus, the increased expression in *Col1a1*, *Fn1* and *TGFβ* genes was reduced in CPT1A KI mice, while the same trend was observed in the case of *Acta2* gene expression (**Figure 35A**). In observance with this concept, the induction of the pro-apoptotic genes *Apaf1* and *Bax* in fibrotic kidneys was moderately reduced in the kidneys from CPT1A KI mice compared with the WT ones, while the gene expression of *Bcl2l1* and the anti-apoptotic gene *Bcl2* were not altered (**Figure 32A**). In addition, 7 days after UUO, expression levels of analyzed pro-inflammatory and anti-inflammatory markers were higher in kidney tissue from mice overexpressing CPT1A than in renal samples from WT mice (**Figure 32B**).

TECs use glucose for anaerobic glycolysis. Metabolic alterations of these cells during kidney fibrosis not only involves a defect in FAO but also in glucose oxidation. However, preventive strategies for kidney fibrosis by improving FAO with genetic or pharmacological approaches did not restore defects in glucose utilization [171]. By contrast, our data shows that levels of the majority of the analyzed regulators of glucose utilization were not altered in obstructed kidneys compared to contralateral ones (**Figure 32C**). In fact, an increased expression of *Ldh1* and *Slc2a1* genes was induced by UUO, which was prevented by CPT1A overexpression (**Figure 32C**). Similarly, CPT1A-gain-of-function did not induce a major shift towards the expression of glycolytic and peroxisome/mitochondrial-related genes in contralateral kidneys (**Figure 32D**).

A similar expression pattern was observed for this subset of genes in the folic acid-induced injury model. QRT-PCR based quantification displayed lower expression of epithelial injury (Kim-1) and fibrotic markers (collagens) in kidneys from CPT1A KI mice (**Figure 33A**). These results were supported by the decrease in the FAN-induced expression of α-SMA and FN at the protein level (**Figure 33B**). Consistently, genes promoting epithelial dedifferentiation (*Twist1* and *Snail*), reflected in the loss of epithelial markers and acquisition of mesenchymal features, showed a reduce trend expression in obstructed kidneys from *Cpt1a* knock-in mice (**Figure 33A**). Some of these data were confirmed by mRNA quantitative analysis using Sybr green. Thus, the increased expression in *Col1a1* and *Fn1* expression was reduced in CPT1A KI mice (**Figure 35B**).

Of note, there was also lower expression of apoptosis (*Apaf1* and *Bax*) (**Figure 34A)** and pro-inflammatory cytokines (*IL6*, *Tnfα*, *Tgfβ*) (**Figure 34B)** in tubules of CPT1A KI mice. In this fibrosis model, there was a general downregulation trend in the expression of glycolysis-related genes, which was not recovered by CPT1A overexpression (**Figure 34C**). By contrast, FAN-induced repression in mRNA levels of the peroxisomal/mitochondrial function-related genes *Acox1*, *Cpt2, Lrpprc, Sdha* and *Tfam* were restored in kidneys from CPT1A mice (**Figure 34D**).

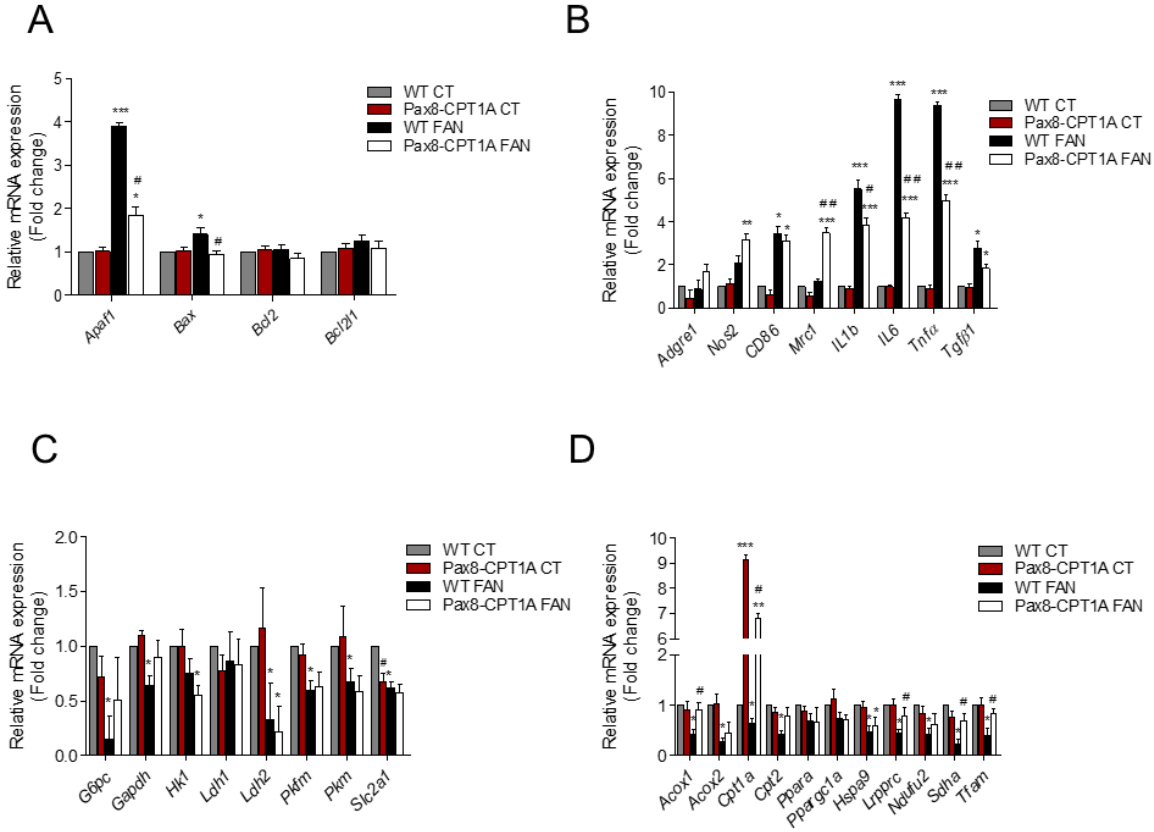

Figure 34. Renal tubule overexpression of CPT1A modifies the FAN response to apoptosis and inflammation. The mRNA levels of apoptosis- (A), inflammation- (B), glucose utilization- (C) and peroxisomal/mitochondrial function- (D) associated genes were determined by qRT-PCR using TaqMan qPCR probes in kidneys from control (CT) and FA-treated (FAN) WT and Pax8-CPT1A mice after doxycycline induction (see methods for details). Bar graphs represent the mean ± s.e.m. of fold changes (n = 6 mice per group). *P < 0.05, **P < 0.01, ***P < 0.01 compared to their corresponding control (CT) kidneys; #P < 0.05, ##P < 0.001 compared to kidneys from WT mice with the same experimental condition. For detailed gene nomenclature see **Supplementary table 1**.

These observations were also confirmed in a third mouse model for CKD, namely the adenine-induced nephrotoxicity (ADN) model. CPT1A KI mice showed a reduction in the induction in the expression of the crucial genes *Col1a1* and α-*SMA* involved in these cellular mechanisms related to kidney fibrosis (**Figure**

35C). Data collected from the three models of CKD in the CPT1A KI mice strongly support that CPT1A is an enzyme which, by itself, has a crucial impact on the outcome of fibrosis most likely due to its critical function in the facilitation of FAO.

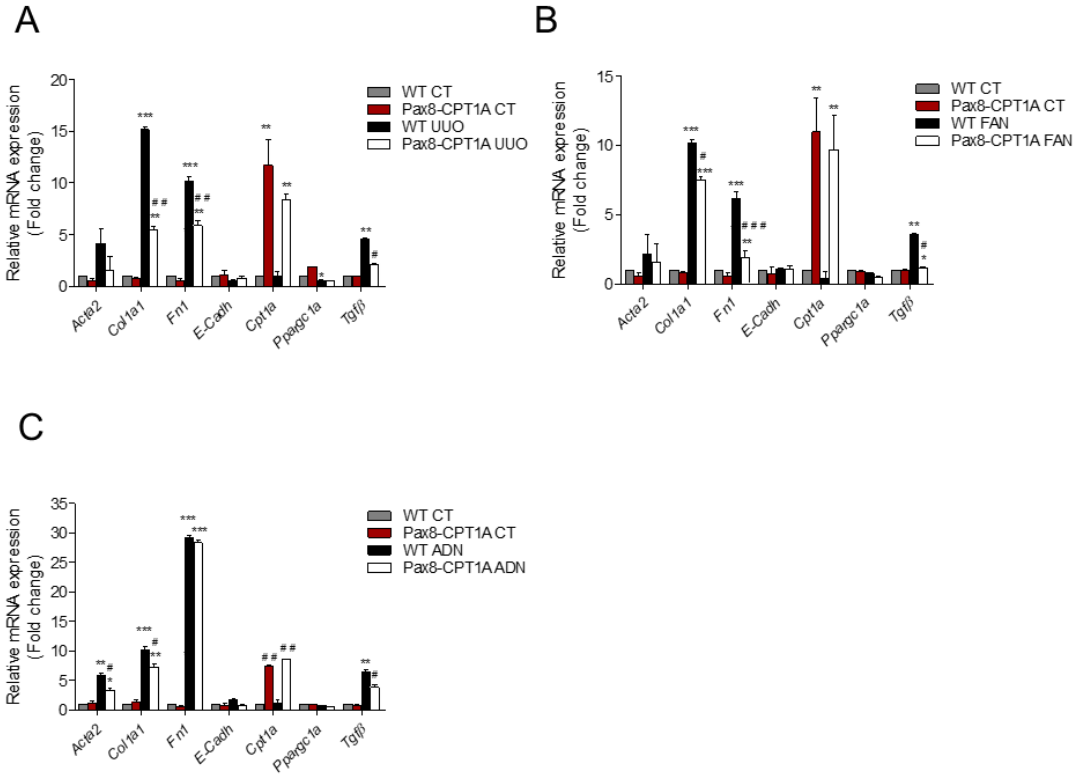

Figure 35. Renal tubule induction of CPT1A prevents kidney damage-induced expression of fibrosis-related genes in three different models. The mRNA levels of alpha-smooth muscle actin (α-SMA), alpha 1 type-1 collagen (Col1α1), fibronectin (FN), E-cadherin (E-cadh), carnitine palmitoyltransferase 1A (CPT1A), peroxisome proliferator-activated receptor gamma coactivator 1 alpha (Ppargc1a) and transforming growth factor beta (TGF-β) were determined by qRT-PCR using Sybr green in kidneys of WT and Pax8-CPT1A mice subjected to UUO (A), FAN (B) or adenine-induced nephrotoxicity (ADN) after doxycycline induction (C). Bar graphs represent the mean ± s.e.m. of fold changes (n = 6 mice per group). *P < 0.05, **P < 0.01, ***P < 0.01 compared to their corresponding control (CT) kidneys; #P < 0.05, ##P < 0.01, ###P < 0.01 compared to kidneys from WT mice with the same experimental condition.

4.2.4. –CPT1A prevents impaired mitochondrial morphology and fatty acid oxidation defect induced by fibrosis in the kidney

Renal mitochondrial abnormalities and dysfunction are common features in the pathogenesis of different forms of renal disease. Cellular pathways promoting kidney damage can compromise mitochondrial homeostasis reflected in increased oxidative stress, apoptosis, microvascular loss and fibrosis, all of which contribute to renal function deterioration [250]. Thus, we then evaluated morphological alterations of mitochondria in cortical proximal tubules by transmission electron microscopy. Cells from tubular segments of healthy kidneys presented regular apical microvilli, intact basement membrane and basal infoldings. Mitochondria were very abundant, most of them presented an elongated shape and were localized in the basolateral part of the cells. They displayed a well-defined arrangement of well-preserved mitochondrial cisternae with a homogeneous inner matrix. Cisternae profiles of ER were located between the mitochondria near the nucleus (**Figure 36A**). In contrast, in FA treated mice group, many epithelial cells were detached from the tubular basement membrane and showed disrupted basal infoldings. Mitochondrial structure was lost and mitochondria presented a fragmented, small and round appearance. Presence of granular materials in renal tubular cells was also clearly noticed. ER is not distinguishably observed in between the mitochondria as observed in the control group but small degraded fragments were observed in the cytoplasm. Cytoplasmic

debris in tubular lumen, vacuole formation, increased number of lysosomes were clearly visible in kidneys from FA-treated animals. Interestingly, most of these morphological alterations in mitochondria as well as the reduction in mitochondrial mass induced by FA were almost abrogated in renal epithelial cells overexpressing CPT1A (**Figure 36A**). This effect was also reflected in the relative mtDNA copy number. In the 3-days UUO and FAN models of kidney damage, CPT1A overexpression prevented the drop of mtDNA copy number (**Figure 36B**).

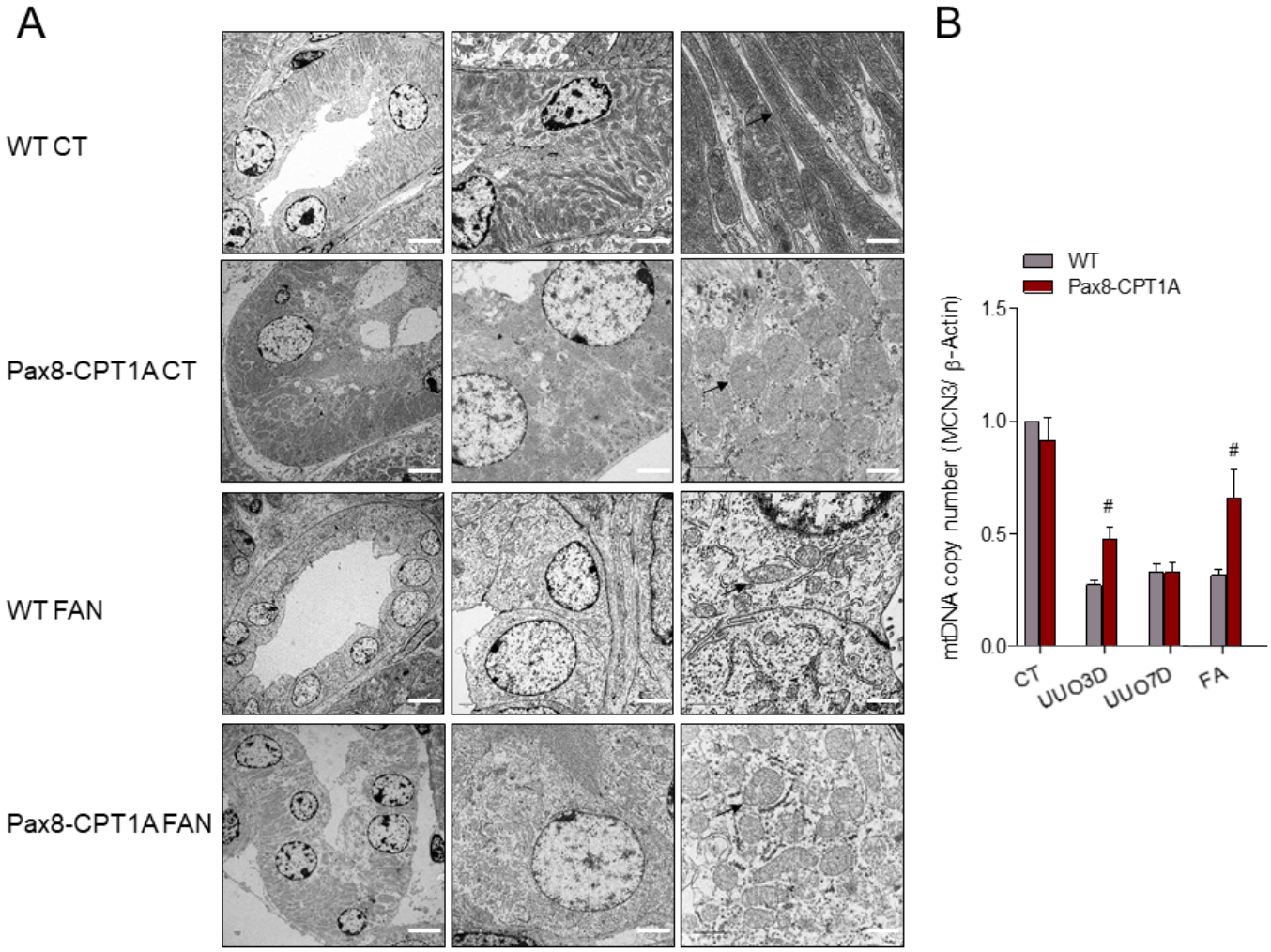

Figure 36. CPT1A overexpression mitigates impaired mitochondrial morphology in FAN-induced kidney fibrosis and prevents mitochondrial loss induced by UUO and FAN. (A) Representative electron microscopy images of cortical proximal tubules from control and Pax8-CPT1A mice subjected to FAN after doxycycline induction. Note reduced mitochondrial mass with a fragmented, small and round appearance in WT mice treated with FA. These changes were markedly abrogated in renal epithelial cells from mice overexpressing CPT1A. Scale bars: 10 µm (left panels), 500 nm (middle panels), 100 nm (right panels). Arrows point at representative mitochondria for each corresponding experimental condition. (B) Mitochondrial DNA copy number (mtDNA) was determined in kidneys of WT and Pax8-CPT1A mice in the UUO (3 and 7 days) and FAN models as specified in Methods. Bar graphs represent the mean ± s.e.m. of fold changes (n = 6 mice per group). $^{\#}P < 0.05$ compared to kidneys from WT mice with the same experimental condition.

As previously shown in **Figure 28**, the increase in CPT1A protein level in renal epithelium increased the capacity of kidney tissue to oxidize ^{14}C-palmitate by 1.5-fold as reflected the measurement of both ^{14}C-palmitate-derived $^{14}CO_2$. As reported, defective FAO was observed in fibrotic kidney from WT mice. However, in the 3-days UUO, FAN and ADN models, CPT1A overexpression counteracted this impairment, maintaining reported FAO rate for healthy kidneys (**Figure 37A, B, C**). Closely related to the improvement in FAO by CPT1A, ATP content in whole kidney tissue was increased from 50 to 80 µM/mg protein by CPT1A

overexpression. In the 3-days UUO, FAN and ADN models, CPT1A overexpression rescued the drop in ATP levels (**Figure 37D, E, F**).

These results suggest that appropriate levels of CPT1A and metabolic function are necessary and sufficient to preserve adequate mitochondrial architecture and morphology.

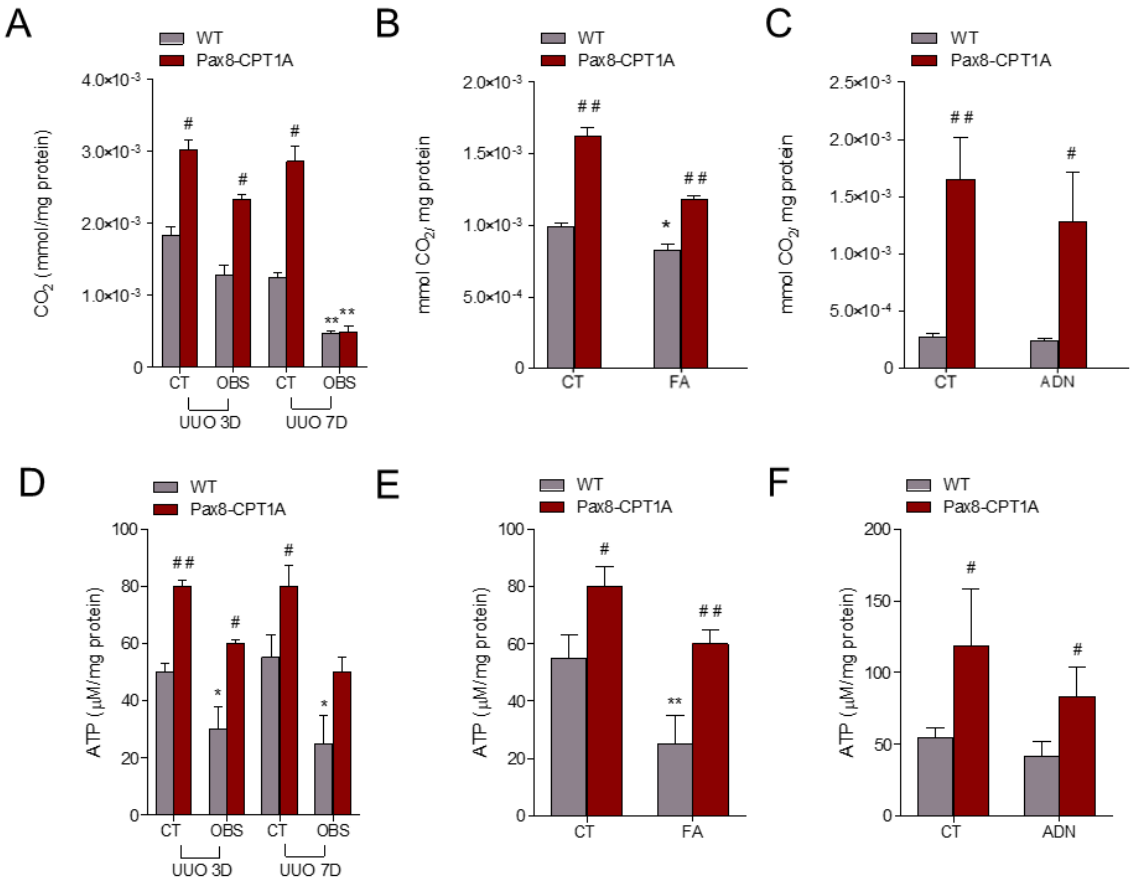

Figure 37. CPT1A overexpression prevents inhibition of fatty acid oxidation induced by UUO, FAN and ADN. Radiolabeled palmitate-derived CO_2 was determined after incubation of ^{14}C-palmitate with kidney tissue from WT and Pax8-CPT1A mice in the 3 and 7-days UUO (A), FAN (B) and adenine-induced nephrotoxicity (ADN) (C) models after doxycycline induction. ATP levels in total kidney tissue determined in mice subjected to UUO (D), FAN (E) or ADN (F). Bar graphs represent the mean ± s.e.m (n = 4 mice per group). *P < 0.05, **P < 0.01 compared to their corresponding control (CT) kidneys; #P < 0.05, ##P < 0.01 compared to kidneys from WT mice with the same experimental condition.

4.2.5. –Increased levels of CPT1A reduces the monocyte/macrophage infiltration pro-inflammatory profile in fibrotic kidneys

Consistent with clinical studies and animal models of kidney disease, there is a strong correlation between infiltrated macrophage polarization and the extent of fibrosis [48]. Flow cytometry analysis revealed that the macrophage subpopulation positive for CD86 (M1) was higher than the positive for CD206 (M2) in fibrotic kidneys from the 3- and 7-days UUO models, while CPT1A overexpression did not affect this trend (**Figure 38 and Figure 39**). However, the M2 macrophage subpopulation was increased in fibrotic kidneys from CPT1A KI mice compared with the WT ones after 7 days UUO (**Figure 39**)**.** Infiltration of macrophage subpopulation positive for both CD86 and CD206 (M1/M2) observed in obstructed kidneys from WT mice 3 or 7 days after UUO, was also enhanced by CPT1A overexpression (**Figure 38 and Figure 39**).

By contrast, in the FAN model, CPT1A overexpression reduced the proportion of renal pro-inflammatory M1 subpopulation (**Figure 40**). In addition, the abundance of this subpopulation was lower in FAN-induced fibrotic kidneys than in UUO-associated ones. These data suggest that the changes in the degree of macrophage infiltration and relative contributions of macrophage subpopulations are dependent

on the model of kidney injury. It is likely that the amplitude of inflammatory changes dictates part of this differential response, thus supporting that the FAN model induces a lesser degree of inflammation and tissue disruption compared to the UUO model.

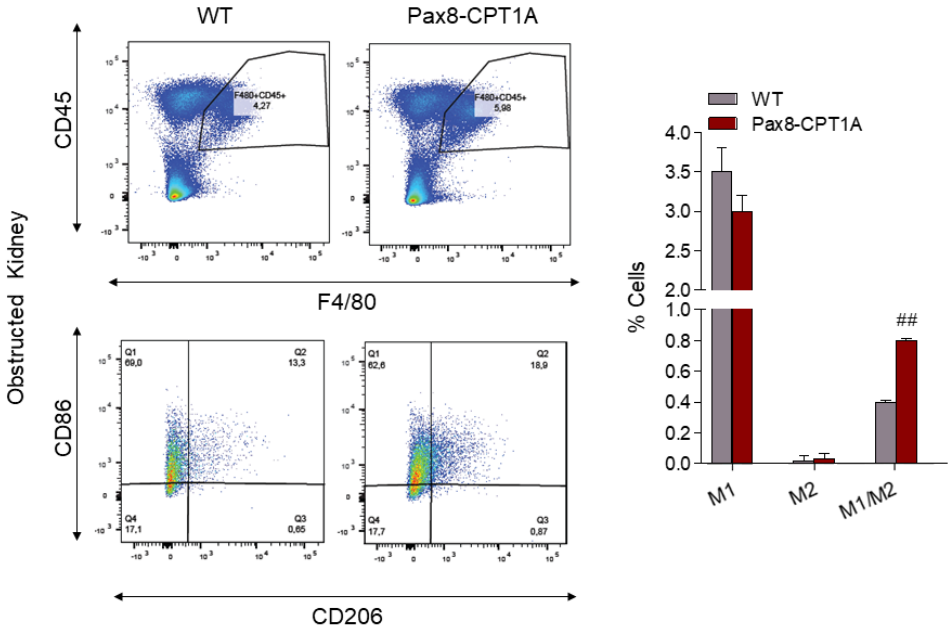

Figure 38. Overexpression of CPT1A increases the infiltration of the macrophage subpopulation positive for both CD86 and CD206 (M1/M2) in the 3-day UUO model. (A) Representative multiparameter flow cytometry dot plots showing the expression of CD45, a panleukocyte antigen also present in hematopoietic cells, monocytes and macrophages and F4/80, a surface marker expressed by monocytes and macrophages, in kidney cells from WT and Pax8-CPT1A mice subjected to 3 days UUO after doxycycline induction (one mouse per group) (upper panels). Numbers in quadrants indicate cell proportions in percent of cells that co-express both markers. CD86 and CD206 were used to determine the proportion of M1 and M2 macrophage subpopulations, respectively, in the total macrophage population (F4/80+, CD45+) (lower panels). Bar graphs represent the percentage of kidney cells expressing CD86 (M1), CD206 (M2) or both (M1/M2) markers. Data represent mean ± s.e.m (n = 4 mice per group). $^{##}P < 0.01$ compared to damaged kidneys from WT mice.

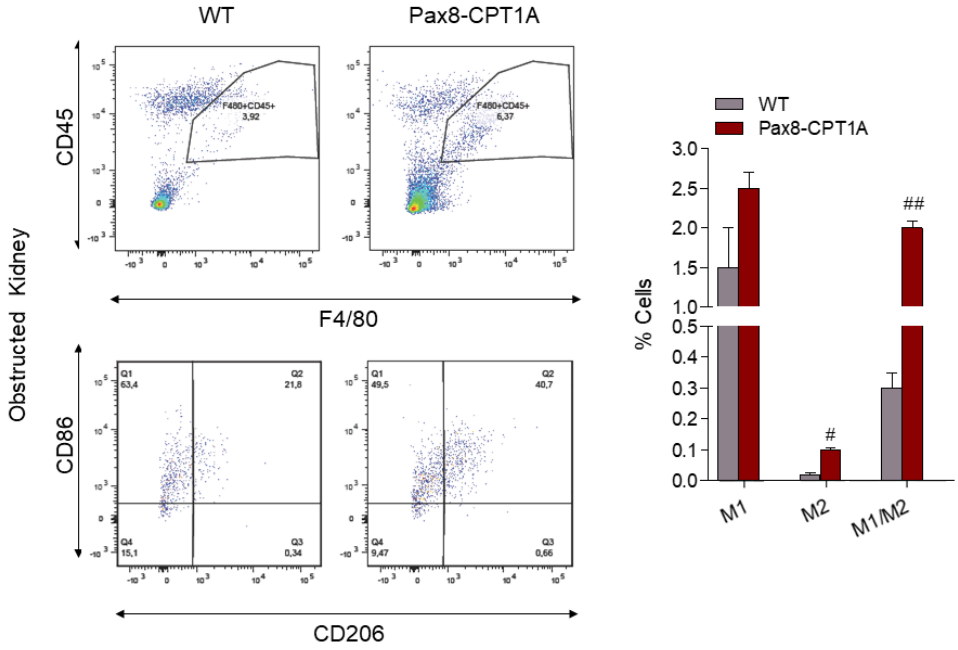

Figure 39. Overexpression of CPT1A increases the infiltration of macrophage subpopulations expressing CD206 (M2) and both CD86 and CD206 (M1/M2) the 7-days UUO model. (A) Representative multiparameter flow cytometry dot plots showing the expression of macrophage populations, studied as in Figure 36, in kidney cells from WT and Pax8-CPT1A mice subjected to 7-days UUO after doxycycline induction (one mouse per group) (upper panels). Numbers in quadrants indicate cell proportions in percent of cells that co-express both markers. CD86 and CD206 were used to determine the proportion of M1 and M2 macrophage subpopulations, respectively, in the total macrophage population (F4/80+, CD45+) (lower panels). Bar graphs represent the percentage of kidney cells expressing CD86 (M1), CD206 (M2) or both (M1/M2) markers. Data represent mean ± s.e.m (n = 4 mice per group). $^{##}P < 0.01$ compared to damaged kidneys from WT mice.

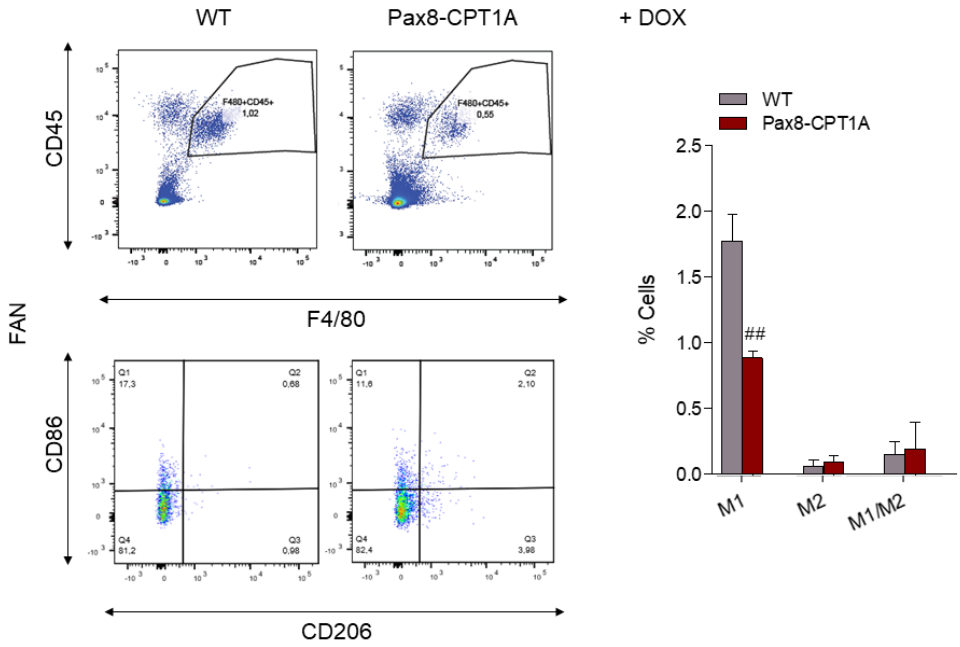

Figure 40. Overexpression of CPT1A reduces M1 macrophage infiltration in the FAN model. (A) Representative multiparameter flow cytometry dot plots showing the expression of macrophage populations, studied as in Figure 36, in kidney cells from WT and Pax8-CPT1A mice subjected to FAN after doxycycline induction (one mouse per group) (upper panels). Numbers in quadrants indicate cell proportions in percent of cells that co-express both markers. CD86 and CD206 were used to determine the proportion of M1 and M2 macrophage subpopulations, respectively, in the total macrophage population (F4/80+, CD45+) (lower panels). Bar graphs represent the percentage of kidney cells expressing CD86 (M1), CD206 (M2) or both (M1/M2) markers. Data represent mean ± s.e.m (n = 4 mice per group). ##P < 0.01 compared to damaged kidneys from WT mice.

4.2.6. –Genetic CPT1A overexpression prevents AMP-activated protein kinase (AMPK) activation associated to kidney fibrosis

Depressed carbohydrate, amino acid and lipid oxidative pathways have been described in patients and animal models of CKD, leading to energy deprivation [251]. AMPK is a highly conserved sensor of the intracellular metabolic status and plays a critical role in systemic energy homeostasis. The AMPK pathway is exquisitely sensitive to alterations in the [AMP]/[ATP] ratio and becomes active when this ratio is shifted towards less ATP. AMPK is activated by phosphorylation of its α-subunit Thr^{172} by upstream kinases. As a result, AMPK promotes catabolic pathways to generate more ATP and inhibits anabolic pathways. AMPK activation subsequently leads to acetyl-CoA carboxylase (ACC) phosphorylation and inactivation and malonyl-CoA decarboxylase (MCD) activation, decreasing malonyl-CoA concentration and hence favoring FAO [252].

To determine if FAO gain of function in kidneys of CPT1A KI mice is mirrored by predictable changes in AMPK activation as a consequence of increased ATP levels, phosphorylation of AMPK was analyzed by immunoblot. In the UUO model, obstructed kidneys presented increased AMPK phosphorylation protein levels compared with contralateral kidneys. Importantly, increasing CPT1A levels attenuated AMPK phosphorylation in fibrotic kidneys in the UUO model. The levels of the ACC phosphorylated form changed accordingly (**Figure 41A**). Similar data were obtained in the FAN and adenine models (**Figure 41B-C**).

These data proved that enhanced FAO in the kidney ameliorates fibrosis-induced energy deprivation associated with kidney fibrosis.

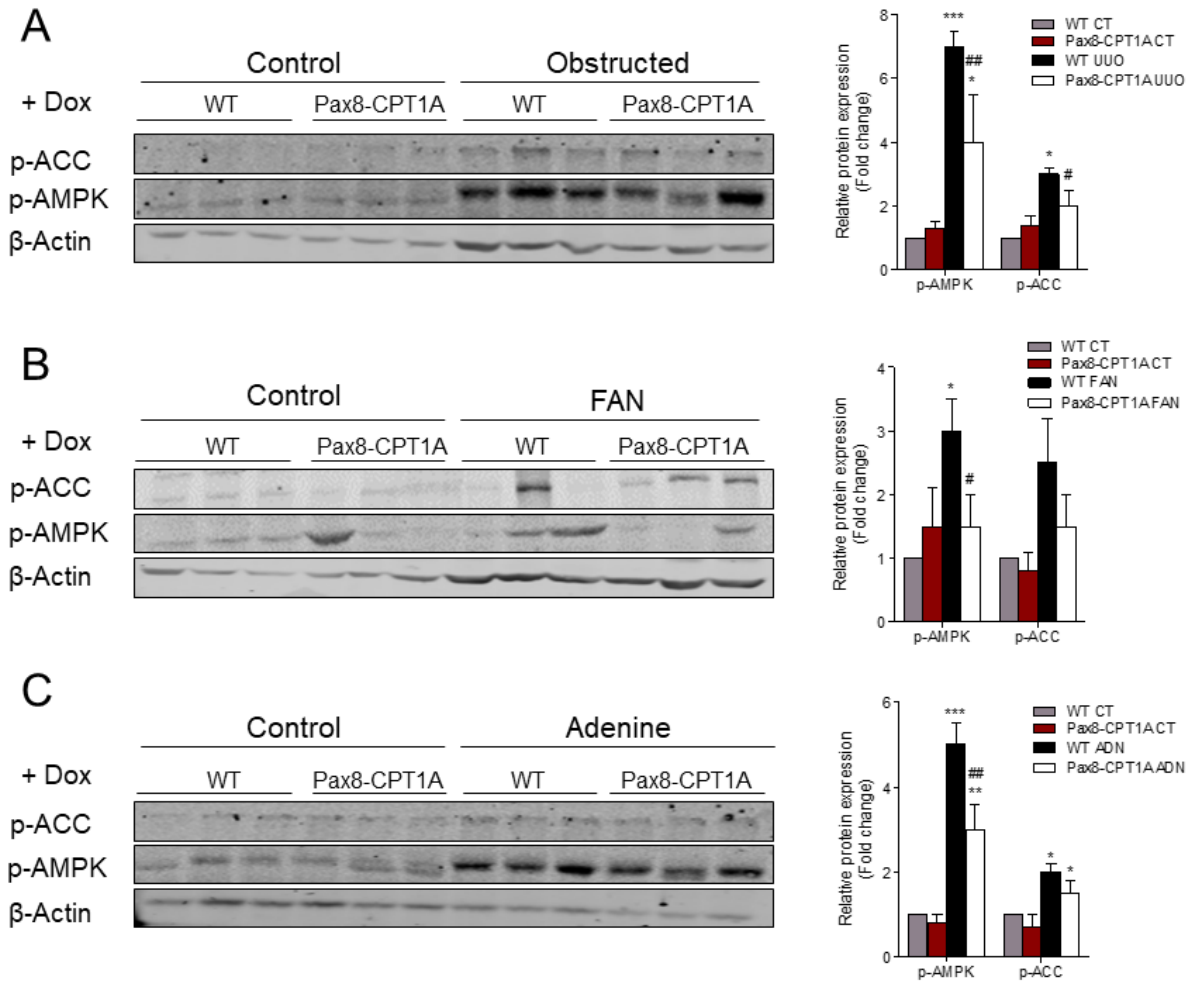

Figure 41. CPT1A overexpression prevents AMP-activated protein kinase (AMPK) phosphorylation associated to kidney fibrosis. Representative immunoblots corresponding to phosphorylated AMP-activated protein kinase (p-AMPK) and acetyl-CoA carboxylase (p-ACC) protein levels in kidneys of WT and Pax8-CPT1A mice subjected to UUO (A), FAN (B) or adenine-induced nephrotoxicity (ADN) (C) after doxycycline induction (represented are 3 mice per each group). Bar graphs represent the mean ± s.e.m. of fold changes corresponding to densitometric analyses (n = 6 mice per group). β-actin was used for normalization purposes. *P < 0.05, **P < 0.01, ***P < 0.01 compared to their corresponding control (CT) kidneys; #P < 0.05, ##P < 0.01 compared to kidneys from WT mice with the same experimental condition.

4.3 Evaluation of TGF-β-induced profibrotic responses in renal cellular models of CPT1A overexpression

4.3.1. –Renal tubule epithelial cells overexpressing CPT1A exhibit higher levels of FAO-associated oxygen consumption rate (OCR) and decreased glucose utilization

Genome wide-associated and transcriptomic profiling have allowed identification of common metabolic derangements in the process of renal fibrogenesis. In particular, the latter has been related to a global defect in fatty acid oxidation (FAO) leading to a compromise in the main source of energy for the tubular epithelial cell [171]. To gain insight about quantitative metabolic changes at the cellular level we examined oxygen consumption (OCR) and extracellular acidification rates (ECAR) of primary RTECs isolated from kidneys from CPT1A KI mice (**Figure 42A**) using a XF24 Extracellular Flux Analyzer (Seahorse Biosciences-Agilent Technologies) using an specific protocol for the evaluation of FAO (see Methods for details). Basal respiration was measured, followed by exposure to oligomycin, an inhibitor of ATP synthase, which allows to determine ATP synthesis-coupled respiration and H+ leak. Then, the uncoupler carbonyl FCCP was added to measure the maximal respiratory capacity, followed by the Complex I inhibitor rotenone and complex III inhibitor antimycin A, which permits to estimate non-mitochondrial respiration (see Methods for details). We found that basal and maximum OCR were markedly higher when palmitic acid was presented to TECs, indicating that TECs efficiently metabolize palmitate. The increase in OCR was sensitive to the CPT1 inhibitor Etomoxir, confirming its specificity (**Figure 42B**).

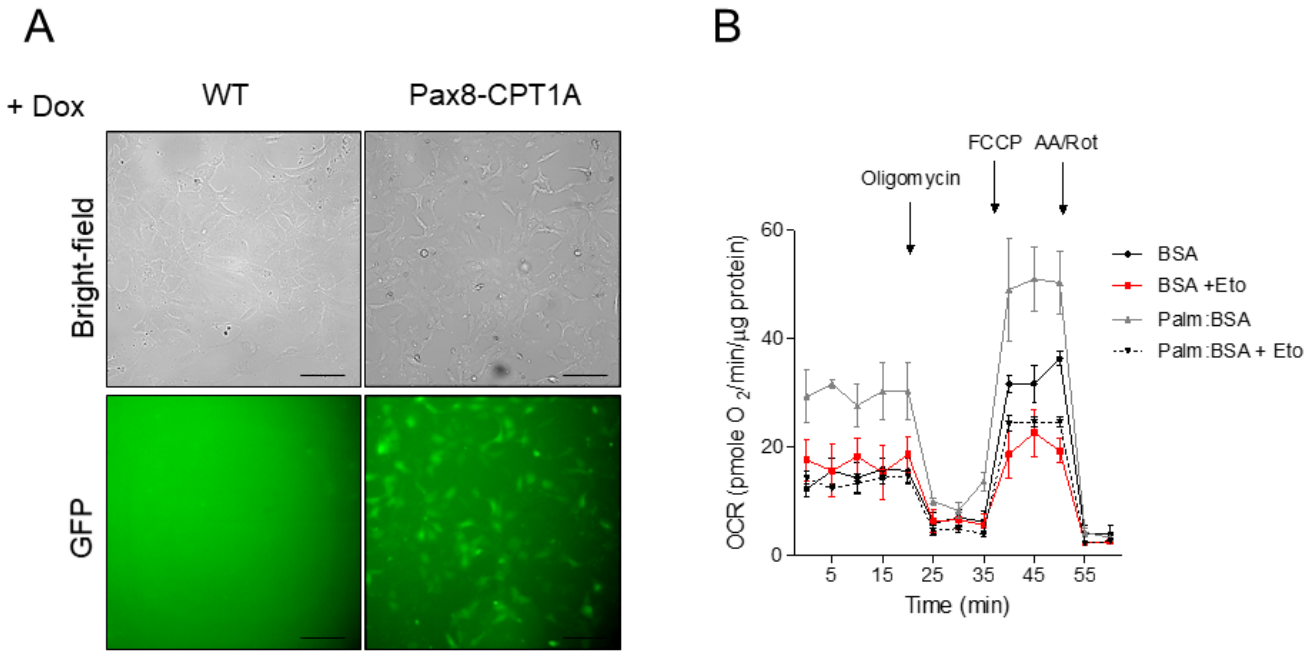

Figure 42. Primary kidney epithelial cells efficiently metabolize palmitate. (A) Bright field or GFP immunofluorescence images of primary kidney epithelial cells (TECs) isolated from kidneys of WT and Pax8-CPT1A mice. Scale bar, 20 µm. (B) Oxygen consumption rate (OCR) of TECs from WT mice was measured with a Seahorse XF24 Extracellular Flux Analyzer. Where indicated, cells were pre-treated with palmitate-BSA FAO Substrate (200 mM) or the CPT1 inhibitor Etomoxir (Eto, 400 µM). Oligomycin (1 µM), FCCP (3 µM) and a combination of antimycin A (1 µM) and rotenone (1 µM) (AA/Rot) were injected sequentially at the time points indicated. Data are represented after normalization by protein amount. Each data point represents the mean ± s.e.m of 4 independent experiments, each performed in triplicate.

FAO-associated OCR was also higher in primary kidney epithelial cells isolated from CPT1A KI compared to the ones isolated from WT mice (**Figure 43A**). We next examined the effect of TGF-β1 on renal epithelial cell metabolism. Cells treated with TGF-β1 had a lower baseline of oxygen consumption levels and showed a reduction in palmitate-induced elevation in OCR, indicating a low activity of fatty acid metabolism (**Figure 43A**). CPT1A overexpression prevented this TGF-β1-induced bioenergetic derangement.

To confirm the metabolic functional consequences of CPT1A overexpression in the human setting, we examined oxygen consumption rate (OCR) and extracellular acidification rate (ECAR) in the human tubular epithelial cell line, HKC-8. Adenovirus carrying CPT1A (AdCPT1A) or GFP (AdGFP) as a negative control were used to infect HKC-8 cells. CPT1A protein level was 2-fold higher in CPT1A-expressing HKC-8 than in GFP control cells (**Figure 44A**). Consistently, the FAO rate was 2-fold higher in AdCPT1A-expressing HKC-8, respectively as confirmed by measurement of both ^{14}C-palmitate-derived $^{14}CO_2$ as well as of ^{14}C-palmitate-derived acid-soluble metabolites (**Figure 44B**).

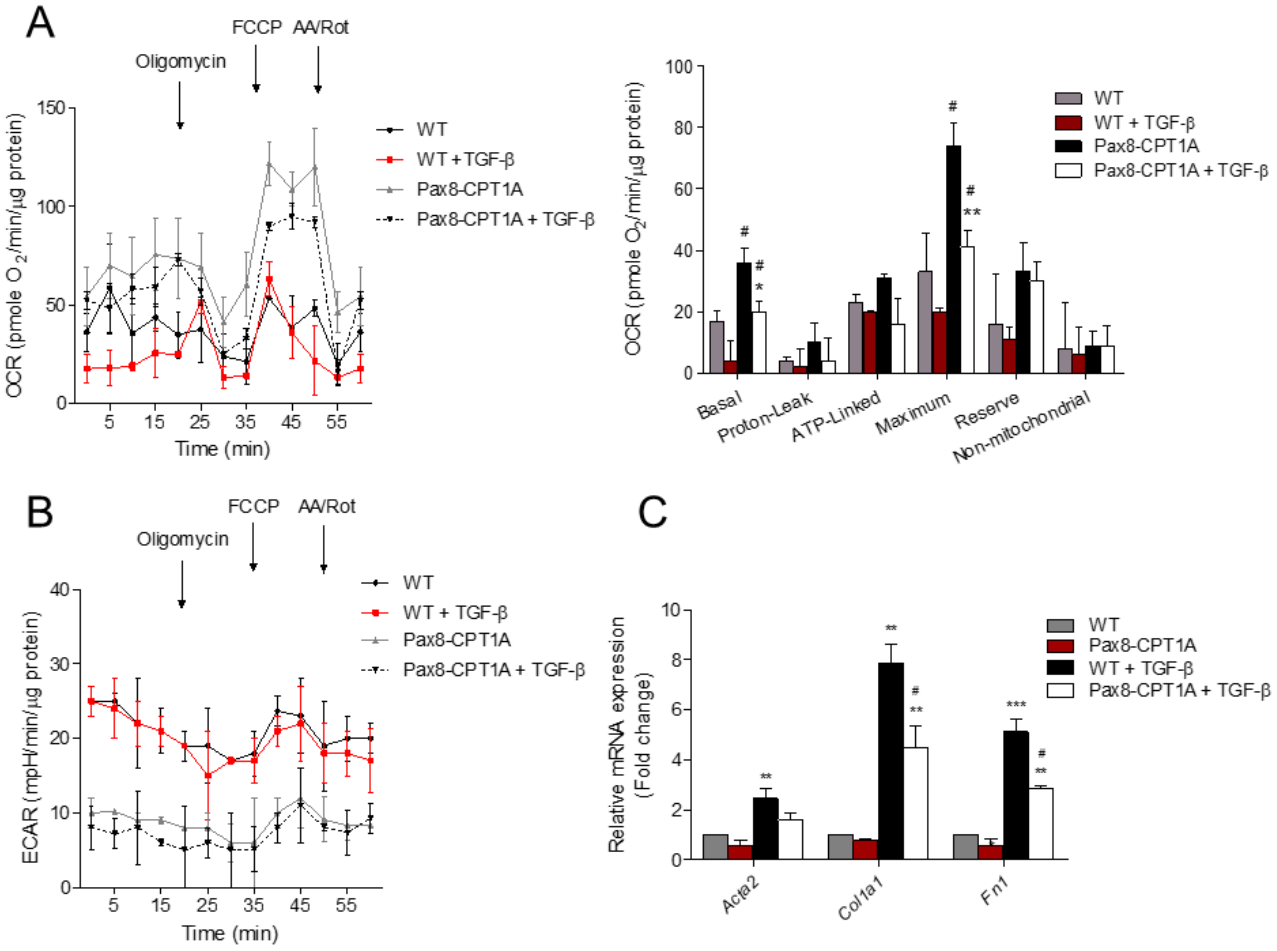

Figure 43. CPT1a overexpression prevents TGF-β1-induced FAO impairment and epithelial cell dediffentiation. (A) Oxygen consumption rate (OCR) of TECs from WT and Pax8-CPT1A mice was measured with a Seahorse XF24 Extracellular Flux Analyser. Cells were pre-treated with palmitate-BSA FAO Substrate (200 mM). Where indicated, cells were treated with TGF-β (10 ng/ml). Oligomycin (1 µM), FCCP (3 µM) and a combination of antimycin A (1 µM) and rotenone (1 µM) (AA/Rot) were injected sequentially at the time points indicated. Bar graphs (right panel) show the rates of OCR associated to basal, proton-leak, ATP-linked, maximum, reserve capacity and non-mitochondrial respiratory statuses. (B) Extracellular acidification rate (ECAR) of cells treated as in (A). Data are normalized by protein amount. Each data point represents the mean ± s.e.m of 4 independent experiments, each performed in triplicate. (C) mRNA levels of alpha-smooth muscle actin (*Acta2*), alpha 1 type-1 collagen (*Col1α1*), fibronectin (*Fn1*) from cells of kidneys from WT and CPT1A KI mice were determined by qRT-PCR using Sybr green. Cells were treated with TGF-β (10 ng/ml) where indicated. Bar graphs represent the mean ± s.e.m. of fold changes from 3 independent experiments, each performed in triplicate.**P < 0.01, ***P < 0.001 compared to their corresponding untreated cells; #P < 0.05 compared to cells from WT mice with the same experimental condition.

In keeping, the bioenergetic profile of CPT1A-expressing HKC-8 was associated with a significant enhancement of basal respiration, H+ leak, maximal respiratory capacity, ATP synthesis-coupled respiration and reserve capacity compared to GFP control cells (**Figure 45A**). Globally, these data show that renal tubule epithelial cells overexpressing CPT1a prevented TGF-β1-induced FAO repression.

Simultaneously, glycolytic function associated to palmitate consumption was determined by ECAR. Oligomycin-induced blockage of OXPHOS, allows to evaluate the maximum glycolytic capacity. We found that CPT1A promoted the inhibition of basal glycolytic function in both cellular models for CPT1A overexpression. TGF-β1 also decreased ECAR rate both in untreated cells and under CPT1A overexpressing conditions (**Figure 43B**-in TECs from mice, **Figure 45B**-in TECs transduced with adenoviral particles).

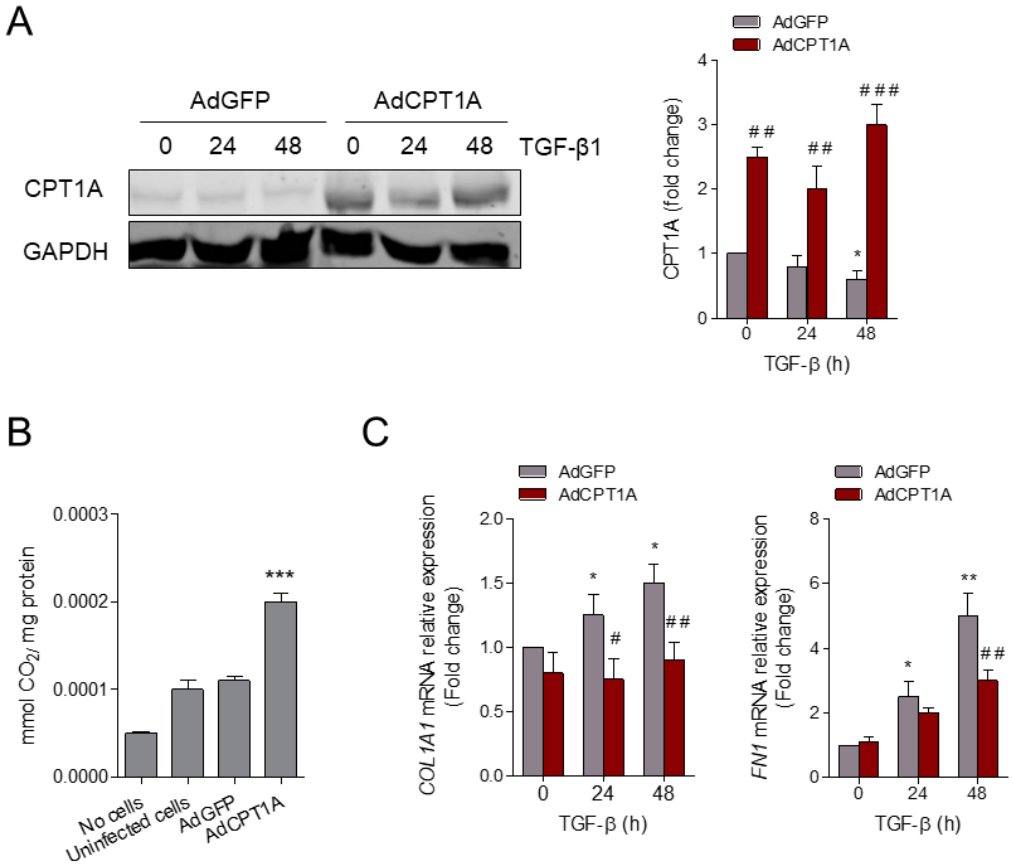

Figure 44. HKC-8 cells transduced with *CPT1A* exhibit decreased TGF-β-induced fibrogenic transformation. (A) Immunoblot depicts CPT1A protein levels in HKC-8 cells infected with adenoviruses carrying CPT1A (AdCPT1A) or GFP (AdGFP) and exposed to 10 ng/ml TGF-β1 for the indicated time points. GAPDH was used for normalization purposes. (B) Radiolabeled palmitate-derived CO_2 was determined after incubation of cells treated as in (A) with ^{14}C-palmitate. (C) mRNA levels of alpha 1 type-1 collagen (*COL1A1*) and fibronectin (*FN1*) of cells treated as in (A) were determined by qRT-PCR using Sybr green. Bar graphs represent the mean ± s.e.m. of fold changes from 3 independent experiments, each performed in triplicate. *P < 0.05, **P < 0.01, ***P < 0.001 compared to their corresponding untreated cells; ##P < 0.01, ###P < 0.001 compared to cells bearing AdGFP with the same experimental treatment.

Thus, data obtained in both cellular models strongly support that FAO gain-of-function acquired through either genetic engineering or adenoviral transduction of CPT1A results in a profound modification of the bioenergetics profile, reflected in a higher level of mitochondrial respiration, even in the presence of negative modulators with profibrotic action such as TGF-β, and a diminished glycolytic activity.

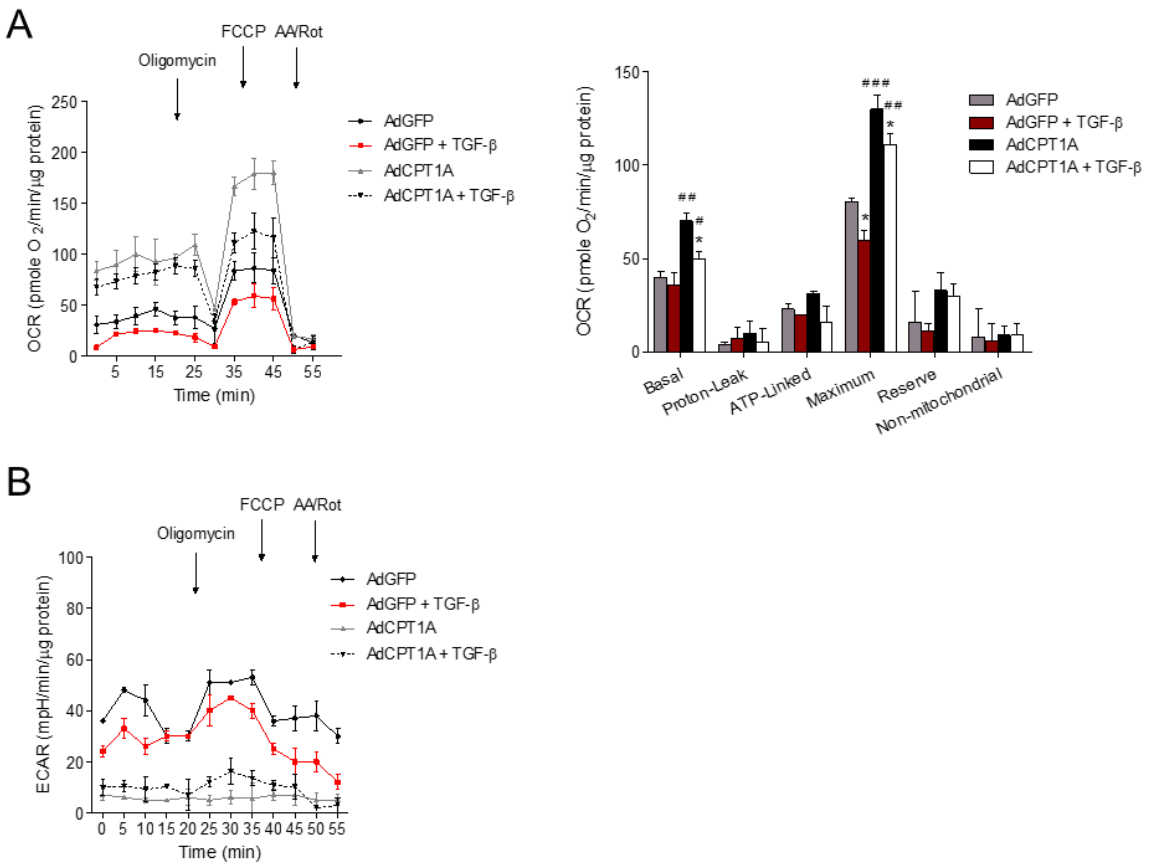

Figure 45. HKC-8 cells transduced with *CPT1A* exhibit reduced TGF-β1-induced FAO inhibition. (A) Oxygen consumption rate (OCR) of HCK-8 cells expressing AdCPT1A or its negative control AdGFP was measured with a Seahorse XF24 Extracellular Flux Analyser. Cells were pre-treated with palmitate-BSA FAO Substrate (200 mM). Where indicated, cells were treated with TGF-β (10 ng/ml). Oligomycin (1 µM), FCCP (3 µM) and a combination of antimycin A (1 µM) and rotenone (1 µM) (AA/Rot) were injected sequentially at the time points indicated. Bar graphs (right panel) show the rates of OCR associated to basal, proton-leak, ATP-linked, maximum, reserve capacity and non-mitochondrial respiratory statuses. (B) Extracellular acidification rate (ECAR) of cells treated as in (A). Data are normalized by protein amount. Each data point represents the mean ± s.e.m of 4 independent experiments, each performed in triplicate. *P < 0.05 compared to their corresponding untreated cells; #P < 0.05, ##P < 0.01, ###P < 0.001 compared to cells bearing AdGFP with the same experimental treatment.

4.3.2. –CPT1A overexpression in renal epithelial cells prevents TGF-β-induced dedifferentiation

Epithelial injury remains a central event in the pathogenesis of CKD. Direct epithelial damage causes dedifferentiation and upregulation of proteins that may themselves orchestrate pro-inflammatory signaling. This dedifferentiation is characterized by the loss of epithelial markers and acquisition of mesenchymal features, a process known as epithelial-to-mesenchymal transition (EMT) [249]. Based on our previous results demonstrating the mitigation of the fibrotic phenotype by increasing CPT1A expression, we hypothesized that FAO gain-of-function in renal epithelial cells could prevent TGF-β-induced dedifferentiation. To test whether enhancing renal epithelial FAO has a protective role in TGF-β-induced dedifferentiation, CPT1A or GFP-expressing HKC-8 were treated with TGF-β1 for different times. Increased expression of CPT1A significantly abrogated TGF-β1-induced transcription of *COL1A1* and *FN1* mRNA levels (**Figure 44C**). Primary kidney epithelial cells isolated from CPT1A KI mice and treated with TGF-β1 for 48 h showed a marked reduction in the increase of these profibrotic markers compared to the cells isolated from WT mice (**Figure 43C**). Consistently, cells from kidneys of mice overexpressing CPT1A presented a reduced population of damaged epithelial cells (CD45- EPCAM+ CD24+) [253] compared to those of WT mice in both the 7-days UUO (A) and FAN (B) models (**Figure 46**). This set of data supports that the protective action of

CPT1A in kidney fibrosis operates, at least in part, through the attenuation of TGF-β1-induced dedifferentiation.

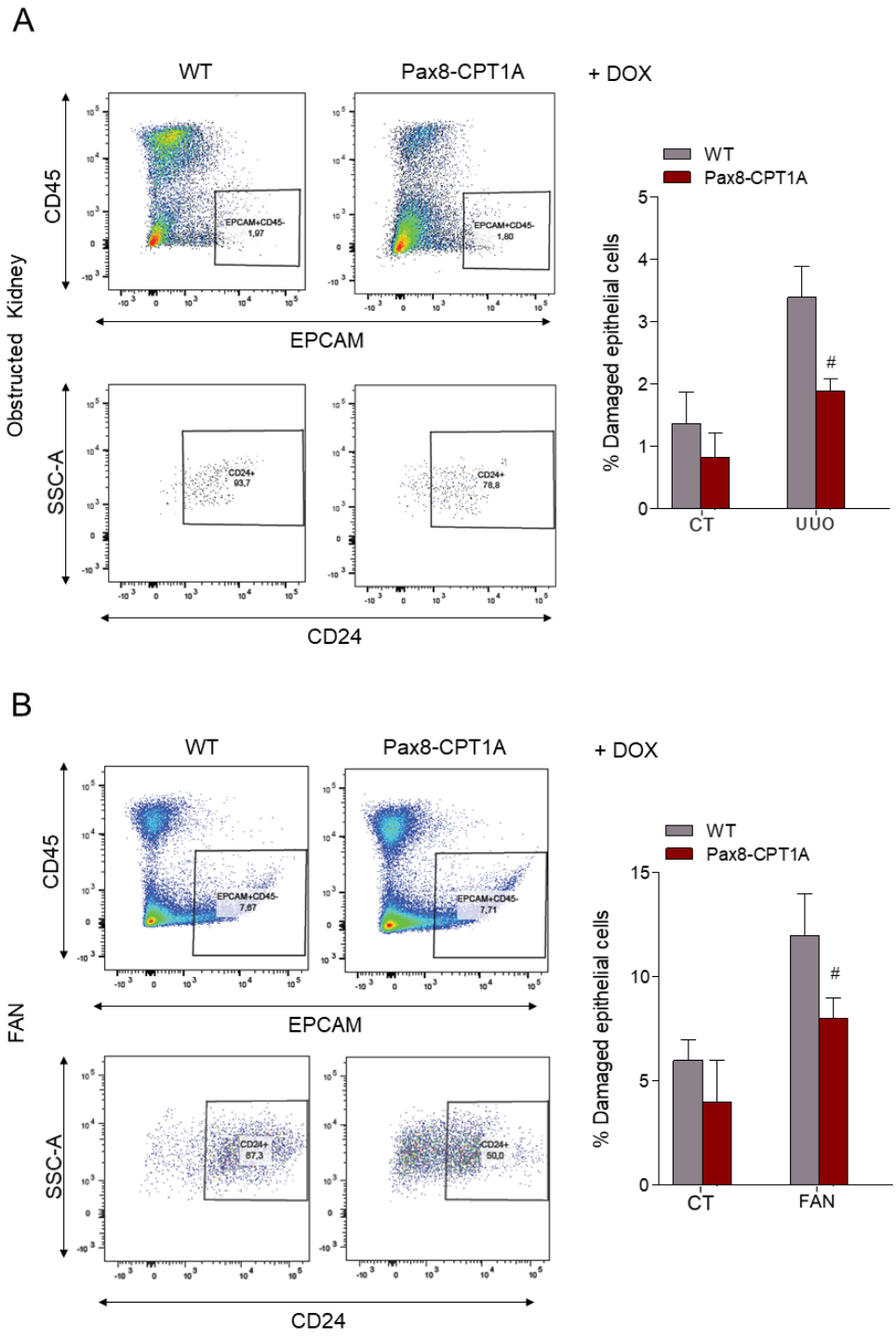

Figure 46. CPT1A overexpression reduces epithelial cell damage in the UUO model. Representative flow cytometry dot plots illustrating cell populations from obstructed kidneys of WT and Pax8-CPT1A mice subjected to UUO for 7 days (A) or FAN (B) after doxycycline treatment. Cells were gated for CD45 negative (-)/Epithelial Cell Adhesion Molecule (EpCAM) positive (+) (upper panels) and then selected for the presence of CD24 (lower panels). Numbers in quadrants indicate cell proportions in percent. SSC-A: Side Scatter Area. Data shown are representative of 4 mice per group. Bar graphs show the percentage of kidney cells positive for CD24. Data represent the mean ± s.e.m (n = 4 mice per group). $^{\#}P < 0.05$ compared to obstructed kidneys in WT mice.

4.4 Identification of specific miRNAs that regulate the fibrotic outcome in the kidney through metabolic pathways

4.4.1. –miRNA expression data in UUO-induced fibrotic kidneys

To decipher the contribution of miRNAs to the metabolic regulation of renal fibrogenesis, the 7-day UUO model was performed in WT mice. RNA was isolated from control and fibrotic kidney samples and the miRNA expression profile was analyzed in a custom microRNA array. Selection of miRNAs was based on their *in silico* targeting of key enzymes involved in the molecular mechanisms we aimed to explore in the context of renal fibrosis: mitochondrial metabolism, redox processes and circadian rhythm (more details in the Methods section). Heat map revealed clearly distinct expression patterns in some miRNAs when comparing fibrotic and control kidney samples (**Figure 47A**). The volcano plot analysis showed that 73 of 175 miRNAs were differentially expressed, 17 up- and 56 down-regulated, in the fibrotic kidney samples compared to the control ones (**Figure 47B, Table 9A, B**).

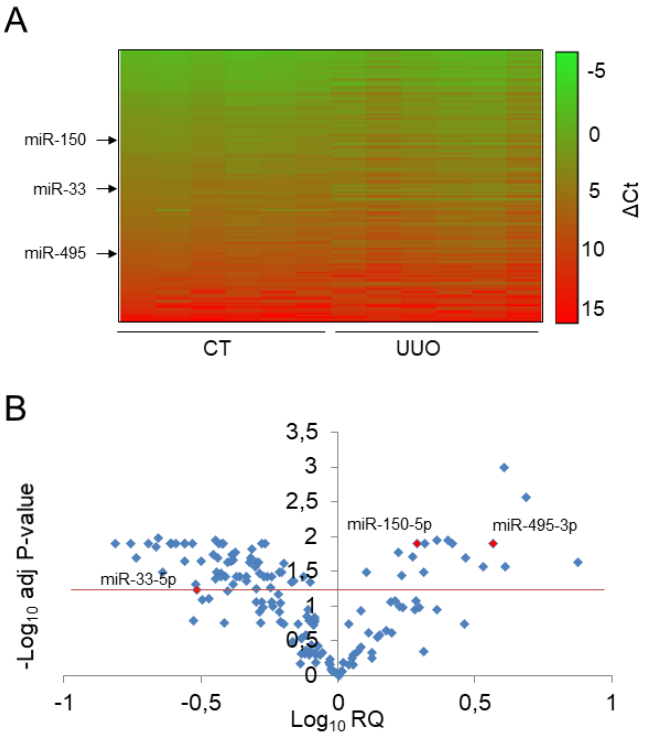

Figure 47. miRNA expression data in UUO-induced fibrosis. (A) Heat map showing relative miRNA expression of contralateral and obstructed kidneys of C57/BL6-J mice subjected to the UUO procedure for 7 days (n=6). The scale bar ranges from green to red (high to low expression) and numbers represent ΔCt values. On the left side are indicated the miRNAs selected for study. (B) Volcano plot analysis of UUO-modulated miRNAs. Log_{10} relative quantification (RQ) and negative (–) log_{10} adjusted (adj.) *P*-values are plotted on the *x*- and *y*-axis, respectively. Each miRNA is represented by a dot. 73 of 175 miRNAs showed an altered expression in the fibrotic samples (adj. P-value ≥ 0.05). Red dots represent selected microRNAs for further analysis.

Among them, specific miRNAs that could regulate the fibrotic outcome in the kidney through metabolic pathways were selected. For that purpose, *in silico* analysis of the 3´UTR of specific genes involved in metabolic and mitochondrial function CPT1A, TFAM, PGC1A was performed with three independent prediction tools (Targetscan, miRWalk and miRanda). Selection criteria also included renal expression level, novelty of targets, degree of knowledge on the metabolic route and biological significance. Link to human pathology, kidney tissue expression level, their role in mitochondrial metabolism and their potential targeting of the fatty acid shuttling enzyme CPT1A encouraged us to focus on three miRNAs, miR-150-5p, miR-495-3p and miR-33-5p, as potential candidates susceptible of regulating metabolic alterations associated to renal

fibrogenesis (**Table 10**). MiR-150-5p and miR-495-3p were upregulated in fibrotic kidney samples compared to the control ones, with a fold change of 3.6 (P-value: 0.012) and 1.99 (P-value: 0.012), respectively. miR-33-5p, by contrast, was downregulated with a fold change of 0.3 (P-value: 0.049).

A

microRNA	Fold change UUO-control	adj.P-Val UUO-control
miR-511-5p	7,508837277	0,023666615
miR-132-3p	4,871691782	0,002681317
miR-127-3p	4,072993544	0,027140175
miR-214-3p	4,028537526	0,001008675
miR-495-3p	3,692051971	0,012767102
miR-382-5p	3,391498515	0,027140175
miR-142-5p	2,920245234	0,020148124
miR-199a-5p	2,625798471	0,012767102
miR-223-3p	2,523202849	0,011453965
miR-342-3p	2,304450632	0,011453965
miR-31-5p	2,082894153	0,012767102
miR-199b-5p	2,061350064	0,032107133
miR-150-5p	1,949029861	0,012767102
miR-183-5p	1,871795548	0,01927754
miR-155-5p	1,70458774	0,035930197
miR-100-5p	1,659892174	0,01669386
miR-99b-5p	1,271845001	0,032652961

B

microRNA	Fold change UUO-control	adj.P-Val UUO-control	microRNA	Fold change UUO-control	adj.P-Val UUO-control
miR-200c-3p	0,789269294	0,04453697	miR-340-3p	0,394862663	0,023589053
miR-145-5p	0,747557364	0,036997098	miR-133a-3p	0,38718354	0,036997098
miR-23b-3p	0,691877978	0,042789997	miR-26a-5p	0,381632567	0,012767102
miR-181c-5p	0,675294882	0,04453697	miR-188-5p	0,376813579	0,012767102
miR-423-3p	0,632259856	0,024593374	miR-340-5p	0,375293063	0,033457941
miR-140-3p	0,620680558	0,032107133	miR-98-5p	0,374210738	0,037528051
let-7b-5p	0,610370099	0,032107133	miR-106a-5p	0,368419891	0,012767102
let-7c-5p	0,57411946	0,037667966	miR-30b-5p	0,363977925	0,020148124
miR-103a-3p	0,551368796	0,037667966	miR-200a-3p	0,36083792	0,032107133
miR-34a-5p	0,543777939	0,012767102	miR-101b-3p	0,357725002	0,04114064
miR-130a-3p	0,535053921	0,037667966	miR-29a-3p	0,356899436	0,011453965
miR-149-5p	0,528297637	0,012767102	miR-107	0,351579501	0,018428087
miR-335-5p	0,516231302	0,033439147	Let-7g-5p	0,315582591	0,022342294
miR-200b-3p	0,512961645	0,023589053	miR-33a-5p	0,302552245	0,049053578
miR-128-3p	0,504440563	0,023589053	miR-9-5p	0,292922218	0,012767102
miR-221-3p	0,497783228	0,027140175	miR-185-5p	0,276322101	0,012767102
miR-30d-5p	0,483612306	0,01516606	miR-101-3p	0,276003065	0,022342294
let-7d-5p	0,479440225	0,020148124	miR-30c-5p	0,275048167	0,012767102
miR-148b-3p	0,478333762	0,023589053	miR-30a-5p	0,25515094	0,012767102
miR-328-3p	0,463108731	0,036997098	miR-216a-5p	0,247744144	0,012767102
miR-872-5p	0,461239997	0,042789997	miR-26b-5p	0,244615805	0,012767102
miR-196a-5p	0,44015682	0,037667966	miR-1	0,229159319	0,032107133
miR-338-3p	0,427132682	0,036997098	miR-29c-3p	0,221097742	0,010686117
miR-27a-3p	0,421495615	0,01669386	miR-383-5p	0,216422569	0,014080317
miR-140-5p	0,415452716	0,04918899	miR-29b-3p	0,203451411	0,012767102
miR-196b-5p	0,412821361	0,021539185	miR-192-5p	0,183572628	0,02007513
miR-203a	0,411393107	0,018428087	miR-194-5p	0,175181564	0,012767102
miR-27b-3p	0,408079703	0,02250354	miR-30e-5p	0,153476484	0,012767102

Table 9. List of microRNAs included in the array with a differential expression in fibrotic kidney samples. 73 out of 175 analyzed miRNAs were differentially expressed in fibrotic kidneys. From these, 17 microRNAs were upregulated (A) and 56 downregulated (B) in fibrotic kidney samples compared to control ones. In red are those miRNAs selected for further study.

A

microRNA	CPT1A	TFAM	PGC1A	Fold change	P-value
miR-495-3p	7mer-A1	7mer-m8 7mer-m8 7mer-A1	7mer-A1 7mer-A1	3.6	0.012
miR-150-5p	7mer-m8	7mer-A1	8mer 7mer-A1	1.99	0.012
miR-33a-5p	8mer 7mer-A1	7mer-A1	7mer-A1	0.302	0.049

Table 10. Selected miRNAs based on *in vitro* targeting of metabolism-related genes. miR-150, miR-495 and miR-33 were selected due to their *in vitro* targeting of the genes CPT1A, TFAM and PGC1A. For each selected microRNA, conserved seed target sites in the 3´UTR of these genes, their fold change and significance (adj. P-value) are indicated.

4.4.2. –Determination of the contribution of miR-33 in regulating kidney FAO and renal fibrosis using the miR-33 knockout mouse model

4.4.2.1. –Loss of miR-33 protects against kidney fibrosis

Decreased levels of fatty acid oxidation (FAO) have been demonstrated to be closely related to fibrotic damage in the kidney [171]. MiR-33 is a key regulator of cholesterol efflux and fatty acid metabolism acting in concert with its SREBP host gene. It is clearly expressed in the kidney (both human and murine), suggesting an important role for this miRNA in controlling FAO during the development of kidney fibrosis. Based on these observations, we sought to determine whether miR-33 plays a direct role in the development of kidney fibrosis by using the two models of kidney fibrosis already described, FAN and UUO, in mice deficient in miR-33 (33KO). Seven days after intraperitoneal (IP) injection of FA, 33KO mice showed a dramatic reduction in the development of kidney fibrosis. Histological analysis of the kidneys revealed that 33KO mice had reduced accumulation of collagen in the interstitial area compared to the WT ones as visualized by Sirius Red staining with light microscopy. This was reflected in a reduction of approximately 40% in the renal fibrotic area (**Figure 48A**). Furthermore, common parameters indicative of kidney function, blood urea nitrogen (BUN) and creatinine, were increased in animals injected with folic acid, but this response was decreased in 33KO animals (**Figure 48B**).

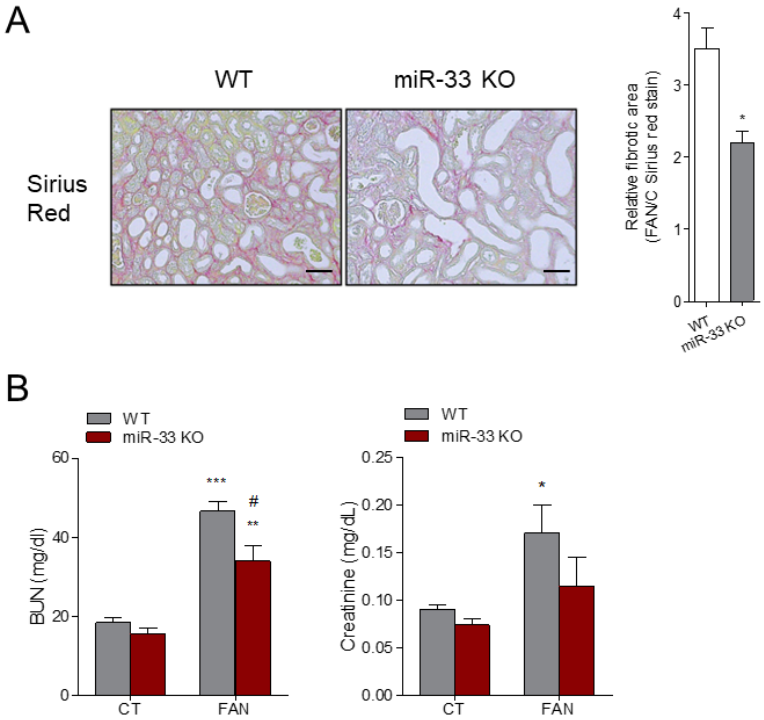

Figure 48. **Loss of miR-33 prevents histological and functional alterations associated with kidney fibrosis.** (A) Representative microphotographs from one mouse per group of Sirius Red staining of kidneys from WT and miR-33 KO mice subjected to FAN. Quantification of Sirius Red staining was calculated as a ratio of the stained area over the total area. The fibrotic area is represented as Sirius Red staining of FA-treated mouse kidneys (FAN) related to control kidneys (right panel). Scale bars: 50 µm. (B) Serum blood urea nitrogen (BUN) and creatinine levels of WT and miR-33 KO mice subjected to FAN. Data are shown as the mean ± s.e.m of 6 mice per group. *P < 0.05, **P < 0.01, ***P < 0.001 compared to corresponding control mice; #P < 0.05, compared to WT mice with the same experimental treatment.

The induction of the fibrosis-associated markers (alpha-smooth muscle actin, fibronectin, and collagen) in response to FA was reduced by 50% in the kidneys from 33KO mice both at the mRNA (**Figure 49A**) and protein levels (**Figure 49B**) compared to the WT ones. Therefore, the absence of miR-33-5p was able to counteract the upregulation of the studied fibrosis-related genes observed in the FAN model.

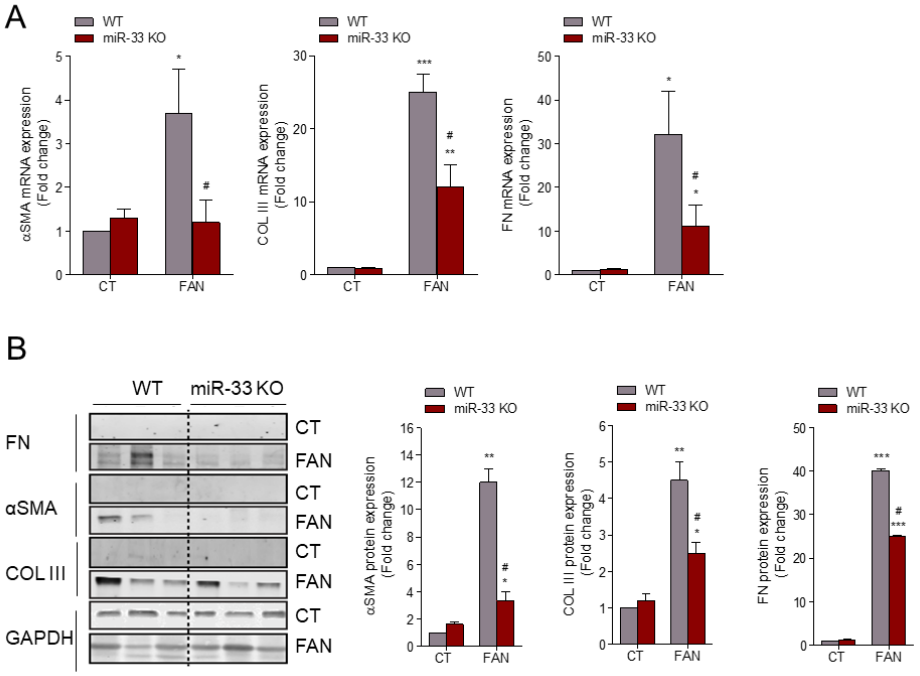

Figure 49. Absence of miR-33 blunts the increased expression of fibrosis-associated markers in the FAN model. (A) mRNA levels of fibrosis-associated genes alpha-smooth muscle actin (α-SMA), type-3 collagen (COL III) and fibronectin (FN) were determined by qRT-PCR using Sybr green in kidneys of WT and miR-33 KO mice subjected to FAN. (B) Immunoblots depicting fibronectin (FN), alpha-smooth muscle actin (α-SMA) and type-3 collagen (COL III) protein levels in control (CT) and FAN kidneys from 3 WT and 3 miR-33 KO mice. Bar graphs represent the mean ± s.e.m. of fold changes after densitometric quantification (n = 6 mice per group). Glyceraldehyde-3-phosphate dehydrogenase (GAPDH) was used for normalization purposes. *P < 0.05, **P < 0.01, ***P < 0.001 compared to their corresponding control kidneys; #P < 0.05 compared to WT mice with the same experimental treatment.

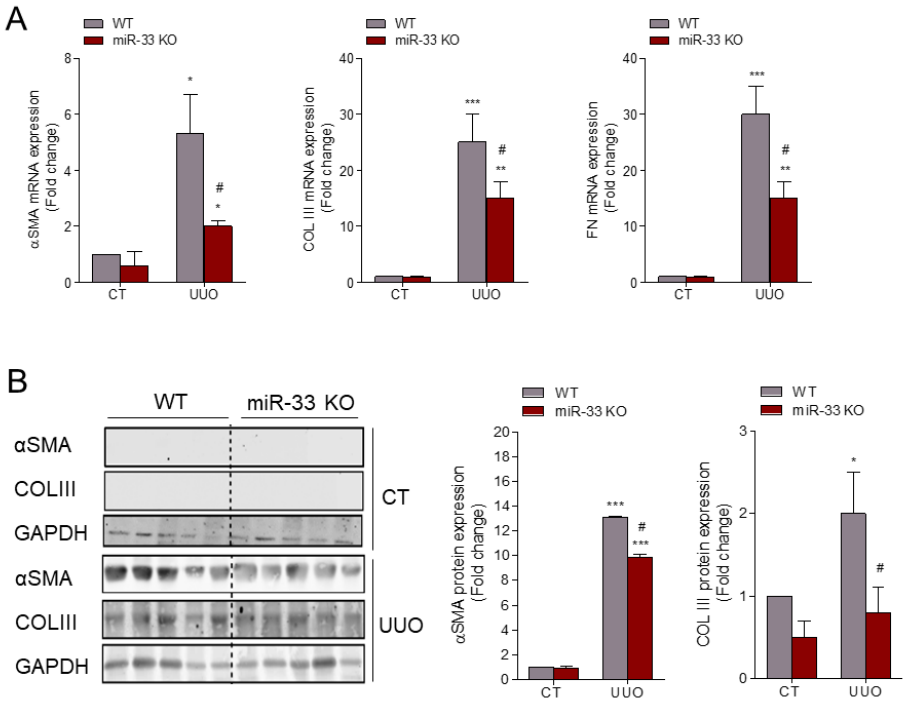

Figure 50. Absence of miR-33 blunts the increased expression of fibrosis-associated markers in the UUO model. (A) mRNA levels of fibrosis-associated genes alpha-smooth muscle actin (α-SMA), type-3 collagen (COL III) and fibronectin (FN) were determined by qRT-PCR using Sybr green in kidneys of WT and miR-33 KO mice subjected to UUO. (B) Immunoblots depicting alpha-smooth muscle actin (α-SMA) and type-3 collagen (COL III) protein levels in obstructed kidneys from 5 WT and 5 miR-33 KO mice. Bar graphs represent the mean ± s.e.m. of fold changes after densitometric quantification (n = 6 mice per group). Glyceraldehyde-3-phosphate dehydrogenase (GAPDH) was used for normalization purposes. *P < 0.05, **P < 0.01, ***P < 0.001 compared to their corresponding control kidneys; #P < 0.05 compared to WT mice with the same experimental treatment.

Similar results were obtained in 33KO and control animals following UUO surgery. miR-33-5p absence prevented the increased expression of key fibrosis-associated genes *Acta2*, *Col1α1*, and *Fn1* induced by the UUO procedure, further confirming the important role of this miRNA in renal fibrogenesis (**Figure 50A, B**).

In addition, the temporal course of renal miR-33-5p expression at 3, 5, 7, 10 and 15 days after the UUO procedure was analyzed by qRT-PCR. It showed that miR-33-5p expression was not altered in the kidney at any analyzed time point after UUO (**Figure 51A**). A similar trend in miR-33-5p kidney levels was observed in response to FA (**Figure 51B**).

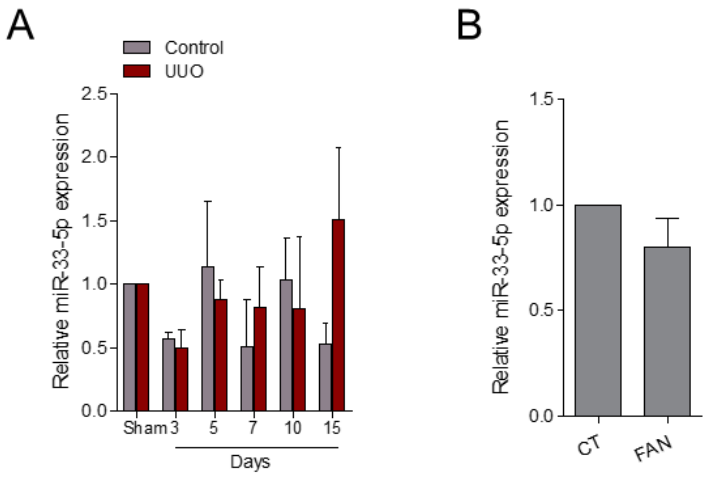

Figure 51. Expression levels of miR-33-5p in kidneys from the UUO and FAN models. qRT-PCR analysis of miR-33-5p expression in kidneys from mice after 3, 5, 7, 10 and 15 days of UUO (A) and FAN (B). Bar graphs represent the mean of the fold change expression levels ± s.e.m. from 3 (A) and 6 (B) mice per group.

4.4.2.2. –Loss of miR-33 enhances FAO-dependent mitochondrial respiration and reduces renal lipid accumulation

As miR-33 is an important regulator of FAO and cholesterol efflux and excessive lipid accumulation is known to be involved in kidney dysfunction [219], we next sought to determine whether alterations in lipid metabolism may be responsible for the protective effects of miR-33 deficiency on renal fibrosis. To gain insight into the consequences of miR-33 on the FAO-associated respiratory capacity, OCR in HKC-8 cells was measured by using the Seahorse apparatus with the modified protocol for FAO evaluation (more details in the Methods section). We observed that, after miR-33 overexpression of HKC-8 cells, there was a consistent abrogation of basal and ATP-linked OCR as well as in maximal respiration compared with cells transfected with the control miRNA. By contrast, a miR-33-5p inhibitor was able to improve the mitochondrial respiratory capacity in HKC-8 cells by inducing a significant increase in basal, ATP-linked respiration, and maximal mitochondrial respiration compared to the control inhibitor (miR-NC inhibitor) (**Figure 53A**). Our data also demonstrate that mitochondrial respiratory capacity was significantly enhanced in primary renal tubular epithelial cells isolated from 33KO mice compared to those from control animals (**Figure 52A**). As already mentioned, CPT1A is the rate-limiting enzyme in FAO and also a well-established target of miR-33 [218]. When this same approach was performed in the presence of the CPT1 inhibitor etomoxir, both HKC-8 cells and primary renal tubular epithelial cells exhibited diminished respiratory capacity. This effect was exacerbated in HKC-8 cells transfected with miR-33-5p, while the enhanced mitochondrial respiratory capacity associated with miR-33 deficiency was partially abolished, indicating that variations in FAO are largely responsible for these observations (**Figure 52A, Figure 53A, B**). Taken together, these data suggest

that the absence of miR-33-5p promotes FAO. In keeping, we found that the amount of TAGs in the kidney was significantly increased in kidneys from WT mice both in the FAN and 3- and 7-days UUO models. This response was blunted in 33KO animals (**Figure 52B, C**).

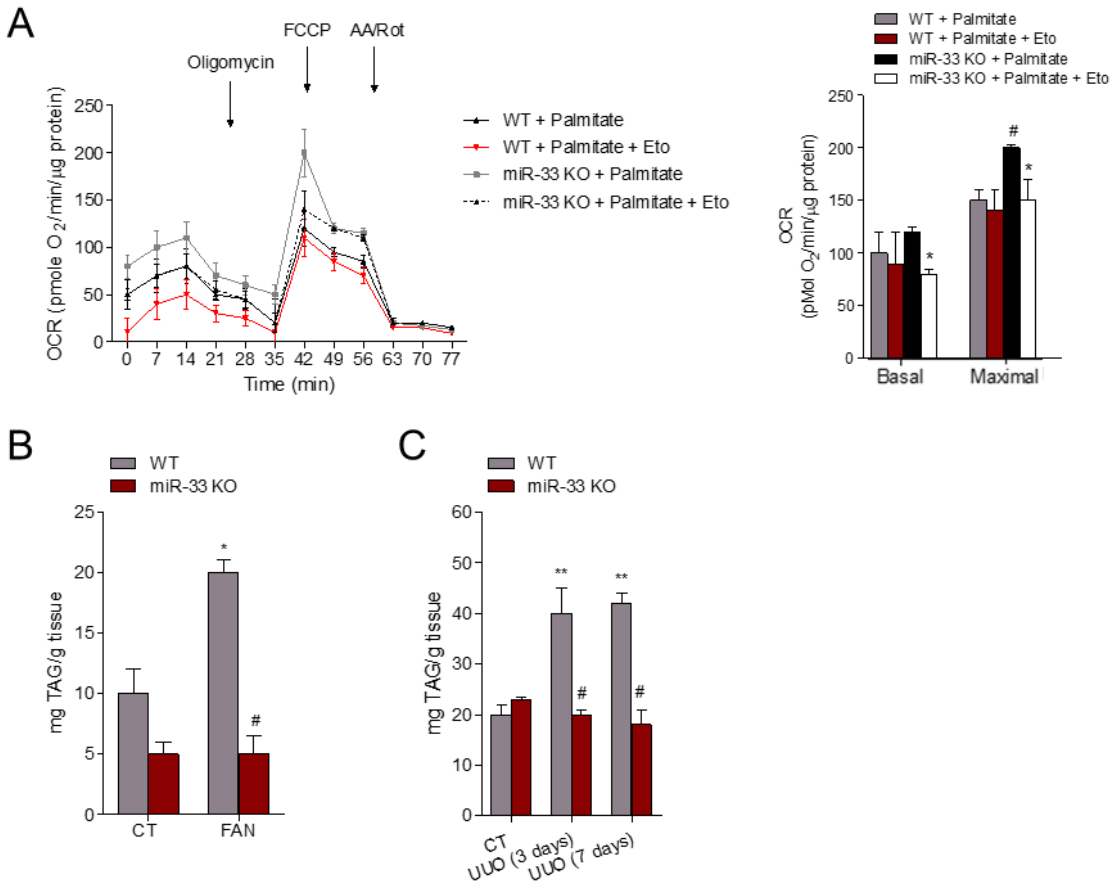

Figure 52. Loss of miR-33 enhances FAO-dependent mitochondrial respiration in TECs and reduces renal triglyceride accumulation in the UUO and FAN models. (A) Oxygen consumption rate (OCR) of TECs isolated from WT and miR-33 KO mice was measured with a Seahorse XF24 Extracellular Flux Analyser. Cells were pre-treated with palmitate-BSA FAO Substrate (200 mM). Where indicated, cells were treated with Etomoxir (Eto) (400 µM). Oligomycin (1 µM), FCCP (3 µM) and a combination of antimycin A (1 µM) and rotenone (1 µM) (AA/Rot) were injected sequentially at the time points indicated. Bar graphs show the values of OCR associated to basal and maximal respiratory statuses. (B) Triglyceride levels in total kidney tissue from WT and miR-33 KO mice subjected to FAN (B) or 3 and 7 days UUO (C). Bar graphs show the mean ± s.e.m triglyceride values (TAG) of 6 mice per group. *P < 0.05, **P < 0.01 compared to their corresponding control conditions; #P < 0.05 compared to WT mice with the same experimental treatment.

Consistently, immunoblot analysis demonstrated that CPT1A protein levels were dramatically reduced in the kidneys of WT mice treated with FA, whereas this decrement was attenuated in the kidneys of 33KO animals (**Figure 54A**). Thus, the loss of miR-33-5p counteracts the decrease in protein levels of CPT1A in response to kidney damage. Of note, the expression of the miR-33 target ABCA1 was increased in FA-induced kidney damage (**Figure 54A**). However, these changes did not reach statistical significance among 33KO and WT mice neither under basal conditions nor after FA administration. Similar results regarding CPT1A and ABCA1 protein levels were observed in the kidneys from 33KO and control animals following UUO (**Figure 54B**). Overall, these data suggest that the absence of miR-33 correlates with increased FAO, reduced accumulation of TAG and increased expression of genes regulating cholesterol efflux, thus providing a basis for the beneficial effects of miR-33 deficiency on kidney fibrosis.

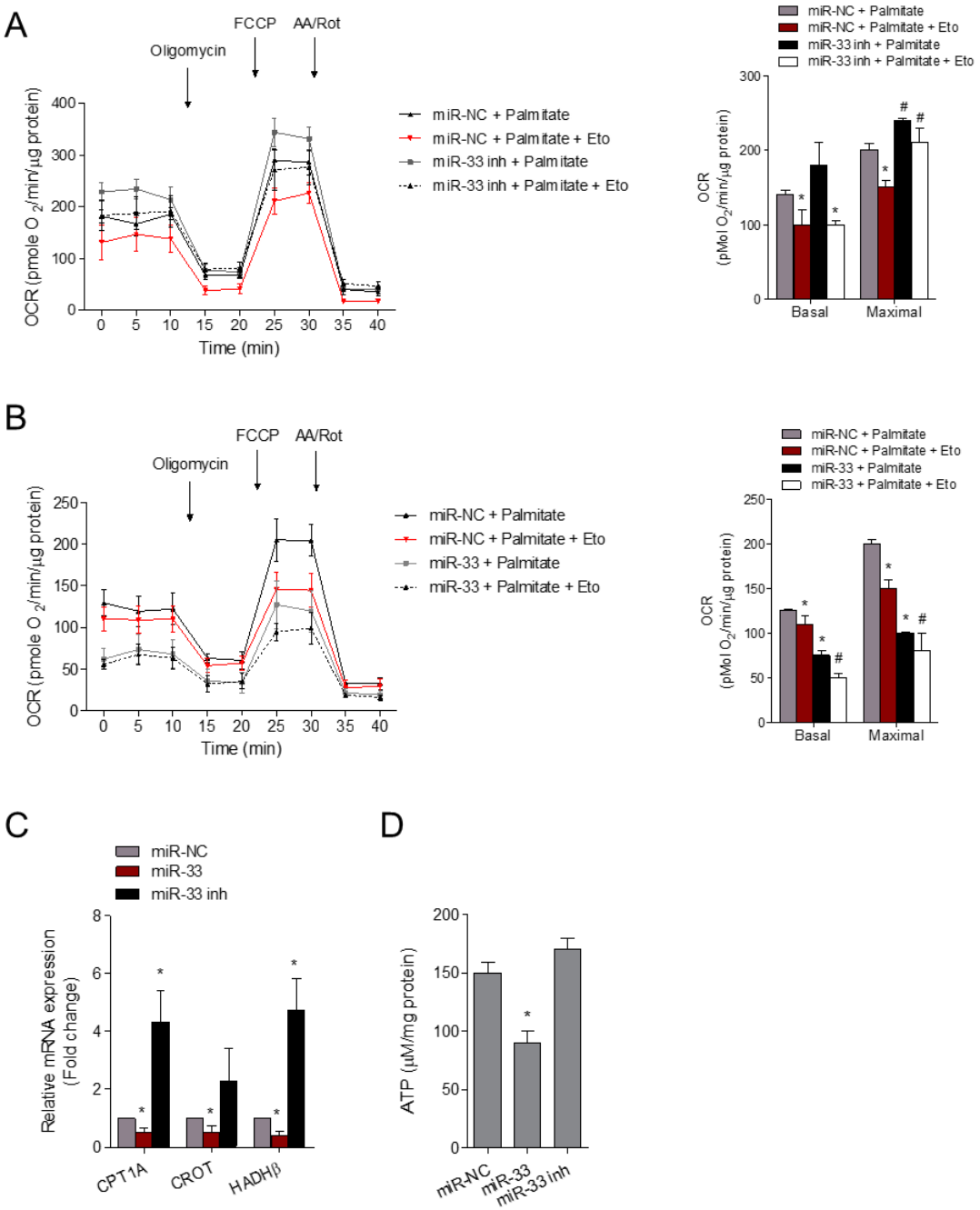

Figure 53. miR-33 regulates FAO-dependent mitochondrial respiration in human tubular renal epithelial cells. Oxygen consumption rate (OCR) of the human tubular cell line HKC-8 transfected with 40 nM miR-NC or miR-33 inhibitor (A)/miR-33-5p mimic (B) and exposed to 400 µM Etomoxir (Eto) for the indicated time points was measured with a Seahorse XF24 Extracellular Flux Analyzer. Cells were pre-treated with palmitate-BSA FAO Substrate (200 mM). Oligomycin (1 µM), FCCP (3 µM) and a combination of antimycin A (1 µM) and rotenone (1 µM) (AA/Rot) were injected sequentially at the indicated time points. Bar graphs (right panels) show the rates of OCR associated to basal and maximal respiratory statuses (n=4). (C) mRNA levels of CPT1A, CROT and HADHβ in HKC-8 cells transfected with miR-NC or miR-33 mimic/miR-33 inhibitor were determined by qRT-PCR using Sybr green. (D) ATP levels in HKC-8 cells transfected with miR-NC or miR-33 mimic/miR-33 inhibitor. Bar graphs show the mean ± s.e.m from 3 independent experiments. *P < 0.05 compared to their corresponding control conditions; #P < 0.05 compared to cells treated with miR-NC with the same experimental condition.

.

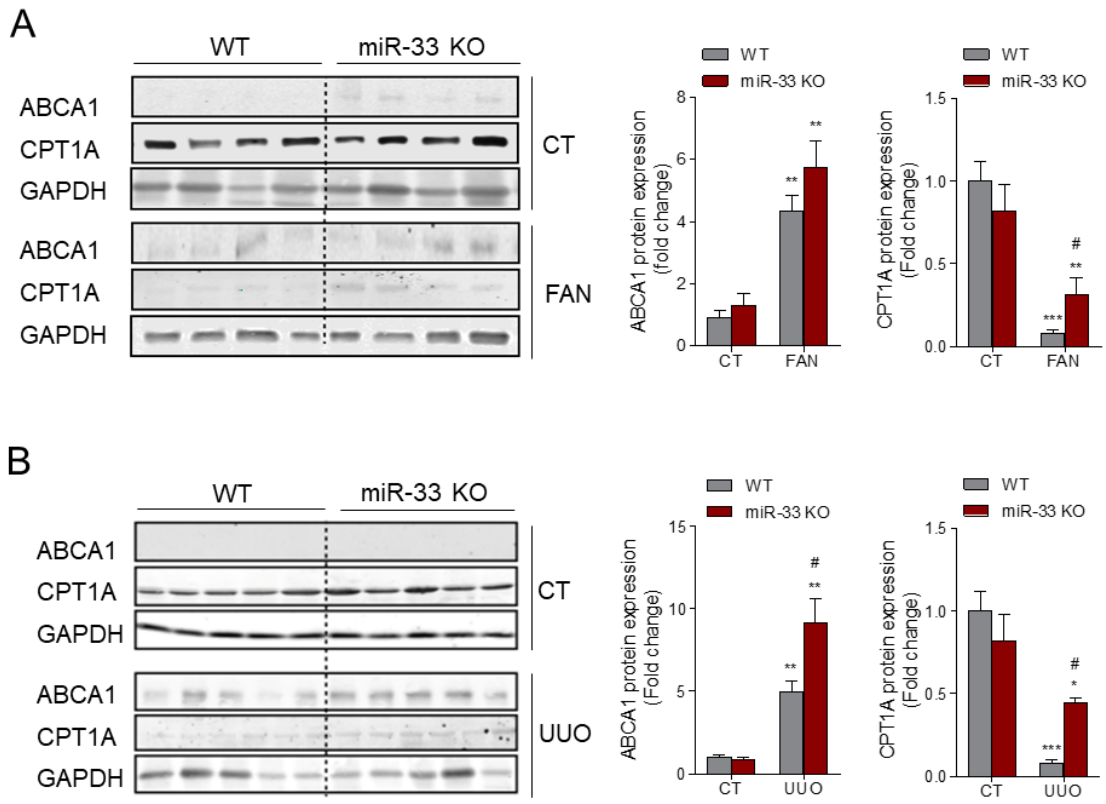

Figure 54. Absence of miR-33 modulates the fibrosis-associated altered kidney expression of its target genes CPT1A and ABCA1. Immunoblots depicting CPT1A and ABCA1 protein levels in control (CT) and FAN kidneys (A) or contralateral (CT) and obstructed (OBS) kidneys (B) from WT and miR-33 KO mice (shown are n=4 in UUO and n=5 in FAN). Bar graphs (right panels) represent the mean of the fold change expression ± s.e.m after densitometric quantification (n = 6 mice per group). Glyceraldehyde-3-phosphate dehydrogenase (GAPDH) was used for normalization purposes. *P < 0.05, **P < 0.01, ***P < 0.001 compared to their corresponding control kidneys; #P < 0.05, compared to WT mice with the same experimental treatment.

4.4.2.3. –miR-33 impairs fatty acid oxidation and promotes kidney dysfunction in human patients.

To explore the human translatability of the results obtained in the array and in the cellular model, we assessed the expression of the selected miRNAs in plasma and kidney biopsies from patients with CKD. Analysis of kidney biopsies from a group of 26 patients (Hospital Ramon y Cajal) did not show correlation between the degree of fibrosis and miR-33-5p levels (**Figure 55A**). Finally, miR-33 circulating plasma levels were assessed in a cohort of 100 CKD patients (Hospital Principe de Asturias). qRT-PCR analysis of miR-33 plasma levels did not show a clear trend toward a differential expression of miR-33 among these subgroups of patients (**Figure 55B**). Interestingly, lipid profiling in plasma of these patients showed a reduction of miR-33 content in the subgroup of patients with higher triglyceride levels (**Figure 55C**).

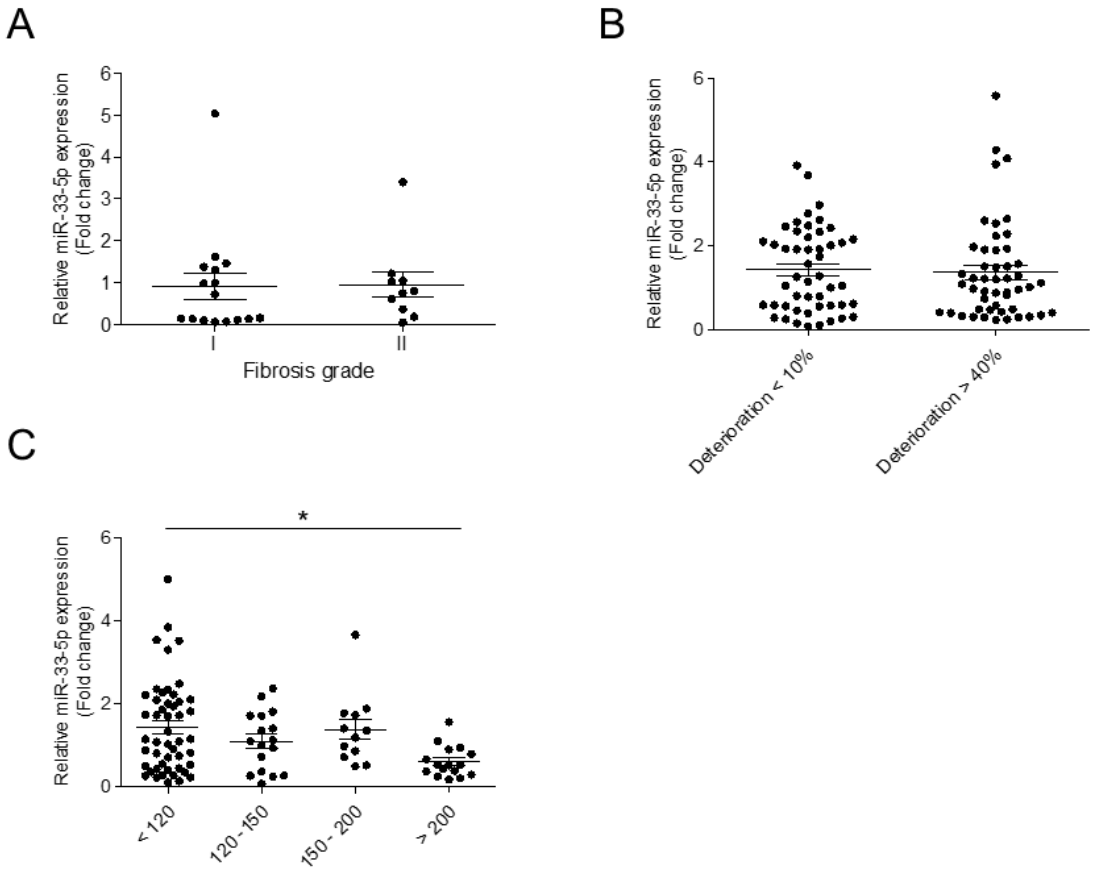

Figure 55. MiR-33-5p levels in kidney samples and plasma from CKD patients. (A) miR-33-5p expression levels in 26 human post-transplant renal biopsies were determined by qRT-PCR using Sybr green. (B) miR-33-5p circulating plasma levels in a cohort of 100 CKD patients were determined by qRT-PCR using Sybr green. (C) Correlation of miR-33 plasma levels and triglyceride levels in plasma samples from patients described in (B). For patient classification see methods section and supplementary tables 2 and 3.

4.4.3. –Role of miR-150, miR-495 as regulators of the profibrotic response by regulating mitochondrial function.

4.4.3.1. –MiR-150 and miR-495 increase the TGF-β profibrotic response in the Human Tubular Renal Epithelial Cell line HKC-8

Quantitative reverse transcription–polymerase chain reaction (qRT–PCR) was performed to confirm the change of miR-150-5p and miR-495-3p expression that had been identified by miRNA expression profiling in the UUO kidney samples. Expression level of these microRNAs was also evaluated in the folic acid nephropathy (FAN) model. We found a 4- and 2-fold upregulation of miR-495-3p and miR-150-5p, respectively in fibrotic kidney samples from both models (**Figure 56A**). In addition, kinetics of miR-150-5p and miR-495-3p expression in the kidneys after 3, 5, 7, 10 and 15 days of UUO procedure was analyzed by qRT-PCR. The expression of these microRNAs was significantly enhanced by 2-fold at 5 days after UUO and remained elevated at 15 days after UUO (**Figure 56B, C**).

TGF-β1, one of the master regulators of fibrogenesis, also induced miR-150 and miR-495 expression in HKC-8 cells more than 2-fold and 3-fold respectively after 24 hours, supporting a potential role for these miRNAs in TGF-β signaling-related events (**Figure 57A and Figure 58A**). To assess whether miR-150 and miR-495 were involved in the pro-fibrogenic transformation of tubular epithelial cells by TGF-β1, the human cell line HKC-8 was transfected with miR-150-5p or miR-495-3p and treated with TGF-β1 for different times. Increasing miR-150-5p and miR-495-3p levels significantly enhanced the TGF-β1-induced mRNA level

expression of the fibrosis-associated markers Acta2, Col1α1 and Fn1 (**Figure 57B and Figure 58B**). Similarly, overexpression of miR-150-5p or miR-495-3p strongly reduced CPT1A and reduced α-SMA protein abundance (**Figure 57C and Figure 58C**). Thus, these microRNAs promote TGF-β1-dependent epithelial dedifferentiation of HKC-8 cells. These data suggest that these microRNAs may participate in the pathogenesis of renal fibrosis caused by UUO or FAN.

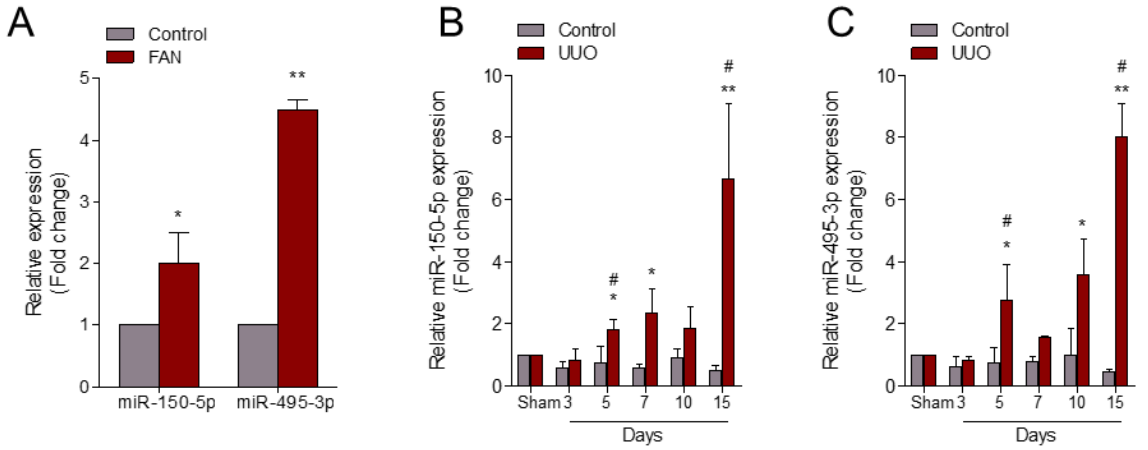

Figure 56. Expression levels of miR-150-5p and miR-495-3p in kidneys from the UUO and FAN models. qRT-PCR analysis of miR-150-5p and miR-495-3p expression in kidneys from mice after FAN (A) and 3, 5, 7, 10 and 15 days UUO for miR-150-5p (B) and miR-495-3p (C). Bar graphs represent the mean of the fold change expression levels ± s.e.m. from 3 (B and C) and 6 (A) mice per group. *P < 0.05, **P < 0.01 compared to their corresponding control conditions; #P < 0.05 compared to control kidneys from mice with the same experimental treatment.

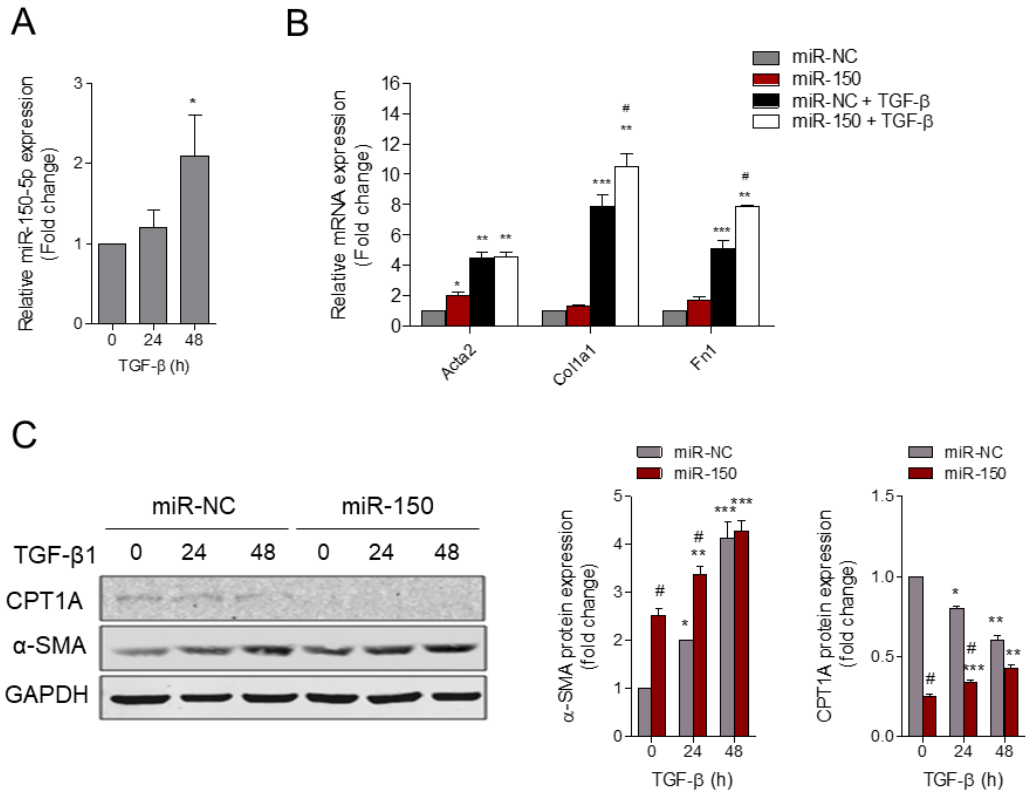

Figure 57. MiR-150 increases TGF-β-dependent profibrotic response in human tubular renal epithelial cells. (A) RT–PCR analysis of miR-150-5p expression in HKC-8 cells treated with 10 ng/ml TGF-β1 for the indicated times. (B) mRNA levels of alpha-smooth muscle actin (α-SMA), alpha 1 type-1 collagen (Col1α1), fibronectin (FN) of cells transfected with miR-NC or mimic miR-150 were determined by qRT-PCR using Sybr green. Cells were treated with TGF-β (10 ng/ml) where indicated. (C) Immunoblots depicting CPT1A and α-SMA levels protein levels in cells transfected with miR-NC and mimic miR-150 for the indicated time points. GAPDH was used for normalization purposes. Bar graphs (right panels) represent the mean of the fold change expression ± s.e.m after densitometric quantification from 3 independent experiments. *P < 0.05, **P < 0.01, ***P < 0.001 compared to their corresponding control conditions; #P < 0.05 compared to cells treated with miR-NC with the same experimental condition.

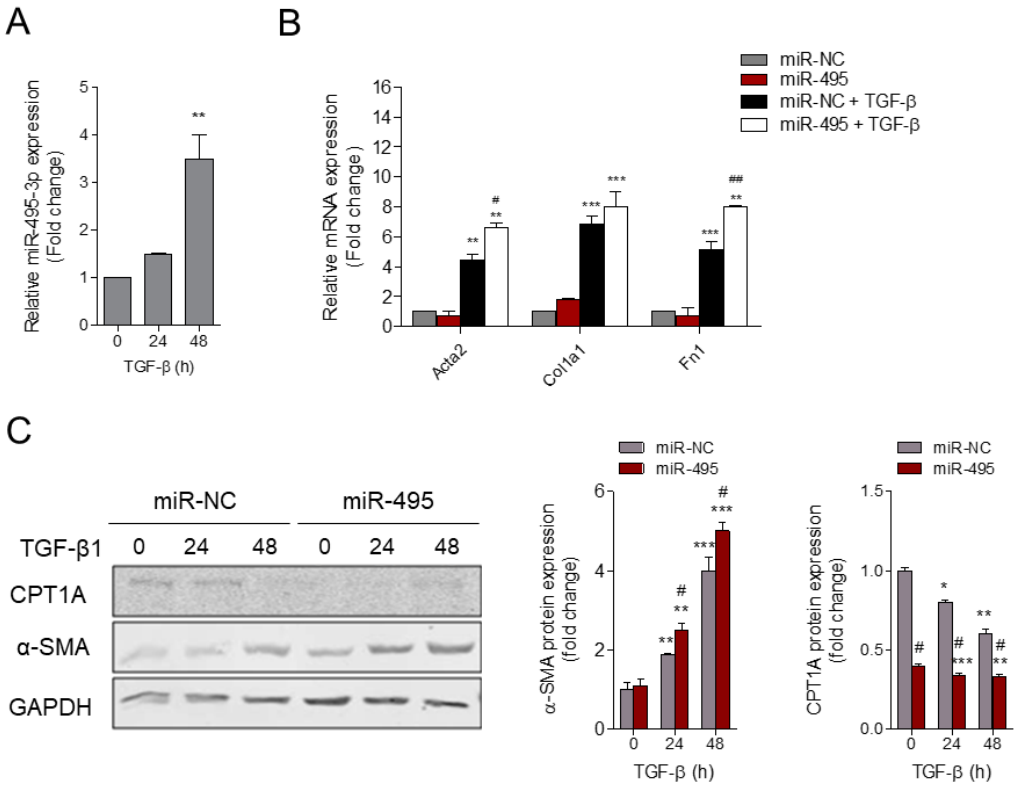

Figure 58. MiR-495 increases TGF-β-dependent profibrotic response in human tubular renal epithelial cells. (A) RT–PCR analysis of miR-495-3p expression in HKC-8 cells treated with 10 ng/ml TGF-β1 for the indicated times. (B) mRNA levels of alpha-smooth muscle actin (α-SMA), alpha 1 type-1 collagen (Col1α1), fibronectin (FN) of cells transfected with miR-NC or mimic miR-495 were determined by qRT-PCR using Sybr green. Cells were treated with TGF-β (10 ng/ml) where indicated. (C) Immunoblots depicting CPT1A and α-SMA levels protein levels in cells transfected with miR-NC and mimic miR-495 for the indicated time points. GAPDH was used for normalization purposes. Bar graphs (right panel) represent the mean of the fold change expression ± s.e.m after densitometric quantification from 3 independent experiments. *P < 0.05, **P < 0.01, ***P < 0.001 compared to their corresponding control conditions; #P < 0.05, ##P < 0.01 compared to cells treated with miR-NC with the same experimental condition.

4.4.3.2. –MiR-150 and miR-495 suppress CPT1A expression and reduce FAO-associated oxygen consumption rate (OCR) in HKC-8 cells

To gain insight into the metabolic consequences induced by the administration of miR-150-5p or miR-495-3p we undertook studies in the human tubular epithelial cell line, HKC-8, and TGF-β1 was used as the model cytokine to induce profibrotic associated changes. To better explore the bioenergetics status of these cells quantitatively, FAO-associated oxygen consumption rate (OCR) and the extracellular acidification rate (ECAR) of HKC-8 cells were measured during sequential treatment with compounds that modulate mitochondrial activity in the presence of palmitate, using a Seahorse XF24 Extracellular Flux Analyzer (more details in the Methods section). After 48h with TGF-β1, HKC-8 cells in the presence of miR-NC showed a consistent decrease in basal, OCR coupled to ATP generation, ATP-linked respiration and in maximal respiration, which relates to 2-4 DNP-sensitive OCR (**Figure 59A, B**). Of note, overexpression of miR-150-5p or miR-495-3p was able to synergize with TGF-β1 in the depression of the mitochondrial respiratory capacity in HKC-8 cells by inducing a significant decrease on basal, ATP-linked respiration, and maximal mitochondrial respiration in comparison to miR-NC-treated cells. We did not observe that these microRNAs induced variations in ECAR (data not shown). The impairment in the OXPHOS induced by miR-150-5p and miR-495 was mirrored by a decrease in ATP content in HKC-8 cells over-expressing each of the miRNAs (**Figure 59C, D**). Consistent with this, mRNA expression levels of their mitochondrial-related target genes CPT1A, PGC1α and the mitochondrial transcription factor A (TFAM), were reduced by half in cells treated

with miR-150 or miR-495 mimics in comparison to miRNA mimic NC-treated cells (**Figure 59E**). Similarly, overexpression of miR-150-5p or miR-495-3p strongly reduced CPT1A protein abundance (**Figure 57C, Figure 58C**). This whole set of results obtained in a cell model of human tubular epithelial cells strongly supports that miR-150 and miR-495 may promote a profibrotic action in kidney fibrosis through the impairment of mitochondrial function.

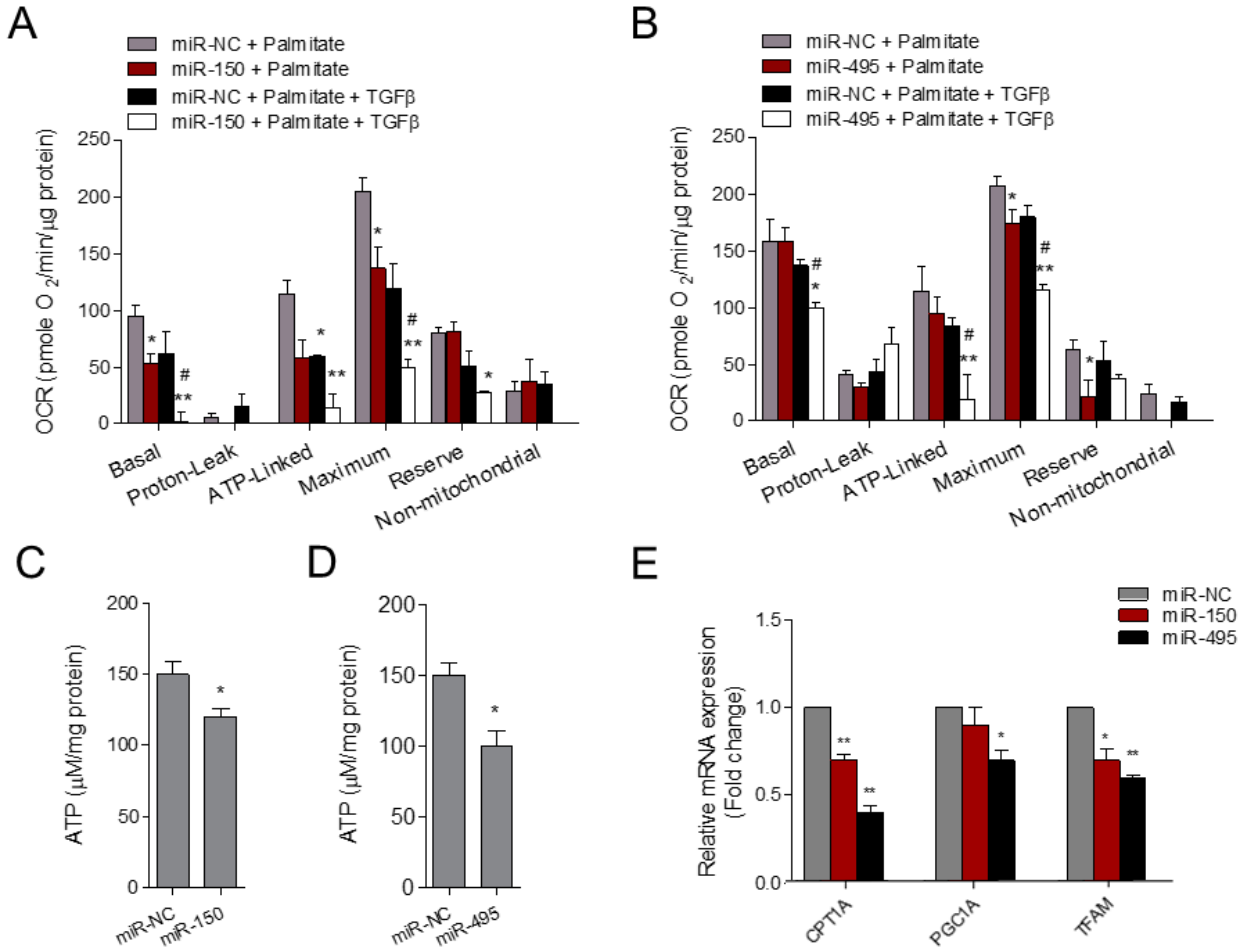

Figure 59. MiR-150 and miR-495 enhance TGFβ1-induced FAO repression in HKC-8 cells. Oxygen consumption rate (OCR) of HKC-8 cells transfected with 40 nM miR-NC or mimic miR-150-5p (A)/miR-495-3p (B) and exposed to 10 ng/ml TGF-β1 for the indicated time points. Cells were pre-treated with palmitate-BSA FAO Substrate (200 mM). Oligomycin (1 µM), FCCP (3 µM) and a combination of antimycin A (1 µM) and rotenone (1 µM) (AA/Rot) were injected sequentially at the time points indicated. Bar graphs show the rates of OCR associated to basal, proton-leak, ATP-linked, maximum, reserve capacity and non-mitochondrial respiratory statuses. Data are represented after normalization by protein amount. (C, D) ATP levels in HKC-8 cells transfected with miR-NC or mimic miR-150-5p (C)/miR-495-3p (D). (E) mRNA levels of CPT1A, PGC1A and TFAM in HKC-8 cells transfected with miR-NC or mimic miR-150-5p (C)/miR-495-3p were determined by qRT-PCR using Sybr green. Bar graphs show the mean ± s.e.m of 4 independent experiments. *P < 0.05, **P < 0.01 compared to their corresponding control conditions; #P < 0.05 compared to cells treated with miR-NC with the same experimental condition.

4.4.3.3. –MiR-150 and miR-495 do not alter mitochondrial transmembrane potential (ΔΨm) and mitochondrial superoxide radical anion production

Mitochondrial membrane potential (ΔΨm) generated by proton pumps (Complexes I, III and IV) is an essential component in the process of energy storage during oxidative phosphorylation. Increased ΔΨm can lead to mitochondrial redox perturbation, while its decrease causes a reduction of ATP production, compromising cell viability [254]. Superoxide radical anion ($O2^{\bullet-}$) is a free radical that can be generated in the mitochondria as a consequence of electron leakage that may occur within several steps of the ETC. Generation of $O2^{\bullet-}$ within the mitochondrial matrix also critically depends on the NADH/NAD^+ and

$CoQH_2$/CoQ ratios and the local O_2 concentration [255]. Its overproduction may lead to the loss of mitochondrial redox homeostasis through different mechanisms, a condition that has been related to many pathological states including AKI and CKD [201]. ΔΨm was examined with the TMRM dye and the superoxide radical anion production with MitoSOX dye. First, we validated these assays by the treatment of cells with FCCP and CCCP as negative controls, for TMRM and MitoSOX respectively, and Oligomycin and Antimycin A as positive controls, for TMRM and MitoSOX respectively, in the human cell line HKC-8. In the case of the TMRM assay, oligomycin treatment induced a 3-fold increase in fluorescence mean of the TMRM compared to the control dye, while FCCP treatment resulted in a 9-fold decrease. Antimycin A and CCCP produced a 35-fold and 2-fold decrease, respectively, in the MitoSOX assay (**Figure 60A, B**). To determine if miR-150 and miR-495 effects on mitochondrial metabolism triggered alterations in these parameters, HKC-8 cells were transfected with a miR-150-5p or miR-495-3p mimic or the corresponding miR-NC. No statistically significant differences in the fluorescence quantification of the TMRM or MitoSOX probes were found between the treatment conditions with the selected miRs and miR-NC (**Figure 60C**).

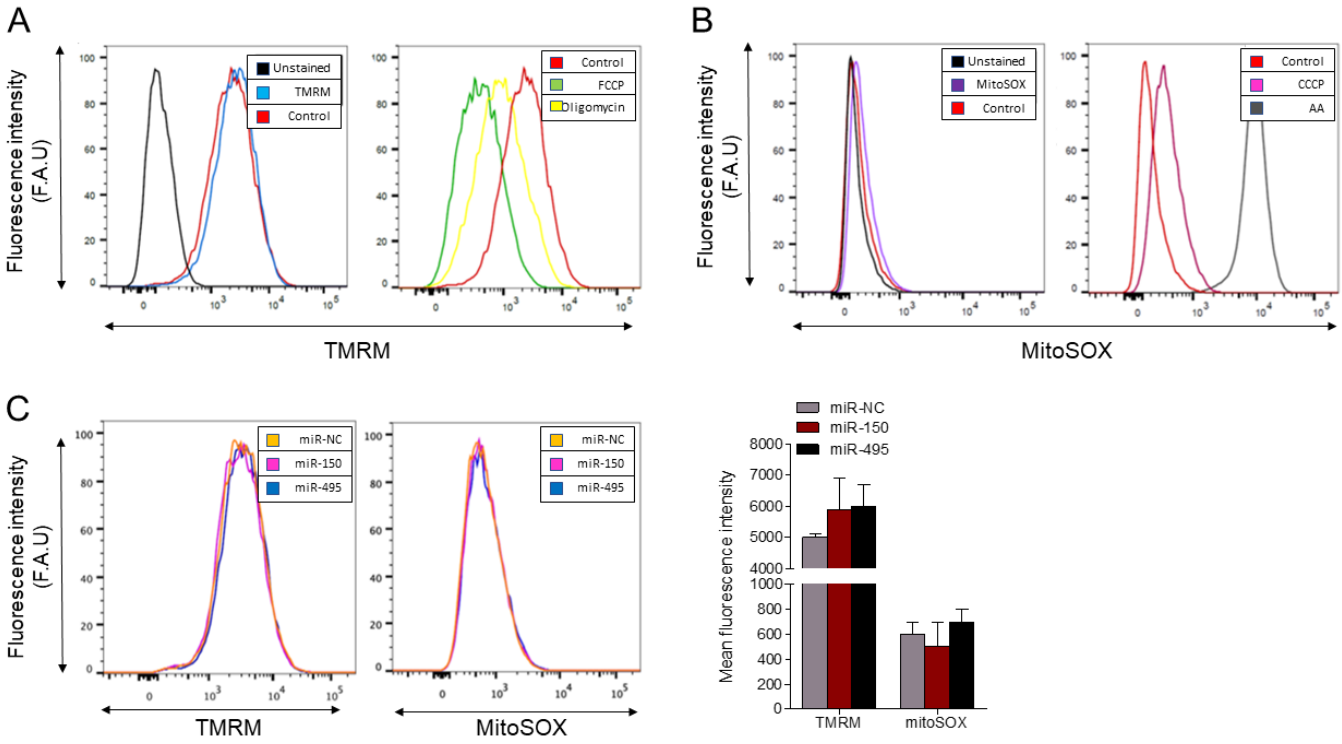

Figure 60. MiR-150 and miR-495 do not alter mitochondrial transmembrane potential (ΔΨm) or mitochondrial superoxide radical production. (A) Representative flow cytometry histograms showing TMRM fluorescence intensities in HKC-8 labeled with the fluorescent dye TMRM (250 nM) exposed to different experimental conditions: unstained, control, FCCP and Oligomycin, measured by flow cytometry. (B) Representative flow cytometry histograms showing mitoSOX fluorescence intensities in HKC-8 labeled with the fluorescent dye MitoSOX (5 µM) exposed to different experimental conditions: unstained, control, CCCP and Antimicyn A, measured by flow cytometry. One from three independent experiments is shown in (A) and (B). (C) TMRM and mitoSOX fluorescence histograms in HKC-8 transfected with 40 nM miR-NC, miR-150 or miR-495. Bar graphs (right panel) represents the mean ± s.e.m of 4 independent experiments. F.A.U: fluorescence arbitrary unit.

4.4.3.4. –MiR-150 and miR-495 levels are not affected in plasma and kidney samples from CKD patients

Finally, we assessed the expression of the selected miRNAs in plasma and kidney biopsies from patients with CKD. Analysis of kidney biopsies from 26 patients (Hospital Ramon y Cajal) did not show correlation between its degree of fibrosis and miR-150-5p and miR-495-3p levels, respectively (**Figure 61A, B**).Circulating plasma levels of miR-150 were determined in a cohort of 100 CKD patients (Hospital Principe de Asturias). These patients were clearly differentiated in two subgroups based on the evolution of their renal

function over a period of 24 months so that 50 patients presented less than 10% of kidney function deterioration while the rest of them had experienced at least a 40% reduction in kidney function. The qRT-PCR quantification of plasma levels of these microRNAs did not show a clear trend towards a differential expression in the two subgroups of patients (**Figure 61C**).

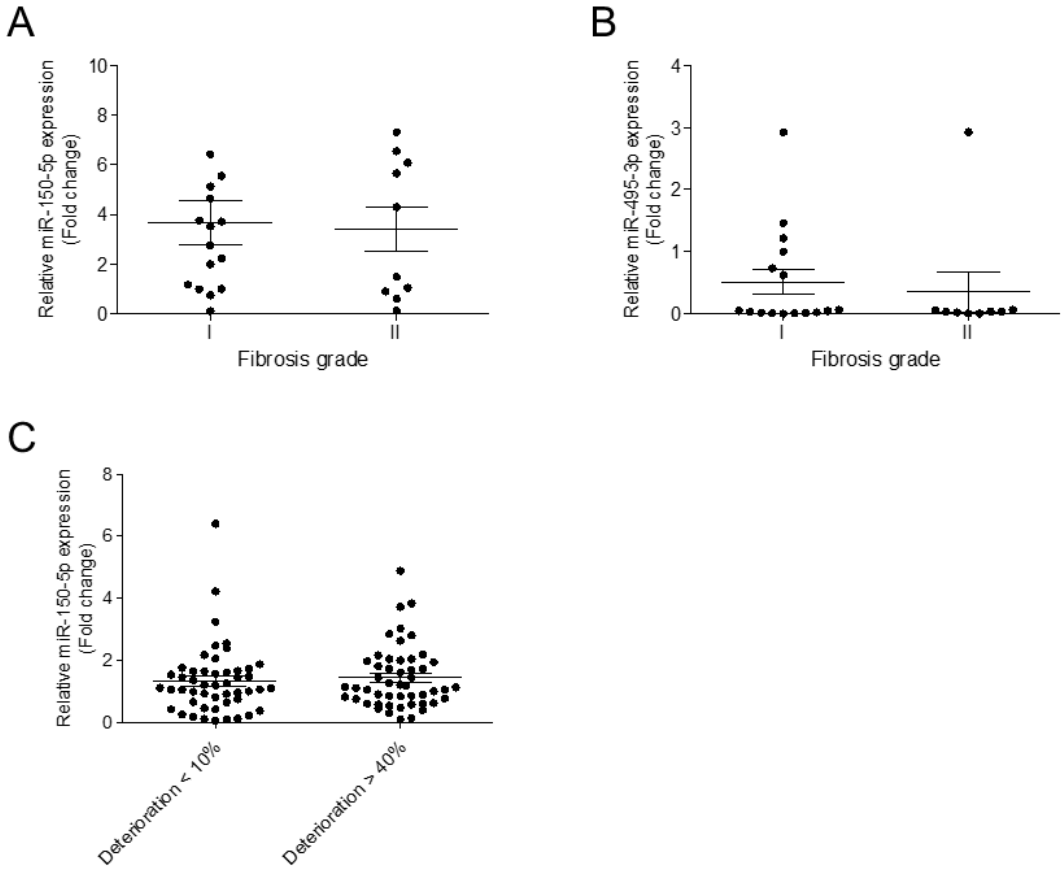

Figure 61. MiR-150-5p and miR-495-3p levels in kidney samples and plasma from CKD patients. (A) miR-150-5p expression levels in 26 human post-transplant renal biopsies were determined by qRT-PCR using Sybr green. (B) miR-495-3p expression levels from the same biopsies as in (A) were determined by qRT-PCR using Sybr green. (C) miR-150-5p circulating plasma levels in a cohort of 100 CKD patients were determined by qRT-PCR using Sybr green. For patient classification see methods section and supplementary tables 2 and 3.

5.Discussion

5.1 Cpt1a enzyme has a protective impact on the outcome of kidney fibrosis

5.1.1. –Protective role of CPT1A in kidney fibrosis development

Epithelial injury is crucial in the pathogenesis of CKD. Direct epithelial damage causes de-differentiation and release of critical fibrogenic cytokines [46]. Tubular epithelial cells are highly energy demanding cells that utilize fatty acid oxidation (FAO) as their main source of ATP [256]. Carnitine palmitoyl-transferase 1 (CPT1) is the rate-limiting enzyme in fatty acid oxidation and is highly expressed in mitochondria-rich organs. CPT1A is the predominant isoform in human and murine kidney tubule mitochondria. It is involving in the translocation of long-chain fatty acids from the cytosol into the mitochondrial matrix using the carnitine shuttle (see Introduction section for details) [257]. A decrease in CPT1A expression and in the rest of the enzymatic machinery involved FAO and mitochondrial biogenesis is commonly observed in patient samples and mouse models of chronic kidney disease [171]. To study the relevance of CPT1A and FAO in renal fibrosis, we generated a transgenic mouse with inducible expression of CPT1A in tubular renal epithelial cells. We found that these mice were partially protected from fibrosis development by using three different models of renal fibrosis: unilateral ureteral obstruction (UUO), folic acid induced nephropathy (FAN) and adenine-induced renal failure (ADN). Genetic overexpression of CPT1A even at moderate levels not only attenuated the profound histopathological changes associated to kidney fibrosis, but also significantly diminished the presence of cellular markers associated to myofibroblast transformation, inflammation and apoptosis. This gain of function counteracted the reduction in FAO associated to fibrosis in the kidney. Moreover, CPT1A was able to abrogate epithelial cell injury and macrophage accumulation in fibrotic kidneys. Studies in human epithelial tubular cells (HKC-8) confirmed that CPT1A prevents from TGF-β-induced dedifferentiation.

5.1.2. –Differences among animal models used for the study of kidney fibrosis

The differences in physiology and in response to injury between mice and humans and the limited number of genes whose modification relates to a specific fibrotic phenotype hamper the precise approach to the complexity of human chronic kidney disease. Thus, animal models do not reflect the broad causality and case histories of the patient population, only allowing for imperfect recapitulations, which lend a basis for oversimplification or misinterpretation of the results. Therefore, considering the specifics and limitations of each model can aid in the adequate interpretation of mechanisms and in the translation into the clinic of potential therapeutic targets [30]. The UUO model is useful to examine mechanisms of tubulointerstitial fibrosis in vivo [229]. In this model, renal blood flow and glomerular filtration rate become significantly reduced within 24 h and interstitial inflammation (peak at 2–3 days), tubular dilation, tubular atrophy and fibrosis are evident after 7 days. UUO involves the activation of TGF-β pathways and a perturbation of the redox status. Among its advantages are consistence and reproducibility, a short time of fibrosis instauration and the availability of the contralateral kidney as a simultaneous control. Among its limitations is the fact that it only mimics human renal fibrosis induced by obstructive uropathy, which represents a small fraction of cases from the etiological standpoint. Also, it lacks standard functional readouts as serum creatinine and BUN are normal due to the presence of the contralateral kidney. Proteinuria is also absent because the injured kidney is completely obstructed and has no urine output [258]. By contrast, folic acid at high dosage induces the formation of crystals rapidly with tubular necrosis in the acute phase (1–14 days) and patchy interstitial

fibrosis in the chronic phase (28–42 days). Folic acid renal injury is induced both by crystal obstruction and direct toxic effect to tubular epithelial cells [230]. In this model, renal function can be assessed as a measure of CKD. It has also been proposed as a model for AKI to CKD transition. However, the effects of folic acid are subject to variability which also depends on FA batches. Significant mortality has been reported in early phases while some changes regress spontaneously after 42 days [30, 259].

Finally, in the adenine-induced modelo f renal failure, orally administered adenine metabolizes to 2,8-dihydroxyadenine, which forms crystals in the proximal tubular epithelia leading to inflammation and subsequent tubulointerstitial fibrosis [231]. This model allows to assess kidney function and induces a stable anemia associated with CKD [260]. Administration by oral gavage avoids the limitations of dietary adenine, as food intake is decreased significantly after mixing adenine with chow, a circumstance that may account for variability in the induction of CKD [231]. Although none of the models adequately represents the generally sluggish progression of CKD in the human setting or recapitulates most common etiologies related to CKD, they are bona-fide models for epithelial cell injury and progressive loss of function. The fact that we observed consistent changes after CPT1A gain-of-function in the three models lends support to the concept that a partial recovery of FAO may prove critical to halt or defer further progression of fibrosis in the kidney.

5.1.3. –Characterization of *in vivo* CPT1A overexpression among transgenic mouse models

A compromise in CPT1 activity will likely have consequences in cell fatty acid metabolism and oxidation. Thus, deletion of CPT1B in the heart causes cardiac hypertrophy and death [261], inhibition of CPT1 in the liver leads to steatosis [262] and skeletal muscle-specific CPT1B deficiency raises the levels of lipotoxic intermediates [263]. By contrast, mice with CPT1C gain-of-function in the brain were protected from high fat diet-induced weight gain [264]. Skeletal muscle specific expression of a malonyl-CoA-insensitive carnitine palmitoyltransferase-1 protected mice against high-fat/high-sucrose diet-induced insulin resistance [265]. This suggests that CPT1 is critical in the control of FAO and has profound implications for the energetic balance of the cell. In the kidney, we are unaware of previous studies addressing the consequences of gain- or loss-of-function strategies for CPT1 at genetic level. Evaluation of CPT1A overexpression in heterozygous mice for this transgene may probe a potential advantage to avoid CPT1A overdose [266, 267]. Our results show that mice overexpressing CPT1A after doxycycline administration presented a 10-fold increase in CPT1A in the whole kidney mRNA levels compared with WT mice. Nevertheless, the level of CPT1A protein expression was only 2.7-fold higher. This asymmetry between mRNA and protein abundance has been previously reported for other genes, mostly mitochondrial proteins or cell cycle regulators [268, 269]. This fact could be attributed to a constant translational rate, microRNA-mediated mRNA translational inhibition, post-translational regulation mechanisms for controlling protein turnover, including the ubitiquitin-proteasome system and the endocytosis-lysosome system [270]. Thus, CPT1A has been reported to be targeted by miR-370 in the liver [271]. Besides, identification of CPT1A residues for ubiquitination and its association with the ubiquitin ligase PARKIN-dependent ubiquitylome [272], experiments with the proteasome inhibitor MG132 did not reflect variations in CPT1A in the cell line HCK-8 (data not shown). Further studies aimed to determine ubiquitin-dependent degradation of mitochondrial proteins did not show that CPT1A was under the control of this mechanism [273]. Due to differential protein stabilities, transcriptional activation is insufficient to provide precision of Tet-on system protein dynamics. Thus, an improved Tet-On based system enhanced with

conditional de/stabilizing elements at the post-translational level has been proposed to deliver simultaneous control of gene expression and protein stability [274]. In addition, increased dox-sensitivity of used optimized reverse tetracyclin-controlled transactivator (rtTA2s-M2) is reported to avoid cellular side effects due to the inhibitory effect of high tetracycline levels on mitochondrial translation and protein synthesis [275].

CPT1A overexpression was also reflected in an increased capacity of kidney tissue to oxidize ^{14}C-palmitate. The enhancement in CPT1A expression levels was similar to other models for CPT1 overexpression. In the murine model with conditional expression in skeletal muscle, CPT1B protein levels were increased by 2.5-fold [265], whereas in the mouse brain model a 3-fold increase in the expression of CPT1C was achieved. In these models, long chain fatty acid oxidation rate was improved by 1.5-fold [264]. These results indicate that the increase in CPT1A expression levels and subsequent gain in FAO in our model are comparable to those reported for other tissue-specific *Cpt1* knock-in mouse models.

5.1.4. –Improved mitochondrial function as a preventive strategy for kidney fibrosis

Alterations in mitochondrial bioenergetics have proven to be decisive in kidney disease, not only in CKD but also in acute kidney injury (AKI) [276]. Several genetic and pharmacological approaches have been attempted in an effort to revert mitochondrial dysfunction associated to CKD and to decipher if this functional alteration is responsible for its progression. In addition to changes in CPT1, multiple enzymes involved in fatty acid metabolism are also affected by CKD. This is likely due to the fact that the levels of the transcriptional regulatory complex, PPAR-α- PGC1α, are also significantly reduced [196, 251, 277]. This complex is also the main transcriptional regulator of most genes involved in mitochondrial biogenesis. It is important to point out that mice null for PGC-1α or PPAR-α do not exhibit renal dysfunction or structural abnormalities in basal conditions [278, 279]. These studies indicate that PGC-1α and PPAR-α are not required to preserve an intact renal function. Nevertheless, increasing their expression or their activity is associated with a protective phenotype against kidney injury [197, 198]. By contrast, tubule-specific deletion of mitochondrial transcription factor A (TFAM), a key activator of mitochondrial transcription and mitochondrial genome replication, was sufficient to induce fibrosis [280].

Insofar as preservation of kidney structure and function requires the concourse of a fully functional mitochondrial critical mass, CPT1A is expected to have a crucial role in the maintenance of energy availability in the kidney. We found that CPT1A not only attenuated the profound histopathological changes associated to kidney fibrosis, but also significantly diminished the presence of cellular markers associated to myofibroblast transformation, inflammation and apoptosis. The extent of the protective role of tubular CPT1A overexpression was comparable to the one reported for PGC-1α against Notch-induced kidney fibrosis and FAN models [197]. Both gain-of-function strategies were able to mitigate the impairment in mitochondrial morphology induced by fibrosis in the kidney albeit the fatty acid oxidation defect induced by fibrosis was not equally prevented by PGC-1α and CPT1A overexpression (this study). Thus, the mRNA expression levels of the FAO-related genes *Acox1* and *Cpt2* were restored in fibrotic kidneys from CPT1A KI mice compared to those of WT ones (**Figure 34**). However, PGC-1*α* overexpression almost completely normalized CPT1 and ACOX1 levels. Noteworthy, neither tubular CPT1A nor PGC-1α overexpression were able to prevent the global downregulation of glycolysis-related genes induced by FAN.

PGC-1*α* also exerts a protective action in other renal pathologies [196]. During acute kidney injury

(AKI) induced by renal ischemia-reperfusion, tubular-epithelial-specific transgenic expression of PGC-1α or NAD^+ supply attenuated pathological changes and were associated with improved renal function [199]. Hypoxia also promotes a decrease in FAO. Increased FAO has been observed in differentiated proximal tubular cells surviving a reversible episode of AKI, highlighting the importance of FAO in renal disease [281]. By contrast, the tolerance window for both high or low PGC-1α levels in less metabolically active renal cells, such as podocytes and endothelial cells, is narrower [200].

Attenuation of renal fibrosis and inflammation induced by CPT1A overexpression had also been documented in the alluded study regarding PPARα gain of function [198]. PPARs are metabolic regulators that also present anti-inflammatory properties in various organs including the kidney [282]. In consistence with our model, the increased expression of pro-inflammatory cytokines including IL-1β, IL-6, and TNF-α found in WT mice was significantly reduced in kidney tissue of mice overexpressing PPARα [198]. In contrast, the expression of the anti-inflammatory cytokine IL-10 and of the enzyme arginase-1 were significantly increased in kidney tissue of these transgenic mice compared to WT mice subjected to UUO. In keeping, the pharmacological activation of PPAR- α by its agonist fenofibrate not only improved FAO but also significantly reduced renal fibrosis development in the UUO and FAN models [171]. Consistently, fenofibrate strongly induced the expression of FAO enzymes CPT1, CPT2 and ACOX1. Similarly to our study in CPT1A KI mice, treatment with fenofibrate restored the expression of FAO-related enzymes but not those involved in glucose utilization[171]. The cause for this selective effect may be multifaceted and possibly related to the complex interaction between these two fundamental energy-providing sources (see below for a detailed discussion of the Randle cycle).

The effect of PPAR-α agonists such as fibrates has been also studied in patients with CKD [283]. However, the obtention of unequivocal conclusions has been hampered by the fact that fibrates interfere with creatinine secretion, which alters creatinine-based eGFR estimations [284]. Both the Fenofibrate Intervention and Event Lowering in Diabetes (FIELD) and the Action to Control Cardiovascular Risk in Diabetes (ACCORD) studies indicated statistical improvement in urinary albuminuria in patients with diabetic kidney disease who were treated with fenofibrate. These studies also indicated a small but significant reduction in GFR; however, the GFR effect seems smaller in patients than in animal models [285, 286].

The phenotype observed in the fibrotic kidneys from CPT1A KI mice in our study should also be analyzed in the light of interventions modulating CPT1A activity. For example, treatment with the CPT1 inhibitor Etomoxir enhanced FAN-dependent kidney injury. Etomoxir shifted metabolism towards glycolysis, evidenced by higher *Glut1* and *Pfk1* expressions. However, this metabolic shift did not improve but rather worsened the development of fibrosis [171]. By contrast, C75, a synthetic compound that increases CPT1 activity and blocks fatty acid synthase, attenuated kidney fibrosis associated to folic acid administration [171]. This treatment restored expression of *Cpt1* and *Acox1* without restoring the defect in glucose utilization, an scenario also consistent with our observations in the CPT1A KI mouse model. In addition, C75 had also a protective role in the ischemia/reperfusion injury model: stimulation of CPT1 activity by C75 recovered ATP depletion, improved renal function, attenuated tissue injury, and inhibited pro-inflammatory cytokine production and neutrophil infiltration [287]. So far, C75 is still under the preclinical stage for developing it as an antitumor agent by utilizing its capability of inhibiting fatty acid synthase activity [288]. However, clinical development of C75 has been hampered by associated anorexia and weight loss caused by the treatment

with this compound [289]. Whether these side effects can be tolerated after short-term administration for treating renal injury needs to be further studied. The toxicity and solubility of C75 are additional considerations for moving it to a phase I clinical trial.

Globally, integration of all these results support that restoring FAO, but not glucose utilization or enhancement of mitochondrial density, is the main responsible event for kidney fibrosis amelioration.

5.1.5. –Molecular mechanisms underlying mitochondrial defects in kidney fibrosis mouse models

At the mechanistic level, TGF-β transcriptionally suppresses FAO though epigenetic downregulation of PGC-1α and PPAR-α in a SMAD3-dependent manner which directly binds to an intronic area on the *PPARGC1A* gene. This region overlaps with an active enhancer specific histone tail modifications (H3K4me1). Consequently, it inhibits PGC-1α expression in many cell types, including RTEC [171, 277]. In addition, a reverse crosstalk of TGF-β and PPARβ/δ signaling has been described. A major class of PPAR target genes, including ANGPTL4, CPT1A, ADRP and PDK4 are reported to be repressed by TGF-β, which is counteracted by PPARβ/δ activation. This is mediated by the TGF-β-induced recruitment of the corepressor SMRT to PPAR response elements and its release by PPARβ/δ ligands. Some TGF-β-induced genes can be in turn downregulated by PPARβ/δ agonists. A cooperative regulation by both ligands was also observed for a minor group of genes, mostly involved in the regulation of cell proliferation [290, 291]. The role of TGF-β in mitochondrial respiration differs among cell types. TGF-β1 induced differentiation of fibroblasts is accompanied by energetic remodeling of myofibroblasts with an increase in mitochondrial respiration and mitochondrial content [292]. In primary human lung fibroblasts, TGF-β has been described to upregulate mitochondrial mass through the SMAD2/3/ C/EBPβ/ PRMT1/ PGC-1α signal pathway [293]. In podocytes, TGF-β increases mitochondrial oxygen consumption and ATP generation via mTOR in the presence of diverse energy substrates, including palmitate [294]. Furthermore, the transcription factor Hes1, a downstream target of the Notch signaling pathway, can directly bind to *PPARGC1A* promoter region and inhibit PGC-1α expression [200]. In addition, the Notch signaling members Jag1 and Notch2 repress the expression of Tfam [280]. However, these observations do not exclude the contribution of other transcription factors also involved in the regulation of FAO and other metabolic processes. Whether TGF-β signaling also regulates the expression levels of CPT1A and other genes involved in FAO in a PGC-1α/PPAR-α-independent manner has not been elucidated.

Activation of AMPK occurs when cells sense that ATP levels are becoming limiting for energy provision. This leads to acetyl-CoA carboxylase (ACC) inactivation and malonyl-CoA decarboxylase (MCD) activation, favoring catabolism [295, 296]. Overexpression of CPT1A counteracted fibrosis-induced activation of AMPK, thus attesting to another protective action by restoring the energy-alarm settings. In a similar fashion another study showed that PGC-1*α* expression almost completely normalized decreased phosphoacetyl-CoA carboxylase protein levels in the kidneys from Notch1-overexpressing mice [197].

ACC catalyzes the formation of malonyl-CoA from acetyl-CoA, while MCD is involved in the conversion of malonyl-CoA into acetyl-CoA and carbon dioxide [297]. ACC inactivation and MCD activation promote the decrease in malonyl-CoA concentration, which can also derive from glucose metabolism. This metabolite inhibits CPT1A activity. This effect reroutes fatty acids towards esterification and FAO inhibition [298] [299]. Given the fact that CPT1A overexpression did not prevent the decrement in the expression of

glucose utilization genes, glucose-derived malonyl-CoA levels were not expected to be different between fibrotic kidneys from CPT1A KI and WT mice. However, activated AMPK form-derived malonyl-CoA levels might be higher in CPT1A KI fibrotic kidneys. Therefore, CPT1A activity should be affected by this enzymatic inhibitory mechanism in a more extensive degree in kidneys from CPT1A KI mice, a fact that could contribute to mask its protective active action in fibrosis development.

5.1.6. –Effect of restoring lipid metabolism on renal epithelial damage

Epithelial dedifferentiation is characterized by the loss of epithelial markers and gain of mesenchymal features. However, the contribution of this phenomenon to the fibrotic response is complex and still not fully understood. While a full EMT conversion remains controversial, some evidence suggests that a partial EMT is sufficient to induce tubular function impairment, triggering cell cycle arrest and promoting the release of critical fibrogenic cytokines that activate interstitial myofibroblasts in a paracrine fashion. This has led researchers in the field to sustain that this partial EMT would account for the transformation of TECs into myofibroblasts [249].

As already mentioned, the reported defect in fatty acid oxidation may jeopardize an adequate input of energy for the tubular epithelial cell. The importance of impaired mitochondrial respiration as a forerunner of tubular damage is also underscored by the fact that a mitochondrial substrate overload surpasses the catabolic capacity of mitochondrial β-oxidation and promotes tubular injury. Under these conditions, free CoA levels decline as increased supply and oxidation of fatty acids lead to accumulation of an excess of acetyl-CoA. This results in an energy deficit, redox imbalance and impaired mitochondrial respiration [300] [301].

In contrast to heart myocardiocytes and other tissues, which may switch to glucose oxidation when fatty acid oxidation is decreased [302, 303], TEC exclusively rely on FAO and they are unable to switch to glycolysis. Thus, pharmacological inhibition of CPT1 results in ATP depletion, cell death, and dedifferentiation [171]. Our data show that FAO gain-of-function acquired through either genetic engineering or adenoviral transduction of *CPT1A* resulted in a profound modification of the bioenergetics profile of TECs, reflected in a higher level of mitochondrial respiration, even in the presence of negative modulators with profibrotic action, such as TGF-β. These results indicate that the TGF-β1-induced FAO blockade is likely mediated by CPT1A. We have observed that this metabolic reprogramming mediated by CPT1A overexpression in renal epithelial cells prevents from TGF-β-induced dedifferentiation through the expression of the mesenchymal markers a-SMA, collagens and fibronectin. This was also the case for Ppargc1a overexpressing epithelial cells, which did not show alterations in their palmitate-induced oxygen consumption rate after TGF-β1 treatment [197]. Increasing *Tfam* expression in RTECs also improved the FAO defect both in the TGF-β1–induced Notch activation models and in the JAG1 co-culture system [280]. In both approaches these cells were protected from TGF-β1-induced dedifferentiation. Similarly, fenofibrate-mediated Ppar-α activation normalized TGF-β1-induced FAO repression and ameliorated TGF-β1-induced dedifferentiation [198]. Conversely, proximal tubule cells (PTCs) treated with the CPT1 inhibitor Etomoxir exhibited expression of mesenchymal genes [171]. Hence, our results as well as those from other groups support that mantaining an adequate level of FAO is critical to prevent TGF-β1-induced TECs dedifferentiation.

Metabolic reprogramming of renal epithelial cells overexpressing CPT1A was also associated with a dramatic decrease in glucose utilization. This observation could relate to a reciprocal regulation between

FAO and glycolysis first described by Randle for hepatic and skeletal muscle tissue (review in [304]. Since then, the term "Randle cycle" was coined and it refers to the occurrence of a competitive regulatory mechanism affecting glucose oxidation enzymes by fatty acid utilization in muscle and adipose tissue [305]. The main mechanism of inhibition of glucose utilization by FAO includes pyruvate dehydrogenase (PDH) inhibition caused by acetyl-CoA and NADH accumulation resulting from FAO, and 6-phosphofructo-1-kinase (PFK) inhibition resulting from citrate accumulation in the cytosol. These effects reroute glucose towards glycogen synthesis and pyruvate to anaplerosis and/or gluconeogenesis [306-308]. Therefore, the glucose-fatty acid cycle, although not determined in the kidney, could be an underlying mechanism that could explain the data related to the metabolic response induced by CPT1A overexpression. Alternatively, it is possible that CPT1A inhibition potentially due to reduced malonyl-CoA levels after glycolytic repression would be only discrete after CPT1A overexpression.

5.1.7. –Macrophage population profile in renal epithelial damage

Our data also reflected that increased levels of CPT1A alters monocyte/macrophage infiltration pro-inflammatory profile in fibrotic kidneys. This reduction strongly correlates with a delayed progression of kidney fibrosis in clinical studies and animal models of kidney disease [48]. Reduced macrophage infiltration was reported in the mouse model of renal metabolic reprogramming mediated by re-expression of PPAR-α after UUO [198]. Of note, lipid accumulation reflected by an imbalance between FA utilization and FA supplies, as in the case of FAO inhibition, can also induce the activation of the pro-inflammatory pathway NF-κB in monocytes. This mediates ER stress and redox distress, creating a pro-inflammatory state in the vicinity of renal PTCs [309, 310]. Nonetheless, the contribution of M1 and M2 macrophage populations to kidney fibrosis is still controversial. M1 cells are replaced by M2 cells during the repair response. M1-to-M2 transition can influence CKD progression [54, 311]. Our data show that CPT1A overexpression reduced the proportion of the M1 (CD86+) subpopulation in the FAN model. In addition, M2 (CD206+) and the double positive (CD86+, CD206+) populations were higher in obstructed kidneys from mice overexpressing CPT1A. Both phenomena may be contributing to the renal protective phenotype of these mice. This is supported by the fact that M1 macrophages have been reported to participate in the injury process by releasing pro-inflammatory molecules. The M2 macrophage population has been generally considered to have an anti-inflammatory role, promoting matrix remodeling and tissue repair [54]. However, recent studies show that M2 macrophage depletion specifically inhibits epithelial-to-mesenchymal transition (EMT) and the subsequent renal fibrosis [312]. In consistence, another study has shown that the transference of M2 macrophages in mice with previous depletion of circulating leukocytes (adoptive transplantation) enhanced renal fibrosis induced by UUO [312]. Whether the balance between M1 and M2 macrophage subpopulations observed in fibrotic kidneys from CPT1A KI is the consequence of changes in the cytokine or metabolic profiles or in both, remains to be established.

Together, these results strongly suggest that CPT1A prevents the fibrotic phenotype in the kidney most likely by a multiplicity of mechanisms that nevertheless stem from a core one, which relates to its critical function in the facilitation of FAO, recovering the deprived energy status associated with kidney fibrosis development.

5.2 MiR-33, a quintessential regulator of lipid metabolism with a new role in kidney fibrosis

5.2.1. –miR-33 as a new regulator of lipid metabolism during kidney fibrosis

Mammalian metabolism is highly regulated through an elaborate control of circuits among cells, tissues and organs, participating in the maintenance of whole-body homeostasis. Regulatory non-coding RNAs such as miRNAs have also recently emerged as important modulators of metabolic homeostasis [313]. The miR-33 miRNA family constitutes one of the most well-characterized examples of miRNA-mediated regulation of lipid metabolism. The miR-33a and miR-33b miRNAs are located in introns of the genes encoding sterol response element binding proteins (SREBP)-2 and SREBP-1, respectively. These are master transcription factors involved in cholesterol/lipid biosynthesis and trafficking. MiR-33a and miR-33b are co-transcribed with their respective host genes, boosting cellular cholesterol and fatty acid levels by regulating genes involved in cellular cholesterol efflux/HDL biogenesis (*ABCA1* and *ABCG1*) and fatty acid oxidation in a negative feedback loop with SREBP proteins [215, 218, 219].

We demonstrated that the absence of miR-33 resulted in a reduced fibrotic response in two models of kidney fibrosis, FAN and UUO. We also proved that this protection was not due to changes in levels of macrophages or other hematopoietic cells (data obtained from experiments with bone marrow transplantation not shown in this thesis). The absence of miR-33 correlated with increased FAO, less accumulation of TAG and increased expression of genes regulating cholesterol efflux, providing a basis for the beneficial action of miR-33 absence in kidney fibrosis.

MiRs play critical roles in normal kidney development and kidney injury by fine-tuning gene expression [118]. Thus, renal tubular-specific deletion of DGCR8 leads to hydronephrosis and renal malformations, whereas DICER deletion in these cells protects against renal ischemia-reperfusion injury [314, 315]. Expression of miR-33a was slightly decreased in UUO fibrotic kidneys. However, in response to FA miR-33-5p kidney level was not altered 33KO WT ones. This discrepancy could be attributed not only to a transcriptional regulation that differs among injury models, but also to a post-transcriptional regulation of miR-33a, involving its processing by DROSHA and DICER.

5.2.2. –Global control of lipid metabolism by miR-33

Our results show that the loss of miR-33 promotes fatty acid oxidation and reduces triglyceride accumulation in fibrotic kidneys. These metabolic features have been associated with a protected fibrotic phenotype in the kidney though different strategies directed towards the improvement of fatty acid consumption. Previous work has described a crucial role for miR-33 in liver and macrophages, regulating lipid metabolism and trafficking, with a profound impact in metabolic syndrome and atherogenesis [316]. MiR-33 regulates the availability of fuel sources used in mitochondrial respiration by targeting genes involved in fatty acid oxidation *CROT*, *HADHB*, *CPT1* as well as expression of *PGC1α* and AMP-activated protein kinase (*AMPK*), a kinase responsive to changes in cellular energy status and required for the activation of PGC1α [215, 317]. Thus, our results are consistent with the effects described for miR-33 inhibition, resulting in enhanced mitochondrial biogenesis and improved mitochondrial function. MiR-33 has also been described to target PPAR-α, the master regulator of the fatty acid oxidative machinery, which could be also contributing to our results regarding miR-33 regulation of mitochondrial function [202, 318]. Beyond the fact that metabolic

alterations have also been reported in the setting of global miR-33 deficiency, we also proved that miR-33 impairs FAO in renal epithelial cells, thus contributing to kidney fibrosis progression. In addition, it has been previously demonstrated that miR-33 also targets critical genes involved in glucose (*IRS2, PGC1α, G6PC*) and cholesterol metabolism (*ABCA1, ABCG1*), fatty acid synthesis (*SREBF1, FASN, ACLY, ACACA*) and bile acid synthesis (CYP7A1) [317].

In addition to transcriptional changes, lipid droplet accumulation has also been repeatedly observed in kidneys of patients with CKD and mouse models of CKD [319]. The incubation of cultured tubule cells in long-chain fatty acid-containing medium resulted in an inflammatory response including ER stress, NF-kB activation and oxidative stress causing lipotoxicity [309, 310]. Lipid toxicity has been proposed as a key mechanism favoring kidney fibrosis. In this setting, overexpression of the long chain fatty acid transporter CD36 resulted in long chain fatty acid and TAG lipid droplet accumulation. However, this lipid overload did not result in kidney disease or fibrosis development, but an increased susceptibility to acute and chronic kidney disease was observed in these animals [171, 195]. miR-33 may also promote the accumulation of lipid droplets in the kidney as described in other organs; contributing to kidney damage. Thus, long-term anti-miR-33 therapy in mice fed a HFD resulted in a derepression of numerous miR-33 target genes involved in cholesterol export and FAO but caused a significant increase in the expression of genes associated with cholesterol and fatty acid synthesis [218]. This also resulted in increased triglyceride levels after a high fat diet. Beyond a defective fatty acid oxidation or an increase in fatty acid uptake, enhanced renal *de novo* lipid synthesis might be an important cause of renal lipid accumulation that may contribute to the progression of CKD [320]. SREBPs regulate cholesterol biosynthesis and uptake and fatty acid biosynthesis. SREBP-1 and fatty acid synthase (FASN) expression are markedly increased in streptozotocin-induced diabetic rats. Cell culture studies showed that high glucose levels increased SREBP1 expression, which in turn led to increased triglyceride accumulation [210, 321]. These findings led the investigators to hypothesize that renal lipid accumulation is due to increased lipid synthesis and is important for progression of CKD promoted by a diabetic state. However, due to the reduced triglyceride accumulation in kidneys from miR-33 KO, lipid accumulation does not seem to be a predominant mechanism promoted by miR-33 in the kidney. Mirroring this scenario, we found that miR-33 was able to exert similar profibrotic actions to those reported for miR-21, which are related to profound and specific metabolic derangements closely associated to mitochondrial dysfunction by targeting PPAR-a [126, 131]. Similarly, miR-21 inhibition prevented the renal profibrotic phenotype by reversing the mitochondrial defects associated with this outcome [131, 148, 322].

5.2.3. –The profibrotic role of miR-33

Gene expression and histological analyses using miR-33KO mice showed that suppression of miR-33 alleviated fibrotic responses to UUO and FA. These data were consistent with recent reports that established miR-33 as an important regulator of hepatic fibrosis. They showed that inhibition of miR-33 reduces liver fibrosis in a nonalcoholic steatohepatitis model. Further, activation of hepatic stellate cells, the liver-specific mesenchymal cells and primary source of liver fibroblasts, induces the expression of the SREBP-2/miR-33 locus, contributing to the fibrotic process [323]. This profibrotic role for miR-33 has been also reported in cardiac fibrosis. Cardiac fibroblast-specific deficiency of miR-33 reduced cardiac fibrosis in response to pressure overload by transverse aortic constriction. The proposed mechanism underlying this

response was that deficiency of miR-33 impaired cardiac fibroblast proliferation, due to altered lipid raft cholesterol content [324, 325]. Whether proliferation of any relevant renal cell type for fibrosis development, such as epithelial cells or myofibroblasts is being affected by miR-33 during the fibrotic response has not been addressed in our work. In the cardiac fibrosis outcome in response to pressure overload, the effect of the absence of miR-33 in cardiofibroblasts was modest compared with that observed in global miR-33–deficient mice, suggesting that other cell types relevant for cardiac fibrosis such as macrophages may also be involved in the fibrotic phenotype observed in miR-33–/– mice.

Macrophage infiltration directs fibrogenesis in the kidney. Proportion of M1 and M2 subpopulations is essential for fibrosis progression. On the other hand, miR-33 has been shown to play an important role in the development of other chronic inflammatory conditions such as atherosclerosis and in the regulation of macrophage polarization. Additional evidence suggests that miR-33 facilitates renal fibrosis in diabetic nephropathy though the activation of the NF-κB/TGF-β inflammation pathway by targeting SIRT6 [326]. Our data show that protection against kidney fibrosis in 33KO mice was not due to changes in bone marrow macrophages or other precursor hematopoietic cells (data obtained from experiments with bone marrow transplantation not shown in this thesis). Macrophage-specific miR-33 deletion shifted macrophage metabolism towards oxidative respiration, enhanced spare respiratory capacity and induced an M2 macrophage polarization–associated gene profile. M2 subpopulation is reported to promote matrix remodeling and tissue repair. Therefore, it would be expected that the M2 macrophage phenotype acquired in the absence of miR-33 could contribute to the abrogation of the fibrotic phenotype.

5.2.4. –Lipid and miR-33 alterations in plasma samples from CKD patients

In our patient samples, miR-33 plasma levels did not differ between patients with different progression stages of kidney disease. In contrast, miRNA-33 levels increased in the sera of diabetic nephropathy patients as well as in the sera and nephridial tissues of a diabetic nephropathy rat model [326]. Differences between patterns of miR-33 levels among human and mouse models can be in part explained by the differential expression of the miR-33b isoform in humans [316, 327]. In humans, miR-33b and miR-33a are present in intron genes of SREBP-1 and SREBP-2 gene, respectively. However, in mice there is only one miR-33 gene, which is conserved with human miR-33a. MiR-33 members co-express with their host genes, which are induced under different metabolic conditions: Srebp-2 gene expression is stimulated during conditions of low intracellular cholesterol, while *Srebp-1* is induced during hyperinsulinemia or insulin resistance [215]. In regard to differences in the profile of specific lipid moieties, our data show that miR-33a plasma levels inversely correlated with the abundance of circulating TAG in CKD patients. These data result paradoxical due to the proposed profibrotic role for miR-33 in kidney fibrosis and the common hypertriglyceridemia reported in ESRD patients. Triglyceride plasma levels mostly depend on VLDLs and their catabolism in oxidative tissues [328]. Enhanced triglyceride levels in ESRD patients have been attributed to the upregulation of ANGPTL4, a protein that reduces the activity of the enzymes lipoprotein lipase and 11betahydroxysteroid dehydrogenase (11beta-HSD), involved in the generation of cortisol and corticosterone [320, 329, 330]. Whether, ANGPTL4 is subject to regulation by miR-33 is yet to be explore. The reported effects of miR-33 on triglyceride levels depend on the species studied and the strategy used to modulate miR-33. Long-term therapeutic silencing of miR-33 in mice increased circulating triglyceride (TAG) levels,

while in non-human primates miR-33 antagonism resulted in a marked suppression of plasma triglyceride levels [218]. MiR-33 KO mice exhibited increased food intake and an insulin resistant phenotype, accompanied by increased circulating levels of TAG [226].

To promote protective effects on kidney fibrosis and to avoid adverse effects on renal dysfunction, effective strategies such as cell- or tissue-specific targeting of miR-33 have been explored and recently submitted (Price NL, Miguel V, Ding W, Singh AK, Malik S, Rotllan N, Goedeke L, Zeiss C, Baldán A, Bahal R, Reshetnyak YK, Rodríguez-Puyol D, Suárez Y, Fernández-Hernando C, Lamas S. Genetic deficiency or pharmacological inhibition of miR-33 enhances renal fatty acid oxidation and protect from kidney fibrosis).

5.3 miR-150 and miR-495 as new regulators of the metabolic derangements of renal fibrosis

5.3.1. –Regulation of mitochondrial function by miR-150 and miR-495 enhance profibrotic responses in renal tubular epithelial cells

The discovery of microRNAs as key regulators of pathophysiological processes has fostered research on their use as therapeutic agents in almost every clinical setting, including kidney disease [85]. Our study with the miRNA array confirmed the altered expression of previously described fibrosis-related miRNAs, such as the upregulation of miR-214 or the downregulation of miR-200, miR-27, miR-29 or miR-196 in UUO fibrotic kidney samples (**Table 9**). Several recent important studies have driven the attention towards perturbations in epithelial cellular metabolism that may provide new mechanistic insight into the molecular basis of fibrosis. MicroRNA-based regulation of this metabolic derangement is a promising avenue for the treatment of this disease [117].

Epithelial injury co-exists with a defect in fatty acid oxidation, the main source of energy for tubular epithelial cells. It leads to their dedifferentiation inducing tubular function impairment, triggering cell cycle arrest and promoting the release of critical fibrogenic cytokines that may contribute to activate interstitial myofibroblasts [171, 277]. MiR-150 and miR-495 expression was increased in mouse fibrotic kidneys and in HKC-8 after the treatment with TGF-β1. They decreased the expression level of their mitochondrial-related potential target genes CPT1A, PGC1α and TFAM. This was reflected in a decreased basal, ATP-linked and maximal OCR and ATP content after miR-150 and miR-495 in HKC-8 cells, while ECAR was only affected by transfection of these miRs in the presence of TGF-β. This effect was accompanied by an enhanced TGF-β profibrotic response in HKC-8 cells.

5.3.2. –MicroRNA regulation of mitochondrial function in renal fibrosis

CPT1A, PGC1α and TFAM genes are closely related to mitochondrial function and biogenesis [164]. Alterations in mitochondrial bioenergetics are critical in kidney disease [276]. The impaired expression of these genes is associated with CKD, while its preservation contributes to kidney integrity as shown in several models of damage. Thus, Han et al found that tubular gain-of-function of PGC-1α protected mice against Notch-induced kidney fibrosis and reversed the mitochondrial derangements associated with this model [197]. Similarly, re-expression of *Tfam* in tubule cells prevented Notch-induced metabolic and profibrotic reprogramming [280], while treatment with the CPT inhibitor Etomoxir, exacerbated kidney injury after folic

acid injection [171]. Therefore, the decreased expression of these mitochondrial genes induced by miR-150 and miR-495 could favor a damaged epithelial phenotype.

The decline we observed in OCR associated with epithelial cell damage is in accordance with previous reports [171]. This study also reported that glucose oxidation was lower in human and mouse models of kidney fibrosis. Our data show that the microRNA-mediated decrease in OCR does not induce per se variations in ECAR, suggesting that the glycolytic shutdown in fibrotic conditions most likely depends on fibrotic stimuli rather than being a consequence of impaired oxidative phosphorylation. The archetypal profibrotic miRNA, miR-21 is related to profound and specific metabolic derangements closely associated to mitochondrial dysfunction [131]. The suppression of PPAR-α expression by miR-21 has been invoked as a mechanism by which this miRNA exerts its pro-fibrogenic action. In addition to inhibiting FAO, the target genes for miR-21 indicated that this miRNA silences a wide range of mitochondrial processes. Thus, miR-21 also downregulates Mpv17-like protein which protects against mitochondrial oxidative stress and apoptosis. Chung et al assessed OCR after miR-21 transfection, finding decreased OCR and ATP levels, while antimiR-21 transfection under TGF-β conditions blocked the TGF-β-induced decrease in OCR and rescued the ATP levels [277]. The delivery of anti-miR-21 oligonucleotides to mice with Alport syndrome markedly retarded the progression of disease, normalized tubular functions and led to an increase in life expectancy of nearly 50% [148]. Another example of metabolic regulation of kidney fibrosis is miR-30e which targets the mitochondrial protein UCP-2 [150, 331]. However, to our knowledge there are few reports addressing the microRNA regulation of CPT1A, PGC1α and TFAM genes in the context of kidney fibrosis. Interestingly, microRNA-214 which promotes EMT during renal fibrosis, directly targets TFAM in colon cancer cells [332]. This repression was also reported for miR-590-3p [333]. The miR-29 family, one of the best characterized regulators of ECM production in organ fibrosis, directly targets PGC1α preserving cardiac homeostasis. Thus, pathologic silencing of miR-29 leads to PGC1α upregulation, generating profound alterations in mitochondrial biogenesis that contribute to cardiac disease [334]. MiR-696 also targets PGC1α in mouse skeletal muscle, modulating mitochondrial biogenesis and fatty acid oxidation in response to physical activity [335]. MiR-370 targets Cpt1α regulating hepatic TAG [336]. On the other hand, miR-150 has already been suggested as a profibrotic miRNA in lupus nephritis by modulating TGF-β signaling [337], while miR-495 shows a protective role in diabetic cardiac fibrosis [338].

To evaluate the integrity of mitochondrial ETC, we focused on two features: $\Delta\Psi m$ and superoxide radical anion production. We observed that miR-150 and miR-495 did not alter these parameters. A stable $\Delta\Psi m$ is required for cell viability and its magnitude varies among cell types [339]. Its maintenance is strictly fine-tuned as an increase in $\Delta\Psi m$ may lead to perturbations in the redox state, while its decrease causes a reduction of ATP production and may trigger apoptosis. Changes in $\Delta\Psi m$ have been quantified with the cationic fluorescent dye TMRM. This lipophilic cation accumulates in negatively charged mitochondria [247]. Some of its advantages are that it is a non-invasive dye, that it is highly fluorescent and that it can be used at low concentrations [340]. However, it has been observed that TMRM can be easily lost from cells if the mitochondria depolarize during any washing steps of the assay and that it may quench its own fluorescence, a phenomenon named ‘autoquenching’, when it exceeds a certain threshold [340]. Mitochondrial superoxide radical anion production was measured with the fluorogenic dye MitoSOX Red. This compound is rapidly and selectively targeted to the mitochondria as a function of $\Delta\Psi m$ and, once there, it is oxidized by superoxide

(Invitrogen; [247]) displaying its fluorescence [341]. The employment of these tools in conditions affecting renal function is not conspicuous in the literature. Song et al evaluated ΔΨm by using TMRM in cardiomyocytes after miR-17 transfection, showing how the apoptotic effect of norepinephrine was significantly decreased by miR-17 [342]. Nevertheless, Tomasetti et al did not find significant differences in ΔΨm after miR-126 transfection in nonmalignant and malignant mesothelioma cells [343]. Otherwise, Mutharasan et al evaluated ROS production after miR-210 transfection in rat cardiomyocytes showing a decrease in ROS generation and mitochondrial biogenesis in contrast with other published reports [344]. In our case it is possible that the employment of other dyes such as TMRE, JC-1 or Rhodamine [345] could allow to confirm or refine our observations.

These results suggest that miR-150 and miR-495 promote renal epithelial cell dedifferentiation most likely through energy deprivation conveyed by the repression of CPT1A, PGC1α and TFAM mitochondrial function-related genes.

5.3.3. –Serum levels of microRNAs as potential biomarkers for CKD progression

Selective cytoplasmic compartmentalization in P-Bodies and MVB participate in miRNA secretion in body fluids [346]. Additional sources of such extracellular miRNAs include passive leakage from broken cells or active secretion using microvesicle-free systems, such as RNA-binding proteins or lipoproteins, which protect them from degradation by ribonucleases [106]. Thus, serum circulating miR-21 levels and abundance of miR-29c in urinary exosomes correlate with kidney fibrosis, suggesting their potential role as biomarkers [132, 347]. However, miR-150 and miR-495 levels were not different either in plasma or kidney samples from CKD patients. The different microRNA expression patterns among species and cell types may explain this absence of difference in miR-150 and miR-495 levels in fibrotic tissue [327]. While in some cases reported microRNA plasma levels could be reflecting those in the kidney tissue, other mechanisms related to the secretion of miRNAs to the circulatory system or a counterbalance of this secretion by other organs should also be considered [107, 125].

In this study, we aimed to demonstrate that the CPT1A enzyme has a protective impact on the outcome of kidney fibrosis, most likely due to its critical function in the facilitation of FAO in renal tubule epithelial cells. Additionally, miR-150, miR-495, miR-33 have been identified as central regulators of the metabolic derangements leading to renal fibrosis (**Figure 62**). The confluence of both avenues in the protective role of restoring FAO in kidney fibrosis may prove useful for the basis of therapies directed towards the treatment of CKD.

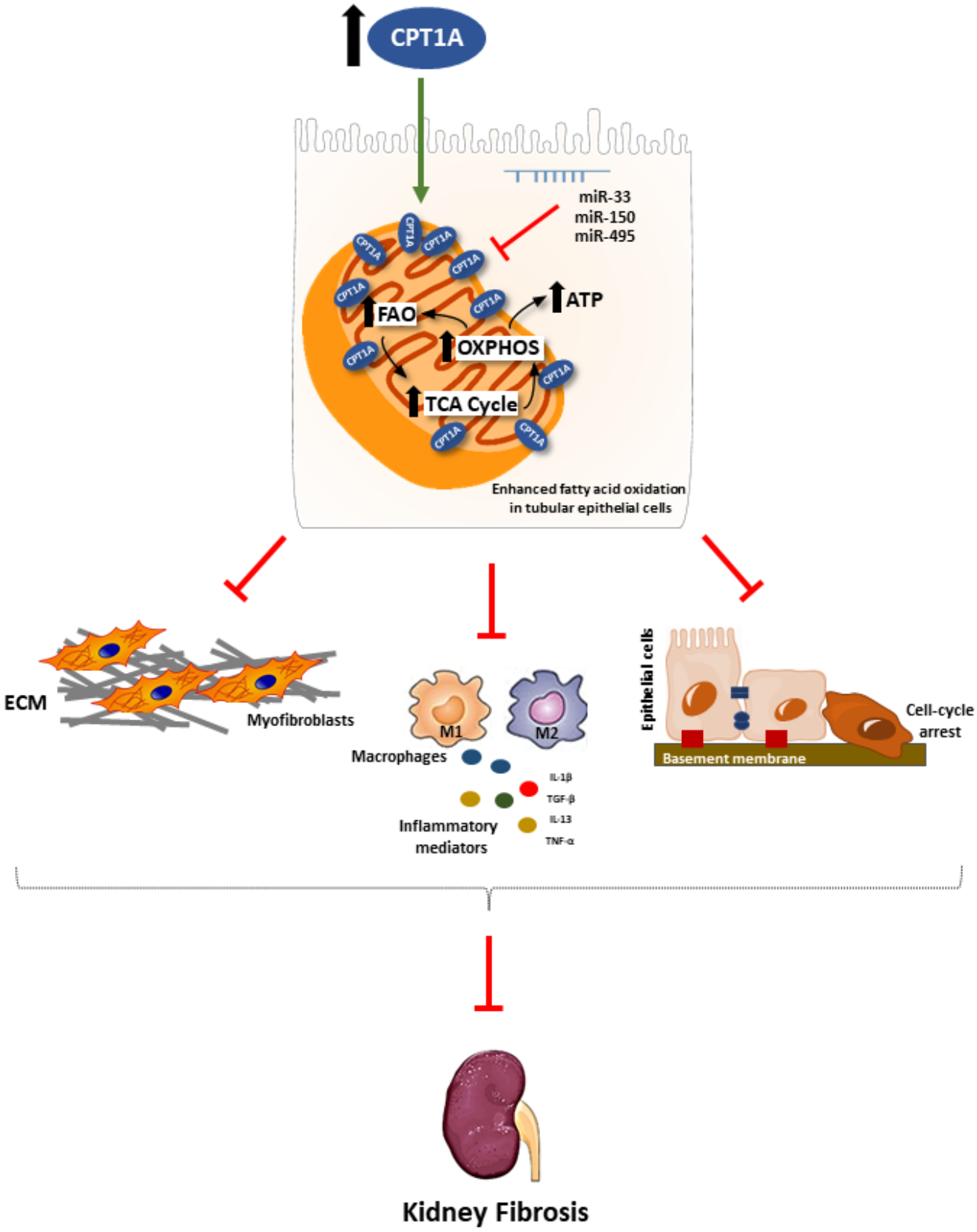

Figure 62. Protection of renal fibrosis promoted by CPT1A. Overexpression of CPT1A prevents tubular epithelial renal cell dedifferentiation, pro-inflammatory phenotype and reprograms fibrosis-related metabolic derangement.

6.Conclusions – Conclusiones

1. The knock-in conditional mouse model for *Cpt1a* in renal tubular epithelial cells resulted in a strong **increment in CPT1A expression** after doxycycline induction. This was also reflected in enhanced **fatty acid oxidation and ATP production**.

2. *Cpt1a* knock-in mice exhibited **decreased expression of fibrotic and apoptotic markers** compared with wild type animals in the different experimental models of kidney fibrosis. This was reflected in **improved renal function** in the FAN model.

3. In the FAN model, CPT1A overexpression **reduced the abundance of the pro-inflammatory M1** subpopulation while in the unilateral ureteral obstruction (UUO) model, it increased the proportion of the M2-subtype macrophage subpopulation.

4. The overexpression of CPT1A **mitigated the distortion of mitochondrial morphology and architecture** in the FAN model.

5. CPT1A overexpression significantly **decreased the descent in FAO and ATP levels** associated to renal fibrosis in the three different experimental models employed. The activation of **AMP-activated protein kinase (AMPK)** associated to kidney fibrosis was also prevented in these models when CPT1 was overexpressed.

6. Renal tubule epithelial cells overexpressing CPT1A were **protected from TGF-β-induced dedifferentiation**. These cells exhibited **higher levels of FAO-associated oxygen consumption rate (mitochondrial respiration) and decreased glycolytic rate**. Epithelial cell damage was reduced in the kidneys from *Cpt1a* knock-in mice in the UUO and FAN models.

7. The absence of miR-33 (global deletion) was associated with an attenuation of the fibrotic phenotype and improved renal function in two experimental models of renal fibrosis. This correlated with **enhanced fatty acid oxidation, mitochondrial respiration** and **reduced renal triglyceride accumulation.**

8. Both miR-150 and miR-495 **promoted TGF-β1-induced fibrogenic transformation** and reduced **FAO-associated oxygen consumption rate (OCR)** in the human tubular renal epithelial cell line HKC-8**.**

1. El modelo murino de ganancia de función condicional de *Cpt1a* en las células epiteliales tubulares renales mostró un **incremento de la expresión de CPT1A** tras la inducción con doxiciclina. Esto se acompañó de un incremento en la **oxidación de ácidos grasos y en la producción de ATP**.

2. Este modelo de ganancia de función de CPT1A mostró una **expresión disminuida de los marcadores de fibrosis y apoptosis** comparada con animales control en diferentes modelos experimentales de fibrosis renal. Esto se reflejó en la mejora de la función renal en el modelo de nefropatía inducida por ácido fólico (FAN).

3. En el modelo de FAN, la sobreexpresión de CPT1A **redujo la presencia de la subpoblación de macrófagos proinflamatorios M1,** mientras que en el modelo de ligadura unilateral del uréter (UUO) incrementó la proporción de la población de macrófagos de subtipo M2.

4. La sobreexpresión de CPT1A **impidió la distorsión de la morfología y arquitectura mitocondrial en el modelo de FAN**.

5. La sobreexpresión de CPT1A **redujo significativamente la disminución de los niveles de oxidación de ácidos grasos y ATP** asociados a la fibrosis renal en los tres modelos experimentales empleados. La **activación de la proteína quinasa activada por AMP (AMPK)** detectada en la fibrosis renal también se redujo en estos modelos tras sobreexpresar CPT1A.

6. Las células epiteliales tubulares renales que sobreexpresan CPT1A mostraron una menor **desdiferenciación inducida por TGF-β**. Estas células presentaron mayores **niveles de consumo de oxígeno asociado a la oxidación de ácidos grasos (respiración mitocondrial) y una tasa glicolítica disminuida**. El daño epitelial estaba reducido en los riñones de los ratones con ganancia de función de CPT1A en el modelo de UUO y FAN.

7. La ausencia de miR-33 (deleción global) se asoció con una disminución del fenotipo fibrótico y una mejora de la función renal en modelos experimentales de fibrosis renal. Esto se correlacionó con un **incremento de la oxidación de ácidos grasos, respiración mitocondrial y una menor acumulación renal de triglicéridos**.

8. Tanto miR-150 como miR-495 **favorecieron la transformación fibrogénica inducida por TGF-β1** y redujeron el **consumo de oxígeno asociado a la oxidación de ácidos grasos** en la línea celular epitelial tubular humana HKC-8**.**

7.Supplementary material

Biological process	Abbreviation	Molecular mechanism
Apoptosis	*Apaf1*	Mediates the cytochrome c-dependent autocatalytic activation of pro-caspase-9 (Apaf-3), leading to the activation of caspase-3 and apoptosis
	Bax	Promotes the opening of the mitochondrial voltage-dependent anion channel (VDAC), which leads to the loss in membrane potential and the release of cytochrome c, activating apoptosis
	Bcl2	Integral outer mitochondrial membrane protein that blocks mitochondrial-mediated apoptosis
	Bcl2l1	Regulate outer mitochondrial membrane channel (VDAC) opening. VDAC regulates mitochondrial membrane potential and the release of cytochrome C by mitochondria, inducing of cell apoptosis It can act as anti- or pro-apoptotic regulator.
Peroxisomal/ mitochondrial function	*Cpt1a*	Transfer of the acyl group of long-chain fatty acid-CoA conjugates onto carnitine, an essential step for the mitochondrial uptake of long-chain fatty acids and their subsequent beta-oxidation in the mitochondrion
	Cpt2	Mediates the export of carnitine from the mitochondrial matrix to the cytosol
	Ppara	Promotes uptake, utilization, and catabolism of fatty acids by upregulation of genes involved in fatty acid transport, fatty acid binding and activation, and peroxisomal and mitochondrial fatty acid β-oxidation
	Ppargc1a	Regulate key mitochondrial genes that contribute to the program of adaptive thermogenesis and glucose and fatty acid metabolism
	Acox1	First enzyme of the peroxisomal fatty acid beta-oxidation pathway, which catalyzes the desaturation of acyl-CoAs to 2-trans-enoyl-CoAs. It donates electrons directly to molecular oxygen, thereby producing hydrogen peroxide
	Acox2	Oxidizes the CoA esters of the bile acid intermediates di- and tri-hydroxycholestanoic acids in the proxisome
	Hspa9	Heat-shock cognate protein, primarily localized in the mitochondria. This protein plays a role in cell proliferation, stress response and maintenance of the mitochondria
	Lrpprc	Promotes translation or stability of mitochondrially encoded cytochrome c oxidase (COX) subunits
	Ndufv2	Component of the complex I in the mitochondrial respiratory chain catalyzes the transfer of electrons from NADH to ubiquinone
	Sdha	Component of the complex II of the mitochondrial electron transport chain and is responsible for transferring electrons from succinate to ubiquinone (coenzyme Q)
	Tfam	Binds to the mitochondrial light strand promoter and functions in mitochondrial transcription regulation
Fibrosis	*Acta2*	Smooth muscle actin involved in cell motility, structure and contractility
	Cdh16	Calcium-dependent membrane cell adhesion protein. Expression is exclusively in kidney where the protein functions as the principal mediator of homotypic cellular recognition
	Col1a1	Fibril-forming collagen found in most connective tissues
	Col3a1	Located in the extracellular space of most soft connective tissues along with type I collagen
	Col4a1	Major structural component of glomerular basement membranes
	Fn1	Binds cell surfaces and various compounds including collagen, fibrin, heparin, DNA, and actin. Involved in cell adhesion, cell motility, opsonization, wound healing, and maintenance of cell shape
	Havrc1	Type-1 transmembrane protein expressed on the proximal tubule apical membrane in kidney injury conditions
	Snai1	Zinc finger transcriptional repressor that decreases the expression of E-cadherin, inducing epithelial to mesenchymal transition (EMT)
	Twist1	Basic helix-loop-helix transcription factor that upregulates N-cadherin and downregulates E-cadherin, induction of the epithelial to mesenchymal transition (EMT)
	Vim	Class-III intermediate filament protein. Along with microtubules and actin microfilaments forms the cytoskeleton. Maintains cell shape, integrity of the cytoplasm and stabilizes cytoskeletal interactions
Glycolysis	*G6pc*	Catalyzes the hydrolysis of D-glucose 6-phosphate to D-glucose and orthophosphate and is a key enzyme in glucose homeostasis, functioning in gluconeogenesis and glycogenolysis
	Gapdh	Catalyzes the conversion of glyceraldehyde 3-phosphate to D-glycerate 1,3-bisphosphate
	Hk1	Phosphorylate glucose to produce glucose-6-phosphate, the first step in glycolysis
	Ldh1	Catalyzes the first step in the pathway that synthesizes (S)-lactate from pyruvate
	Ldh2	Catalyzes the conversion of lactate to pyruvate
	Pgk1	Catalyzes the step 2 of the pathway that synthesizes pyruvate from D-glyceraldehyde 3-phosphate
	Pkfm	Catalyzes the conversion of fructose 6-phosphate and ATP to fructose 1,6-bisphosphate and ADP
	Pkm	Catalyzes the transfer of a phosphate group from phosphoenolpyruvate (PEP) to adenosine diphosphate (ADP), yielding one molecule of pyruvate and one molecule of ATP
	Slc2a1	Facilitates the transport of glucose across the plasma membranes of mammalian cells
Inflammation	*Adgre1*	Involved in cell adhesion and cell-cell interactions. Macrophage marker
	Cd86	M1 macrophage marker
	IL1b	Pro-inflammatory cytokine, produced by M1 macrophages
	IL6	Pro-inflammatory cytokine, produced by M1 macrophages
	Nos2	Produces nitric oxide, M1 macrophage marker
	Tgfb1	Pro-fibrotic cytoquine
	Tnfα	Pro-fibrotic cytoquine

Supplementary table 1. Molecular mechanism of genes analyzed by TaqMan probes.

Sample number	ΔCt (miR-33)	ΔCt (miR-150)	Basal Cr (mg/dL)	Basal MDRD (ml/min)	Basal CKD-EPI (mg/dl)	Cr (24 months) (mg/dL)	MDRD (24 months) (ml/min)	CKD-EPI (24 months) (mg/dl)	MDRD Deterioration	TG (mg/dL)
1402	4,44	0,01	1,55	34,86	32,64	1,545	34,67	32,41	-0,55	62
1487	3,62	0,38	2,99	22	19,64					58
1506	1,49	0,23	2,08	34,34	32,44	4,46	14,15	12,81	-58,79	71
1676	4,95	-1,03	1,04	57,26	57,72	1,05	56,26	56,66	-1,75	111
1683	4,74	-1,3	1,1	52,04	50,28	1,09	52,3	50,48	0,5	81
1736	3,24	-1,25	1,14	49,66	47,48	1,14	49,39	47,15	-0,54	81
1745	5,3	-1,93	2,64	25,15	24,31	5,39	10,94	10,11	-56,5	76
1783	3,02	0,26	4,1	18,99	18,91					95
1827	4,36	-0,72	1,14	50,53	49,53	1,15	49,73	48,66	-1,58	49
1869	2,2	-0,08	1,7	43,21	41,4	1,7	42,94	40,82	-0,62	119
1914	3,72	-0,99	2,27	33,5	33,82	4,35	15,67	15,3	-53,22	65
1920	5,62	0,17	3,13	15,57	14,2					90
2104	2,67	-0,06	2,58	22,21	22,94					116
2167	4,3	-0,27	1,5	49,32	46,5	1,47	50,19	47,32	1,76	60
2169	1,61	-2,28	2,6	21,35	21,79	4,05	12,69	12,57	-40,56	66
2172	3,4	-0,78	1,4	54,76	53,84	1,37	55,78	54,5	1,86	96
2177	5,32	-0,24	3,2	20,57	18,6					70
2289	3,94	0,11	2,1	33,07	30,31	2,1	32,89	30,1	-0,54	42
2294	3,76	-1,39	2,87	17,99	17,4					91
2307	4,92	-0,75	4,08	16,66	16,07					95
2319	3,57	-0,78	1,69	32,28	31,2	4,44	10,52	9,64	-67,41	50
2356	2,65	-0,13	1,41	53,78	51,9	1,4	53,89	51,99	0,2	81
2384	5,6	-0,08	1,21	48,24	48,41	1,19	48,85	49,05	1,26	90
2435	2,36	-0,55	1,43	51,96	49,27	1,4	52,95	49,84	1,91	51
2471	2,37	-0,25	1,6	45,65	43,01	1,58	46,05	43,06	0,88	119
2533	3,33	-1,12	2,24	31,63	30,08	4,82	12,98	11,74	-58,96	97
2548	4,69	-0,06	3,47	19,92	19,28					91
2590	3,87	0,29	2,12	32,99	30,61	7,38	7,78	6,68	-76,42	94
2640	2,65	1,41	1,6	45,13	41,82	1,62	44,25	40,62	-1,95	84
2648	1,11	-0,52	4,1	15,5	13,88					101
2678	2,57	-0,15	1,9	38,89	38,01	1,9	38,62	37,48	-0,69	77
2877	4,63	-1,89	3,7	18,02	16,86					51
2884	2,4	1,07	2,5	20,12	18,63					98
2890	1,62	-2,67	2,3	23,76	23,72	2,3	23,58	23,55	-0,76	79
2973	2,28	3,38	1,14	58,34	63,33	1,14	57,65	62,45	-1,18	98
3017	3,31	-1,59	1,7	48,71	50,4	4,2	16,97	16,77	-65,16	87
3048	2,25	1,77	1,94	28,58	28,73	3,73	13,39	12,94	-53,15	82
3130	2,64	1,26	1,6	34,28	33,11	1,58	34,57	33,38	0,85	69
3450	2,48	3,25	1,5	52,03	52,4	1,5	51,64	51,67	-0,75	99
3452	1,71	0,62	1,9	39,31	38,82	1,9	39,03	38,28	-0,71	115
3683	2,12	1,28	2	36,53	35,48	2	36,28	34,98	-0,68	104
3689	2,21	-0,27	3,34	19,95	18,56	6,58	9,06	8,06	-54,59	102
3711	5,39	0,69	1,3	45	46,62	4,35	11,17	10,67	-75,18	81
3807	2,43		4,3	15,95	15,51					42
3994	3,23	-0,85	3,4	19,67	18,29					117
4286	2,29	0,42	1,35	43,12	43,92	1,35	42,81	43,61	-0,72	113
4369	2,54	1,14	3,4	19,13	17,29	3,33	19,48	17,48	1,83	70
4449	6,34	-1,11	1,75	42,47	41,11	1,77	41,64	40,27	-1,95	98
4464	6,8	4,11	1,2	47,34	46,22	1,2	47,07	45,58	-0,57	70

Supplementary table 2. Relative miR-150 and miR-33 expression (ΔCt) and kidney functional parameters (Creatinine (Cr), MDRD, CKD-EPI) of CKD patients with triglyceride levels lower than 120 mg/dL.

Sample number	ΔCt (miR-33)	ΔCt (miR-150)	Basal Cr (mg/dL)	Basal MDRD (ml/min)	Basal CKD-EPI (mg/dl)	Cr (24 months) (mg/dL)	MDRD (24 months) (ml/min)	CKD-EPI (24 months) (mg/dl)	MDRD Deterioration	TG (mg/dL)
1570	2,66	-0,64	1,47	50,5	47,48	1,466	50,21	47,14	-0,57	136
1755	5,48	-0,52	1,2	46,8	44,63	1,2	46,55	44,31	-0,53	121
1772	4,9	-0,68	1,4	54,06	52,35	3,1	21,47	19,74	-60,28	145
1793	3,26	-1,69	3,2	20,63	18,74	3,19	20,53	18,68	-0,48	123
1804	5,36	-1,48	2,87	21,27	21,94	4,84	11,46	11,5	-46,12	136
1863	3,53	-0,44	1,4	40,5	40,3	1,4	40,24	39,73	-0,64	140
1997	5,32	-0,61	2,03	36,42	35,59	2	36,79	35,98	1,02	146
2344	3,91	-0,9	1,27	44,48	43,16	1,25	45,03	43,69	1,24	122
2514	2,19	-0,33	2,76	24,06	21,48					126
2573	2,58	0,14	1,47	52,29	51,84	1,47	51,94	51,12	-0,67	128
2939	2,31	2,53	2,59	25,96	23,52	2,6	25,7	23,09	-1	146
3387	2,94	3,39	2,31	22,44	21,39	4,74	9,73	8,84	-56,64	122
3664	3	-0,13	4,1	15,95	14,9					148
3704	2,66	0,8	1,93	29,21	29,53	3,33	15,44	15,16	-47,14	137
4036	3,3	1,19	3,1	21,88	20,59					139
4283	3,43	0,16	2,43	27,94	25,23	3,99	15,68	13,76	-43,88	127
4458	7,35	2,93	1,49	40,79	43,01	1,47	41,04	43,11	0,61	144
1450	2,94	0,81	2,13	33,31	31,3	2,11	33,47	31,44	0,48	192
1826	3,47	0,64	3,85	16,57	14,77	9,17	6,04	5,14	-63,55	198
2497	2,64	-0,95	2,7	24,81	22,53					168
2595	3,93	0,23	1,73	42,34	40,53	1,74	41,8	39,69	-1,28	169
2601	3	-0,32	3,41	19,87	18,88					162
2849	1,56	-1,1	3,66	17,78	16,27	7,78	7,4	6,45	-58,38	175
2893	4,4	-0,97	2,4	31,13	31,18	4	17,12	16,58	-45	156
2995	2,52	-0,18	1,5	49,77	47,49	1,51	49,09	46,78	-1,37	156
3097	3,19	-0,81	2,1	38,85	39,87	3,9	18,79	18,73	-51,63	163
3678	4,45	0,74	1,6	48,3	48,46	1,6	47,94	47,79	-0,75	167
3979	3,65	0,02	2,71	26,29	25,63	5,99	10,45	9,76	-60,25	153
4034	2,61	-0,17	3,5	18,96	17,66					181
1681	5,45	0,06	2,48	27,61	25,32	2,5	27,19	24,9	-1,52	205
1820	4,88	-0,71	3,88	18,4	18,07					453
1896	2,79	-1,02	1,01	58,11	57,74	0,99	59,11	58,33	1,72	207
1917	5,24	-1,02	3,75	18,01	17,06					256
1923	4,37	0,31	1,86	42,35	43,04	1,85	42,23	43,01	-0,28	225
2001	4,03	1,35	2,67	18,55	16,85					499
2193	4,82	-0,78	3,28	20,94	19,92	9,2	6,32	5,69	-69,82	308
2389	3,53	-0,72	1,62	46,27	45,13	1,63	45,64	44,17	-1,36	297
2559	3,78	-0,52	2,61	19,49	18,32	4,66	9,92	9,03	-49,1	221
2567	5,93	-1,34	1,86	38,95	37,13	1,87	38,47	36,63	-1,23	234
2600	0	0	4,36	15,13	14,22					348
2603	4,36	-0,53	2,19	32,68	31,35	2,2	32,29	30,74	-1,19	248
2630	4,64	0,42	2,79	24,03	21,96	4,8	12,77	11,24	-46,86	223
2711	3,3	0,73	3,8	17,6	16,68					267
2804	4,39	-2,07	1,2	47,2	45,9	1,2	46,94	45,26	-0,55	384
3444	3,59	-0,68	1,1	56,83	59,93	1,1	56,35	59,51	-0,84	585
4459	5,74	2,86	2,42	22,59	22,78					238
1484	5,14	-1,5	1,78	40,6	38,07	2,9	22,91	20,81	-43,57	
2360	2,02	-0,07	1,46	51,66	49,76	1,45	51,75	49,83	0,17	
3459	2,23	2,17	1,6	45,51	42,41	1,6	45,26	42,11	-0,55	
3797	2,45	1,98	3,31	19,62	17,61	3,26	19,85	17,69	1,17	

Supplementary table 3. Relative miR-150 and miR-33 expression (ΔCt) and kidney functional parameters (Creatinine (Cr), MDRD, CKD-EPI) of CKD patients with triglyceride levels: 120-150 mg/dL (white), 150-200 mg/dL (soft grey) and higher than 200 mg/dL (dark grey).

8.References

1. Webster, A.C., E.V. Nagler, R.L. Morton and P. Masson, *Chronic Kidney Disease.* Lancet, 2017. **389**(10075): p. 1238-1252.
2. Kazancioglu, R., *Risk factors for chronic kidney disease: an update.* Kidney Int Suppl (2011), 2013. **3**(4): p. 368-371.
3. Ojo, A., *Addressing the global burden of chronic kidney disease through clinical and translational research.* Trans Am Clin Climatol Assoc, 2014. **125**: p. 229-43; discussion 243-6.
4. Reidy, K., H.M. Kang, T. Hostetter and K. Susztak, *Molecular mechanisms of diabetic kidney disease.* J Clin Invest, 2014. **124**(6): p. 2333-40.
5. Drawz, P.E. and M.E. Rosenberg, *Slowing progression of chronic kidney disease.* Kidney Int Suppl (2011), 2013. **3**(4): p. 372-376.
6. Lopez-Novoa, J.M., A.B. Rodriguez-Pena, A. Ortiz, C. Martinez-Salgado and F.J. Lopez Hernandez, *Etiopathology of chronic tubular, glomerular and renovascular nephropathies: clinical implications.* J Transl Med, 2011. **9**: p. 13.
7. Preuss, H.G., *Basics of renal anatomy and physiology.* Clin Lab Med, 1993. **13**(1): p. 1-11.
8. Soriano, R.M. and S.W. Leslie, *Anatomy, Abdomen and Pelvis, Kidneys*, in *StatPearls*. 2019: Treasure Island (FL).
9. Richards, A.N., *Physiology of the Kidney: The Wesley M. Carpenter Lecture.* Bull N Y Acad Med, 1938. **14**(1): p. 5-20.
10. Lacombe, C., J.L. Da Silva, P. Bruneval, N. Casadevall, J.P. Camilleri, J. Bariety, P. Tambourin and B. Varet, *Erythropoietin: sites of synthesis and regulation of secretion.* Am J Kidney Dis, 1991. **18**(4 Suppl 1): p. 14-9.
11. Khundmiri, S.J., R.D. Murray and E. Lederer, *PTH and Vitamin D.* Compr Physiol, 2016. **6**(2): p. 561-601.
12. Bonventre, J.V. and R. Nemenoff, *Renal tubular arachidonic acid metabolism.* Kidney Int, 1991. **39**(3): p. 438-49.
13. Weir, M.R. and V.J. Dzau, *The renin-angiotensin-aldosterone system: a specific target for hypertension management.* Am J Hypertens, 1999. **12**(12 Pt 3): p. 205S-213S.
14. Chmielewski, C., *Renal anatomy and overview of nephron function.* Nephrol Nurs J, 2003. **30**(2): p. 185-90; quiz 191-2.
15. Arif, E. and D. Nihalani, *Glomerular Filtration Barrier Assembly: An insight.* Postdoc J, 2013. **1**(4): p. 33-45.
16. Zhuo, J.L. and X.C. Li, *Proximal nephron.* Compr Physiol, 2013. **3**(3): p. 1079-123.
17. Wynn, T.A., *Cellular and molecular mechanisms of fibrosis.* J Pathol, 2008. **214**(2): p. 199-210.
18. Agarwal, I., N.L. Glazer, E. Barasch, M.L. Biggs, L. Djousse, A.L. Fitzpatrick, J.S. Gottdiener, J.H. Ix, J.R. Kizer, E.B. Rimm, D.S. Siscovick, R.P. Tracy, S.J. Zieman and K.J. Mukamal, *Fibrosis-related biomarkers and risk of total and cause-specific mortality: the cardiovascular health study.* Am J Epidemiol, 2014. **179**(11): p. 1331-9.
19. Hutchison, N., C. Fligny and J.S. Duffield, *Resident mesenchymal cells and fibrosis.* Biochim Biophys Acta, 2013. **1832**(7): p. 962-71.
20. Huebener, P. and R.F. Schwabe, *Regulation of wound healing and organ fibrosis by toll-like receptors.* Biochim Biophys Acta, 2013. **1832**(7): p. 1005-17.
21. Wynn, T.A. and T.R. Ramalingam, *Mechanisms of fibrosis: therapeutic translation for fibrotic disease.* Nat Med, 2012. **18**(7): p. 1028-40.
22. Bochaton-Piallat, M.L., G. Gabbiani and B. Hinz, *The myofibroblast in wound healing and fibrosis: answered and unanswered questions.* F1000Res, 2016. **5**.
23. Kendall, R.T. and C.A. Feghali-Bostwick, *Fibroblasts in fibrosis: novel roles and mediators.* Front Pharmacol, 2014. **5**: p. 123.
24. Glasser, S.W., J.S. Hagood, S. Wong, C.A. Taype, S.K. Madala and W.D. Hardie, *Mechanisms of Lung Fibrosis Resolution.* Am J Pathol, 2016. **186**(5): p. 1066-77.
25. Jun, J.I. and L.F. Lau, *Resolution of organ fibrosis.* J Clin Invest, 2018. **128**(1): p. 97-107.
26. Brew, K. and H. Nagase, *The tissue inhibitors of metalloproteinases (TIMPs): an ancient family with structural and functional diversity.* Biochim Biophys Acta, 2010. **1803**(1): p. 55-71.

27. Aryal, S. and S.D. Nathan, *An update on emerging drugs for the treatment of idiopathic pulmonary fibrosis.* Expert Opin Emerg Drugs, 2018. **23**(2): p. 159-172.
28. Li, X. and S. Zhuang, *Recent advances in renal interstitial fibrosis and tubular atrophy after kidney transplantation.* Fibrogenesis Tissue Repair, 2014. **7**: p. 15.
29. Zeisberg, M. and E.G. Neilson, *Mechanisms of tubulointerstitial fibrosis.* J Am Soc Nephrol, 2010. **21**(11): p. 1819-34.
30. Zeisberg, M., M.A. Soubasakos and R. Kalluri, *Animal models of renal fibrosis.* Methods Mol Med, 2005. **117**: p. 261-72.
31. Nakagawa, N. and J.S. Duffield, *Myofibroblasts in Fibrotic Kidneys.* Curr Pathobiol Rep, 2013. **1**(3).
32. LeBleu, V.S., G. Taduri, J. O'Connell, Y. Teng, V.G. Cooke, C. Woda, H. Sugimoto and R. Kalluri, *Origin and function of myofibroblasts in kidney fibrosis.* Nat Med, 2013. **19**(8): p. 1047-53.
33. Lin, S.L., T. Kisseleva, D.A. Brenner and J.S. Duffield, *Pericytes and perivascular fibroblasts are the primary source of collagen-producing cells in obstructive fibrosis of the kidney.* Am J Pathol, 2008. **173**(6): p. 1617-27.
34. Smith, S.W., C. Schrimpf, D.J. Parekh, M. Venkatachalam and J.S. Duffield, *Kidney pericytes: a novel therapeutic target in interstitial fibrosis.* Histol Histopathol, 2012. **27**(12): p. 1503-14.
35. Grgic, I., J.S. Duffield and B.D. Humphreys, *The origin of interstitial myofibroblasts in chronic kidney disease.* Pediatr Nephrol, 2012. **27**(2): p. 183-93.
36. Humphreys, B.D., *Mechanisms of Renal Fibrosis.* Annu Rev Physiol, 2018. **80**: p. 309-326.
37. Grande, M.T., B. Sanchez-Laorden, C. Lopez-Blau, C.A. De Frutos, A. Boutet, M. Arevalo, R.G. Rowe, S.J. Weiss, J.M. Lopez-Novoa and M.A. Nieto, *Snail1-induced partial epithelial-to-mesenchymal transition drives renal fibrosis in mice and can be targeted to reverse established disease.* Nat Med, 2015. **21**(9): p. 989-97.
38. Lovisa, S., V.S. LeBleu, B. Tampe, H. Sugimoto, K. Vadnagara, J.L. Carstens, C.C. Wu, Y. Hagos, B.C. Burckhardt, T. Pentcheva-Hoang, H. Nischal, J.P. Allison, M. Zeisberg and R. Kalluri, *Epithelial-to-mesenchymal transition induces cell cycle arrest and parenchymal damage in renal fibrosis.* Nat Med, 2015. **21**(9): p. 998-1009.
39. Li, J., J.A. Deane, N.V. Campanale, J.F. Bertram and S.D. Ricardo, *The contribution of bone marrow-derived cells to the development of renal interstitial fibrosis.* Stem Cells, 2007. **25**(3): p. 697-706.
40. Kramann, R., F. Machado, H. Wu, T. Kusaba, K. Hoeft, R.K. Schneider and B.D. Humphreys, *Parabiosis and single-cell RNA sequencing reveal a limited contribution of monocytes to myofibroblasts in kidney fibrosis.* JCI Insight, 2018. **3**(9).
41. Kramann, R., R.K. Schneider, D.P. DiRocco, F. Machado, S. Fleig, P.A. Bondzie, J.M. Henderson, B.L. Ebert and B.D. Humphreys, *Perivascular Gli1+ progenitors are key contributors to injury-induced organ fibrosis.* Cell Stem Cell, 2015. **16**(1): p. 51-66.
42. Mugford, J.W., P. Sipila, J.A. McMahon and A.P. McMahon, *Osr1 expression demarcates a multi-potent population of intermediate mesoderm that undergoes progressive restriction to an Osr1-dependent nephron progenitor compartment within the mammalian kidney.* Dev Biol, 2008. **324**(1): p. 88-98.
43. Pan, S.Y., Y.T. Chang and S.L. Lin, *Microvascular pericytes in healthy and diseased kidneys.* Int J Nephrol Renovasc Dis, 2014. **7**: p. 39-48.
44. Duffield, J.S., *Cellular and molecular mechanisms in kidney fibrosis.* J Clin Invest, 2014. **124**(6): p. 2299-306.
45. Park, J., R. Shrestha, C. Qiu, A. Kondo, S. Huang, M. Werth, M. Li, J. Barasch and K. Susztak, *Single-cell transcriptomics of the mouse kidney reveals potential cellular targets of kidney disease.* Science, 2018. **360**(6390): p. 758-763.
46. Liu, Y., *Cellular and molecular mechanisms of renal fibrosis.* Nat Rev Nephrol, 2011. **7**(12): p. 684-96.
47. Campanholle, G., G. Ligresti, S.A. Gharib and J.S. Duffield, *Cellular mechanisms of tissue fibrosis. 3. Novel mechanisms of kidney fibrosis.* Am J Physiol Cell Physiol, 2013. **304**(7): p. C591-603.
48. Imig, J.D. and M.J. Ryan, *Immune and inflammatory role in renal disease.* Compr Physiol, 2013. **3**(2): p. 957-76.

49. Guiteras, R., A. Sola, M. Flaquer, G. Hotter, J. Torras, J.M. Grinyo and J.M. Cruzado, *Macrophage Overexpressing NGAL Ameliorated Kidney Fibrosis in the UUO Mice Model.* Cell Physiol Biochem, 2017. **42**(5): p. 1945-1960.
50. Lebleu, V.S., H. Sugimoto, C.A. Miller, V.H. Gattone, 2nd and R. Kalluri, *Lymphocytes are dispensable for glomerulonephritis but required for renal interstitial fibrosis in matrix defect-induced Alport renal disease.* Lab Invest, 2008. **88**(3): p. 284-92.
51. Ascon, M., D.B. Ascon, M. Liu, C. Cheadle, C. Sarkar, L. Racusen, H.T. Hassoun and H. Rabb, *Renal ischemia-reperfusion leads to long term infiltration of activated and effector-memory T lymphocytes.* Kidney Int, 2009. **75**(5): p. 526-35.
52. Nishida, M. and K. Hamaoka, *Macrophage phenotype and renal fibrosis in obstructive nephropathy.* Nephron Exp Nephrol, 2008. **110**(1): p. e31-6.
53. Mosser, D.M. and J.P. Edwards, *Exploring the full spectrum of macrophage activation.* Nat Rev Immunol, 2008. **8**(12): p. 958-69.
54. Guiteras, R., M. Flaquer and J.M. Cruzado, *Macrophage in chronic kidney disease.* Clin Kidney J, 2016. **9**(6): p. 765-771.
55. Italiani, P. and D. Boraschi, *From Monocytes to M1/M2 Macrophages: Phenotypical vs. Functional Differentiation.* Front Immunol, 2014. **5**: p. 514.
56. Ishizuka, E.K., M.J. Ferreira, L.Z. Grund, E.M. Coutinho, E.N. Komegae, A.A. Cassado, K.R. Bortoluci, M. Lopes-Ferreira and C. Lima, *Role of interplay between IL-4 and IFN-gamma in the in regulating M1 macrophage polarization induced by Nattectin.* Int Immunopharmacol, 2012. **14**(4): p. 513-22.
57. Wilson, H.M., S. Chettibi, C. Jobin, D. Walbaum, A.J. Rees and D.C. Kluth, *Inhibition of macrophage nuclear factor-kappaB leads to a dominant anti-inflammatory phenotype that attenuates glomerular inflammation in vivo.* Am J Pathol, 2005. **167**(1): p. 27-37.
58. Lee, S., S. Huen, H. Nishio, S. Nishio, H.K. Lee, B.S. Choi, C. Ruhrberg and L.G. Cantley, *Distinct macrophage phenotypes contribute to kidney injury and repair.* J Am Soc Nephrol, 2011. **22**(2): p. 317-26.
59. Lu, J., Q. Cao, D. Zheng, Y. Sun, C. Wang, X. Yu, Y. Wang, V.W. Lee, G. Zheng, T.K. Tan, X. Wang, S.I. Alexander, D.C. Harris and Y. Wang, *Discrete functions of M2a and M2c macrophage subsets determine their relative efficacy in treating chronic kidney disease.* Kidney Int, 2013. **84**(4): p. 745-55.
60. Zhang, M.Z., X. Wang, Y. Wang, A. Niu, S. Wang, C. Zou and R.C. Harris, *IL-4/IL-13-mediated polarization of renal macrophages/dendritic cells to an M2a phenotype is essential for recovery from acute kidney injury.* Kidney Int, 2017. **91**(2): p. 375-386.
61. Lisi, L., E. Stigliano, L. Lauriola, P. Navarra and C. Dello Russo, *Proinflammatory-activated glioma cells induce a switch in microglial polarization and activation status, from a predominant M2b phenotype to a mixture of M1 and M2a/B polarized cells.* ASN Neuro, 2014. **6**(3): p. 171-83.
62. Kim, M.G., S.C. Kim, Y.S. Ko, H.Y. Lee, S.K. Jo and W. Cho, *The Role of M2 Macrophages in the Progression of Chronic Kidney Disease following Acute Kidney Injury.* PLoS One, 2015. **10**(12): p. e0143961.
63. Geeraerts, X., E. Bolli, S.M. Fendt and J.A. Van Ginderachter, *Macrophage Metabolism As Therapeutic Target for Cancer, Atherosclerosis, and Obesity.* Front Immunol, 2017. **8**: p. 289.
64. Lee, S.A., S. Noel, M. Sadasivam, A.R.A. Hamad and H. Rabb, *Role of Immune Cells in Acute Kidney Injury and Repair.* Nephron, 2017. **137**(4): p. 282-286.
65. Audiger, C., M.J. Rahman, T.J. Yun, K.V. Tarbell and S. Lesage, *The Importance of Dendritic Cells in Maintaining Immune Tolerance.* J Immunol, 2017. **198**(6): p. 2223-2231.
66. Blank, U., M. Essig, L. Scandiuzzi, M. Benhamou and Y. Kanamaru, *Mast cells and inflammatory kidney disease.* Immunol Rev, 2007. **217**: p. 79-95.
67. Dai, H. and R.J. Korthuis, *Mast Cell Proteases and Inflammation.* Drug Discov Today Dis Models, 2011. **8**(1): p. 47-55.
68. Chawla, A., *Control of macrophage activation and function by PPARs.* Circ Res, 2010. **106**(10): p. 1559-69.
69. Anders, H.J., E. Belemezova, V. Eis, S. Segerer, V. Vielhauer, G. Perez de Lema, M. Kretzler, C.D. Cohen, M. Frink, R. Horuk, K.L. Hudkins, C.E. Alpers, F. Mampaso and D. Schlondorff, *Late onset of treatment*

with a chemokine receptor CCR1 antagonist prevents progression of lupus nephritis in MRL-Fas(lpr) mice. J Am Soc Nephrol, 2004. **15**(6): p. 1504-13.
70. Jones, L.K., K.M. O'Sullivan, T. Semple, M.P. Kuligowski, K. Fukami, F.Y. Ma, D.J. Nikolic-Paterson, S.R. Holdsworth and A.R. Kitching, *IL-1RI deficiency ameliorates early experimental renal interstitial fibrosis.* Nephrol Dial Transplant, 2009. **24**(10): p. 3024-32.
71. Khan, S.B., H.T. Cook, G. Bhangal, J. Smith, F.W. Tam and C.D. Pusey, *Antibody blockade of TNF-alpha reduces inflammation and scarring in experimental crescentic glomerulonephritis.* Kidney Int, 2005. **67**(5): p. 1812-20.
72. Kanwar, Y.S., *TGF-beta and renal fibrosis: a Pandora's box of surprises.* Am J Pathol, 2012. **181**(4): p. 1147-50.
73. Sweetwyne, M.T., J. Tao and K. Susztak, *Kick it up a notch: Notch signaling and kidney fibrosis.* Kidney Int Suppl (2011), 2014. **4**(1): p. 91-96.
74. Edeling, M., G. Ragi, S. Huang, H. Pavenstadt and K. Susztak, *Developmental signalling pathways in renal fibrosis: the roles of Notch, Wnt and Hedgehog.* Nat Rev Nephrol, 2016. **12**(7): p. 426-39.
75. Singh, K.D. and S.S. Karnik, *Angiotensin Receptors: Structure, Function, Signaling and Clinical Applications.* J Cell Signal, 2016. **1**(2).
76. Noh, H., H. Ha, M.R. Yu, Y.O. Kim, J.H. Kim and H.B. Lee, *Angiotensin II mediates high glucose-induced TGF-beta1 and fibronectin upregulation in HPMC through reactive oxygen species.* Perit Dial Int, 2005. **25**(1): p. 38-47.
77. Biernacka, A., M. Dobaczewski and N.G. Frangogiannis, *TGF-beta signaling in fibrosis.* Growth Factors, 2011. **29**(5): p. 196-202.
78. Heldin, C.H. and A. Moustakas, *Signaling Receptors for TGF-beta Family Members.* Cold Spring Harb Perspect Biol, 2016. **8**(8).
79. Inman, G.J., *Linking Smads and transcriptional activation.* Biochem J, 2005. **386**(Pt 1): p. e1-e3.
80. Toda, N., M. Mukoyama, M. Yanagita and H. Yokoi, *CTGF in kidney fibrosis and glomerulonephritis.* Inflamm Regen, 2018. **38**: p. 14.
81. Neumann, C., A. Yu, U. Welge-Lussen, E. Lutjen-Drecoll and M. Birke, *The effect of TGF-beta2 on elastin, type VI collagen, and components of the proteolytic degradation system in human optic nerve astrocytes.* Invest Ophthalmol Vis Sci, 2008. **49**(4): p. 1464-72.
82. Breyer, M.D. and K. Susztak, *The next generation of therapeutics for chronic kidney disease.* Nat Rev Drug Discov, 2016. **15**(8): p. 568-88.
83. Sureshbabu, A., S.A. Muhsin and M.E. Choi, *TGF-beta signaling in the kidney: profibrotic and protective effects.* Am J Physiol Renal Physiol, 2016. **310**(7): p. F596-F606.
84. Kobori, H., H. Mori, T. Masaki and A. Nishiyama, *Angiotensin II blockade and renal protection.* Curr Pharm Des, 2013. **19**(17): p. 3033-42.
85. Badal, S.S. and F.R. Danesh, *MicroRNAs and their applications in kidney diseases.* Pediatr Nephrol, 2015. **30**(5): p. 727-40.
86. Anglicheau, D., T. Muthukumar and M. Suthanthiran, *MicroRNAs: small RNAs with big effects.* Transplantation, 2010. **90**(2): p. 105-12.
87. Winter, J., S. Jung, S. Keller, R.I. Gregory and S. Diederichs, *Many roads to maturity: microRNA biogenesis pathways and their regulation.* Nat Cell Biol, 2009. **11**(3): p. 228-34.
88. Gebert, L.F.R. and I.J. MacRae, *Regulation of microRNA function in animals.* Nat Rev Mol Cell Biol, 2019. **20**(1): p. 21-37.
89. Lee, R.C., R.L. Feinbaum and V. Ambros, *The C. elegans heterochronic gene lin-4 encodes small RNAs with antisense complementarity to lin-14.* Cell, 1993. **75**(5): p. 843-54.
90. Pasquinelli, A.E., B.J. Reinhart, F. Slack, M.Q. Martindale, M.I. Kuroda, B. Maller, D.C. Hayward, E.E. Ball, B. Degnan, P. Muller, J. Spring, A. Srinivasan, M. Fishman, J. Finnerty, J. Corbo, M. Levine, P. Leahy, E. Davidson and G. Ruvkun, *Conservation of the sequence and temporal expression of let-7 heterochronic regulatory RNA.* Nature, 2000. **408**(6808): p. 86-9.
91. Lewis, B.P., C.B. Burge and D.P. Bartel, *Conserved seed pairing, often flanked by adenosines, indicates that thousands of human genes are microRNA targets.* Cell, 2005. **120**(1): p. 15-20.
92. Esteller, M., *Non-coding RNAs in human disease.* Nat Rev Genet, 2011. **12**(12): p. 861-74.

93. Lee, Y., M. Kim, J. Han, K.H. Yeom, S. Lee, S.H. Baek and V.N. Kim, *MicroRNA genes are transcribed by RNA polymerase II.* EMBO J, 2004. **23**(20): p. 4051-60.
94. Borchert, G.M., W. Lanier and B.L. Davidson, *RNA polymerase III transcribes human microRNAs.* Nat Struct Mol Biol, 2006. **13**(12): p. 1097-101.
95. St Laurent, G., C. Wahlestedt and P. Kapranov, *The Landscape of long noncoding RNA classification.* Trends Genet, 2015. **31**(5): p. 239-51.
96. Treiber, T., N. Treiber and G. Meister, *Regulation of microRNA biogenesis and function.* Thromb Haemost, 2012. **107**(4): p. 605-10.
97. Cai, X., C.H. Hagedorn and B.R. Cullen, *Human microRNAs are processed from capped, polyadenylated transcripts that can also function as mRNAs.* RNA, 2004. **10**(12): p. 1957-66.
98. Han, J., Y. Lee, K.H. Yeom, Y.K. Kim, H. Jin and V.N. Kim, *The Drosha-DGCR8 complex in primary microRNA processing.* Genes Dev, 2004. **18**(24): p. 3016-27.
99. Chendrimada, T.P., R.I. Gregory, E. Kumaraswamy, J. Norman, N. Cooch, K. Nishikura and R. Shiekhattar, *TRBP recruits the Dicer complex to Ago2 for microRNA processing and gene silencing.* Nature, 2005. **436**(7051): p. 740-4.
100. Krol, J., I. Loedige and W. Filipowicz, *The widespread regulation of microRNA biogenesis, function and decay.* Nat Rev Genet, 2010. **11**(9): p. 597-610.
101. Su, H., M.I. Trombly, J. Chen and X. Wang, *Essential and overlapping functions for mammalian Argonautes in microRNA silencing.* Genes Dev, 2009. **23**(3): p. 304-17.
102. Hu, W. and J. Coller, *What comes first: translational repression or mRNA degradation? The deepening mystery of microRNA function.* Cell Res, 2012. **22**(9): p. 1322-4.
103. Pillai, R.S., S.N. Bhattacharyya, C.G. Artus, T. Zoller, N. Cougot, E. Basyuk, E. Bertrand and W. Filipowicz, *Inhibition of translational initiation by Let-7 MicroRNA in human cells.* Science, 2005. **309**(5740): p. 1573-6.
104. Grimson, A., K.K. Farh, W.K. Johnston, P. Garrett-Engele, L.P. Lim and D.P. Bartel, *MicroRNA targeting specificity in mammals: determinants beyond seed pairing.* Mol Cell, 2007. **27**(1): p. 91-105.
105. Gibbings, D.J., C. Ciaudo, M. Erhardt and O. Voinnet, *Multivesicular bodies associate with components of miRNA effector complexes and modulate miRNA activity.* Nat Cell Biol, 2009. **11**(9): p. 1143-9.
106. Chen, X., H. Liang, J. Zhang, K. Zen and C.Y. Zhang, *Secreted microRNAs: a new form of intercellular communication.* Trends Cell Biol, 2012. **22**(3): p. 125-32.
107. Angelini, T.G. and C. Emanueli, *MicroRNAs as clinical biomarkers?* Front Genet, 2015. **6**: p. 240.
108. Gantier, M.P., C.E. McCoy, I. Rusinova, D. Saulep, D. Wang, D. Xu, A.T. Irving, M.A. Behlke, P.J. Hertzog, F. Mackay and B.R. Williams, *Analysis of microRNA turnover in mammalian cells following Dicer1 ablation.* Nucleic Acids Res, 2011. **39**(13): p. 5692-703.
109. Liu, H., C. Lei, Q. He, Z. Pan, D. Xiao and Y. Tao, *Nuclear functions of mammalian MicroRNAs in gene regulation, immunity and cancer.* Mol Cancer, 2018. **17**(1): p. 64.
110. Budak, H., R. Bulut, M. Kantar and B. Alptekin, *MicroRNA nomenclature and the need for a revised naming prescription.* Brief Funct Genomics, 2016. **15**(1): p. 65-71.
111. Zhang, H., B. Shykind and T. Sun, *Approaches to manipulating microRNAs in neurogenesis.* Front Neurosci, 2012. **6**: p. 196.
112. Chen, Y., D.Y. Gao and L. Huang, *In vivo delivery of miRNAs for cancer therapy: challenges and strategies.* Adv Drug Deliv Rev, 2015. **81**: p. 128-41.
113. Trionfini, P., A. Benigni and G. Remuzzi, *MicroRNAs in kidney physiology and disease.* Nat Rev Nephrol, 2015. **11**(1): p. 23-33.
114. Cheng, C.J., R. Bahal, I.A. Babar, Z. Pincus, F. Barrera, C. Liu, A. Svoronos, D.T. Braddock, P.M. Glazer, D.M. Engelman, W.M. Saltzman and F.J. Slack, *MicroRNA silencing for cancer therapy targeted to the tumour microenvironment.* Nature, 2015. **518**(7537): p. 107-10.
115. Chen, Y., H. Zhao, Z. Tan, C. Zhang and X. Fu, *Bottleneck limitations for microRNA-based therapeutics from bench to the bedside.* Pharmazie, 2015. **70**(3): p. 147-54.
116. Chandrasekaran, K., D.S. Karolina, S. Sepramaniam, A. Armugam, E.M. Wintour, J.F. Bertram and K. Jeyaseelan, *Role of microRNAs in kidney homeostasis and disease.* Kidney Int, 2012. **81**(7): p. 617-27.

117. Fierro-Fernandez, M., V. Miguel and S. Lamas, *Role of redoximiRs in fibrogenesis.* Redox Biol, 2016. **7**: p. 58-67.
118. Gomez, I.G., N. Nakagawa and J.S. Duffield, *MicroRNAs as novel therapeutic targets to treat kidney injury and fibrosis.* Am J Physiol Renal Physiol, 2016. **310**(10): p. F931-44.
119. Meng, X.M., P.M. Tang, J. Li and H.Y. Lan, *TGF-beta/Smad signaling in renal fibrosis.* Front Physiol, 2015. **6**: p. 82.
120. Eble, J.A. and F.F. de Rezende, *Redox-relevant aspects of the extracellular matrix and its cellular contacts via integrins.* Antioxid Redox Signal, 2014. **20**(13): p. 1977-93.
121. Herrera, J., D.J. Beisang, M. Peterson, C. Forster, A. Gilbertsen, A. Benyumov, K. Smith, C.E. Korenczuk, V.H. Barocas, K. Guenther, R. Hite, L. Zhang, C.A. Henke and P.B. Bitterman, *Dicer1 Deficiency in the Idiopathic Pulmonary Fibrosis Fibroblastic Focus Promotes Fibrosis by Suppressing MicroRNA Biogenesis.* Am J Respir Crit Care Med, 2018. **198**(4): p. 486-496.
122. Chung, A.C., Y. Dong, W. Yang, X. Zhong, R. Li and H.Y. Lan, *Smad7 suppresses renal fibrosis via altering expression of TGF-beta/Smad3-regulated microRNAs.* Mol Ther, 2013. **21**(2): p. 388-98.
123. Davis, B.N., A.C. Hilyard, P.H. Nguyen, G. Lagna and A. Hata, *Smad proteins bind a conserved RNA sequence to promote microRNA maturation by Drosha.* Mol Cell, 2010. **39**(3): p. 373-84.
124. Petrillo, F., A. Iervolino, M. Zacchia, A. Simeoni, C. Masella, G. Capolongo, A. Perna, G. Capasso and F. Trepiccione, *MicroRNAs in Renal Diseases: A Potential Novel Therapeutic Target.* Kidney Dis (Basel), 2017. **3**(3): p. 111-119.
125. Wonnacott, A., T. Bowen and D.J. Fraser, *MicroRNAs as biomarkers in chronic kidney disease.* Curr Opin Nephrol Hypertens, 2017. **26**(6): p. 460-466.
126. Zhong, X., A.C. Chung, H.Y. Chen, X.M. Meng and H.Y. Lan, *Smad3-mediated upregulation of miR-21 promotes renal fibrosis.* J Am Soc Nephrol, 2011. **22**(9): p. 1668-81.
127. Denby, L., V. Ramdas, M.W. McBride, J. Wang, H. Robinson, J. McClure, W. Crawford, R. Lu, D.Z. Hillyard, R. Khanin, R. Agami, A.F. Dominiczak, C.C. Sharpe and A.H. Baker, *miR-21 and miR-214 are consistently modulated during renal injury in rodent models.* Am J Pathol, 2011. **179**(2): p. 661-72.
128. Loboda, A., M. Sobczak, A. Jozkowicz and J. Dulak, *TGF-beta1/Smads and miR-21 in Renal Fibrosis and Inflammation.* Mediators Inflamm, 2016. **2016**: p. 8319283.
129. McClelland, A.D., M. Herman-Edelstein, R. Komers, J.C. Jha, C.E. Winbanks, S. Hagiwara, P. Gregorevic, P. Kantharidis and M.E. Cooper, *miR-21 promotes renal fibrosis in diabetic nephropathy by targeting PTEN and SMAD7.* Clin Sci (Lond), 2015. **129**(12): p. 1237-49.
130. Chen, J., A. Zmijewska, D. Zhi and R.B. Mannon, *Cyclosporine-mediated allograft fibrosis is associated with micro-RNA-21 through AKT signaling.* Transpl Int, 2015. **28**(2): p. 232-45.
131. Chau, B.N., C. Xin, J. Hartner, S. Ren, A.P. Castano, G. Linn, J. Li, P.T. Tran, V. Kaimal, X. Huang, A.N. Chang, S. Li, A. Kalra, M. Grafals, D. Portilla, D.A. MacKenna, S.H. Orkin and J.S. Duffield, *MicroRNA-21 promotes fibrosis of the kidney by silencing metabolic pathways.* Sci Transl Med, 2012. **4**(121): p. 121ra18.
132. Glowacki, F., G. Savary, V. Gnemmi, D. Buob, C. Van der Hauwaert, J.M. Lo-Guidice, S. Bouye, M. Hazzan, N. Pottier, M. Perrais, S. Aubert and C. Cauffiez, *Increased circulating miR-21 levels are associated with kidney fibrosis.* PLoS One, 2013. **8**(2): p. e58014.
133. Li, R., A.C. Chung, Y. Dong, W. Yang, X. Zhong and H.Y. Lan, *The microRNA miR-433 promotes renal fibrosis by amplifying the TGF-beta/Smad3-Azin1 pathway.* Kidney Int, 2013. **84**(6): p. 1129-44.
134. Rogler, C.E., L. Levoci, T. Ader, A. Massimi, T. Tchaikovskaya, R. Norel and L.E. Rogler, *MicroRNA-23b cluster microRNAs regulate transforming growth factor-beta/bone morphogenetic protein signaling and liver stem cell differentiation by targeting Smads.* Hepatology, 2009. **50**(2): p. 575-84.
135. Meng, J., L. Li, Y. Zhao, Z. Zhou, M. Zhang, D. Li, C.Y. Zhang, K. Zen and Z. Liu, *MicroRNA-196a/b Mitigate Renal Fibrosis by Targeting TGF-beta Receptor 2.* J Am Soc Nephrol, 2016. **27**(10): p. 3006-3021.
136. Guo, R., G. Hao, Y. Bao, J. Xiao, X. Zhan, X. Shi, L. Luo, J. Zhou, Q. Chen and X. Wei, *MiR-200a negatively regulates TGF-beta1-induced epithelial-mesenchymal transition of peritoneal mesothelial cells by targeting ZEB1/2 expression.* Am J Physiol Renal Physiol, 2018. **314**(6): p. F1087-F1095.

137. Wang, B., P. Koh, C. Winbanks, M.T. Coughlan, A. McClelland, A. Watson, K. Jandeleit-Dahm, W.C. Burns, M.C. Thomas, M.E. Cooper and P. Kantharidis, *miR-200a Prevents renal fibrogenesis through repression of TGF-beta2 expression.* Diabetes, 2011. **60**(1): p. 280-7.
138. Srivastava, S.P., D. Koya and K. Kanasaki, *MicroRNAs in kidney fibrosis and diabetic nephropathy: roles on EMT and EndMT.* Biomed Res Int, 2013. **2013**: p. 125469.
139. Chung, A.C., X.R. Huang, X. Meng and H.Y. Lan, *miR-192 mediates TGF-beta/Smad3-driven renal fibrosis.* J Am Soc Nephrol, 2010. **21**(8): p. 1317-25.
140. Li, H., R. Yang, X. Fan, T. Gu, Z. Zhao, D. Chang and W. Wang, *MicroRNA array analysis of microRNAs related to systemic scleroderma.* Rheumatol Int, 2012. **32**(2): p. 307-13.
141. Makino, K., M. Jinnin, A. Hirano, K. Yamane, M. Eto, T. Kusano, N. Honda, I. Kajihara, T. Makino, K. Sakai, S. Masuguchi, S. Fukushima and H. Ihn, *The downregulation of microRNA let-7a contributes to the excessive expression of type I collagen in systemic and localized scleroderma.* J Immunol, 2013. **190**(8): p. 3905-15.
142. Pandit, K.V., D. Corcoran, H. Yousef, M. Yarlagadda, A. Tzouvelekis, K.F. Gibson, K. Konishi, S.A. Yousem, M. Singh, D. Handley, T. Richards, M. Selman, S.C. Watkins, A. Pardo, A. Ben-Yehudah, D. Bouros, O. Eickelberg, P. Ray, P.V. Benos and N. Kaminski, *Inhibition and role of let-7d in idiopathic pulmonary fibrosis.* Am J Respir Crit Care Med, 2010. **182**(2): p. 220-9.
143. Mayr, C., M.T. Hemann and D.P. Bartel, *Disrupting the pairing between let-7 and Hmga2 enhances oncogenic transformation.* Science, 2007. **315**(5818): p. 1576-9.
144. Denby, L., V. Ramdas, R. Lu, B.R. Conway, J.S. Grant, B. Dickinson, A.B. Aurora, J.D. McClure, D. Kipgen, C. Delles, E. van Rooij and A.H. Baker, *MicroRNA-214 antagonism protects against renal fibrosis.* J Am Soc Nephrol, 2014. **25**(1): p. 65-80.
145. Liu, M., L. Liu, M. Bai, L. Zhang, F. Ma, X. Yang and S. Sun, *Hypoxia-induced activation of Twist/miR-214/E-cadherin axis promotes renal tubular epithelial cell mesenchymal transition and renal fibrosis.* Biochem Biophys Res Commun, 2018. **495**(3): p. 2324-2330.
146. Morizane, R., S. Fujii, T. Monkawa, K. Hiratsuka, S. Yamaguchi, K. Homma and H. Itoh, *miR-34c attenuates epithelial-mesenchymal transition and kidney fibrosis with ureteral obstruction.* Sci Rep, 2014. **4**: p. 4578.
147. Casalena, G., S. Krick, I. Daehn, L. Yu, W. Ju, S. Shi, S.Y. Tsai, V. D'Agati, M. Lindenmeyer, C.D. Cohen, D. Schlondorff and E.P. Bottinger, *Mpv17 in mitochondria protects podocytes against mitochondrial dysfunction and apoptosis in vivo and in vitro.* Am J Physiol Renal Physiol, 2014. **306**(11): p. F1372-80.
148. Gomez, I.G., D.A. MacKenna, B.G. Johnson, V. Kaimal, A.M. Roach, S. Ren, N. Nakagawa, C. Xin, R. Newitt, S. Pandya, T.H. Xia, X. Liu, D.B. Borza, M. Grafals, S.J. Shankland, J. Himmelfarb, D. Portilla, S. Liu, B.N. Chau and J.S. Duffield, *Anti-microRNA-21 oligonucleotides prevent Alport nephropathy progression by stimulating metabolic pathways.* J Clin Invest, 2015. **125**(1): p. 141-56.
149. Espinosa-Diez, C., M. Fierro-Fernandez, F. Sanchez-Gomez, F. Rodriguez-Pascual, M. Alique, M. Ruiz-Ortega, N. Beraza, M.L. Martinez-Chantar, C. Fernandez-Hernando and S. Lamas, *Targeting of Gamma-Glutamyl-Cysteine Ligase by miR-433 Reduces Glutathione Biosynthesis and Promotes TGF-beta-Dependent Fibrogenesis.* Antioxid Redox Signal, 2015. **23**(14): p. 1092-105.
150. Jiang, L., W. Qiu, Y. Zhou, P. Wen, L. Fang, H. Cao, K. Zen, W. He, C. Zhang, C. Dai and J. Yang, *A microRNA-30e/mitochondrial uncoupling protein 2 axis mediates TGF-beta1-induced tubular epithelial cell extracellular matrix production and kidney fibrosis.* Kidney Int, 2013. **84**(2): p. 285-96.
151. Wang, B., R. Komers, R. Carew, C.E. Winbanks, B. Xu, M. Herman-Edelstein, P. Koh, M. Thomas, K. Jandeleit-Dahm, P. Gregorevic, M.E. Cooper and P. Kantharidis, *Suppression of microRNA-29 expression by TGF-beta1 promotes collagen expression and renal fibrosis.* J Am Soc Nephrol, 2012. **23**(2): p. 252-65.
152. Yamada, Y., M. Takanashi, K. Sudo, S. Ueda, S.I. Ohno and M. Kuroda, *Novel form of miR-29b suppresses bleomycin-induced pulmonary fibrosis.* PLoS One, 2017. **12**(2): p. e0171957.
153. Zhang, Y., X.R. Huang, L.H. Wei, A.C. Chung, C.M. Yu and H.Y. Lan, *miR-29b as a therapeutic agent for angiotensin II-induced cardiac fibrosis by targeting TGF-beta/Smad3 signaling.* Mol Ther, 2014. **22**(5): p. 974-85.

154. Kriegel, A.J., Y. Liu, Y. Fang, X. Ding and M. Liang, *The miR-29 family: genomics, cell biology, and relevance to renal and cardiovascular injury.* Physiol Genomics, 2012. **44**(4): p. 237-44.
155. Rayego-Mateos, S., J.L. Morgado-Pascual, R.R. Rodrigues-Diez, R. Rodrigues-Diez, L.L. Falke, S. Mezzano, A. Ortiz, J. Egido, R. Goldschmeding and M. Ruiz-Ortega, *Connective tissue growth factor induces renal fibrosis via epidermal growth factor receptor activation.* J Pathol, 2018. **244**(2): p. 227-241.
156. Ruperez, M., O. Lorenzo, L.M. Blanco-Colio, V. Esteban, J. Egido and M. Ruiz-Ortega, *Connective tissue growth factor is a mediator of angiotensin II-induced fibrosis.* Circulation, 2003. **108**(12): p. 1499-505.
157. Wang, J., L. Duan, T. Guo, Y. Gao, L. Tian, J. Liu, S. Wang and J. Yang, *Downregulation of miR-30c promotes renal fibrosis by target CTGF in diabetic nephropathy.* J Diabetes Complications, 2016. **30**(3): p. 406-14.
158. Bijkerk, R., R.G. de Bruin, C. van Solingen, J.M. van Gils, J.M. Duijs, E.P. van der Veer, T.J. Rabelink, B.D. Humphreys and A.J. van Zonneveld, *Silencing of microRNA-132 reduces renal fibrosis by selectively inhibiting myofibroblast proliferation.* Kidney Int, 2016. **89**(6): p. 1268-80.
159. Macconi, D., S. Tomasoni, P. Romagnani, P. Trionfini, F. Sangalli, B. Mazzinghi, P. Rizzo, E. Lazzeri, M. Abbate, G. Remuzzi and A. Benigni, *MicroRNA-324-3p promotes renal fibrosis and is a target of ACE inhibition.* J Am Soc Nephrol, 2012. **23**(9): p. 1496-505.
160. O'Connor, P.M., *Renal oxygen delivery: matching delivery to metabolic demand.* Clin Exp Pharmacol Physiol, 2006. **33**(10): p. 961-7.
161. Hamm, L.L., N. Nakhoul and K.S. Hering-Smith, *Acid-Base Homeostasis.* Clin J Am Soc Nephrol, 2015. **10**(12): p. 2232-42.
162. Naifeh, J. and M. Varacallo, *Biochemistry, Aerobic Glycolysis*, in *StatPearls*. 2019: Treasure Island (FL).
163. Cargill, K. and S. Sims-Lucas, *Metabolic requirements of the nephron.* Pediatr Nephrol, 2018.
164. Jornayvaz, F.R. and G.I. Shulman, *Regulation of mitochondrial biogenesis.* Essays Biochem, 2010. **47**: p. 69-84.
165. Klahr, S., L. Hamm, M. Hammerman and L. Mandel, *Renal metabolism: integrated responses. In: Handbook of Physiology.* Compr Physiol, 2011: p. 2263–2333.
166. Weidemann, M.J. and H.A. Krebs, *The fuel of respiration of rat kidney cortex.* Biochem J, 1969. **112**(2): p. 149-66.
167. Mather, A. and C. Pollock, *Glucose handling by the kidney.* Kidney Int Suppl, 2011(120): p. S1-6.
168. Gerich, J.E., C. Meyer, H.J. Woerle and M. Stumvoll, *Renal gluconeogenesis: its importance in human glucose homeostasis.* Diabetes Care, 2001. **24**(2): p. 382-91.
169. Imasawa, T. and R. Rossignol, *Podocyte energy metabolism and glomerular diseases.* Int J Biochem Cell Biol, 2013. **45**(9): p. 2109-18.
170. Ding, H., L. Jiang, J. Xu, F. Bai, Y. Zhou, Q. Yuan, J. Luo, K. Zen and J. Yang, *Inhibiting aerobic glycolysis suppresses renal interstitial fibroblast activation and renal fibrosis.* Am J Physiol Renal Physiol, 2017. **313**(3): p. F561-F575.
171. Kang, H.M., S.H. Ahn, P. Choi, Y.A. Ko, S.H. Han, F. Chinga, A.S. Park, J. Tao, K. Sharma, J. Pullman, E.P. Bottinger, I.J. Goldberg and K. Susztak, *Defective fatty acid oxidation in renal tubular epithelial cells has a key role in kidney fibrosis development.* Nat Med, 2015. **21**(1): p. 37-46.
172. Rakhshandehroo, M., B. Knoch, M. Muller and S. Kersten, *Peroxisome proliferator-activated receptor alpha target genes.* PPAR Res, 2010. **2010**.
173. Iwao, Y., K. Nakajou, R. Nagai, K. Kitamura, M. Anraku, T. Maruyama and M. Otagiri, *CD36 is one of important receptors promoting renal tubular injury by advanced oxidation protein products.* Am J Physiol Renal Physiol, 2008. **295**(6): p. F1871-80.
174. Sassa, T. and A. Kihara, *Metabolism of very long-chain Fatty acids: genes and pathophysiology.* Biomol Ther (Seoul), 2014. **22**(2): p. 83-92.
175. Vasko, R., *Peroxisomes and Kidney Injury.* Antioxid Redox Signal, 2016. **25**(4): p. 217-31.
176. Houten, S.M. and R.J. Wanders, *A general introduction to the biochemistry of mitochondrial fatty acid beta-oxidation.* J Inherit Metab Dis, 2010. **33**(5): p. 469-77.
177. Jernberg, J.N., C.E. Bowman, M.J. Wolfgang and S. Scafidi, *Developmental regulation and localization of carnitine palmitoyltransferases (CPTs) in rat brain.* J Neurochem, 2017. **142**(3): p. 407-419.

178. McCoin, C.S., T.A. Knotts and S.H. Adams, *Acylcarnitines--old actors auditioning for new roles in metabolic physiology.* Nat Rev Endocrinol, 2015. **11**(10): p. 617-25.
179. Ahmad, M. and C.I. Kahwaji, *Biochemistry, Electron Transport Chain*, in *StatPearls*. 2019: Treasure Island (FL).
180. Ceccarelli, S.M., O. Chomienne, M. Gubler and A. Arduini, *Carnitine palmitoyltransferase (CPT) modulators: a medicinal chemistry perspective on 35 years of research.* J Med Chem, 2011. **54**(9): p. 3109-52.
181. Gobin, S., J.P. Bonnefont, C. Prip-Buus, C. Mugnier, M. Ferrec, F. Demaugre, J.M. Saudubray, H. Rostane, F. Djouadi, W. Wilcox, S. Cederbaum, R. Haas, W.L. Nyhan, A. Green, G. Gray, J. Girard and L. Thuillier, *Organization of the human liver carnitine palmitoyltransferase 1 gene (CPT1A) and identification of novel mutations in hypoketotic hypoglycaemia.* Hum Genet, 2002. **111**(2): p. 179-89.
182. Ramsay, R.R., R.D. Gandour and F.R. van der Leij, *Molecular enzymology of carnitine transfer and transport.* Biochim Biophys Acta, 2001. **1546**(1): p. 21-43.
183. Kerner, J., A.M. Distler, P. Minkler, W. Parland, S.M. Peterman and C.L. Hoppel, *Phosphorylation of rat liver mitochondrial carnitine palmitoyltransferase-I: effect on the kinetic properties of the enzyme.* J Biol Chem, 2004. **279**(39): p. 41104-13.
184. Fukumoto, K., A. Pierro, V.A. Zammit, L. Spitz and S. Eaton, *Tyrosine nitration of carnitine palmitoyl transferase I during endotoxaemia in suckling rats.* Biochim Biophys Acta, 2004. **1683**(1-3): p. 1-6.
185. Morillas, M., E. Lopez-Vinas, A. Valencia, D. Serra, P. Gomez-Puertas, F.G. Hegardt and G. Asins, *Structural model of carnitine palmitoyltransferase I based on the carnitine acetyltransferase crystal.* Biochem J, 2004. **379**(Pt 3): p. 777-84.
186. Fraser, F., C.G. Corstorphine and V.A. Zammit, *Topology of carnitine palmitoyltransferase I in the mitochondrial outer membrane.* Biochem J, 1997. **323 (Pt 3)**: p. 711-8.
187. Shi, J., H. Zhu, D.N. Arvidson and G. Woldegiorgis, *The first 28 N-terminal amino acid residues of human heart muscle carnitine palmitoyltransferase I are essential for malonyl CoA sensitivity and high-affinity binding.* Biochemistry, 2000. **39**(4): p. 712-7.
188. Lopez-Vinas, E., A. Bentebibel, C. Gurunathan, M. Morillas, D. de Arriaga, D. Serra, G. Asins, F.G. Hegardt and P. Gomez-Puertas, *Definition by functional and structural analysis of two malonyl-CoA sites in carnitine palmitoyltransferase 1A.* J Biol Chem, 2007. **282**(25): p. 18212-24.
189. Faye, A., K. Borthwick, C. Esnous, N.T. Price, S. Gobin, V.N. Jackson, V.A. Zammit, J. Girard and C. Prip-Buus, *Demonstration of N- and C-terminal domain intramolecular interactions in rat liver carnitine palmitoyltransferase 1 that determine its degree of malonyl-CoA sensitivity.* Biochem J, 2005. **387**(Pt 1): p. 67-76.
190. Faye, A., C. Esnous, N.T. Price, M.A. Onfray, J. Girard and C. Prip-Buus, *Rat liver carnitine palmitoyltransferase 1 forms an oligomeric complex within the outer mitochondrial membrane.* J Biol Chem, 2007. **282**(37): p. 26908-16.
191. Song, S., R.R. Attia, S. Connaughton, M.I. Niesen, G.C. Ness, M.B. Elam, R.T. Hori, G.A. Cook and E.A. Park, *Peroxisome proliferator activated receptor alpha (PPARalpha) and PPAR gamma coactivator (PGC-1alpha) induce carnitine palmitoyltransferase IA (CPT-1A) via independent gene elements.* Mol Cell Endocrinol, 2010. **325**(1-2): p. 54-63.
192. Louet, J.F., G. Hayhurst, F.J. Gonzalez, J. Girard and J.F. Decaux, *The coactivator PGC-1 is involved in the regulation of the liver carnitine palmitoyltransferase I gene expression by cAMP in combination with HNF4 alpha and cAMP-response element-binding protein (CREB).* J Biol Chem, 2002. **277**(41): p. 37991-8000.
193. Zhou, D. and Y. Liu, *Renal fibrosis in 2015: Understanding the mechanisms of kidney fibrosis.* Nat Rev Nephrol, 2016. **12**(2): p. 68-70.
194. Simon, N. and A. Hertig, *Alteration of Fatty Acid Oxidation in Tubular Epithelial Cells: From Acute Kidney Injury to Renal Fibrogenesis.* Front Med (Lausanne), 2015. **2**: p. 52.
195. Yang, X., D.M. Okamura, X. Lu, Y. Chen, J. Moorhead, Z. Varghese and X.Z. Ruan, *CD36 in chronic kidney disease: novel insights and therapeutic opportunities.* Nat Rev Nephrol, 2017. **13**(12): p. 769-781.

196. Lynch, M.R., M.T. Tran and S.M. Parikh, *PGC1alpha in the kidney.* Am J Physiol Renal Physiol, 2018. **314**(1): p. F1-F8.
197. Han, S.H., M.Y. Wu, B.Y. Nam, J.T. Park, T.H. Yoo, S.W. Kang, J. Park, F. Chinga, S.Y. Li and K. Susztak, *PGC-1alpha Protects from Notch-Induced Kidney Fibrosis Development.* J Am Soc Nephrol, 2017. **28**(11): p. 3312-3322.
198. Li, S., N. Mariappan, J. Megyesi, B. Shank, K. Kannan, S. Theus, P.M. Price, J.S. Duffield and D. Portilla, *Proximal tubule PPARalpha attenuates renal fibrosis and inflammation caused by unilateral ureteral obstruction.* Am J Physiol Renal Physiol, 2013. **305**(5): p. F618-27.
199. Tran, M.T., Z.K. Zsengeller, A.H. Berg, E.V. Khankin, M.K. Bhasin, W. Kim, C.B. Clish, I.E. Stillman, S.A. Karumanchi, E.P. Rhee and S.M. Parikh, *PGC1alpha drives NAD biosynthesis linking oxidative metabolism to renal protection.* Nature, 2016. **531**(7595): p. 528-32.
200. Li, S.Y. and K. Susztak, *The Role of Peroxisome Proliferator-Activated Receptor gamma Coactivator 1alpha (PGC-1alpha) in Kidney Disease.* Semin Nephrol, 2018. **38**(2): p. 121-126.
201. Ratliff, B.B., W. Abdulmahdi, R. Pawar and M.S. Wolin, *Oxidant Mechanisms in Renal Injury and Disease.* Antioxid Redox Signal, 2016. **25**(3): p. 119-46.
202. Yang, Z., T. Cappello and L. Wang, *Emerging role of microRNAs in lipid metabolism.* Acta Pharm Sin B, 2015. **5**(2): p. 145-50.
203. Yang, Z. and L. Wang, *Regulation of microRNA expression and function by nuclear receptor signaling.* Cell Biosci, 2011. **1**(1): p. 31.
204. Li, J., Y. Zhang, R. Kuruba, X. Gao, C.R. Gandhi, W. Xie and S. Li, *Roles of microRNA-29a in the antifibrotic effect of farnesoid X receptor in hepatic stellate cells.* Mol Pharmacol, 2011. **80**(1): p. 191-200.
205. Lee, C.G., Y.W. Kim, E.H. Kim, Z. Meng, W. Huang, S.J. Hwang and S.G. Kim, *Farnesoid X receptor protects hepatocytes from injury by repressing miR-199a-3p, which increases levels of LKB1.* Gastroenterology, 2012. **142**(5): p. 1206-1217 e7.
206. Esau, C., S. Davis, S.F. Murray, X.X. Yu, S.K. Pandey, M. Pear, L. Watts, S.L. Booten, M. Graham, R. McKay, A. Subramaniam, S. Propp, B.A. Lollo, S. Freier, C.F. Bennett, S. Bhanot and B.P. Monia, *miR-122 regulation of lipid metabolism revealed by in vivo antisense targeting.* Cell Metab, 2006. **3**(2): p. 87-98.
207. Ahn, J., H. Lee, C.H. Jung and T. Ha, *Lycopene inhibits hepatic steatosis via microRNA-21-induced downregulation of fatty acid-binding protein 7 in mice fed a high-fat diet.* Mol Nutr Food Res, 2012. **56**(11): p. 1665-74.
208. Fernandez-Hernando, C., C.M. Ramirez, L. Goedeke and Y. Suarez, *MicroRNAs in metabolic disease.* Arterioscler Thromb Vasc Biol, 2013. **33**(2): p. 178-85.
209. Shirasaki, T., M. Honda, T. Shimakami, R. Horii, T. Yamashita, Y. Sakai, A. Sakai, H. Okada, R. Watanabe, S. Murakami, M. Yi, S.M. Lemon and S. Kaneko, *MicroRNA-27a regulates lipid metabolism and inhibits hepatitis C virus replication in human hepatoma cells.* J Virol, 2013. **87**(9): p. 5270-86.
210. Horton, J.D., J.L. Goldstein and M.S. Brown, *SREBPs: activators of the complete program of cholesterol and fatty acid synthesis in the liver.* J Clin Invest, 2002. **109**(9): p. 1125-31.
211. Marquart, T.J., R.M. Allen, D.S. Ory and A. Baldan, *miR-33 links SREBP-2 induction to repression of sterol transporters.* Proc Natl Acad Sci U S A, 2010. **107**(27): p. 12228-32.
212. Najafi-Shoushtari, S.H., F. Kristo, Y. Li, T. Shioda, D.E. Cohen, R.E. Gerszten and A.M. Naar, *MicroRNA-33 and the SREBP host genes cooperate to control cholesterol homeostasis.* Science, 2010. **328**(5985): p. 1566-9.
213. Rosenson, R.S., H.B. Brewer, Jr., W.S. Davidson, Z.A. Fayad, V. Fuster, J. Goldstein, M. Hellerstein, X.C. Jiang, M.C. Phillips, D.J. Rader, A.T. Remaley, G.H. Rothblat, A.R. Tall and L. Yvan-Charvet, *Cholesterol efflux and atheroprotection: advancing the concept of reverse cholesterol transport.* Circulation, 2012. **125**(15): p. 1905-19.
214. Allen, R.M., T.J. Marquart, C.J. Albert, F.J. Suchy, D.Q. Wang, M. Ananthanarayanan, D.A. Ford and A. Baldan, *miR-33 controls the expression of biliary transporters, and mediates statin- and diet-induced hepatotoxicity.* EMBO Mol Med, 2012. **4**(9): p. 882-95.

215. Rayner, K.J., Y. Suarez, A. Davalos, S. Parathath, M.L. Fitzgerald, N. Tamehiro, E.A. Fisher, K.J. Moore and C. Fernandez-Hernando, *MiR-33 contributes to the regulation of cholesterol homeostasis.* Science, 2010. **328**(5985): p. 1570-3.
216. Rottiers, V., S. Obad, A. Petri, R. McGarrah, M.W. Lindholm, J.C. Black, S. Sinha, R.J. Goody, M.S. Lawrence, A.S. deLemos, H.F. Hansen, S. Whittaker, S. Henry, R. Brookes, S.H. Najafi-Shoushtari, R.T. Chung, J.R. Whetstine, R.E. Gerszten, S. Kauppinen and A.M. Naar, *Pharmacological inhibition of a microRNA family in nonhuman primates by a seed-targeting 8-mer antimiR.* Sci Transl Med, 2013. **5**(212): p. 212ra162.
217. Rotllan, N., C.M. Ramirez, B. Aryal, C.C. Esau and C. Fernandez-Hernando, *Therapeutic silencing of microRNA-33 inhibits the progression of atherosclerosis in Ldlr-/- mice--brief report.* Arterioscler Thromb Vasc Biol, 2013. **33**(8): p. 1973-7.
218. Goedeke, L., A. Salerno, C.M. Ramirez, L. Guo, R.M. Allen, X. Yin, S.R. Langley, C. Esau, A. Wanschel, E.A. Fisher, Y. Suarez, A. Baldan, M. Mayr and C. Fernandez-Hernando, *Long-term therapeutic silencing of miR-33 increases circulating triglyceride levels and hepatic lipid accumulation in mice.* EMBO Mol Med, 2014. **6**(9): p. 1133-41.
219. Davalos, A., L. Goedeke, P. Smibert, C.M. Ramirez, N.P. Warrier, U. Andreo, D. Cirera-Salinas, K. Rayner, U. Suresh, J.C. Pastor-Pareja, E. Esplugues, E.A. Fisher, L.O. Penalva, K.J. Moore, Y. Suarez, E.C. Lai and C. Fernandez-Hernando, *miR-33a/b contribute to the regulation of fatty acid metabolism and insulin signaling.* Proc Natl Acad Sci U S A, 2011. **108**(22): p. 9232-7.
220. Gerin, I., L.A. Clerbaux, O. Haumont, N. Lanthier, A.K. Das, C.F. Burant, I.A. Leclercq, O.A. MacDougald and G.T. Bommer, *Expression of miR-33 from an SREBP2 intron inhibits cholesterol export and fatty acid oxidation.* J Biol Chem, 2010. **285**(44): p. 33652-61.
221. Hochedlinger, K., Y. Yamada, C. Beard and R. Jaenisch, *Ectopic expression of Oct-4 blocks progenitor-cell differentiation and causes dysplasia in epithelial tissues.* Cell, 2005. **121**(3): p. 465-77.
222. Beard, C., K. Hochedlinger, K. Plath, A. Wutz and R. Jaenisch, *Efficient method to generate single-copy transgenic mice by site-specific integration in embryonic stem cells.* Genesis, 2006. **44**(1): p. 23-8.
223. Ly, J.P., T. Onay and S.E. Quaggin, *Mouse models to study kidney development, function and disease.* Curr Opin Nephrol Hypertens, 2011. **20**(4): p. 382-90.
224. Kuzmichev, A.N., S.K. Kim, A.C. D'Alessio, J.G. Chenoweth, I.M. Wittko, L. Campanati and R.D. McKay, *Sox2 acts through Sox21 to regulate transcription in pluripotent and differentiated cells.* Curr Biol, 2012. **22**(18): p. 1705-10.
225. Buchholz, F., P.O. Angrand and A.F. Stewart, *Improved properties of FLP recombinase evolved by cycling mutagenesis.* Nat Biotechnol, 1998. **16**(7): p. 657-62.
226. Price, N.L., A.K. Singh, N. Rotllan, L. Goedeke, A. Wing, A. Canfran-Duque, A. Diaz-Ruiz, E. Araldi, A. Baldan, J.P. Camporez, Y. Suarez, M.S. Rodeheffer, G.I. Shulman, R. de Cabo and C. Fernandez-Hernando, *Genetic Ablation of miR-33 Increases Food Intake, Enhances Adipose Tissue Expansion, and Promotes Obesity and Insulin Resistance.* Cell Rep, 2018. **22**(8): p. 2133-2145.
227. Kumar, R.M., P. Cahan, A.K. Shalek, R. Satija, A. DaleyKeyser, H. Li, J. Zhang, K. Pardee, D. Gennert, J.J. Trombetta, T.C. Ferrante, A. Regev, G.Q. Daley and J.J. Collins, *Deconstructing transcriptional heterogeneity in pluripotent stem cells.* Nature, 2014. **516**(7529): p. 56-61.
228. Livak, K.J. and T.D. Schmittgen, *Analysis of relative gene expression data using real-time quantitative PCR and the 2(-Delta Delta C(T)) Method.* Methods, 2001. **25**(4): p. 402-8.
229. Chevalier, R.L., M.S. Forbes and B.A. Thornhill, *Ureteral obstruction as a model of renal interstitial fibrosis and obstructive nephropathy.* Kidney Int, 2009. **75**(11): p. 1145-1152.
230. Fink, M., M. Henry and J.D. Tange, *Experimental folic acid nephropathy.* Pathology, 1987. **19**(2): p. 143-9.
231. Rahman, A., D. Yamazaki, A. Sufiun, K. Kitada, H. Hitomi, D. Nakano and A. Nishiyama, *A novel approach to adenine-induced chronic kidney disease associated anemia in rodents.* PLoS One, 2018. **13**(2): p. e0192531.
232. Griffiths-Jones, S., H.K. Saini, S. van Dongen and A.J. Enright, *miRBase: tools for microRNA genomics.* Nucleic Acids Res, 2008. **36**(Database issue): p. D154-8.

233. Friedman, R.C., K.K. Farh, C.B. Burge and D.P. Bartel, *Most mammalian mRNAs are conserved targets of microRNAs.* Genome Res, 2009. **19**(1): p. 92-105.
234. Krek, A., D. Grun, M.N. Poy, R. Wolf, L. Rosenberg, E.J. Epstein, P. MacMenamin, I. da Piedade, K.C. Gunsalus, M. Stoffel and N. Rajewsky, *Combinatorial microRNA target predictions.* Nat Genet, 2005. **37**(5): p. 495-500.
235. Dweep, H. and N. Gretz, *miRWalk2.0: a comprehensive atlas of microRNA-target interactions.* Nat Methods, 2015. **12**(8): p. 697.
236. Betel, D., M. Wilson, A. Gabow, D.S. Marks and C. Sander, *The microRNA.org resource: targets and expression.* Nucleic Acids Res, 2008. **36**(Database issue): p. D149-53.
237. Benjamini, Y., D. Drai, G. Elmer, N. Kafkafi and I. Golani, *Controlling the false discovery rate in behavior genetics research.* Behav Brain Res, 2001. **125**(1-2): p. 279-84.
238. Bligh, E.G. and W.J. Dyer, *A rapid method of total lipid extraction and purification.* Can J Biochem Physiol, 1959. **37**(8): p. 911-7.
239. Huynh, F.K., M.F. Green, T.R. Koves and M.D. Hirschey, *Measurement of fatty acid oxidation rates in animal tissues and cell lines.* Methods Enzymol, 2014. **542**: p. 391-405.
240. Matsushita, K., B.K. Mahmoodi, M. Woodward, J.R. Emberson, T.H. Jafar, S.H. Jee, K.R. Polkinghorne, A. Shankar, D.H. Smith, M. Tonelli, D.G. Warnock, C.P. Wen, J. Coresh, R.T. Gansevoort, B.R. Hemmelgarn, A.S. Levey and C. Chronic Kidney Disease Prognosis, *Comparison of risk prediction using the CKD-EPI equation and the MDRD study equation for estimated glomerular filtration rate.* JAMA, 2012. **307**(18): p. 1941-51.
241. Solez, K., R.B. Colvin, L.C. Racusen, M. Haas, B. Sis, M. Mengel, P.F. Halloran, W. Baldwin, G. Banfi, A.B. Collins, F. Cosio, D.S. David, C. Drachenberg, G. Einecke, A.B. Fogo, I.W. Gibson, D. Glotz, S.S. Iskandar, E. Kraus, E. Lerut, R.B. Mannon, M. Mihatsch, B.J. Nankivell, V. Nickeleit, J.C. Papadimitriou, P. Randhawa, H. Regele, K. Renaudin, I. Roberts, D. Seron, R.N. Smith and M. Valente, *Banff 07 classification of renal allograft pathology: updates and future directions.* Am J Transplant, 2008. **8**(4): p. 753-60.
242. Acebo, P., D. Giner, P. Calvo, A. Blanco-Rivero, A.D. Ortega, P.L. Fernandez, G. Roncador, E. Fernandez-Malave, M. Chamorro and J.M. Cuezva, *Cancer abolishes the tissue type-specific differences in the phenotype of energetic metabolism.* Transl Oncol, 2009. **2**(3): p. 138-45.
243. Varga, J., D. Brenner and S. Phan, *Fibrosis research: methods and protocols*, N.J.H. Press, Editor. 2005.
244. van der Windt, G.J., C.H. Chang and E.L. Pearce, *Measuring Bioenergetics in T Cells Using a Seahorse Extracellular Flux Analyzer.* Curr Protoc Immunol, 2016. **113**: p. 3 16B 1-3 16B 14.
245. Ravi, S., B. Chacko, P.A. Kramer, H. Sawada, M.S. Johnson, D. Zhi, M.B. Marques and V.M. Darley-Usmar, *Defining the effects of storage on platelet bioenergetics: The role of increased proton leak.* Biochim Biophys Acta, 2015. **1852**(11): p. 2525-34.
246. Chazotte, B., *Labeling mitochondria with TMRM or TMRE.* Cold Spring Harb Protoc, 2011. **2011**(7): p. 895-7.
247. Li, R., N. Jen, F. Yu and T.K. Hsiai, *Assessing mitochondrial redox status by flow cytometric methods: vascular response to fluid shear stress.* Curr Protoc Cytom, 2011. **Chapter 9**: p. Unit9 37.
248. Calderon-Dominguez, M., D. Sebastian, R. Fucho, M. Weber, J.F. Mir, E. Garcia-Casarrubios, M.J. Obregon, A. Zorzano, A.M. Valverde, D. Serra and L. Herrero, *Carnitine Palmitoyltransferase 1 Increases Lipolysis, UCP1 Protein Expression and Mitochondrial Activity in Brown Adipocytes.* PLoS One, 2016. **11**(7): p. e0159399.
249. Huang, S. and K. Susztak, *Epithelial Plasticity versus EMT in Kidney Fibrosis.* Trends Mol Med, 2016. **22**(1): p. 4-6.
250. Eirin, A., A. Lerman and L.O. Lerman, *The Emerging Role of Mitochondrial Targeting in Kidney Disease.* Handb Exp Pharmacol, 2017. **240**: p. 229-250.
251. Stadler, K., I.J. Goldberg and K. Susztak, *The evolving understanding of the contribution of lipid metabolism to diabetic kidney disease.* Curr Diab Rep, 2015. **15**(7): p. 40.
252. Mihaylova, M.M. and R.J. Shaw, *The AMPK signalling pathway coordinates cell growth, autophagy and metabolism.* Nat Cell Biol, 2011. **13**(9): p. 1016-23.

253. Kusaba, T., M. Lalli, R. Kramann, A. Kobayashi and B.D. Humphreys, *Differentiated kidney epithelial cells repair injured proximal tubule.* Proc Natl Acad Sci U S A, 2014. **111**(4): p. 1527-32.
254. Kuznetsov, A.V., R. Margreiter, A. Amberger, V. Saks and M. Grimm, *Changes in mitochondrial redox state, membrane potential and calcium precede mitochondrial dysfunction in doxorubicin-induced cell death.* Biochim Biophys Acta, 2011. **1813**(6): p. 1144-52.
255. Radi, R., *Oxygen radicals, nitric oxide, and peroxynitrite: Redox pathways in molecular medicine.* Proc Natl Acad Sci U S A, 2018. **115**(23): p. 5839-5848.
256. Bhargava, P. and R.G. Schnellmann, *Mitochondrial energetics in the kidney.* Nat Rev Nephrol, 2017. **13**(10): p. 629-646.
257. Lee, K., J. Kerner and C.L. Hoppel, *Mitochondrial carnitine palmitoyltransferase 1a (CPT1a) is part of an outer membrane fatty acid transfer complex.* J Biol Chem, 2011. **286**(29): p. 25655-62.
258. Martinez-Klimova, E., O.E. Aparicio-Trejo, E. Tapia and J. Pedraza-Chaverri, *Unilateral Ureteral Obstruction as a Model to Investigate Fibrosis-Attenuating Treatments.* Biomolecules, 2019. **9**(4).
259. Bao, Y.W., Y. Yuan, J.H. Chen and W.Q. Lin, *Kidney disease models: tools to identify mechanisms and potential therapeutic targets.* Zool Res, 2018. **39**(2): p. 72-86.
260. Jia, T., H. Olauson, K. Lindberg, R. Amin, K. Edvardsson, B. Lindholm, G. Andersson, A. Wernerson, Y. Sabbagh, S. Schiavi and T.E. Larsson, *A novel model of adenine-induced tubulointerstitial nephropathy in mice.* BMC Nephrol, 2013. **14**: p. 116.
261. Haynie, K.R., B. Vandanmagsar, S.E. Wicks, J. Zhang and R.L. Mynatt, *Inhibition of carnitine palymitoyltransferase1b induces cardiac hypertrophy and mortality in mice.* Diabetes Obes Metab, 2014. **16**(8): p. 757-60.
262. Vickers, A.E., *Characterization of hepatic mitochondrial injury induced by fatty acid oxidation inhibitors.* Toxicol Pathol, 2009. **37**(1): p. 78-88.
263. Shi, W., S. Hu, W. Wang, X. Zhou and W. Qiu, *Skeletal muscle-specific CPT1 deficiency elevates lipotoxic intermediates but preserves insulin sensitivity.* J Diabetes Res, 2013. **2013**: p. 163062.
264. Reamy, A.A. and M.J. Wolfgang, *Carnitine palmitoyltransferase-1c gain-of-function in the brain results in postnatal microencephaly.* J Neurochem, 2011. **118**(3): p. 388-98.
265. Vavrova, E., V. Lenoir, M.C. Alves-Guerra, R.G. Denis, J. Castel, C. Esnous, J.R. Dyck, S. Luquet, D. Metzger, F. Bouillaud and C. Prip-Buus, *Muscle expression of a malonyl-CoA-insensitive carnitine palmitoyltransferase-1 protects mice against high-fat/high-sucrose diet-induced insulin resistance.* Am J Physiol Endocrinol Metab, 2016. **311**(3): p. E649-60.
266. Matthaei, K.I., *Genetically manipulated mice: a powerful tool with unsuspected caveats.* J Physiol, 2007. **582**(Pt 2): p. 481-8.
267. Unger, R.H., *Lipid overload and overflow: metabolic trauma and the metabolic syndrome.* Trends Endocrinol Metab, 2003. **14**(9): p. 398-403.
268. Nie, L., G. Wu and W. Zhang, *Correlation between mRNA and protein abundance in Desulfovibrio vulgaris: a multiple regression to identify sources of variations.* Biochem Biophys Res Commun, 2006. **339**(2): p. 603-10.
269. Wang, D., *Discrepancy between mRNA and protein abundance: insight from information retrieval process in computers.* Comput Biol Chem, 2008. **32**(6): p. 462-8.
270. Liu, Y., A. Beyer and R. Aebersold, *On the Dependency of Cellular Protein Levels on mRNA Abundance.* Cell, 2016. **165**(3): p. 535-50.
271. Fernandez-Hernando, C., Y. Suarez, K.J. Rayner and K.J. Moore, *MicroRNAs in lipid metabolism.* Curr Opin Lipidol, 2011. **22**(2): p. 86-92.
272. Sarraf, S.A., M. Raman, V. Guarani-Pereira, M.E. Sowa, E.L. Huttlin, S.P. Gygi and J.W. Harper, *Landscape of the PARKIN-dependent ubiquitylome in response to mitochondrial depolarization.* Nature, 2013. **496**(7445): p. 372-6.
273. Lavie, J., H. De Belvalet, S. Sonon, A.M. Ion, E. Dumon, S. Melser, D. Lacombe, J.W. Dupuy, C. Lalou and G. Benard, *Ubiquitin-Dependent Degradation of Mitochondrial Proteins Regulates Energy Metabolism.* Cell Rep, 2018. **23**(10): p. 2852-2863.

274. Almogy, G. and G.P. Nolan, *Conditional protein stabilization via the small molecules Shld-1 and rapamycin increases the signal-to-noise ratio with tet-inducible gene expression.* Biotechniques, 2009. **46**(1): p. 44-50.
275. Das, A.T., L. Tenenbaum and B. Berkhout, *Tet-On Systems For Doxycycline-inducible Gene Expression.* Curr Gene Ther, 2016. **16**(3): p. 156-67.
276. Duann, P. and P.H. Lin, *Mitochondria Damage and Kidney Disease.* Adv Exp Med Biol, 2017. **982**: p. 529-551.
277. Chung, K.W., E.K. Lee, M.K. Lee, G.T. Oh, B.P. Yu and H.Y. Chung, *Impairment of PPARalpha and the Fatty Acid Oxidation Pathway Aggravates Renal Fibrosis during Aging.* J Am Soc Nephrol, 2018. **29**(4): p. 1223-1237.
278. Tran, M., D. Tam, A. Bardia, M. Bhasin, G.C. Rowe, A. Kher, Z.K. Zsengeller, M.R. Akhavan-Sharif, E.V. Khankin, M. Saintgeniez, S. David, D. Burstein, S.A. Karumanchi, I.E. Stillman, Z. Arany and S.M. Parikh, *PGC-1alpha promotes recovery after acute kidney injury during systemic inflammation in mice.* J Clin Invest, 2011. **121**(10): p. 4003-14.
279. Ozkok, A. and C.L. Edelstein, *Pathophysiology of cisplatin-induced acute kidney injury.* Biomed Res Int, 2014. **2014**: p. 967826.
280. Huang, S., J. Park, C. Qiu, K.W. Chung, S.Y. Li, Y. Sirin, S.H. Han, V. Taylor, U. Zimber-Strobl and K. Susztak, *Jagged1/Notch2 controls kidney fibrosis via Tfam-mediated metabolic reprogramming.* PLoS Biol, 2018. **16**(9): p. e2005233.
281. Bataille, A., P. Galichon, N. Chelghoum, B.M. Oumoussa, M.J. Ziliotis, I. Sadia, S. Vandermeersch, N. Simon-Tillaux, D. Legouis, R. Cohen, Y.C. Xu-Dubois, M. Commereuc, E. Rondeau, S. Le Crom and A. Hertig, *Increased Fatty Acid Oxidation in Differentiated Proximal Tubular Cells Surviving a Reversible Episode of Acute Kidney Injury.* Cell Physiol Biochem, 2018. **47**(4): p. 1338-1351.
282. Wahli, W. and L. Michalik, *PPARs at the crossroads of lipid signaling and inflammation.* Trends Endocrinol Metab, 2012. **23**(7): p. 351-63.
283. Cheng, C.F., H.H. Chen and H. Lin, *Role of PPARalpha and Its Agonist in Renal Diseases.* PPAR Res, 2010. **2010**: p. 345098.
284. Samra, M. and A.C. Abcar, *False estimates of elevated creatinine.* Perm J, 2012. **16**(2): p. 51-2.
285. Bonds, D.E., T.E. Craven, J. Buse, J.R. Crouse, R. Cuddihy, M. Elam, H.N. Ginsberg, K. Kirchner, S. Marcovina, J.C. Mychaleckyj, P.J. O'Connor and J.A. Sperl-Hillen, *Fenofibrate-associated changes in renal function and relationship to clinical outcomes among individuals with type 2 diabetes: the Action to Control Cardiovascular Risk in Diabetes (ACCORD) experience.* Diabetologia, 2012. **55**(6): p. 1641-50.
286. Scott, R., J. Best, P. Forder, M.R. Taskinen, J. Simes, P. Barter, A. Keech and F.S. Investigators, *Fenofibrate Intervention and Event Lowering in Diabetes (FIELD) study: baseline characteristics and short-term effects of fenofibrate [ISRCTN64783481].* Cardiovasc Diabetol, 2005. **4**: p. 13.
287. Idrovo, J.P., W.L. Yang, J. Nicastro, G.F. Coppa and P. Wang, *Stimulation of carnitine palmitoyltransferase 1 improves renal function and attenuates tissue damage after ischemia/reperfusion.* J Surg Res, 2012. **177**(1): p. 157-64.
288. Corominas-Faja, B., L. Vellon, E. Cuyas, M. Buxo, B. Martin-Castillo, D. Serra, J. Garcia, R. Lupu and J.A. Menendez, *Clinical and therapeutic relevance of the metabolic oncogene fatty acid synthase in HER2+ breast cancer.* Histol Histopathol, 2017. **32**(7): p. 687-698.
289. Loftus, T.M., D.E. Jaworsky, G.L. Frehywot, C.A. Townsend, G.V. Ronnett, M.D. Lane and F.P. Kuhajda, *Reduced food intake and body weight in mice treated with fatty acid synthase inhibitors.* Science, 2000. **288**(5475): p. 2379-81.
290. Yang, L., Y.S. Roh, J. Song, B. Zhang, C. Liu, R. Loomba and E. Seki, *Transforming growth factor beta signaling in hepatocytes participates in steatohepatitis through regulation of cell death and lipid metabolism in mice.* Hepatology, 2014. **59**(2): p. 483-95.
291. Stockert, J., T. Adhikary, K. Kaddatz, F. Finkernagel, W. Meissner, S. Muller-Brusselbach and R. Muller, *Reverse crosstalk of TGFbeta and PPARbeta/delta signaling identified by transcriptional profiling.* Nucleic Acids Res, 2011. **39**(1): p. 119-31.

292. Negmadjanov, U., Z. Godic, F. Rizvi, L. Emelyanova, G. Ross, J. Richards, E.L. Holmuhamedov and A. Jahangir, *TGF-beta1-mediated differentiation of fibroblasts is associated with increased mitochondrial content and cellular respiration.* PLoS One, 2015. **10**(4): p. e0123046.
293. Sun, Q., L. Fang, X. Tang, S. Lu, M. Tamm, D. Stolz and M. Roth, *TGF-beta Upregulated Mitochondria Mass through the SMAD2/3-->C/EBPbeta-->PRMT1 Signal Pathway in Primary Human Lung Fibroblasts.* J Immunol, 2019. **202**(1): p. 37-47.
294. Abe, Y., T. Sakairi, C. Beeson and J.B. Kopp, *TGF-beta1 stimulates mitochondrial oxidative phosphorylation and generation of reactive oxygen species in cultured mouse podocytes, mediated in part by the mTOR pathway.* Am J Physiol Renal Physiol, 2013. **305**(10): p. F1477-90.
295. Hardie, D.G., D. Carling and M. Carlson, *The AMP-activated/SNF1 protein kinase subfamily: metabolic sensors of the eukaryotic cell?* Annu Rev Biochem, 1998. **67**: p. 821-55.
296. Hue, L. and M.H. Rider, *The AMP-activated protein kinase: more than an energy sensor.* Essays Biochem, 2007. **43**: p. 121-37.
297. Saha, A.K. and N.B. Ruderman, *Malonyl-CoA and AMP-activated protein kinase: an expanding partnership.* Mol Cell Biochem, 2003. **253**(1-2): p. 65-70.
298. Itani, S.I., A.K. Saha, T.G. Kurowski, H.R. Coffin, K. Tornheim and N.B. Ruderman, *Glucose autoregulates its uptake in skeletal muscle: involvement of AMP-activated protein kinase.* Diabetes, 2003. **52**(7): p. 1635-40.
299. Grabacka, M., M. Pierzchalska, M. Dean and K. Reiss, *Regulation of Ketone Body Metabolism and the Role of PPARalpha.* Int J Mol Sci, 2016. **17**(12).
300. Kruger, C., T.T. Nguyen, C. Breaux, A. Guillory, M. Mangelli, K.T. Fridianto, J.P. Kovalik, D.H. Burk, R.C. Noland, R. Mynatt and K. Stadler, *Proximal Tubular Cell-Specific Ablation of Carnitine Acetyltransferase Causes Tubular Disease and Secondary Glomerulosclerosis.* Diabetes, 2019. **68**(4): p. 819-831.
301. Liu, L., X. Shi, K.G. Bharadwaj, S. Ikeda, H. Yamashita, H. Yagyu, J.E. Schaffer, Y.H. Yu and I.J. Goldberg, *DGAT1 expression increases heart triglyceride content but ameliorates lipotoxicity.* J Biol Chem, 2009. **284**(52): p. 36312-23.
302. Chatham, J.C. and M.E. Young, *Metabolic remodeling in the hypertrophic heart: fuel for thought.* Circ Res, 2012. **111**(6): p. 666-8.
303. Lopaschuk, G.D., *Fatty Acid Oxidation and Its Relation with Insulin Resistance and Associated Disorders.* Ann Nutr Metab, 2016. **68 Suppl 3**: p. 15-20.
304. Hue, L. and H. Taegtmeyer, *The Randle cycle revisited: a new head for an old hat.* Am J Physiol Endocrinol Metab, 2009. **297**(3): p. E578-91.
305. Randle, P.J., *Metabolic fuel selection: general integration at the whole-body level.* Proc Nutr Soc, 1995. **54**(1): p. 317-27.
306. Gibala, M.J., M.E. Young and H. Taegtmeyer, *Anaplerosis of the citric acid cycle: role in energy metabolism of heart and skeletal muscle.* Acta Physiol Scand, 2000. **168**(4): p. 657-65.
307. Garland, P.B., P.J. Randle and E.A. Newsholme, *Citrate as an Intermediary in the Inhibition of Phosphofructokinase in Rat Heart Muscle by Fatty Acids, Ketone Bodies, Pyruvate, Diabetes, and Starvation.* Nature, 1963. **200**: p. 169-70.
308. Sugden, M.C. and M.J. Holness, *Mechanisms underlying regulation of the expression and activities of the mammalian pyruvate dehydrogenase kinases.* Arch Physiol Biochem, 2006. **112**(3): p. 139-49.
309. Kaser, A., E. Martinez-Naves and R.S. Blumberg, *Endoplasmic reticulum stress: implications for inflammatory bowel disease pathogenesis.* Curr Opin Gastroenterol, 2010. **26**(4): p. 318-26.
310. Snodgrass, R.G., M. Boss, E. Zezina, A. Weigert, N. Dehne, I. Fleming, B. Brune and D. Namgaladze, *Hypoxia Potentiates Palmitate-induced Pro-inflammatory Activation of Primary Human Macrophages.* J Biol Chem, 2016. **291**(1): p. 413-24.
311. Meng, X.M., P.M. Tang, J. Li and H.Y. Lan, *Macrophage Phenotype in Kidney Injury and Repair.* Kidney Dis (Basel), 2015. **1**(2): p. 138-46.
312. Pan, B., G. Liu, Z. Jiang and D. Zheng, *Regulation of renal fibrosis by macrophage polarization.* Cell Physiol Biochem, 2015. **35**(3): p. 1062-9.

313. Rottiers, V. and A.M. Naar, *MicroRNAs in metabolism and metabolic disorders.* Nat Rev Mol Cell Biol, 2012. **13**(4): p. 239-50.
314. Bartram, M.P., C. Dafinger, S. Habbig, T. Benzing, B. Schermer and R.U. Muller, *Loss of Dgcr8-mediated microRNA expression in the kidney results in hydronephrosis and renal malformation.* BMC Nephrol, 2015. **16**: p. 55.
315. Wei, Q., K. Bhatt, H.Z. He, Q.S. Mi, V.H. Haase and Z. Dong, *Targeted deletion of Dicer from proximal tubules protects against renal ischemia-reperfusion injury.* J Am Soc Nephrol, 2010. **21**(5): p. 756-61.
316. Price, N.L., N. Rotllan, A. Canfran-Duque, X. Zhang, P. Pati, N. Arias, J. Moen, M. Mayr, D.A. Ford, A. Baldan, Y. Suarez and C. Fernandez-Hernando, *Genetic Dissection of the Impact of miR-33a and miR-33b during the Progression of Atherosclerosis.* Cell Rep, 2017. **21**(5): p. 1317-1330.
317. Price, N.L. and C. Fernandez-Hernando, *Novel Role of miR-33 in Regulating of Mitochondrial Function.* Circ Res, 2015. **117**(3): p. 225-8.
318. Portius, D., C. Sobolewski and M. Foti, *MicroRNAs-Dependent Regulation of PPARs in Metabolic Diseases and Cancers.* PPAR Res, 2017. **2017**: p. 7058424.
319. Scerbo, D., N.H. Son, A. Sirwi, L. Zeng, K.M. Sas, V. Cifarelli, G. Schoiswohl, L.A. Huggins, N. Gumaste, Y. Hu, S. Pennathur, N.A. Abumrad, E.E. Kershaw, M.M. Hussain, K. Susztak and I.J. Goldberg, *Kidney triglyceride accumulation in the fasted mouse is dependent upon serum free fatty acids.* J Lipid Res, 2017. **58**(6): p. 1132-1142.
320. Wahl, P., G.M. Ducasa and A. Fornoni, *Systemic and renal lipids in kidney disease development and progression.* Am J Physiol Renal Physiol, 2016. **310**(6): p. F433-45.
321. Ghadge, A., A. Harsulkar, M. Karandikar, V. Pandit and A. Kuvalekar, *Comparative anti-inflammatory and lipid-normalizing effects of metformin and omega-3 fatty acids through modulation of transcription factors in diabetic rats.* Genes Nutr, 2016. **11**: p. 10.
322. Schauerte, C., A. Hubner, S. Rong, S. Wang, N. Shushakova, M. Mengel, A. Dettling, C. Bang, K. Scherf, M. Koelling, A. Melk, H. Haller, T. Thum and J.M. Lorenzen, *Antagonism of profibrotic microRNA-21 improves outcome of murine chronic renal allograft dysfunction.* Kidney Int, 2017. **92**(3): p. 646-656.
323. Tomita, K., T. Teratani, T. Suzuki, M. Shimizu, H. Sato, K. Narimatsu, Y. Okada, C. Kurihara, R. Irie, H. Yokoyama, K. Shimamura, S. Usui, H. Ebinuma, H. Saito, C. Watanabe, S. Komoto, A. Kawaguchi, S. Nagao, K. Sugiyama, R. Hokari, T. Kanai, S. Miura and T. Hibi, *Free cholesterol accumulation in hepatic stellate cells: mechanism of liver fibrosis aggravation in nonalcoholic steatohepatitis in mice.* Hepatology, 2014. **59**(1): p. 154-69.
324. Nishiga, M., T. Horie, Y. Kuwabara, K. Nagao, O. Baba, T. Nakao, T. Nishino, D. Hakuno, Y. Nakashima, H. Nishi, F. Nakazeki, Y. Ide, S. Koyama, M. Kimura, R. Hanada, T. Nakamura, T. Inada, K. Hasegawa, S.J. Conway, T. Kita, T. Kimura and K. Ono, *MicroRNA-33 Controls Adaptive Fibrotic Response in the Remodeling Heart by Preserving Lipid Raft Cholesterol.* Circ Res, 2017. **120**(5): p. 835-847.
325. Zhang, X. and C. Fernandez-Hernando, *miR-33 Regulation of Adaptive Fibrotic Response in Cardiac Remodeling.* Circ Res, 2017. **120**(5): p. 753-755.
326. Cao, M., L. Bai, D. Wang, Q. Zhai, Y. Li, J. Hai and W. Wang, *miRNA-33 expression and its mechanism in patients and model rats with type 2 diabetic nephropathy.* Int J Clin Exp Med, 2018. **11**(3): p. 1661-1668.
327. Weber, M.J., *New human and mouse microRNA genes found by homology search.* FEBS J, 2005. **272**(1): p. 59-73.
328. Feingold, K.R. and C. Grunfeld, *Introduction to Lipids and Lipoproteins*, in *Endotext*, K.R. Feingold, B. Anawalt, A. Boyce, G. Chrousos, K. Dungan, A. Grossman, J.M. Hershman, G. Kaltsas, C. Koch, P. Kopp, M. Korbonits, R. McLachlan, J.E. Morley, M. New, L. Perreault, J. Purnell, R. Rebar, F. Singer, D.L. Trence, A. Vinik and D.P. Wilson, Editors. 2000: South Dartmouth (MA).
329. Mace, C. and S.S. Chugh, *Nephrotic syndrome: components, connections, and angiopoietin-like 4-related therapeutics.* J Am Soc Nephrol, 2014. **25**(11): p. 2393-8.
330. Dijk, W., S. Schutte, E.O. Aarts, I.M.C. Janssen, L. Afman and S. Kersten, *Regulation of angiopoietin-like 4 and lipoprotein lipase in human adipose tissue.* J Clin Lipidol, 2018. **12**(3): p. 773-783.

331. Ding, E., Q. Zhao, Y. Bai, M. Xu, L. Pan, Q. Liu, B. Wang, X. Song, J. Wang, L. Chen and B. Zhu, *Plasma microRNAs expression profile in female workers occupationally exposed to mercury.* J Thorac Dis, 2016. **8**(5): p. 833-41.
332. Wu, K., J. Ma, Y. Zhan, K. Liu, Z. Ye, J. Chen, K. Xu, H. Huang and Y. He, *Down-Regulation of MicroRNA-214 Contributed to the Enhanced Mitochondrial Transcription Factor A and Inhibited Proliferation of Colorectal Cancer Cells.* Cell Physiol Biochem, 2018. **49**(2): p. 545-554.
333. Wu, K., Z. Zhao, Y. Xiao, J. Peng, J. Chen and Y. He, *Roles of mitochondrial transcription factor A and microRNA5903p in the development of colon cancer.* Mol Med Rep, 2016. **14**(6): p. 5475-5480.
334. Caravia, X.M., V. Fanjul, E. Oliver, D. Roiz-Valle, A. Moran-Alvarez, G. Desdin-Mico, M. Mittelbrunn, R. Cabo, J.A. Vega, F. Rodriguez, A. Fueyo, M. Gomez, M. Lobo-Gonzalez, H. Bueno, G. Velasco, J.M.P. Freije, V. Andres, B. Ibanez, A.P. Ugalde and C. Lopez-Otin, *The microRNA-29/PGC1alpha regulatory axis is critical for metabolic control of cardiac function.* PLoS Biol, 2018. **16**(10): p. e2006247.
335. Aoi, W., Y. Naito, K. Mizushima, Y. Takanami, Y. Kawai, H. Ichikawa and T. Yoshikawa, *The microRNA miR-696 regulates PGC-1{alpha} in mouse skeletal muscle in response to physical activity.* Am J Physiol Endocrinol Metab, 2010. **298**(4): p. E799-806.
336. Iliopoulos, D., K. Drosatos, Y. Hiyama, I.J. Goldberg and V.I. Zannis, *MicroRNA-370 controls the expression of microRNA-122 and Cpt1alpha and affects lipid metabolism.* J Lipid Res, 2010. **51**(6): p. 1513-23.
337. Zhou, H., S.A. Hasni, P. Perez, M. Tandon, S.I. Jang, C. Zheng, J.B. Kopp, H. Austin, 3rd, J.E. Balow, I. Alevizos and G.G. Illei, *miR-150 promotes renal fibrosis in lupus nephritis by downregulating SOCS1.* J Am Soc Nephrol, 2013. **24**(7): p. 1073-87.
338. Wang, X., H. Jin, S. Jiang and Y. Xu, *MicroRNA-495 inhibits the high glucose-induced inflammation, differentiation and extracellular matrix accumulation of cardiac fibroblasts through downregulation of NOD1.* Cell Mol Biol Lett, 2018. **23**: p. 23.
339. Zorova, L.D., V.A. Popkov, E.Y. Plotnikov, D.N. Silachev, I.B. Pevzner, S.S. Jankauskas, V.A. Babenko, S.D. Zorov, A.V. Balakireva, M. Juhaszova, S.J. Sollott and D.B. Zorov, *Mitochondrial membrane potential.* Anal Biochem, 2018. **552**: p. 50-59.
340. Billis, P., Y. Will and S. Nadanaciva, *High-Content Imaging Assays for Identifying Compounds that Generate Superoxide and Impair Mitochondrial Membrane Potential in Adherent Eukaryotic Cells.* Curr Protoc Toxicol, 2014. **59**: p. 25 1 1-14.
341. Mukhopadhyay, P., M. Rajesh, G. Hasko, B.J. Hawkins, M. Madesh and P. Pacher, *Simultaneous detection of apoptosis and mitochondrial superoxide production in live cells by flow cytometry and confocal microscopy.* Nat Protoc, 2007. **2**(9): p. 2295-301.
342. Song, S., H.H. Seo, S.Y. Lee, C.Y. Lee, J. Lee, K.J. Yoo, C. Yoon, E. Choi, K.C. Hwang and S. Lee, *MicroRNA-17-mediated down-regulation of apoptotic protease activating factor 1 attenuates apoptosome formation and subsequent apoptosis of cardiomyocytes.* Biochem Biophys Res Commun, 2015. **465**(2): p. 299-304.
343. Tomasetti, M., S. Staffolani, L. Nocchi, J. Neuzil, E. Strafella, N. Manzella, L. Mariotti, M. Bracci, M. Valentino, M. Amati and L. Santarelli, *Clinical significance of circulating miR-126 quantification in malignant mesothelioma patients.* Clin Biochem, 2012. **45**(7-8): p. 575-81.
344. Mutharasan, R.K., V. Nagpal, Y. Ichikawa and H. Ardehali, *microRNA-210 is upregulated in hypoxic cardiomyocytes through Akt- and p53-dependent pathways and exerts cytoprotective effects.* Am J Physiol Heart Circ Physiol, 2011. **301**(4): p. H1519-30.
345. Perry, S.W., J.P. Norman, J. Barbieri, E.B. Brown and H.A. Gelbard, *Mitochondrial membrane potential probes and the proton gradient: a practical usage guide.* Biotechniques, 2011. **50**(2): p. 98-115.
346. Parker, R. and U. Sheth, *P bodies and the control of mRNA translation and degradation.* Mol Cell, 2007. **25**(5): p. 635-46.
347. Sole, C., J. Cortes-Hernandez, M.L. Felip, M. Vidal and J. Ordi-Ros, *miR-29c in urinary exosomes as predictor of early renal fibrosis in lupus nephritis.* Nephrol Dial Transplant, 2015. **30**(9): p. 1488-96.